Stellingen behorende bij het proefschrift

Catalytic Diesel Exhaust Purification
A DRIFT Spectroscopic and Mechanistic Study of Soot Oxidation

door G. Mul

1. De aanduiding Universitair Docent (UD) of Universitair Hoofd Docent (UHD), in plaats van bijvoorbeeld Universitair Fundamenteel Onderzoeker (UFO), suggereert ten onrechte dat medewerkers die onder de catagorie UD of UHD vallen zich voornamelijk met onderwijs bezig houden.

2. Het geven van de achternaam van de moeder aan pas geboren kinderen, i.p.v. de achternaam van de vader, vermindert schijnbaar de biologische relatie tussen vader en kind. Gelukkig wordt het kind in eerste instantie toch nog naar een man vernoemd, namelijk naar opa (van moeders kant). Het is in zekere zin te betreuren dat dit een transient verschijnsel is.

3. Het verdient aanbeveling wetenschappelijke documentaires op de Nederlandse televisie op een wat eerder tijdstip te programmeren dan nu het geval is, daar de gemiddelde kijker op het huidige tijdstip al lang is uitgezapped ten gevolge van een overdosis Ende/Mol.

4. Qua tijdsbesteding is het voor AIO's op een experimenteel wetenschapsgebied noodzakelijk de gulden middenweg te kiezen tussen denken en doen.

5. NO was in 1994 het molecuul van het jaar, voornamelijk ten gevolge van publicaties over biologische reacties van dit molecuul in het menselijk lichaam. Gezien het grote aantal publikaties in katalytische tijdschriften over 'deNOx', zou het best in 1997 weer het molecuul van het jaar mogen worden.

6. Tot de catagorie metaal oxiden waarvan uitsluitend het aanwezige zuurstof aan het oppervlak beschikbaar is voor uitwisseling, worden in een proefschrift naast Fe_2O_3 en Cr_2O_3, ook V_2O_5, MoO_3 en WO_3 gerekend [1]. Voor de laatste drie metaal oxiden geldt echter dat niet alleen het aanwezige oppervlakte zuurstof, maar tevens bulk zuurstof uitwisselbaar is [2].

   [1] F. v. Looij, 'The catalytic partial oxidation of methane to synthesis gas', PhD Thesis, Utrecht University, 1994.
   [2] J. Novakova, 'Isotopic exchange of oxygen ^{18}O between the gaseous phase and oxide catalysts', *Catal. Rev.* 4 (1970) 77.

7. De chemische reactiviteit van KBr wordt onderschat [3,4].

   [3] C. Setzer, W. Scheutz, and F. Scheuth, 'Transition metal compound oxide catalysts for lowering the light-off temperature of particles from diesel exhaust.', Proc. 10th International Congress on Catalysis, Budapest, 1992, P.309.
   [4] Hoofdstuk 2 van bijgaand proefschrift

8. De gewoonte om alleen na het plassen de handen te wassen laat zien dat de gemiddelde man meer consideratie voor anderen, dan voor zichzelf heeft.

9. De opmerking dat kunstmatig gefabriceerd vitamine C veel minder effectief zijn werking doet in het menselijk lichaam dan vitamine C uit vruchten, en soms zelfs schadelijk kan zijn [5], is zowel lachwekkend als misleidend.

   [5] H. Diamond en M. Diamond, 'Een leven lang fit', 33e druk, Uitgeverij De Kern, Baarn, 1987, p. 145.

10. De naam 'Titanic Reisen', die een reisbureau in Berlijn voert, is vooral wervend voor diegene die het leven moe zijn...

11. Promoveren is als een avond in de kroeg. Voor je het weet is het sluitingstijd.

Catalytic Diesel Exhaust Purification

A DRIFT Spectroscopic and Mechanistic Study of Soot Oxidation

Proefschrift

ter verkrijging van de graad van doctor
aan de Technische Universiteit Delft,
op gezag van de Rector Magnificus Prof. dr. ir. Blaauwendraad,
in het openbaar te verdedigen ten overstaan van een commissie,
door het college van Dekanen aangewezen,
op dinsdag 25 maart 1997 te 13.30 uur

door

Guido MUL

doctorandus in de scheikunde

geboren te Hoorn

Dit proefschrift is goedgekeurd door de promotor: Prof. dr. J.A. Moulijn

Toegevoegd promotor: Dr. F. Kapteijn

Samenstelling promotiecommissie

Rector Magnificus	Technische Universiteit Delft, voorzitter
Prof. dr. J.A. Moulijn	Technische Universiteit Delft, promotor
Dr. F. Kapteijn	Technische Universiteit Delft, toegevoegd promotor
Prof. Dr. R. Schlögl	Fritz Haber Institut der Max Planck Gesellschaft
Prof. dr. J.W. Geus	Universiteit Utrecht
Prof. dr. J. v.d. Maas	Universiteit Utrecht
Prof. dr. V. Ponec	Rijksuniversiteit Leiden
Dr. M. Makkee	Technische Universiteit Delft

Mul, Guido

Catalytic Diesel Exhaust Purification
A DRIFT Spectroscopic and Mechanistic Study of Soot Oxidation

Proefschrift, Technische Universiteit Delft
-met samenvatting in het Nederlands

PREFACE

Regarding the emission of hydrocarbons and nitrogen oxides (NO_x), diesel engines are environmentally friendlier than otto engines. However, they are main contributors to the emission of particulates. The particulates, consisting of soot (*i.e.* the carbonaceous part), adsorbed poly-aromatic hydrocarbons (PAH's, compounds which are toxic and thought to have a carcinogenic effect), sulfates and inorganic substances, are blamed for decreasing environmental conditions, particularly in large cities. Furthermore, after the development of platinum/rhodium three-way catalysts for otto engines, the amount of nitrogen oxides (NO_x) emitted by diesel engines is higher than the amount emitted by otto engines. Unfortunately, platinum/rhodium catalysts cannot be used for the clean-up of diesel-exhaust gas, because of the presence of a relatively high amount of oxygen: the reaction of CO with NO, essential in the three-way catalysis, does not take place.

The Dutch Ministry of Environmental Affairs granted a project to the Faculty of Chemical Technology and Materials Science of the Delft University to develop a method for the conversion of diesel soot (including adsorbed hydrocarbons) and NO_x into harmless substances. The removal of NO_x and soot might be accomplished in two stages: in the first stage the particulates, including the adsorbed hydrocarbons, are filtered using a ceramic filter (wall flow monolith) and simultaneously converted into CO_2 by reaction with oxygen at the exhaust gas temperatures. In a second stage NO_x is catalytically converted with ammonia, yielding water and N_2.

This thesis deals with the catalytic oxidation of soot particulates. As the oxidation of soot occurs around 875 K, and the temperature of diesel exhaust (dependent on the loading of the diesel-engine) hardly ever exceeds 625 K, catalytic oxidation of soot is required. Three major groups of catalytically active materials are known: catalysts based on transition metal chlorides, catalysts based on alkali metal oxides and -carbonates, and catalysts based on transition metal oxides. However, knowledge of the mechanism by which catalytic soot or carbon oxidation occurs, is limited. Elucidation of this mechanism might result in design rules for the development of highly active catalysts. Fourier Transformed InfraRed (FT-IR) spectroscopy is an excellent analytical technique to study the surface composition of carbonaceous materials. Moreover, FT-IR spectroscopy allows a characterization of metal oxides and other catalysts. Therefore, this is the main technique used throughout this thesis, with the objective to reveal the mechanism of catalytic soot oxidation. The activity of the mentioned groups of catalysts will be evaluated, as well as the effect of other components of diesel exhaust, *i.e.* NO and CO, on the catalytic performance.

Outline

A description of the literature on the FT-IR spectroscopic analysis of carbonaceous materials is given in *chapter 1*. It will be shown that oxygen and hydrogen containing functionalities on carbon surfaces (the terminology Surface Oxygen Complexes (SOCs)

is used throughout this thesis) can be analyzed in detail. *Chapter 2* describes the experimental procedures for an optimal accuracy in the recording of Diffuse Reflectance Infrared Fourier Transformed (DRIFT) spectra of mixtures of catalysts and soot. Drawbacks of the use of KBr as sample diluent will be dealt with. Furthermore, the reader is introduced to the chemistry of fullerene C60, which is shown to be a useful compound as a model for soot. In *chapter 3* a mechanistic study on the most active catalyst described in the literature, *i.e.* a Cu/K/Mo/Cl catalyst, is dealt with. In *chapter 4* the activity of other chlorine containing catalysts is evaluated. It will be shown that these catalysts are of little practical use. *Chapters 5 and 6* describe the mechanism of catalytic soot oxidation by alkali metal oxides as revealed by (*in-situ*) DRIFT analyses and activity measurements. The effects of CO and NO (other constituents of the diesel exhaust gas) on the catalytic activity are included, as well as an evaluation of the possibility to use K-based catalysts in practice. *Chapters 7 and 8* deal with the catalytic action of transition metal catalysts in soot oxidation. The contributions of lattice oxygen, gas phase oxygen and carbon surface oxygen complexes to the mechanism will be evaluated. *Chapter 9* deals with the soot oxidation activity of Ag- and Au modified transition metal oxides. A possible mechanistic explanation for the observed phenomena will be given. Finally, *chapter 10* describes the effects of CO and NO on the activity of transition metal oxides. The activity of these catalysts in the oxidation of NO and in the NO_2/soot reaction will be evaluated, as well as the opportunities to use the NO_2/soot reaction for the conversion of soot particulates from diesel exhaust.

CONTENTS

Preface

1

Infrared analysis of carbonaceous materials : a literature survey

Abstract

In this introductory chapter, literature dealing with IR analyses of coal, soot, and related carbonaceous materials is reviewed. Many IR analyses performed in the 1950s-1970s, were aimed to elucidate the composition of coal and its structure. Furthermore, extensive *in-situ* FT-IR studies of the pyrolysis and oxidation of coal and other carbonaceous materials have been performed in the 1980s-1990s. These studies are described and the observed spectral phenomena evaluated, as well as the effect of diluting agents (KBr) and the use of mathematical transformations (Fourier Self Deconvolution). Also chemical methods to justify the assignments of the surface species are dealt with, such as the reaction of hydroxylic species with acetic acid. An overview of the assignments of the absorption frequencies of several hydrogen and oxygen containing functionalities on carbon surfaces, is presented. The functional groups located on the surfaces of chars, carbon black and coal, appear to be quite similar. Literature dealing with the (*in-situ*) IR analysis of the catalytic oxidation of carbon is limited and mainly focused on the K_2CO_3 catalyzed CO_2 gasification. The results of these studies are described and evaluated.

1.1. *The composition of coal and soot : a comparison*

Several chapters in this thesis deal with the (*in-situ*) Diffuse Reflectance Infrared Fourier Transformed (DRIFT) spectroscopic characterization of the catalytic oxidation of soot. In this chapter, the reader is introduced to Fourier Transformed Infrared (FT-IR) analyses of carbonaceous materials. The number of papers dealing with IR analyses of soot are limited, whereas an enormous amount of papers concerning the IR analyses of coal is available. It will be shown that IR spectra of coal, (oxidized) soot, chars, and other carbonaceous materials are quite similar. First, a general description of the structures of coal and soot is given.

The typology, physics, chemistry and constitution of coal has been extensively described by van Krevelen [1]. Moreover, at least five theses have been written as a result of the Dutch National Coal Research Program (NOK), dealing with the pyrolysis [2], gasification [3-5], and combustion [6] of carbonaceous materials. Coal is a heterogeneous kind of rock which mainly consists of organic material (macerals, which are fossilized plant remains) and different kinds of minerals [2,7]. The macerals can be divided into three major classes: vitrinite is believed to be derived from wood-like substances, exinite from lipids and waxy plant like substances, and inertinite is probably formed by prehistoric pyrolysis processes [1].

Depending on the pressure of overlying sediments and time, various coals can be arranged in the following rank order: peat, lignite, subbituminous coal, bituminous coal and anthracite. The C/H and $C_{aromatic}/C_{total}$ ratio increases with rank [7]. Several models for a description of the coal structure have been postulated, such as one hypothetical average molecule, characterizing coal of a specific rank. The proposition of an aromatic/hydroaromatic model [1,2,8] probably is a better description: a variety of aromatics and functional groups, such as aliphatic and oxygen containing functionalities, are added together to synthesize a coal structure. Some examples are given in figure 1.

Fluorenone   Phenantrene   Xanthone   Benzonaphtofuran
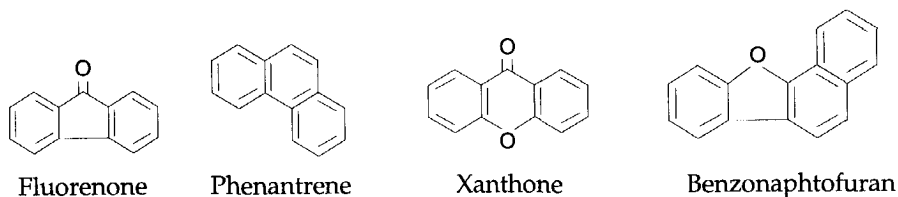
Figure 1. Examples of aromatic functionalities present in coal [8].

The aromatic units are linked together through short aliphatic and ether bridges, yielding macromolecular aggregates. Within these aggregates smaller molecules are embedded, which can be dissolved, and contribute to the composition of coal extracts (figure 2). The presence of these aggregates also explains solvent swelling of coal [1].
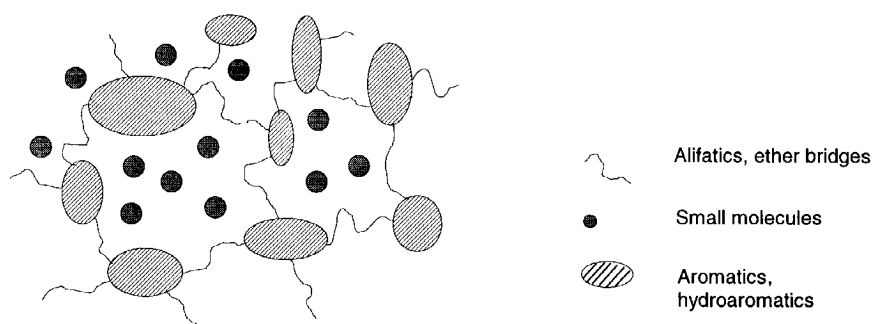
Figure 2. Representation of a two component model proposed for the structure of coal [8].

Diesel particulate consists of a mixture of so-called acinoform (Latin for "clustered like grapes") carbon, which is usually referred to as soot, and a Soluble Organic Fraction (SOF). Acinoform carbon (soot) consists of spherical particles, which are fused together in aggregates of colloidal dimensions. Carbon black should be considered as an artificial, manufactured product, which almost entirely consists of acinoform carbon. Carbon blacks are used for rubber reinforcement and for ink and paint coloring [9]. The soluble organic fraction of diesel particulate is much larger than the fraction of carbon black samples. An extract of the organics (poly-nuclear aromatic compounds and poly-nuclear aromatic hydrocarbons) of diesel particulate in methylene chloride mainly consists of unburned hydrocarbons also present in the original diesel-fuel [10]. Summarizing, a number of similarities between coal and diesel particulate exist: they both contain a solid carbon and a soluble organic fraction, of which the chemical composition is also essentially identical.

1.2. *IR analysis of coal : qualitative assignments of C=O and C-H functionalities*

The hydrocarbon functionalities present on the surface of coal have been analyzed extensively by means of IR spectroscopy in the 1950s and 1960s using dispersive IR instruments [1,8]. Furthermore, extensive FT-IR studies of the pyrolysis and oxidation of coal have been performed in the 1980s-1990s. A nice evaluation of the literature dealing with the FT-IR spectra of (oxidized) carbonaceous materials, is given by Painter [11] and Zawadski [12]. The main advantage of FT-IR compared to dispersive IR, is the higher throughput to the detector (see appendix I). In this way, a better signal to noise ratio can be obtained, and a better determination of the absorption frequencies is possible. The assignments of the IR absorptions to aromatic hydrocarbons, aliphatic hydrocarbons and oxygenated species are summarized in Table 1. A spectrum of ozonized soot is shown in figure 3a. Assignments to various oxygen containing aromatic compounds, are given in figure 3b.

Table 1. *Functionalities on carbon surfaces and their infrared assignments.*

Spectral regions (cm^{-1})	O-functionality**	CH-functionality
3300	OH, hydrogen bonded	
3030		Aromatic CH stretch
2500-3300	OH, Carboxylic acids	
2850-2950		Aliphatic CH stretch
1835	C=O, anhydride	
1765-1775	C=O ester + E.W.G.*	
1665-1760	C=O, ketone, COOH	
1735	Lactones, C=O ester	
1600	Quinones	C=C, aromatic ring
1560-1590	COO⁻, salt form	
1490		C=C, aromatic ring
1450		CH$_2$, CH$_3$ bend
1375		CH$_3$ bend
1110-1300	C-O stretch, OH bend	
1000-1100	Alcohols, aliph. ethers	
700-900 ***		Aromatic C-H bending

* E.W.G. = Electron Withdrawing Group attached to single bonded oxygen (EWG-O-(C=O)-Carbon).
** See figure 3 for a spectrum and a description of the molecular structures
*** See figure 4 for a detailed assignment.
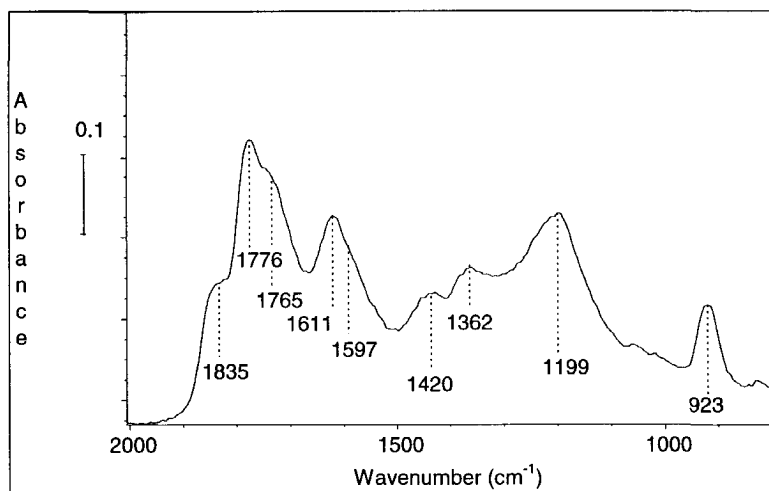
Figure 3a. *DRIFT spectrum of ozonized soot, recorded in KBr (8 cm⁻¹, 256 scans) [14].*
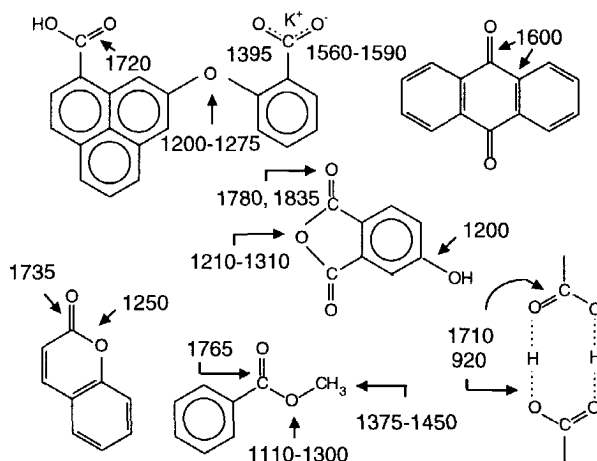
Figure 3b. *Carbonylic (C=O), C-OH and C-O-C stretching vibrations of various aromatic oxygen containing compounds. The assignments are based on Conley [15] and Zawadski [12].*

The carbonylic stretching region ranges from 1600-1850 cm^{-1} (figures 3a and 3b). Generally, the C=O absorption frequency of aromatic species increases in the series: ketones (1665-1690) < aldehydes (1700) < acids (1710-1730) < esters, lactones (1725-1745) < anhydrides (1830-1810) (compare Table 1) [15].

The vibrational modes of the two carbonylic groups of <u>anhydrides</u> are coupled. This results in an asymmetric and symmetric stretching vibration of the anhydride group, of which the asymmetric vibration is located at an approximately 60 cm^{-1} higher frequency than the symmetric vibration. A distinction between linear and cyclic anhydrides can be made: in linear anhydrides, the high frequency band is stronger and sharper than the low frequency band, whereas the reverse is true for cyclic anhydrides. Moreover, the stretching vibrations of linear anhydrides are usually located below 1800 cm^{-1}. In cyclic <u>esters</u> (<u>lactones</u>) the frequency of the carbonyl functionality increases with decreasing ring size: the C=O frequency of a 5-membered ring is located at approximately 1770 cm^{-1} [15], whereas it is located at 1735 cm^{-1} in the case of a 6-membered ring. The carbonyl frequency of <u>acids</u> is largely affected by hydrogen bonding. The double bond character is decreased, resulting in a shift to lower frequency (compare figure 3b). In the salt form (COO-K), symmetric and asymmetric stretching vibrations of the C=O group are located at 1560-1590 cm^{-1} and around 1395 cm^{-1}, respectively.

There is still disagreement about two regions of the IR-spectrum of carbonaceous materials: the region near 1600 cm^{-1} and the region between 1000 cm^{-1} and 1350 cm^{-1}. The first cannot be assigned to simple vibrations of specific functional groups, but has a complex, mixed character. Painter extensively discussed the absorption profile at 1600 cm^{-1} [11]. The intensity of the 1600 cm^{-1} band was found to increase with the amount of phenolic OH. Furthermore, after treatment of coal in HCl, changes in the absorption

profile were observed. This effect is explained by the assumption that COO⁻ groups, which absorb near 1580 cm⁻¹, contribute to the intensity of the 1600 cm⁻¹ band. The carboxyl groups are converted to the carboxylic acid form, COOH, yielding absorptions around 1720 cm⁻¹. These observations lead to the assignment of the 1600 cm⁻¹ band to aromatic stretching vibrations, whose intensity is enhanced by phenolic groups and R-COO⁻ functionalities. Morterra and Low [13] provide further evidence for the assignment of the 1600 cm⁻¹ to aromatic stretching vibrations, by comparing the spectrum of carbon oxidized in $^{16}O_2$ with that of carbon oxidized in $^{18}O_2$. Shifts in wavenumbers occurred at 1760 cm⁻¹ (to 1725 cm⁻¹) and 1260 cm⁻¹ (to 1235 cm⁻¹), whereas the 1600 cm⁻¹ band remained at the same position.

Vibrations involving C-O-C stretching, C-C stretching, O-H bending and C-H bending appear in the region between 1000 cm⁻¹ and 1350 cm⁻¹ of the spectrum [11]. The C-O-C stretching vibration of <u>anhydrides</u> can be found around 1210-1310 cm⁻¹. The C-O-C frequencies of <u>esters</u> are dependent on the nature of the substituents (aliphatic or aromatic). Aromatic esters show absorptions at 1080-1150 cm⁻¹ and at 1240-1310 cm⁻¹. The OH stretching of <u>acidic</u> species, yields a broad complex band structure ranging from 2500-3000 cm⁻¹. In addition coupled frequencies in dimeric species (figure 3b) between O-H and C-O stretching are located near 1250 and 1420 cm⁻¹. Furthermore, a strong out of plane bending vibration of dimeric acidic species is located around 920 cm⁻¹. The C-O-C asymmetric stretching mode of aromatic <u>ethers</u> are located around 1200-1275 cm⁻¹. The symmetric stretching mode is of weaker intensity and located around 1050 cm⁻¹. Internal <u>ethers (epoxides)</u> show vibrations due to bending modes of the ring structure, which are located at 810-950 and 1250 cm⁻¹. The absorption frequencies of <u>phenols</u> are located near 3610 cm⁻¹ (O-H stretch) and 1310-1410 cm⁻¹ (O-H bend). Furthermore, the C-O stretching vibration is located near 1230 cm⁻¹.

Based on the characteristic frequencies given, the absorption bands present in the spectrum of ozonized soot can be assigned to anhydrides (1835 and 1776 cm⁻¹), lactones (five membered ring (1765 cm⁻¹)), esters (1765, 1199 cm⁻¹), dimeric acids (1710, 1420, 920 cm⁻¹), possibly epoxides (923 cm⁻¹, 1199 cm⁻¹) and phenols (1362, 1199 cm⁻¹). The 1611 cm⁻¹ band is assigned to aromatic C=C ring stretch.

Absorptions occurring in coal spectra at 2920 and 3030 cm⁻¹ have been ascribed to aliphatic and aromatic C-H vibrations, respectively. The 3030 cm⁻¹ absorption was shown to increase with rank. This is explained by an increasing aromatic to total hydrogen ratio [7]. Absorptions at 760, 814 and 870 cm⁻¹ were assigned to out-of-plane vibrations of one isolated, two adjacent, or four adjacent aromatic CH-groups (shown in figure 4). A more detailed description of the C-H bending and stretching vibrations will be given in the next paragraph.

1.3. *Quantitative IR analysis of coal : the C-H content*

Carbonaceous materials are strong absorbers of IR radiation. The extinction coefficients of carbon blacks and graphite are typically around 0.7 [12]. Spectral data of

carbonaceous materials are usually obtained by dilution of the samples with KBr. In this way, the overall absorption of the samples can be reduced.

| **A.** Isolated CH groups (760 cm^{-1}) | **B.** Two adjacent CH groups (814 cm^{-1}) | **C.** Four adjacent CH groups (870 cm^{-1}) |
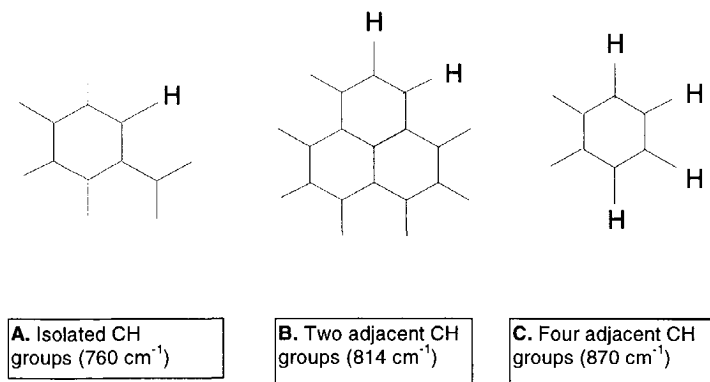
Figure 4. Assignment of the out of plane bending vibrations of C-H bonds in the 700-1000 cm^{-1} region of IR spectra of carbonaceous materials.

When a diluting agent is applied, some aspects have to be considered, especially if a quantitative analysis is aimed for. The maximum peak intensity depends on the grinding time of a coal/KBr mixture, before pellets are pressed [11]. Ito [16] prepared coal-samples by grinding and dilution with KBr. The smaller (<< 200 mesh) the particle size, the better the obtained resolution and intensity of the recorded spectral bands. Furthermore, a quantitative IR analysis of the hydrocarbon content of coal samples, requires the elimination of spectral features caused by minerals (kaolinite and illite, which are clay like materials). Also a proper baseline adjustment of the spectra is necessary. The baseline of the IR spectra of carbonaceous materials usually has a parabolic shape, and a baseline correction by using one sloping straight line is not applicable.

Cagniant [17] used the whole characteristic spectral region (2800 cm^{-1} to 3000 cm^{-1}) to determine the amount of aliphatic hydrocarbons in different kinds of coal. The resolution can be improved by calculating the second derivative of the spectral lines. In this way, the 2800 to 3000 cm^{-1} region of the spectrum can be shown to consist of three main components: CH$_3$, (CH$_2$)$_n$, and CH (compare Table 1). By separation of the spectral contributions a better insight in the structure of coal and a better estimation of the aliphatic to aromatic C-H ratio is obtained [16].

Generally, if two IR bands overlap, they can be resolved by a method called Fourier Self Deconvolution (FSD). Nowadays, FT-IR software usually contains the option to perform these deconvolution calculations [18]. FSD can be applied when the instrumental resolution is higher than the intrinsic line-widths [18]. Kauppinen describes mathematical operations and provides examples of the application of the deconvolution procedure. A nice feature of FSD is the possibility to remove

contributions of interfering spectral lines to the surface area of a certain absorption band. This is illustrated in figure 5. After deconvolution of the original pattern, one contribution can be removed. Reconvolution of the remaining band results in the original shape of the absorption frequency and allows a reliable calculation of the original surface area.
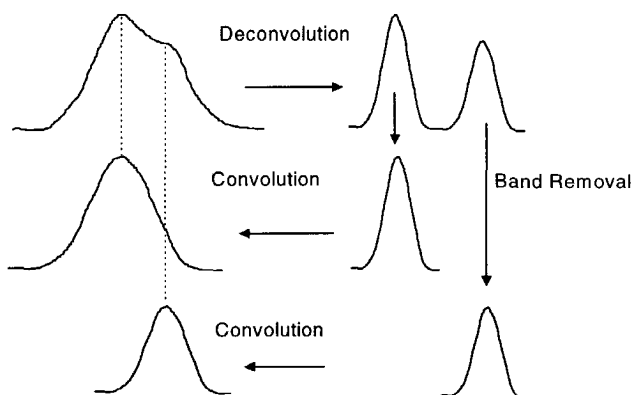
Figure 5. *FSD, followed by elimination of spectral lines, to enable a better calculation of the surface area.*

The FSD method was used to resolve the contributions of different aliphatic C-H vibrations in the 2700-3000 cm^{-1} spectral region. The following assignments are in excellent agreement with standard works [19,20]:

2745 cm^{-1} : C-H stretch in aldehyde groups
2859 cm^{-1} : Symmetric C-H stretch in methylene (CH$_2$) groups
2885 cm^{-1} : C-H stretch of a C-H group of tertiary carbon components (R$_3$C-H)
2926 cm^{-1} : C-H antisymmetric stretch in methylene groups
2954 cm^{-1} : C-H antisymmetric stretch in methyl groups.

Within the 700 to 1000 cm^{-1} spectral region, various absorption frequencies can be assigned to aromatic out of plane C-H vibrations (compare the assignments given in figure 3). After FSD Wang and Griffiths [20] conclude that each frequency contains (at least) a doublet. The high frequency absorption of each doublet is assigned to C-H vibrations of poly-aromatic structures, whereas the low frequency absorption is assigned to C-H groups attached to isolated rings. The results indicate that FSD, when it is applied properly (eliminating artificial bands), is a powerful mathematical technique to obtain additional spectral information, obscured in the original spectra of carbonaceous materials [19,20].

1.4. *Quantitative IR analysis of coal : oxygen containing functionalities*

If a quantitative IR analysis of OH-groups is aimed for, several issues have to be taken into consideration [11]. Residual absorptions, mainly due to traces of water present in KBr (used to dilute the sample), introduce a significant systematic error in the determination of the intensity of the 3450 cm^{-1} band. Moreover, water is always present in coal itself. Recently, Boehm reviewed the surface chemistry of carbon blacks and activated carbons [21]. The paper is focused on chemical methods for a quantitative analysis of surface oxides. Chemical methods have also been combined with IR analyses to obtain a better identification and quantification of surface oxygen complexes. For example, the acetylation of R-OH groups with acetic anhydride has been quite successful [11,22]. IR bands appearing at 1770 cm^{-1} and 1725 cm^{-1} can be assigned to C=O vibrations of acetylated phenolic-OH and alkyl-OH moieties, respectively [11,22]. Separation of the bands is necessary to obtain quantitative results. This can be accomplished by calculating the second derivative of the obtained difference-spectrum or using the FSD procedure. Furthermore, fitting programs can be used to calculate the area under the different curves. However, a fitting program suitable for a certain set of bands, cannot be applied to the whole spectrum, because band shapes (Gaussian or Lorentzian shape) are usually dependent on the spectral region.

Fuller and Smyrl measured the *in-situ* acetylation reaction of coal samples, using DRIFT spectroscopy [19,22,23]. In this way, pellet pressing is not necessary, and unknown factors due to sample manipulations are excluded. Moreover, the sequential steps, in which the acetylation reaction proceeds, can be visualized, thus permitting the reaction to be followed kinetically. A sequence of *in-situ* DRIFT spectra showed a growing band in the 1770 cm^{-1} region. Moreover a broad negative band was formed in the 3000 cm^{-1} to 3600 cm^{-1} region. The 1770 cm^{-1} band did not contain a contribution of a 1725 cm^{-1} absorption. Therefore, Fuller and Smyrl [22] conclude that the analyzed coals only contain phenolic OH-groups. After completion of the acetylation reaction, relatively sharp bands were observed at 3550 cm^{-1} and 3440 cm^{-1}. These bands were assigned to OH-groups that did not react with the acetylation agent, probably because they were inaccessible. Fuller confirmed this conclusion by reacting the residual OH-groups with D$_2$O. An exchange of protons for deuterons was observed.

The FSD procedure was used for the analysis of OH-groups by Haley [24]. The spectral region of 400-2300 cm^{-1} was deconvoluted to analyze the amount of different hydroxylic functionalities. In peat, only aliphatic OH-vibrations were observed. Hydrogen-bonding is claimed to be a major force in this material, holding several structures together. Five distinct types of hydrogen bonding exist. The more rigid the coal structure, the stronger the hydrogen bonds are, as was deduced from lower specific absorption frequencies and sharper peaks of the OH-vibrations. The content of hydrogen-bonding was found to decrease with rank [24].

1.5. *Oxidation of coals at ambient temperatures*

The reaction of coal with oxygen at low temperatures, *i.e.* below 425 K, has been extensively studied, because low temperature oxidation changes the physical and chemical properties [25]. The self-ignition temperature of coal depends on the number of carboxylic acid moieties, undergoing endothermic thermolysis, and the number of highly substituted aromatic rings which undergo an exothermic oxidation. Moreover, low temperature oxidation increases the hetero atom content of the coal, resulting in a greater number of sites available for chemical reaction and catalyst binding. Gethner used *in-situ* FT-IR spectroscopy to analyze the low temperature oxidation of coal [25]. Pre-treatment at 375 K under vacuum or a flowing helium atmosphere resulted in a decreasing intensity of the bands in the carbonyl region. Decomposition of carboxylic acid moieties was observed between room temperature and 375 K:

$$\text{Coal-COOH} \rightarrow \text{Coal} + CO_2 + CO + H_2O \qquad (1)$$
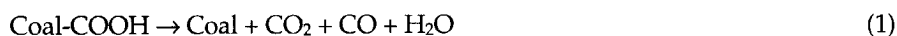
After this pre-treatment oxygen was introduced into the vacuum chamber, resulting in increasing bands at 1670, 1600, 1090 and 1020 cm^{-1}, due to the formation of various oxygenated species (compare figure 3b). These species were formed by reaction of oxygen with unsaturated hydrocarbons.

The oxidation of carbon black by various oxygen containing gasification agents (O_2, O_3, NO_2, SO_2) at ambient temperatures, has been extensively studied by Smith and co-workers [37-42]. Various oxygen, nitrogen and even sulfur containing functionalities can be formed on the soot surface. From the oxidation studies the authors derive a detailed three-dimensional model for the composition of soot. It is thought to consist of layered aromatic sheets, which contain several oxygen containing functionalities on the edges. These functionalities are quite similar to those proposed for different coal ranks, and the IR spectra of oxidized soots are in reasonable agreement with those observed in the analyses of the oxidation of coal.

1.6. *Pyrolysis of coal at elevated temperatures*

By using a DRIFT accessory and a sensitive MCT detector (Mercury, Cadmium, Tellurium), Meldrum and Rochester obtained spectra of undiluted coal samples [26]. Pyrolysis (or carbonization) of the coal samples initially resulted in the loss of aliphatic hydrocarbons (at about 775 K), followed by the loss of aromatic species at about 875 K. Simultaneously, a reduction of the intensity of the IR-bands assigned to C=O and C-O functionalities occurred, accompanied by the formation of carbon dioxide and carbon monoxide. After complete pyrolysis (established at 1075 K) spectral features were no longer present. Pyrolysis enhanced the resistance of the carbon surface towards oxidation. This was shown for tar pitch which had been carbonized at 975 K. Up to 775 K the formation of oxygen containing species was not observed. This can be explained

by the enhancement of the size and stability of polyaromatic components in the carbon structure upon pyrolysis.

A pyrolysis study of coal performed by Ibarra and Moliner [27] revealed the evolution of CO_2, CO, CH_4 (and other hydrocarbons), COS, and H_2S. Obviously, the amounts of H_2S and COS are large for sulfur containing coal-samples. The evolution temperature of CO_2 depends on the nature of oxygen containing species in the coal. Low rank coals (especially peat) contain more oxygen and therefore more CO_2 is evolved. The tars, which are the products of pyrolysis, were analyzed with FT-IR, using a transmittance cell and KBr pellets. The analysis revealed that oxygen containing species like C=O (1700 cm^{-1}, broad band) and C-O (1035 cm^{-1}) were still present in the resulting tars.

An *in-situ* FT-IR study of the pyrolysis of coal was also performed by Vassallo [28]. For resinites aliphatic carbon features were lost and structural changes in the carboxylic region occurred. Vitrinite showed increasing absorptions in the aromatic region. The authors discovered that CO_2 was evolved at temperatures as low as 425 K, explained by potassium catalyzed decomposition of carboxylic acids (KBr pellets were used to obtain the IR spectra). Appreciable changes in the IR spectra of inertinite were not detected below 575 K.

Diffuse Reflectance Near IR spectroscopy (wavenumbers 4000-6000 cm^{-1}) was applied by Ito [29] and co-workers to study the pyrolysis of coal. An increase in the electron transition band at 6000 cm^{-1} together with decreasing aliphatic C-H bands was observed. The aliphatic hydrocarbons were totally evaporated at 725 K. At 875 K the aromatic hydrocarbons were vaporized, yielding an increasing intensity of the electron transition band. This is an indication that evaporation of aliphatic and aromatic hydrocarbons is accompanied by the formation of condensed polyaromatic structures.

1.7. *Oxidation of carbonaceous materials at elevated temperatures*

An extensive study of the oxidation of different coal samples was performed by Meldrum and Rochester [26,30-33]. A DTGS detector appeared to be too insensitive to obtain useful spectra of the oxidation of undiluted carbonaceous materials [30]. Therefore KBr was used as a diluting agent. Although a catalytic effect of KBr was not observed, the ionic salt was involved in interactions with surface oxygenates. Probably phenolate-type structures, described by others as intermediates in the potassium carbonate catalyzed coal gasification [34], were formed. Cyclic acid anhydride structures could be identified at moderate temperatures: destruction occurred at slightly higher temperatures, resulting in epoxides, heterocyclic rings containing C-O-C-O-C groupings, C-O-K$^+$ groups and probably peroxy-groups [30].

Meldrum and Rochester also performed an *in-situ* DRIFT spectroscopic analysis of the oxidation of coal by oxygen and CO_2 [32]. The spectra of untreated carbon samples showed bands due to C=O, C-O-C, and aromatic C-H species. Cyclic anhydride, C=O groups associated with poly-nuclear aromatic groups and C-O bonds were formed

upon oxidation. Oxidation of coal in an aqueous peroxide solution yielded oxygenated species similar to those formed by gas-phase oxidation at elevated temperatures.

DRIFT was also utilized by Fuller [23] to identify the processes occurring upon high temperature air oxidation of coal. Temperature, pressure, reactant concentration and other factors appeared to affect the oxidation rate. The DRIFT analyses revealed that aliphatic hydrocarbons are more labile than aromatic compounds. Incorporation of oxygen in the carbon structure starts by aldehyde and ketone formation, followed by transformation in acidic structures, and finally proceeding to the formation of acid anhydride and carbonate functionalities. Inherent oxygenated species have a major influence on the oxidative behavior. Also hydroxyl-groups might contribute to the oxidation characteristics [23].

Fanning [35] also analyzed the formation of surface groups on carbon black (Black Pearls 2000, Cabot). A hydrogen pre-treatment decreased the oxidation rate of the investigated carbonaceous material. The nature of the functional groups on carbon surfaces and their corresponding IR assignments is extensively discussed. The assignments correspond quite well to those given in table I and figure 3b.

Raman spectroscopy was applied by van Doorn *et al.* [36] to investigate the (high temperature) oxidation of coal. Two absorption frequencies were observed at 1580 cm^{-1} and 1350 cm^{-1}. The first band (G-band) is assigned to graphitic carbon, whereas the latter (D-band) is due to defects in the structural order. Carbonaceous materials which have an ordered structure were found to have a lower reactivity towards oxygen, which is in agreement with the results of Meldrum and Rochester [26].

Wicke [43] investigated the non catalyzed oxidation of soot within a temperature range of 523 to 873 K by using oxygen atoms. These atoms were created by striking a microwave discharge on an argon-oxygen mixture at the inlet of the reactor. The mixture was analyzed by chemiluminescence and mass spectrometry. The results pointed out that production of CO, CO_2 and oxygen recombination processes on the soot surface took place. Also extensive oxygen adsorption on the surface was observed. The formation of CO and CO_2 appeared to be first order in oxygen atom number density. The authors do not give any mechanistic details [43].

Tomita and coworkers [44] studied the oxidation of a phenol-formaldehyde char by DRIFT spectroscopy. Dilution by KBr was not applied. Absorptions occurred at 1735, 1600 and 1250 cm^{-1}, which were assigned to lactone, carbonyl/quinone, and ether like species. The determination of the intensity of the frequencies was combined with temperature programmed desorption experiments. A decreasing intensity of the 1735 cm^{-1} band primarily resulted in the formation of CO_2 at approximately 775 K, whereas decreasing intensities of the 1600 and 1250 cm^{-1} bands predominantly yielded CO at higher temperatures (up to 1075 K). Apparently, lactones decompose at lower temperatures than quinones and ether-like species.

1.8. *Catalytic oxidation of soot and carbonaceous materials*

IR analyses have hardly been used for the elucidation of fundamental chemical reactions in the catalytic oxidation of soot and carbonaceous materials. Only the alkali metal catalyzed carbon gasification (potassium carbonate) has been analyzed by Cerfontain using IR spectroscopy [34]. Absorptions at 1100-1150 cm^{-1} have been assigned to phenoxide functionalities, which were formed by an electron transfer from the aromatic carbon structure to the alkali metal ion. However, the band position does not correspond with model compounds such as potassium phenoxide. A better assignment of the 1100 cm^{-1} band will be extensively discussed in chapter 5 of this thesis. IR spectra of the potassium carbonate catalyzed carbon gasification were also presented by Mims [45], Freriks [46], and Yuh [47]. Mims used chemical methods to identify potassium containing species on the surface of carbonaceous materials by NMR (Nucleair Magnetic Resonance). The use of a methanation reaction resulted in a proposal for the catalytically active potassium complex, based on potassium phenoxide (*i.e.* phenolate). Similar structures have been proposed by Freriks and Yuh.

The interaction of alkali metals with surface oxygen complexes was reviewed by Zawadski [12]. Various IR spectra of oxidized carbon films are presented. Ion exchange of acid functionalities with Na$^+$ and K$^+$ causes a decreasing 1720 cm^{-1} band, (C=O vibrations in carboxylic acids (figure 3b)), a rising absorption intensity at 1590 cm^{-1} (asymmetric COO$^-$ vibrations) and the formation of a 1380 cm^{-1} band (symmetric COO$^-$ vibrations). By treatment of the samples with HCl, the original acidic structures are reformed (the 1380 cm^{-1} band disappears and the 1590 cm^{-1} band decreases). The studies described by Zawadski [12] were performed to elucidate the acidity of the carboxylic acid functionalities, and not focused on catalytic phenomena.

An *in-situ* DRIFT spectroscopic study on the catalytic oxidation of diesel soot has been performed by Setzer [48]. Catalysts were mixed with soot in a ratio of 1:1 and mixed 1:4 with KBr afterwards. Copper metavanadate appeared to be a good catalyst for the catalytic oxidation of soot. Several bands appeared and disappeared in the 900-1000 cm^{-1} spectral region, due to modifications of the catalyst structure. The changes in band intensities were ascribed to the reduction of copper species. However, it will be shown in chapter 2 of this thesis that reactions between KBr and copper metavanadate are likely to affect the spectral changes.

1.9. *Conclusions*

- The application of dispersive IR spectrometers in the 1950s and 1960s, led to a first description of the nature of oxygenates and hydrocarbons present on the surface of coal particles.
- The introduction of FT-IR instruments and the application of advanced calculation techniques (Second Derivative, Fourier Self Deconvolution), resulted in a more detailed description of the structure of coal and related carbonaceous materials. In this way, C-H vibrations of poly- and monoaromatic species have been resolved.

- Also DRIFT spectroscopy appeared to be a useful technique for the recording of high quality spectra of carbonaceous materials. Pellet-pressing can be avoided and in some cases dilution of the samples with KBr is not necessary.
- Chemical methods can be applied to modify oxygen containing functionalities, in order to enable a better assignment of the IR bands observed in the spectra of carbonaceous materials. Acetylation has been used successfully to identify different kinds of hydroxylic groups.
- The IR absorption frequencies observed in the IR spectra of coal, soot, chars and carbon blacks, are very similar. Apparently, the nature of hydrogenated and oxygenated species is relatively independent of the carbonaceous material.
- Several reaction steps have been proposed for the non-catalytic oxidation and pyrolysis of carbonaceous materials at elevated temperatures. Evaporation and cracking of aliphatic and aromatic hydrocarbons occurs simultaneously, resulting in the loss of spectral features and the formation of polycyclic aromatic compounds.
- It is generally agreed that the ordering of the carbon structure, which is related to the amount of condensed polycyclic aromatic hydrocarbons, affects the oxidation resistance. The higher the aromaticity of the carbon, the less the number of sites available for oxidative attack. An initial amount of surface hydroxyls and carbonyl-groups, appears to enhance the oxidation rate.
- IR analysis of catalytic gasification/oxidation of carbon is limited to alkali metal catalyzed carbon oxidation. Although the observed spectral features have been assigned to phenoxide functionalities, the exact nature of the formed potassium species is still unknown.

1.10. *References*

[1] D.W. v.Krevelen, 'Coal, typology-physics-chemistry-constitution', Elsevier, Amsterdam, 1993.
[2] P.J.J. Tromp, 'Coal pyrolysis-basic phenomena relevant to conversion processes.', Ph.D. Thesis University of Amsterdam (1987).
[3] T. Wigmans, 'Catalytic gasification of carbon; a mechanistic study', Ph.D. Thesis University of Amsterdam (1982).
[4] M.B. Cerfontain, 'Alkali catalyzed carbon gasification', Ph.D. Thesis University of Amsterdam (1987).
[5] R. Meijer, 'Kinetics and mechanism of the alkali-catalyzed gasification of carbon', Ph.D. Thesis University of Amsterdam (1992).
[6] O.S.L. Bruinsma, 'Coal combustion; pyrolysis & oxidation of hydrocarbons & chars', Ph.D. Thesis University of Amsterdam (1988).
[7] M.W. Haenel, Fuel, 71 (1992) 1211.
[8] J.G. Speight, Analytical methodes for coal and coal products, vol II, (1978).
[9] M.L. Studebaker and E.W.D. Huffman, Ind.Eng.Chem. 48 (1956) 162.
[10] P.T. Williams, K.D. Bartle and G.E. Andrews, Fuel, 65 (1986) 1150.
[11] P.C. Painter, R.W. Snyder and M. Starcinic, Appl. Spectrosc., 35 (1981) 475.
[12] J. Zawadski, Chem. Phys. Carbon, 21 (1989) 147.

[13] C. Morterra and M.J.D. Low, Spectrosc. Lett., 15(9) (1982) 689.
[14] G. Mul, J.P.A. Neeft, F. Kapteijn and J.A. Moulijn, Fuel, in preparation.
[15] R.T. Conley, Infrared Spectroscopy, Allyn and Bacon, Boston, 1972.
[16] O. Ito, S. Akiho, T. Nozawa, M. Hatano and M. Iino, Fuel, 68 (1989) 335.
[17] D. Cagniant, R. Gruber, C. Lacordaire, A.P. Legrand, D. Sderi, H. Sfihi, P. Tougne, M.F. Quinton, G. Bunte, S. Jasienko and H. Machinkowska, Fuel, 70 (1991) 675.
[18] J.K. Kauppinen and D.J. Moffatt, Appl. Spectrosc., 35 (1981) 271.
[19] E.L. Fuller and N.R. Smyrl, Appl. Spectrosc., 44 (1990) 451.
[20] S.H. Wang and P.R. Griffiths, Fuel, 64 (1985) 229.
[21] H.P. Boehm, Carbon, 32 (1994) 759.
[22] N.R. Smyrl and E.L. Fuller, Appl. Spectrosc., 41 (1987) 1023.
[23] E.L. Fuller and N.R. Smyrl, Fuel, 64 (1985) 1143.
[24] E. Haley, Proc. 19th Biennial Conf. on carbon, State College, USA, (1989) 556.
[25] J.S. Gethner, Appl. Spectrosc., 41 (1987) 50.
[26] B.J. Meldrum and C.H. Rochester, Fuel, 70 (1991) 57.
[27] J.V. Ibarra and R. Moliner, J. Anal. Appl. Pyrolysis, 20 (1991) 171.
[28] A.M. Vassallo, Y.L. Liu, L.S.K. Pang and M.A. Wilson, Fuel, 70 (1991) 635.
[29] O. Ito, H. Seki and M. Lino, Fuel, 67 (1988) 573.
[30] B.J. Meldrum and C.H. Rochester, J.Chem.Soc.Faraday Trans. 86 (1990) 2997.
[31] B.J. Meldrum and H. Rochester, J.Chem.Soc.Faraday Trans. 86 (1990) 1881.
[32] C.H. Rochester and B.J. Meldrum, J.Chem.Soc.Faraday Trans. 86 (1990) 861.
[33] B.J. Meldrum, J.C. Orr and C.H. Rochester, J. Chem. Soc. Chem. Comm. (1985) 1176.
[34] M.B. Cerfontain and J.A. Moulijn, Fuel, 62 (1983) 256.
[35] P.E. Fanning and M.A. Vannice, Carbon, 31 (1993) 721.
[36] J. van Doorn, M.A. Vuurman and J.A. Moulijn, Proc. 19th Biennial Conf. on Carbon, State College, USA, (1989) 558.
[37] D.M. Smith, J.R. Keifer, M. Novicky and A.R. Chughtai, Appl.Spectrosc. 43 (1983) 103.
[38] D.M. Smith, W.F. Welch, S.M. Graham, A.R. Chughtai, B. Wicke and K.A. Grady, Appl.Spectrosc. 42 (1988) 674.
[39] C.A. Sergides, J.A. Jassim, A.R. Chughtai and D.M. Smith, Appl.Spectrosc. 41 (1987) 482.
[40] J.A. Jassim, H.P. Lu, A.R. Chughtai and D.M. Smith, Appl.Spectrosc. 40 (1986) 113.
[41] M.S. Akhter, A.R. Chughtai and D.M. Smith, Appl.Spectrosc. 45 (1991) 653.
[42] A.R. Chughtai, W.F. Welch and D.M. Smith, Carbon, 28 (1990) 411.
[43] B.G. Wicke and K.A. Grady, Proc. 19th Biennial Conf. on Carbon, State College, USA, (1989) 562.
[44] Q.-L. Zhuang, T. Kyotani and A. Tomita, Energy & Fuels, (1994) 714.
[45] C.A. Mims and K.D. Rose, J.Am.Chem.Soc. 104 (1982) 6886.
[46] I.L.C. Freriks, H.M.H. Wechum, J.C.M. Stuiver and R. Bouwman, Fuel, 60 (1981) 463.
[47] J.Y. Yuh and E.E. Wolf, Fuel, 62 (1981) 252.
[48] C. Setzer, W. Scheutz and F. Schüth, in Proc. 10th International Congress on Catalysis, Budapest, 1992, P.309.

2

Development of experimental procedures for the *in-situ* DRIFT analysis of metal oxide/soot mixtures

Abstract

In general, DRIFT spectroscopy is a powerful technique for the *in-situ* recording of IR spectra of powdered samples at elevated temperatures. Unfortunately, carbonaceous materials are strong absorbers of IR radiation. To increase the quality of IR spectra, usually KBr is used as a diluent. However, several metal oxides, like V_2O_5 and MoO_3, are shown to react with KBr. Changes occurring in the V_2O_5 spectrum can be explained by the formation of potassium vanadium oxides. Reaction of KBr with MoO_3 is shown to yield several potassium molybdates. Furthermore, the *in-situ* DRIFT analysis of metal chlorides in KBr is affected by the formation of eutectics. This results in melting and/or oxidation below the temperatures characteristic for the pure metal chlorides. Additionally, oxygenated species on the soot surface might react with KBr, yielding potassium benzoate type complexes. If the *in-situ* DRIFT analysis of the interactions between soot, oxygen and transition metal oxides is aimed for, the use of KBr as a diluent is not recommended. Si powder can be used as an alternative, although it has a higher overall extinction coefficient than KBr. Another alternative is to use Fullerene C60 as a soot model compound, which, upon oxidation, is shown to yield surface oxygen complexes quite similar to those observed in the spectra of oxidized soot.

2.1. *Introduction*

Several IR recording techniques can be used to obtain IR spectra of (oxidized) carbonaceous materials: conventional recording in transmittance mode (the sample is diluted with KBr and pressed into an infrared transparent pellet), Photo Acoustic Spectroscopy (PAS), and Diffuse Reflectance Infrared Fourier Transformed (DRIFT) spectroscopy have been applied. Although useful spectra have been obtained by the conventional method, sample preparation is time consuming and 'flow-through' conditions are not achieved. PAS can only be used to record spectra at room temperature, and requires a He flow in the vicinity of the sample. Moreover, this technique can not be applied for *in-situ* studies at elevated temperatures. The DRIFT technique has been used extensively to study the non-catalytic oxidation of carbonaceous materials with CO_2, H_2O or O_2. However, *in-situ* recording of DRIFT spectra of carbonaceous materials at elevated temperatures usually yields poor quality spectra, because carbon has a high overall extinction coefficient: little radiation is available for detection.

In this chapter several aspects of *in-situ* DRIFT analyses of mixtures of soot with catalysts will be discussed. A description of the spectrometer, the DRIFT accessory and the principles of the DRIFT technique will be given. Experimental procedures for the acquirement of high quality spectra, and drawbacks of the use of KBr as a diluting agent will be dealt with. The latter is focused on the interaction of V_2O_5, CuCl and oxidized soot with KBr. The use of an alternative diluent (Si powder) and fullerene C-60 as a soot model compound will be evaluated. Finally, examples will be given of the *in-situ* analyses of the reduction of metal oxides.

2.2. *The Nicolet Magna 550 spectrometer*

The FT-IR spectra published in this thesis were recorded on a Nicolet Magna 550 FT-IR spectrometer. It contains an air cooled Ever Glow IR source, an interferometer to modulate the IR radiation (to make it detectable), and a DTGS (Deuterated Tri Glycine Sulfate) detector. The apparatus has the option to use a second, MCT (Mercury Cadmium Telluride) detector, which is nitrogen cooled. The latter has a higher sensitivity, but a less linear response. A laser (a monochromatic source) is incorporated in the apparatus as a reference for the other frequencies (the reproducibility of the wavenumber is 0.01 cm^{-1}). The alignment of the spectrometer can be automatically adjusted, needed for a consistent performance. The spectrometer is controlled by the OMNIC™ 2.1. software, which is compatible with Word™ and other programs using Windows™. The theories behind FT-IR spectroscopy and mathematical options incorporated in the software, are dealt with in Appendix I of this thesis.

2.3. *The Spectratech DRIFT accessory*

DRIFT (Diffuse Reflectance Infrared Fourier Transform) spectroscopy is a sampling technique used for IR measurements on solid powdered samples. Time consuming pressing of KBr or self supporting wafers is not necessary.
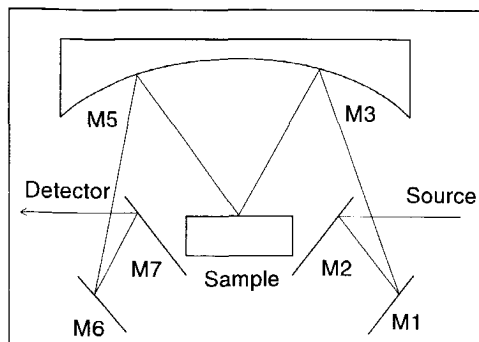
Figure 1. *The optics of the Spectratech DRIFT accessory.*

Figure 2. *Possible modes of interaction between IR radiation and a sample in the DRIFT accessory.*

Moreover, environmental chamber accessories are available, that enable measurements of powdered samples at elevated temperatures.
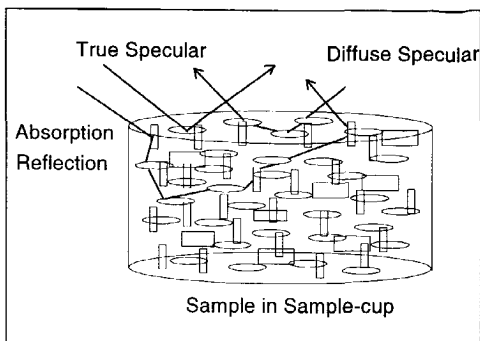
The spectra published in this thesis were collected using a Spectratech Collector diffuse reflectance accessory, equipped with a compatible environmental cell. The optics of the accessory are shown in figure 1 [1]. Two flat mirrors are used to pass the focused beam to spherical mirror M3. The mirror refocuses the beam onto the sample. After interaction with the sample the different components of radiation are collected by spherical mirror M5 and subsequently sent to the detector by mirrors M6 and M7.

The incoming beam interacts with the sample yielding three types of reflected radiation (figure 2). True specular radiation is directly reflected from the surface, without any penetration into the sample. Diffuse specular radiation penetrates into the sample, but does not interact with the particles: it is reflected radiation, which does not contain any spectral information. Only rays that penetrate the particles contribute to the spectrum and contain information about the structure and chemical composition of the sample. When strongly reflecting substances are analyzed, the spectra usually contain large contributions of specular and diffuse specular reflections, causing negative absorption bands. To reduce the contribution of specular reflection a 'blocker' can be placed on the surface of the sample. Furthermore, a mathematical transformation, called the Kramers-Kronig (K-K) transformation, can be used to correct these spectra. The OMNIC™ 2.1 software contains the formulae to perform the K-K transformation.

As the Magna 550 spectrometer is a single beam apparatus, DRIFT spectra are recorded against a background spectrum. Usually, an IR transparent salt, such as KBr,

is used to record the background. Analogous to the transmittance T, the fractional reflectance R is defined as in equation (1).

$$R = \frac{reflectance\ sample}{reflectance\ KBr} * 100 \tag{1}$$

The concentration of the sample is related to the so-called absorption reflectance A_r (equation (2)):

$$A_r = k * c \tag{2}$$

k is a constant, which is dependent on the intrinsic properties of the sample, and c represents the concentration. Two expressions can be used to obtain a linear relation between the concentration of a sample and the fractional reflectance R :

$$A_r = \log\left(\frac{1}{R}\right) \tag{3}$$

$$A_r = \frac{(1-R)^2}{2*R} \tag{4}$$
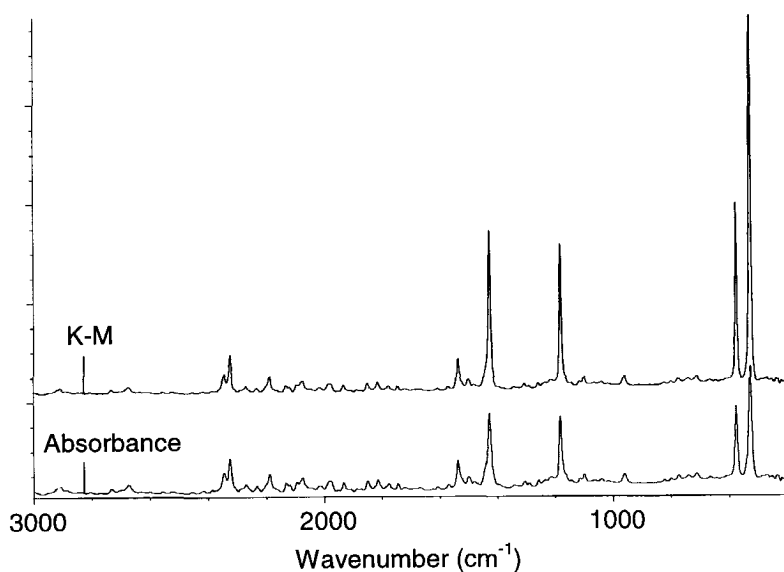
Figure 3. *The IR spectrum of undiluted Fullerene C60 in the K-M and absorbance reflectance format (256 scans, 8 cm^{-1} resolution).*

Equation (3) yields a linear relation between the concentration (represented by A_r) and the fractional reflectance in the near infrared region when the sample is highly absorbing. Equation (4), known as the Kubelka-Munk (K-M) equation, is a corrected expression that was derived under the condition of infinite dilution in a non-absorbing

matrix. If a quantitative analysis is aimed for, expressions (3) and (4) should be evaluated. The expression which gives the most linear response between the fractional reflectance and the sample concentration can then be properly selected. Figure 3 shows the effect of the K-M calculation: strong bands are relatively more amplified than weak bands. The assignment of the IR vibrations occurring in the fullerene C60 spectra will be further discussed in paragraph 2.7.

2.4. *Experimental*

The *in-situ* DRIFT spectra presented in the next 3 paragraphs, were recorded on a Nicolet Magna 550 spectrometer, equipped with a Spectratech DRIFT accessory and environmental cell. The spectra were obtained by collection of 256 scans at 8 cm^{-1} resolution and are displayed in absorption reflectance units, unless otherwise stated. An overview of the samples is given in Table I. Si-powder (-325 mesh, 99%) and KBr (FT-IR grade) were used as received from Aldrich.

**Table 1.** *Various experimental data of the mixtures investigated by in-situ DRIFT spectroscopy.*

SAMPLE	TEMP. RANGE	GAS PHASE
KBr/V$_2$O$_5$	570-690 K	Air
KBr/V$_2$O$_5$/soot	Prepared @ 775K [8]	N$_2$
V$_2$O$_5$/C60	640 K (60 minutes)	N$_2$
KBr/MoO$_3$	575-775 K	Air
KBr/CuCl	400-550 K	Air
KBr/Soot-SOC	530-680 K	N$_2$
KBr/CuO	375-725 K	10% H$_2$ in N$_2$
KBr/Red. Co$_3$O$_4$	375-725 K	Air
Si-powder/V$_2$O$_5$	550-800 K	Air
KBr/Coronene/Co$_3$O$_4$	675-775 K	Air
C60	@ 575 K	Air

K$_2$O.4V$_2$O$_5$ and K$_2$O.V$_2$O$_5$ were prepared by solid state reaction of stoichiometric amounts of K$_2$CO$_3$ (Baker *p.a.*) and V$_2$O$_5$ (Aldrich) at 775 K in static air for 12 hours [5]. K$_2$Mo$_3$O$_{10}$ was prepared by solid state reaction of MoO$_3$ with K$_2$CO$_3$ for 16 hours at 800 K in static air. MoO$_3$ and CuO were used as received from Merck (*p.a.*) and Co$_3$O$_4$ was prepared by decomposition of Co(NO$_3$)$_2$ at 675 K [8]. Ozonized soot (Printex-U, kindly provided by Degussa) was prepared by reaction at 375 K in 10% O$_3$ in O$_2$ for 60 minutes. Coronene (sublimed) was used as received from Aldrich.

Sublimed fullerene C60 (>99%) was used as received from Bucky-USA. The FT-Raman spectrum of C60 was recorded on a Perkin-Elmer 1760 X FT-Raman spectrometer by co-addition of 64 scans at 2 cm^{-1} resolution and 50 mW laser power.

2.5. *Interactions of KBr with catalyst/soot mixtures*

Carbonaceous materials are strong absorbers of IR radiation, thus causing a low signal to noise ratio. To obtain spectra of a better quality, dilution of the samples with KBr (1 wt% sample) is usually applied. Metal oxides, which generally have spectral features in the far IR region (1000-100 cm^{-1}), might react with KBr. This is clearly demonstrated by an *in-situ* analysis (in 20% oxygen in nitrogen) of V_2O_5 (figure 4) at elevated temperatures.
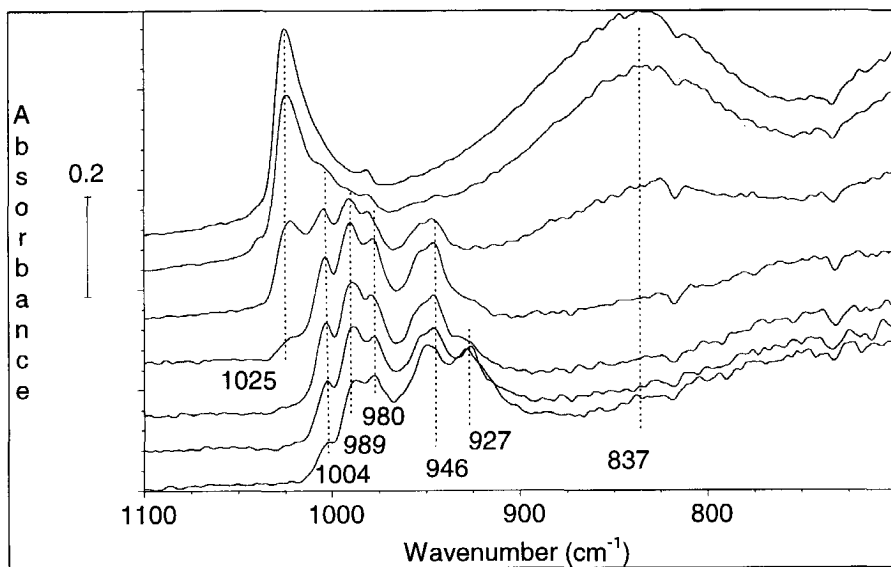
Figure 4. *In-situ DRIFT analysis of the reaction of V_2O_5 with KBr. The spectra (256 scans, 8 cm^{-1} resolution) were collected at 570, 590, 610, 630, 650, 670, and 690 K, respectively (Top to bottom).*

The DRIFT spectrum of V_2O_5 consists of two major bands in the 600-1200 cm^{-1} region, located at 1025 cm^{-1} and centered around 837 cm^{-1} [2-4]. The spectra in figure 4 clearly show a diminishing 1025 cm^{-1} band, accompanied by increasing absorptions at 1004, 989 and 980 cm^{-1}. At even higher temperatures the bands at 1004 and 989 cm^{-1} are replaced by bands at 946 and 927 cm^{-1}. The spectral changes can be explained by the reduction of V_2O_5, which is induced by KBr [4] :

$$V_2O_5 + 2\,KBr \rightarrow V_2O_4 + K_2O + Br_2 \Uparrow \qquad\qquad (5)$$

Reaction (5) is likely to be accompanied by a solid-state reaction of V_2O_4 and V_2O_5 with the formed K_2O, yielding potassium vanadates (*e.g.* $K_2O.4V_2O_5$ or $K_2O.V_2O_5$) or so-called potassium bronzes, such as $K_{0.23}V_2O_5$ [2].
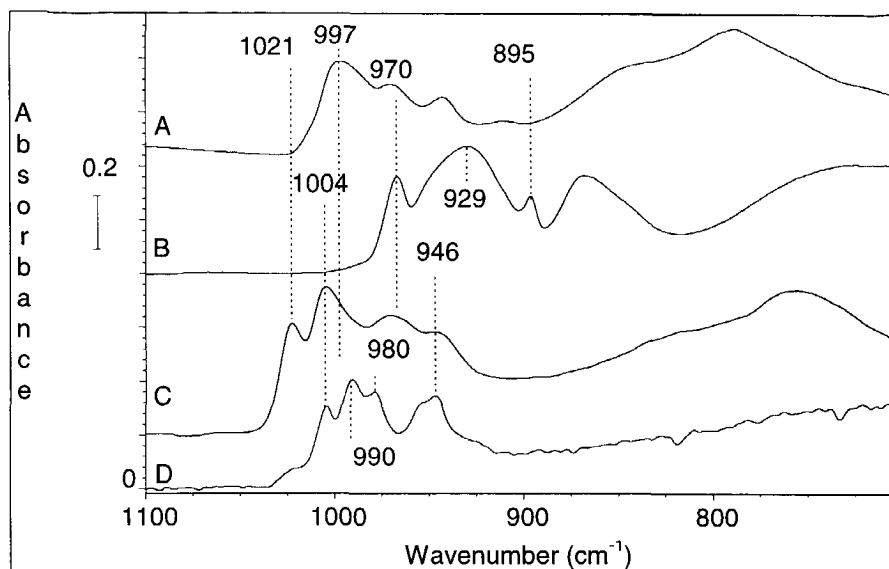
Figure 5. *DRIFT spectra (256 scans, 8 cm^{-1}) of K$_2$O.4V$_2$O$_5$ (A), K$_2$O.V$_2$O$_5$ (B), K$_{0.23}$V$_2$O$_5$ (C) and KBr/V$_2$O$_5$ at 650 K (D). The spectra of the bronze and potassium vanadates were recorded at 300 K.*

The spectrum of the KBr/V$_2$O$_5$ mixture at 650 K (D), is compared with the spectra of K$_{0.23}$V$_2$O$_5$ (C), K$_2$O.V$_2$O$_5$ (B), and K$_2$O.4V$_2$O$_5$ (A) in figure 5. Although several features are similar, the KBr/V$_2$O$_5$ spectrum does not entirely correspond to the spectrum of K$_{0.23}$V$_2$O$_5$, nor to that of the vanadates. However, the series of spectra displayed in figure 4, indicate a shift of the vanadyl vibrations to lower wavenumbers with increasing temperature, which might be explained by a progressive incorporation of K in the V$_2$O$_5$ or V$_2$O$_4$ lattice: a band at 927 cm^{-1} is developing, which might be assigned to K$_2$O.V$_2$O$_5$ (figure 5). Evaluating the experimental data, the spectral changes observed in KBr/V$_2$O$_5$ samples at elevated temperatures, might be explained by the formation potassium vanadates and potassium bronzes [2].

The spectrum of K$_2$O.V$_2$O$_5$, as shown in figure 5, corresponds quite well to the one published by Frederickson *et al.* [6]. However, IR absorption frequencies of meta-vanadate compounds determined by dilution in KBr pellets, were significantly different from the ones obtained by the so-called Nujol Mull technique [6]: interactions of K$^+$ ions with vanadate anions already occur at ambient temperatures during the preparation of the KBr pellet. To determine the effect of KBr on an *ex-situ* analysis of carbothermally reduced V$_2$O$_5$, the spectrum recorded in KBr is compared with a spectrum of V$_2$O$_5$ *in-situ* reduced by fullerene C60 (without KBr dilution).
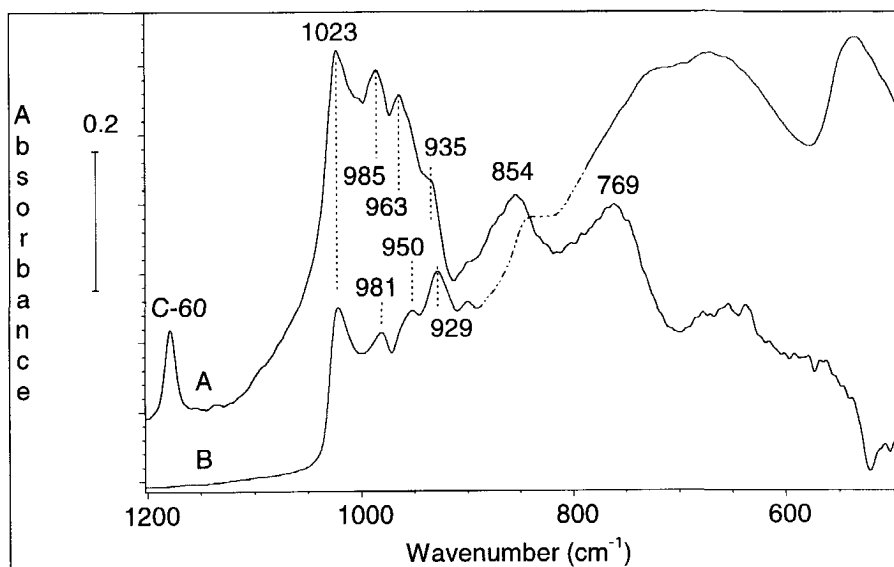
Figure 6. DRIFT spectrum in KBr (256 scans, 8 cm⁻¹) (B) of carbothermally reduced V_2O_5 (obtained by reaction with Printex-U in a thermobalance in N_2 up to 775 K) compared with the in-situ spectrum of a $V_2O_5/C60$ mixture, recorded at 640 K after 60 minutes in N_2 (A).

If differences in the reduction degree are taken into consideration, there is no need to assume that KBr dilution severely affects the spectra of reduced V_2O_5 recorded at ambient temperatures. The K^+ exchange observed by Frederickson, might be the result of the high pressures applied to press KBr pellets.

Several absorptions in the 900-1000 cm⁻¹ region have also been observed upon an *in-situ* DRIFT analysis of a copper vanadate/soot mixture in KBr [7]. The observed spectral changes were assigned to reduced copper species, and claimed to be related to the presence of soot: treatment of copper vanadate at high temperatures in KBr did not result in alterations of the spectrum. However, the spectra of several vanadium oxide based compounds, shown in figures 4, 5 and 6, also contain absorptions in the 980-1000 cm⁻¹ region: an assignment of the spectral features reported by Setzer [7] to reduced vanadium species formed by reaction with KBr, seems more appropriate than to copper species. By evaluating the experimental data given above, the *in-situ* analysis of vanadium based catalysts in KBr at elevated temperatures, is not recommended.

An *in-situ* DRIFT analysis of the reaction of MoO_3 with KBr is shown in figure 7. Changes occur in the 800-1000 cm⁻¹ region of the spectra, which can be assigned to the formation of $K_2Mo_3O_{10}$. The IR spectra of various potassium molybdates will be further discussed in chapter 3 of this thesis. It is obvious that *in-situ* DRIFT studies of molybdenum containing catalysts cannot be performed in a KBr matrix.
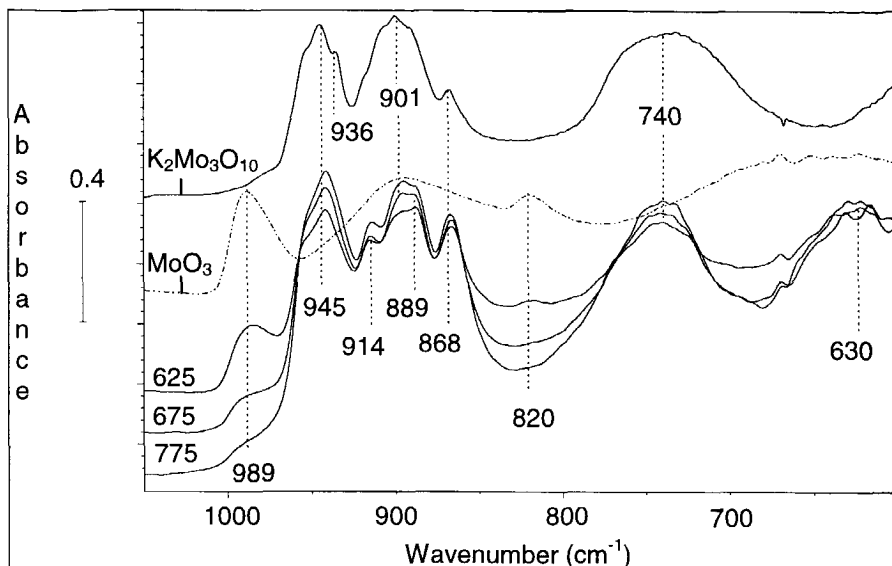
Figure 7. *In-situ DRIFT spectra (256 scans, 8 cm⁻¹ resolution) of MoO₃ in KBr recorded at 625, 675 and 775 K (top to bottom). The spectra of MoO₃ and K₂Mo₃O₁₀, recorded at 300 K in KBr, are shown for comparison.*

Besides metal oxides, metal chlorides are very active soot oxidation catalysts [8]. The *in-situ* DRIFT analyses of metal chloride/soot mixtures could reveal the formation of possible chloride and/or oxygen containing intermediates. An *in-situ* analysis of CuCl mixed with KBr in air is shown in figure 8. The transformation of bands at 901, 851 and 805 cm⁻¹, assigned to hydrated CuCl species [9], into a broad band centered around 528 cm⁻¹, is explained by dehydration and simultaneous oxidation of CuCl. The broad absorption band centered around 528 cm⁻¹ can be assigned to CuO. Cu₂O formation is not observed [2]. Oxidation starts already at 475-500 K, which is below the oxidation temperature characteristic for bulk CuCl (600 K). Apparently, the oxidation of CuCl to CuO is affected by the presence of KBr. The activity and stability of metal chlorides in the oxidation of soot will be extensively discussed in chapter 4 of this thesis.

Although KBr has often been applied for *in-situ* FT-IR analysis of the oxidation of coal, as was reviewed in chapter 1 of this thesis, interactions of potassium ions with surface oxygen complexes might interfere with spectral interpretations. Figure 9 shows an *in-situ* DRIFT analysis of the decomposition of surface oxygen complexes on soot in KBr. The oxygen functionalities were formed by the oxidation of soot in ozone (chapter 7). A decreasing intensity in the 1700-1900 cm⁻¹ region and a shift to lower wavenumbers of the absorption band around 1621 cm⁻¹ to 1590 cm⁻¹ is observed. The shift in wavenumbers is accompanied by an increasing absorption intensity.
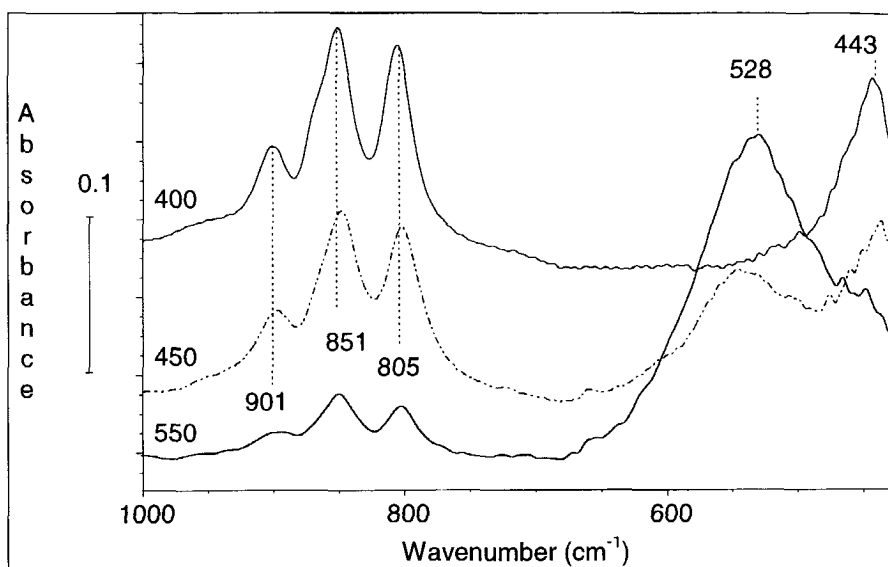
Figure 8. *In-situ DRIFT spectra (256 scans, 8 cm⁻¹ resolution) of CuCl in KBr, recorded in air at 400, 450, and 550 K (top to bottom).*
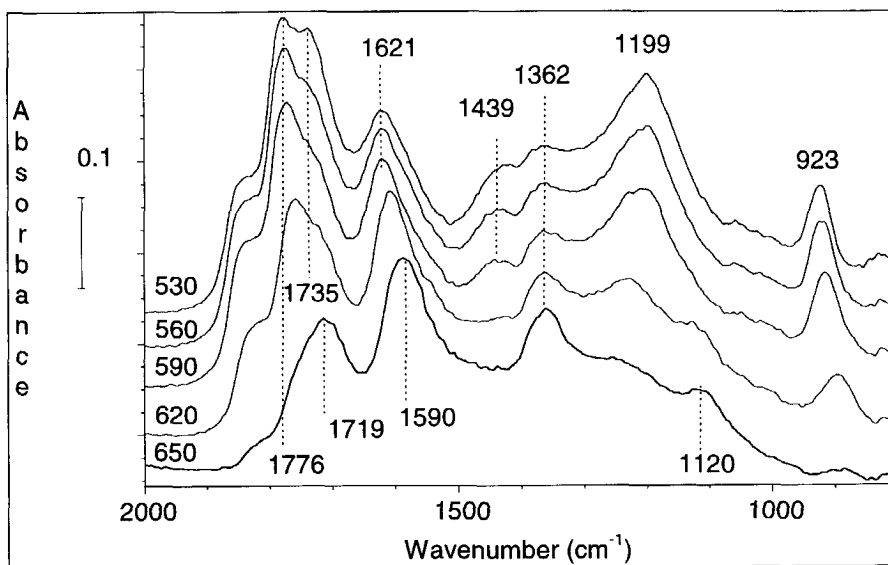
Figure 9. *In-situ DRIFT spectra (256 scans, 8 cm⁻¹ resolution) of the decomposition of surface oxygen complexes of ozonized soot in KBr. Spectra were recorded at 530, 560, 590, 620 and 650 K (top to bottom).*

Furthermore bands at 923 and centered around 1200-1250 cm⁻¹ decrease in intensity, accompanied by an increasing 1362 cm⁻¹ band. The spectral changes can be explained by the formation of potassium benzoate (causing the frequency shift of the 1600 cm⁻¹ band). The absorption pattern above 1700 cm⁻¹ can be assigned to acid, acid anhydride, and lactone functionalities. The bands at 1200-1250 cm⁻¹ are assigned to ether-like functionalities [10], and the 1362 cm⁻¹ band to a benzoate functionality [11]. Furthermore, bands at 1439 cm⁻¹ and 1120 cm⁻¹ indicate that CO_2, formed by decomposition of the functionalities, interacts with potassium species. The nature of the compounds causing the 1439 and 1120 cm⁻¹ bands, as well as the other spectral phenomena, will be extensively discussed in chapter 5 of this thesis. It is obvious that an *in-situ* DRIFT study on the interaction of transition metal oxides with carbon surface oxygen complexes, cannot be performed in a KBr matrix: interactions of the oxygen complexes with potassium anions strongly interfere with the absorptions of interest.

Some examples of successful *in-situ* DRIFT analyses performed in a KBr matrix are shown in figures 10 and 11. In figure 10 the development of the IR vibrations upon CuO reduction in H_2 is shown. The broad absorption band centered around 502 cm⁻¹, is replaced by a band at 608 cm⁻¹, which is assigned to Cu_2O [2]. Eventually, total reduction of the oxide occurs, yielding metallic Cu, which does not have any spectral features in the region presented.
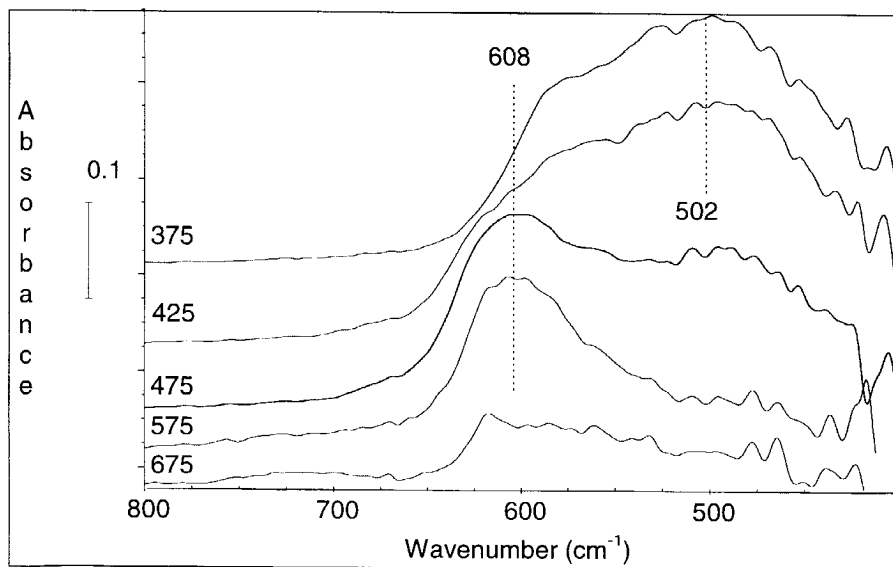
Figure 10. *In-situ DRIFT spectra of the CuO reduction in 10 % H_2 in N_2 in KBr. Spectra were recorded at 375, 425, 475, 575, and 675 K (top to bottom).*
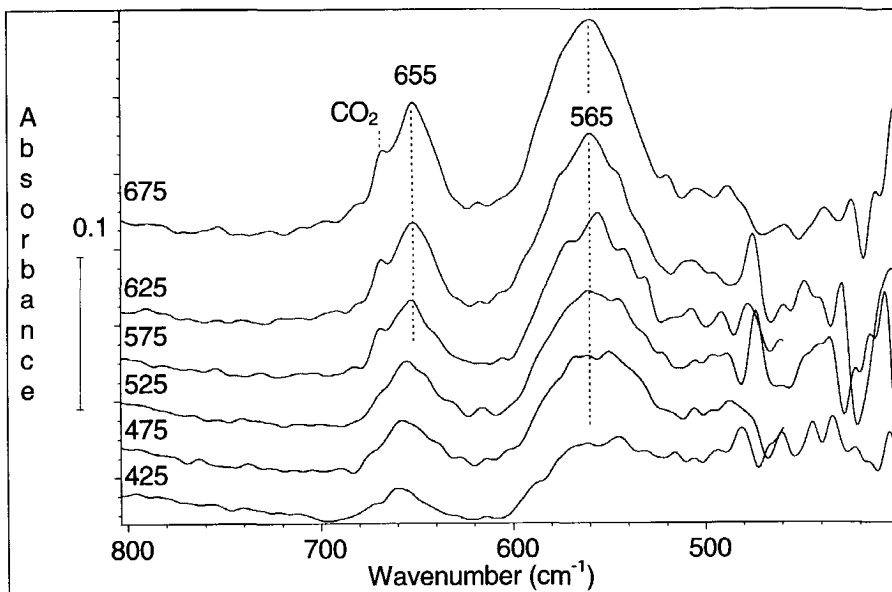
Figure 11. In-situ DRIFT spectra in a KBr matrix of the reoxidation of carbothermically reduced Co_3O_4. Spectra were recorded in a temperature range of 375-675 K, with intervals of 50 K (bottom to top).

Although soot causes a reduced signal to noise ratio in a CuO/soot spectrum, similar spectral changes have been observed in the carbothermic reduction of CuO. Interactions of KBr with CuO have not been observed: reoxidation of the reduced copper species yields the original CuO spectrum.

The *in-situ* analysis of the reoxidation of reduced Co_3O_4 in a KBr matrix is shown in figure 11. Reduced Co_3O_4 (by soot, *i.e.* carbothermically) is characterized by the spectrum recorded at 425 K. The 655 and 565 cm^{-1} absorptions can be assigned to the spinel vibrations of some remaining Co_3O_4 and are characteristic for metal oxides crystallized in the spinel conformation. The spectrum is in agreement with that published by Fattakhova [12]. The *in-situ* analysis shows an increase in the spinel vibrations upon oxidation. Eventually, the spectrum of Co_3O_4 is completely restored. Apparently KBr does not form any potassium substituted compounds with Co_3O_4. Mechanistic details of the carbothermic reduction of various metal oxides will be extensively discussed in chapters 8 and 9 of this thesis.

2.6. *The use of other diluents*

Besides KBr, many other inorganic salts, such as NaCl, CaF_2, KCl and ZnSe, can be used to increase the spectral quality of highly absorbing samples. However, NaCl and KCl also react with several metal oxides and interact with carbon surface oxygen complexes. CaF_2 becomes opaque below approximately 850 cm^{-1}: absorptions of

(transition) metal oxides occur below this frequency, and are not available for analysis if CaF_2 is applied. ZnSe is not stable at high temperatures in air and is oxidized at approximately 525-575 K. Moreover, interactions with V_2O_5 have been observed (unpublished results). The use of Si powder is another alternative. The IR spectra of a V_2O_5/soot mixture in Si-powder are shown in figure 12. The spectrum was recorded against a Si-powder background.

Although the overall extinction coefficient is rather high and a background signal of water is present in the spectra (located around 1600 cm^{-1}), the spectral features of V_2O_5 are very well resolved. The V_2O_5 vibrations remain unchanged upon catalytic soot oxidation. A negative absorption band is located at 1250 cm^{-1}. As Si-powder was used to collect the background, the negative absorption might be related to this compound: a different concentration during the background and sample collection, caused by 'dilution' with the V_2O_5/soot sample, yields a negative absorption band. Soot conversion is witnessed by the formation of gas-phase CO_2, which has strong absorptions in the 2300-2400 cm^{-1} region. Soot oxidation occurs around 700 K. Negative CO_2 absorptions are caused by different concentrations in the environment at the time of the background and sample recording.
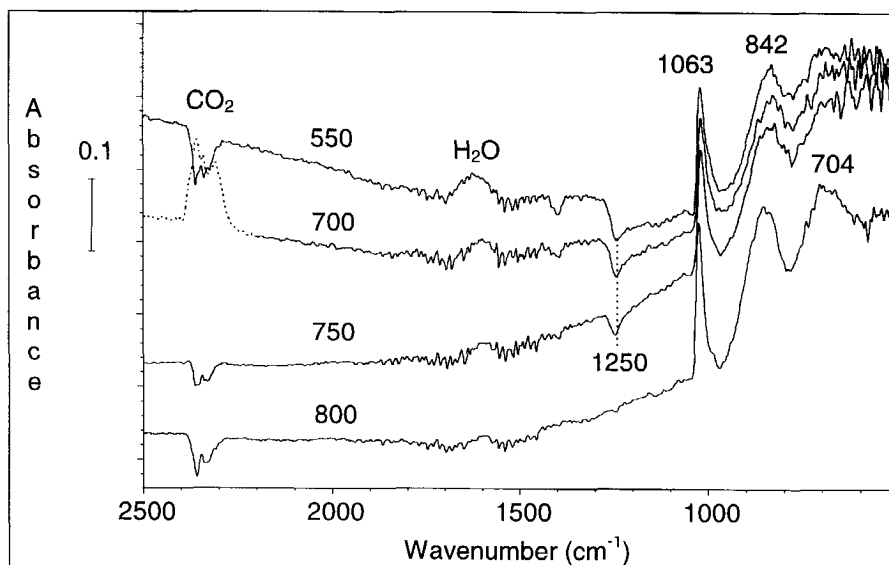
Figure 12. DRIFT spectra of a V_2O_5 soot sample in Si powder (256 scans, 8 cm^{-1} resolution). Spectra were recorded in air at 550, 700, 750, and 800 K, respectively.

After complete conversion of the soot (spectrum recorded at 800 K), the V_2O_5 bands are better resolved: a vibration at 704 cm^{-1} is clearly visible. Also the negative absorption at 1250 cm^{-1} has disappeared, which was apparently related to the presence of soot. Si-powder is shown to be a reasonable alternative for KBr: reactions between V_2O_5 and Si-powder did not occur.

2.7. *The use of soot model compounds: Coronene and Fullerene C-60*

In order to obtain a better spectral quality during *in-situ* analyses of catalytic soot oxidation, model compounds such as coronene and fullerene C60 might be applied. As an example, the Co_3O_4-catalyzed coronene oxidation is shown in figure 13. Around 725 K evaporation occurs, as is witnessed by decreasing absorptions of coronene at 554, 843, and 1314 cm^{-1}. Intermediate oxygen complexes cannot be observed, with the exception of a small absorption band at 1283 cm^{-1}, which might be assigned to an oxygen containing functionality [13].

Fullerene C60 is another suitable soot model compound in spectroscopic studies. The carbon atoms of C60 are totally sp^2 hybridized, just like in graphite. The chemical properties of this compound are extensively reviewed in references [14-17]. An FT-Raman and DRIFT spectrum of fullerene C60, recorded without KBr dilution, are shown in figure 14.
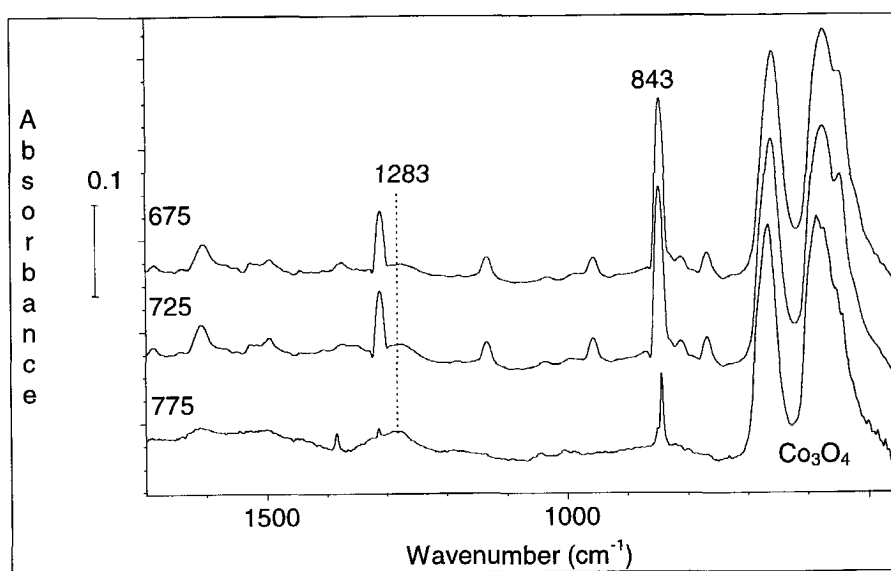
Figure 13. In-situ DRIFT spectra (256 scans, 8 cm^{-1} resolution) of the Co_3O_4 catalyzed coronene oxidation in air, recorded in KBr at 675, 725, and 775 K, respectively.

Note that the Raman and IR spectra are quite different, which indicates that several vibrations are exclusively Raman and others exclusively IR allowed. The Raman absorptions at 1463, 495, and 272 cm^{-1} have been assigned to vibrational modes of the C60 crystals [16]. The four IR active modes are located at 1427, 1181, 576 and 527 cm^{-1}. Several minor absorptions above 1700 cm^{-1} are induced by contaminations, such as polyaromatic solvents used for the purification of fullerene. Obviously, dilution with KBr is superfluous: a high quality DRIFT spectrum of fullerene C60 can be obtained without KBr dilution.
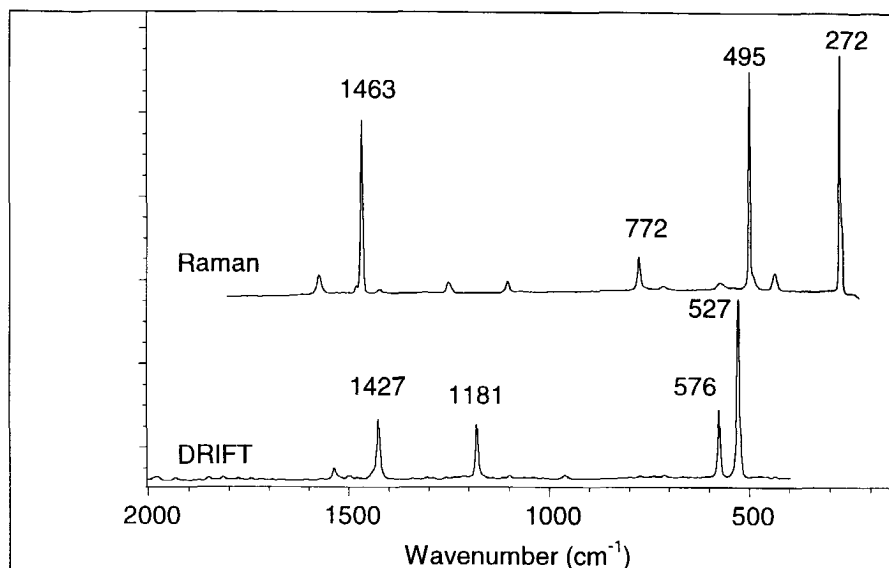
Figure 14. *DRIFT (256 scans, 8 cm⁻¹ resolution) and FT-Raman spectrum (128 scans, 2 cm⁻¹ resolution, 50 mW laser power) of Fullerene C60. The intensity of the bands in the DRIFT spectrum is increased by a twentyfold multiplication, to enable a better comparison with the Raman spectrum.*
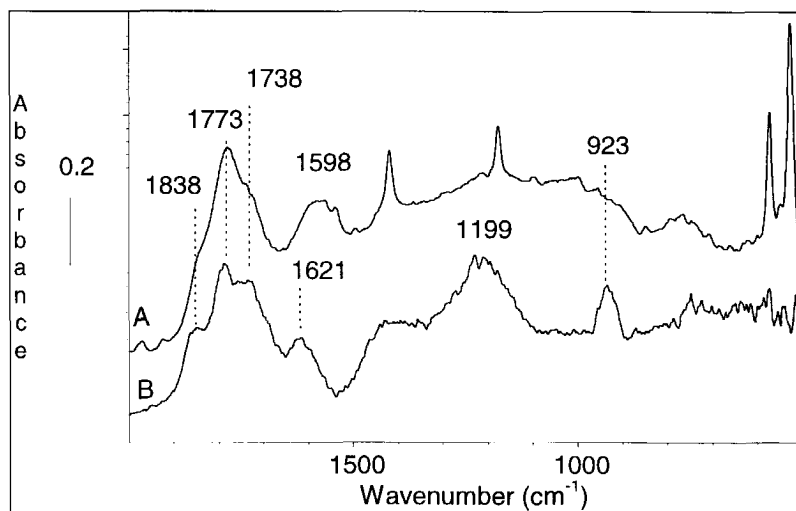
Figure 15. *DRIFT spectra (256 scans, 8 cm⁻¹ resolution) of oxidized C60 at 575 K (A) and ozonized soot at 575 K (B). Ozonized soot was prepared by reaction at 375 K in 10% O_3 in O_2 for 60 minutes.*

In inert atmospheres, fullerene C60 is quite stable up to relatively high temperatures (785-875 K) and evaporation does not occur at temperatures where catalytic oxidation takes place [18-20]. The spectrum of oxidized fullerene C60 is compared with that of ozonized soot in figure 15. The spectrum of the oxidized fullerene corresponds excellently with the spectra published by Wohlers [21,22]. Typical vibrations at 1785, 1730 and around 1050 cm^{-1} were assigned to linear anhydrides [22]. The absorption band at 1500-1630 cm^{-1} is due to carbonaceous C=C vibrations, induced by oxygenated species [23]. A small absorption band at 2126 cm^{-1} (not shown) can be assigned to CO intercalated in the fullerene molecule. The absorption at 923 cm^{-1} in the spectrum of ozonized soot is induced by dimeric acidic functionalities [10]. The spectra of oxidized fullerene C60 and ozonized soot are quite similar, especially in the 1700-1850 cm^{-1} region. The spectra will be further evaluated in chapters 5 and 7 of this thesis.

2.8. *Conclusions*

- *In-situ* FT-IR analysis of catalytic reactions involving V_2O_5 and MoO_3 cannot be performed in a KBr matrix at elevated temperatures, because solid state reactions between KBr and these metal oxides occur.
- *In-situ* analysis of a carbon/metal oxide mixture in KBr, might not reveal bands formed by the interaction of the metal oxide with soot at high temperatures, because potassium will interact with those complexes yielding benzoate functionalities. Therefore, the use of undiluted samples is recommended. *Ex-situ analysis at low temperatures is not associated with these parasitic phenomena.*
- The application of Si powder is a promising alternative for *in-situ* analyses of catalytic soot oxidation, although this material possesses a rather high extinction coefficient.
- Fullerene C-60 can be used as a model compound for *in-situ* DRIFT studies on the catalytic oxidation of soot. Fullerene C60 behaves quite similarly to soot, and has a well defined IR spectrum. As a consequence, the use of a diluting agent can be avoided.

2.9. *References*

[1] M.P. Fuller and P.R. Griffiths, Anal. Chem., 50 (1978) 1906.
[2] R.A. Nyquist and R.O. Kagel, Infrared Spectra of Inorganic Compounds, Academic Press, New York, 1971.
[3] J. Van den Berg, 'Stoichiometry and Catalytic Activity of Vanadia Based Oxides for the Oxidation of CO and H2.', Ph.D. Thesis Utrecht University (1984).
[4] M.T. Vandenborre, C. Sanchez and J. Livage, in Proc. 10th Intern. Symp. on the Reactivity of Solids, 1984, pp. 291-292.
[5] F. Holtzberg, A. Reisman, M. Berry and M. Berkenblit, J.Am.Chem.Soc. 78 (1955) 1536.
[6] L.D. Frederickson and D.M. Hausen, Anal. Chem., 35 (1963) 818.

[7] C. Setzer, W. Scheutz and F. Schüth, in Proc. 10th International Congress on Catalysis, Budapest, 1992, P.309.

[8] G. Mul, F. Kapteijn and J.A. Moulijn,. Appl. Catal. B: Env. (1996), accepted.

[9] C.F. Ng, K.S. Leung and C.K. Chan, J. Catal. 78 (1982) 51.

[10] G. Cardini, R. Bini, P.R. Salvi, V. Schettino, M.L. Klein, R.M. Strongin, L. Brard and A.B. Smith, J. Phys. Chem. 98 (1994) 9966.

[11] G. Mul, chapter 5 of this thesis.

[12] Z.T. Fattakhova, A. Ukharskii, P.A. Shiryaev and A.D. Berman, Kinet.Katal., 27 (1987) 884.

[13] Q.-L. Zhuang, T. Kyotani and A. Tomita, Energy & Fuels, (1994) 714.

[14] A.M. Vassallo, L.S.K. Pang, P.A. Cole-Clarke and M.A. Wilson, J. Am. Chem. Soc. 113 (1991) 7820.

[15] H.W. Kroto, J.E. Fischer and D.E. Cox, The Fullerenes, Pergamon Press, Oxford, 1993.

[16] P.W. Stephens, Physics and Chemistry of Fullerenes, ACS Symposium Series, 1992.

[17] R. Taylor, The Chemistry of Fullerenes, ACS Symposium Series, 1995.

[18] J.D. Saxby, S.P. Chatfield, J. Palmisano, A.M. Vassallo, M.A. Wilson and L.S.K. Pang, J. Phys. Chem. 96 (1992) 17.

[19] A. Cuesta, M. Jamond, A. Martinez-Alonso and J.M.D. Tascon, in Proc. 21st Biennial Conf. on Carbon. Santa Barbara, USA, 1993, pp. 221-222.

[20] I.M.K. Ismail and E.J. Wucherer, in Proc. 21st Biennial Conf. on Carbon, Santa Barbara, USA, 1993, pp. 223-224.

[21] M. Wohlers, A. Bauer and R. Schloegl, Microchim. Acta, submitted.

[22] M. Wohlers, H. Werner, D. Herien, T. Schedel-Niedrig, A. Bauer and R. Schlögl, Synthetic Metals, 77 (1996) 299.

[23] C. Morterra and M.J.D. Low, Spectrosc. Lett., 15 (1982) 689.

3

Soot oxidation catalyzed by a Cu/K/Mo/Cl catalyst : Evaluation of the chemistry and performance of the catalyst

Abstract

The combination of different oxidic compounds potentially present in a highly active Cu/K/Mo/Cl soot oxidation catalyst (copper-molybdates, potassium-molybdates, and a mixed copper-potassium-molybdate ($K_2Cu_2(MoO_4)_3$), a novel compound, never synthesized before) have been tested individually on their activity in soot oxidation. After intensive mixing in a ball mill, *i.e.* in 'tight contact' conditions, the oxides induce oxidation between 685 K and 720 K, whereas it non-catalytically oxidizes at 875 K. Without the ball mill procedure, *i.e.* in 'loose contact', the oxides are less active and only show a high activity above approximately 790 K. A ZrO_2 supported Cu/K/Mo/Cl catalyst shows a high 'loose contact' activity around 670 K. Hence, the 'loose contact' activity of this catalyst is not induced by the presence of an oxidic compound.

DRIFT and XRD analyses have shown that addition of KCl to $CuMoO_4$ (two compounds present within the Cu/K/Mo/Cl catalysts) followed by calcination at 950 K in air, eventually results in the formation of a mixed potassium-copper-molybdate. Simultaneously several volatile copper, potassium and chlorine containing compounds (*e.g.* K_2CuCl_4) are formed. These copper and chlorine containing compounds possess a high 'loose contact' soot oxidation activity between 600 and 690 K. A catalytic cycle, involving Cu_2OCl_2, is proposed to explain the high 'loose contact' activity of copper chlorides and supported Cu/K/Mo/Cl catalysts. The activity of the latter will be maintained as long as Cu_2OCl_2 can be restored by reaction of copper molybdates with KCl, which serves as a chlorine supplier.

3.1. *Introduction*

Recently the interest in diesel exhaust gas cleaning has increased significantly. Although diesel exhaust gas was accepted to be rather clean in comparison with otto engine exhaust, this point of view changed after the introduction of the three-way catalyst. The amount of NO_x and soot emitted by diesel engines is much larger than that emitted by otto engines equipped with catalytic converters.

Soot emission from diesel engines can be reduced in various ways [1]. Collection of soot in a filter in combination with simultaneous oxidation, seems to be the best option to minimize the contamination of the environment. However, soot oxidation takes place at temperatures of 825 - 875 K, while the temperature of diesel exhaust at high loads on the engine is typically 450 - 675 K. Therefore, a catalyst is needed to prevent accumulation of soot in the monolithic filter. Several investigators have focused their attention on the application of oxidic materials to lower the oxidation temperature of soot. Reported active soot oxidation catalysts are, among others, PbO, Co_3O_4, V_2O_5, MoO_3, and CuO [1, 2], copper vanadates [3], and perovskite type oxides [4]. Also noble metals, in combination with metal oxides have been tested as soot oxidation catalysts [5]. Ciambelli *et al.* [6, 7, 21] report a catalyst containing copper, potassium, and vanadium compounds stabilized on an Al_2O_3 support. This catalyst is prepared by impregnation of the Al_2O_3 carrier with a solution containing KCl, $CuCl_2$, and NH_4VO_3. A similar catalyst is described by Watabe *et al.* [8], based on KCl, $CuCl_2$ and $(NH_4)_6Mo_7O_{24}$ and supported on TiO_2. These two catalysts are able to lower the soot oxidation temperature from 825-875 K to 600 K, thus being active in the temperature range of interest. Moreover, they are the most active catalysts reported so far. Although Yuan *et al.* [9] give a possible explanation for the increase in activity in soot oxidation after addition of a potassium compound to a TiO_2 supported copper catalyst (*i.e.* stabilization of the support material), little is known about the nature of the active component in the Cu/K/Mo/Cl catalyst, nor about the reason why three metals (copper, potassium, and molybdenum, (or vanadium)) are needed. X-Ray Diffraction (XRD) and X-Ray Fluorescence (XRF) analyses of the Cu/K/Mo/Cl and Cu/K/V/Cl catalysts revealed that several potassium- and copper molybdates or vanadates are present in these catalytic mixtures and that the catalysts still contain considerable amounts of chlorine (predominantly present as KCl) [6, 7, 10].

This chapter describes the activity of potassium- and copper molybdates in the oxidation of soot. The activities of possible chlorine containing compounds (KCl, $MoCl_5$, $CuCl_2$, CuCl, and Cu_2OCl_2) and the activities of $CuMoO_4$/KCl, $CuMoO_4$/K_2CO_3, $CuMoO_4$/LiCl, $CuMoO_4$/CsCl, and $CuWO_4$/KCl mixtures are also reported. The results obtained are related to the chemistry taking place within the Cu/K/Mo/Cl catalyst. A possible catalytic cycle, involving the active component, is suggested. Finally the applicability of this system as a catalyst for diesel soot oxidation is evaluated.

3.2. *Experimental*

3.2.1. *Preparation*

A Cu/K/Mo/Cl catalyst supported on ZrO_2 was prepared by wet impregnation according to the procedure given by Neeft [10]. The catalyst consisted of 10.3 wt% Cu, 6 wt% K, and 8.3 wt% Mo. Starting materials for the synthesis of the individual (non-supported) molybdates were K_2CO_3 (Baker, *p.a.*), CuO, and MoO_3 (Merck, *p.a.*). Thorough mixing in an agate mortar of stoichiometric mixtures of CuO/MoO_3, and K_2CO_3/MoO_3, respectively, and calcination for 16 hours at 800 K (heating rate 10 K/min) in static air were needed to prepare the desired copper- and potassium molybdates [11, 12]. The potassium molybdates (K_2MoO_4, $K_2Mo_2O_7$, $K_2Mo_3O_{10}$, and $K_2Mo_4O_{13}$) obtained consisted of white crystalline compounds, $CuMoO_4$ had a light green color, and $Cu_3Mo_2O_9$ was light brown. $K_2Cu_2(MoO_4)_3$ was prepared by mixing stoichiometric amounts of K_2MoO_4 and $CuMoO_4$ and calcining the mixture for 12 hours at 820 K in static air. After calcination a compound with a bright green color was obtained.

The chlorides of the three metals present in the Cu/K/Mo/Cl catalyst were used as received from Merck (KCl, *p.a.*) and Aldrich (CuCl (99+%), $CuCl_2.2H_2O$ (99+%), oxychlorination catalyst (30 wt% $CuCl_2$ on alumina), and $MoCl_5$ (99.9+%)). Copper-oxy-chloride (Cu_2OCl_2) was synthesized according to a procedure described by Goreaud [13]. A brownish compound was obtained, which changed within a few days to bright green due to the adsorption of water.

The Cu/K/Mo/Cl catalyst on ZrO_2 and mixtures of KCl and $CuMoO_4$ and KCl and $CuWO_4$ were calcined in flowing air for 3 hours at 923, 723, and 923 K, respectively. During these calcination procedures a cold trap was placed in the oven in order to trap possible volatile compounds formed within the Cu/K/Mo/Cl catalyst and upon reaction between KCl and $CuMoO_4$ and $CuWO_4$, respectively. $CuWO_4$ was used to study the effect of the Cu counter ion on the formation of volatile components.

3.2.2. *Analysis*

The molybdates obtained and the compounds formed by calcination of $KCl/CuMoO_4$ and the Cu/K/Mo/Cl-ZrO_2 catalyst were analyzed by means of XRD. XRD analysis of the powdered samples was performed with Cu-$K\alpha_1$ radiation on a Guinier-Johansson camera. DRIFT (Diffuse Reflectance Infrared Fourier Transformed) spectra of the molybdates were recorded on a Nicolet Magna 550 Spectrometer, equipped with a Spectratech DRIFT accessory, after dilution with KBr to approximately 2 wt%, against a KBr background. Several KCl and copper (oxy) chloride containing samples were analyzed without dilution in KBr. A number of 128 scans and a resolution of 8 cm^{-1} were applied to record the spectra. The spectra are presented without further data processing.

3.2.3. Activity determination in soot oxidation

As it is difficult to obtain diesel soot with constant properties (the composition strongly depends on the engine load) a model soot was applied (Printex-U, a flame soot obtained from Degussa). This soot contains low amounts of Poly Aromatic Hydrocarbons and little surface oxygen, nitrogen and sulfur compounds [10]. The activities of the investigated catalysts in the soot oxidation were determined in a STA 1500H thermobalance by measurement of the weight loss (TG) and the heat flow (DSC). Before an experiment the molybdates and metal oxides were milled with soot in a ratio of 2 : 1 (by weight) for one hour in a ball mill at speed '6'. These samples (referred to as being in 'tight contact') were diluted with SiC in order to prevent thermal runaways [2, 10]. About 4 mg catalyst, 2 mg soot and 54 mg SiC were applied as a sample. In this way, smooth DSC curves could be obtained. A heating rate of 10 K/min and a flow rate of 50 ml/min of 21 vol% O_2 in N_2 were used. The maximum of the DSC curve is defined as the 'oxidation temperature'. This temperature coincided within 10 K with the temperature of the maximum weight loss rate.

The activities of the $Cu/K/Mo/Cl-ZrO_2$ catalyst and possible chlorine containing compounds present (or formed) within this catalyst (KCl, $MoCl_5$, CuCl, $CuCl_2.2H_2O$ and Cu_2OCl_2, and non-calcined mixtures of KCl with copper chlorides ($K_2Cu_2OCl_4$, K_2CuCl_3, $K_2CuCl_4.2H_2O$)) were determined by mixing with soot in a ratio of 2:1 by weight with a spatula (*i.e.* 'loose contact') before dilution with SiC and thermal analysis. The activities of mixtures of LiCl (Baker) and CsCl (Baker) with $CuMoO_4$, KCl with $CuMoO_4$ and $CuWO_4$, and K_2CO_3 with $CuMoO_4$ (2:1 by weight) were determined in a similar way. $CuWO_4$ was used as received from Aldrich.

The activity of K_2MoO_4 was determined both in 'tight contact' and 'loose contact'. A TG/DSC reduction profile of Cu_2OCl_2 in the presence of soot (Cu_2OCl_2 : soot = 4:1 wt%) was recorded in nitrogen without SiC dilution.

3.3. Results

3.3.1. Catalyst characterization by means of DRIFT and XRD

The DRIFT spectra of the potassium- and copper molybdates are given in figures 1 and 2. The spectrum of MoO_3 is included in figure 2 for comparison. None of the molybdate spectra features the 990 cm^{-1} absorption or any absorption around 1400 cm^{-1}, which could be ascribed to residual MoO_3 or K_2CO_3, possibly left over after synthesis. The spectra of the potassium molybdates are similar to the ones published by Caillet *et al.* [14]. Especially the spectrum of $K_2Mo_4O_{13}$ contains a number of absorptions between 500 and 1000 cm^{-1}, due to several Mo=O and Mo-O-Mo vibrations [14].
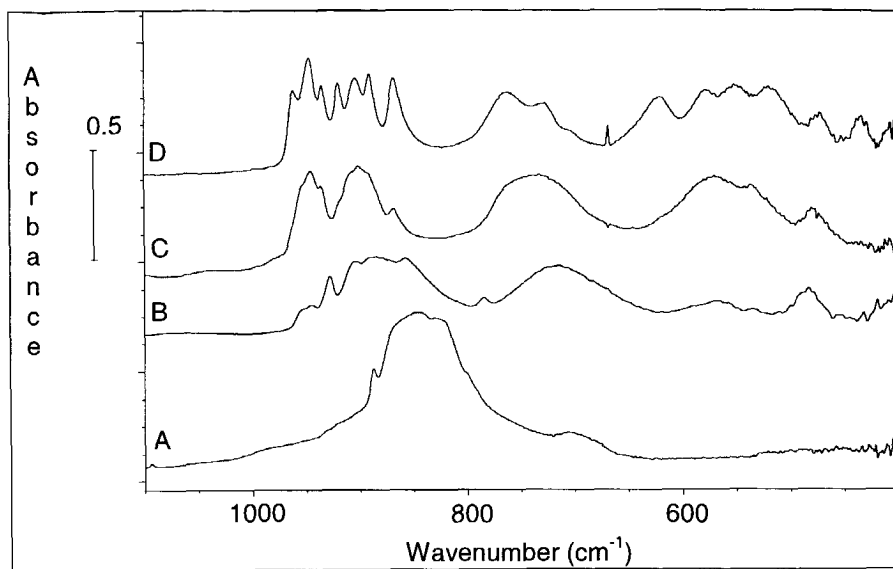
Figure 1. DRIFT spectra of K_2MoO_4 (A), $K_2Mo_2O_7$ (B), $K_2Mo_3O_{10}$ (C), and $K_2Mo_4O_{13}$ (D).
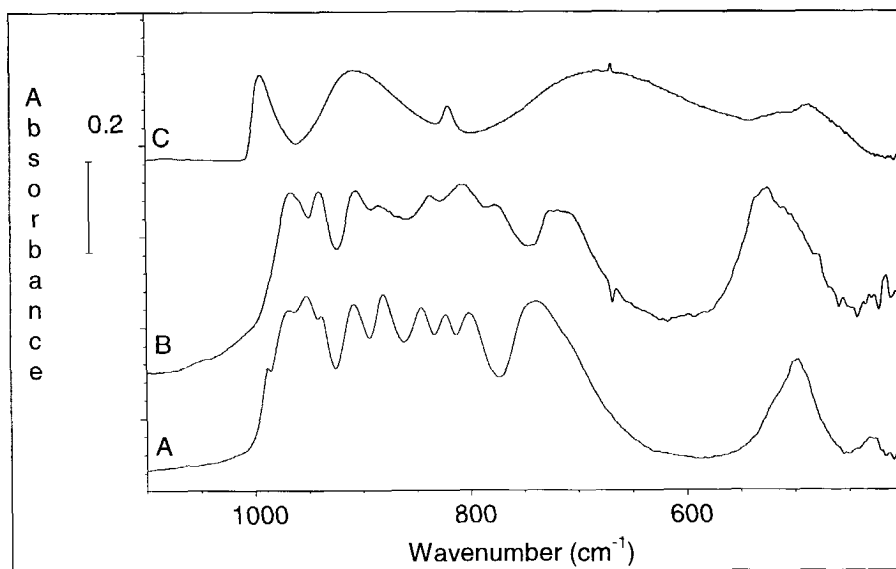
Figure 2. DRIFT spectra of $CuMoO_4$ (A), $Cu_3Mo_2O_9$ (B), and MoO_3 (C).

CuMoO$_4$ and Cu$_3$Mo$_2$O$_9$ can be identified by their individual DRIFT spectrum. The DRIFT spectra displayed in figure 2 are somewhat different than the spectra published by Machej [12]. The observed differences in intensity are probably due to the sampling technique applied (DRIFT *vs.* transmission). The XRD data of the molybdates correspond to those published in the Joint Committee on Powder Diffraction System files (JCPDS): Cu$_3$Mo$_2$O$_9$ [24-0055], CuMoO$_4$ [22-0242], K$_2$Mo$_4$O$_{13}$ [21-0666], K$_2$Mo$_3$O$_{10}$ [21-0662], and K$_2$Mo$_2$O$_7$ [21-0663].

To the best of my knowledge the potassium/copper double molybdate (K$_2$Cu$_2$(MoO$_4$)$_3$) has never been synthesized before. Only the nickel and cobalt analogues were synthesized by Klevtsov *et al.* [15]. Based on the chemical composition, the absence of several diffraction lines of either copper- or potassium molybdates, and the results of a crystallographic analysis, a new compound (with the stoichiometry K$_2$Cu$_2$(MoO$_4$)$_3$) is proposed to be formed.
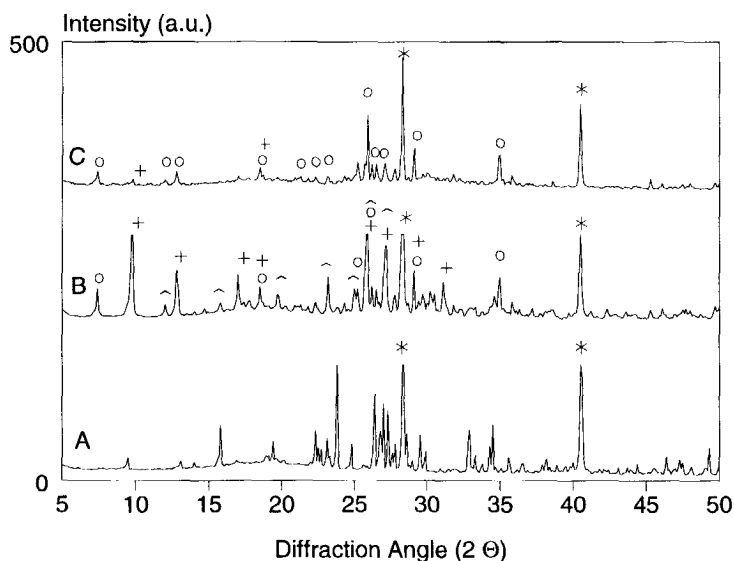
Figure 3. *X-Ray diffractograms of the compounds formed after reaction of CuMoO$_4$ and KCl in air at 723 K after 0 (A), 1 (B) and 3 (C) hours. Key : CuMoO$_4$ (none), KCl (*), K$_2$Mo$_3$O$_{10}$ (+), K$_2$Cu$_2$(MoO$_4$)$_3$ (o), and Cu$_3$Mo$_2$O$_9$ (^).*

Characteristic in the XRD pattern of this compound is a diffraction line of very strong intensity at a d-value of 1.1796 nm. In figure 3 the XRD spectra of the products after reaction of a mixture of KCl and CuMoO$_4$ (2:1 by weight) in air at 723 K, after 0, 1, and 3 hours, are given. Clearly the composition of products varies with time. First a potassium molybdate, *i.e.* K$_2$Mo$_3$O$_{10}$, together with Cu$_3$Mo$_2$O$_9$ are formed. After a prolonged period of time, the double molybdate (K$_2$Cu$_2$(MoO$_4$)$_3$) can be identified.

After reaction of $CuMoO_4$ still a lot of KCl is present, because the initial amount of KCl (on a molar basis) was six times the amount of $CuMoO_4$.
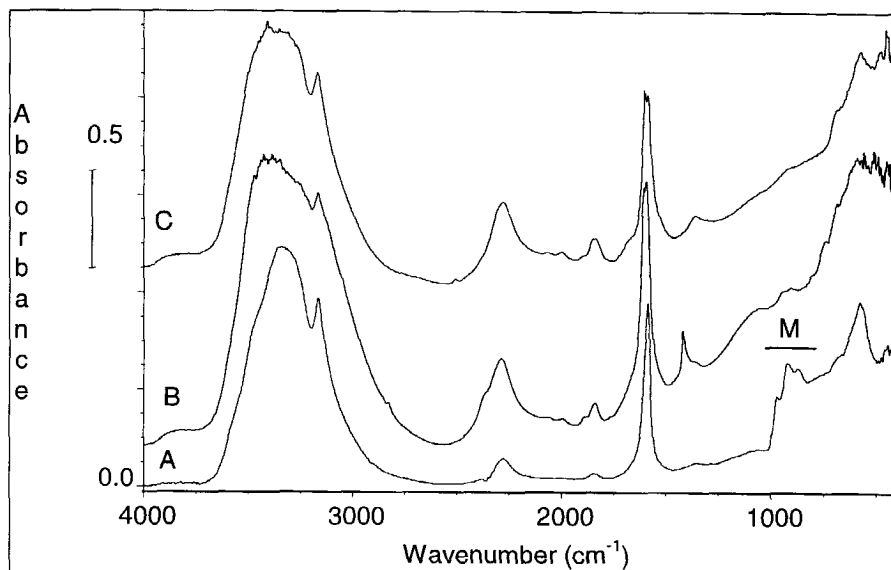
Figure 4. DRIFT spectra of the volatile compounds formed by calcination at 925 K of a Cu/K/Mo/(Cl)-ZrO₂ catalyst ((A), "M" indicates molybdates) and a non-supported KCl/CuWO₄ mixture (B). The spectrum of KCl mixed with CuCl₂.2H₂O (C) is shown for comparison.

In Figure 4 DRIFT spectra of the trapped volatile products formed by calcination at 925 K of a *non*-supported KCl/CuWO$_4$ mixture and a Cu/K/Mo/Cl-ZrO$_2$ catalyst are given. Most of the absorptions observed in the DRIFT spectra can be assigned to water adsorbed on copper chlorides. CuCl, Cu$_2$OCl$_2$ and CuCl$_2$ adsorb water differently, resulting in different DRIFT spectra. Comparing the spectra of the volatiles with the CuCl$_2$.2H$_2$O spectrum (figure 4), it is concluded that the volatile products mainly consist of CuCl$_2$.2H$_2$O. The presence of KCl, possibly mixed with potassium copper chlorides (*e.g.* K$_2$CuCl$_4$.2H$_2$O), cannot be identified by infrared, because KCl is infrared-transparent in the recorded spectral region (400-4000 cm^{-1}). The sample obtained from the Cu/K/Mo/Cl-ZrO$_2$ catalyst, also contains some molybdenum containing compounds (identified by the absorptions between 900 and 1000 cm^{-1}, indicated with 'M' in figure 4).

The results of the DRIFT analyses were confirmed by XRD. After comparison of the XRD-spectra shown in figure 5 with the JCPDS-files, CuCl$_2$.2H$_2$O, KCuCl$_3$ and K$_2$CuCl$_4$.2H$_2$O can be identified in the volatile fractions of the KCl/CuWO$_4$ mixture and the Cu/K/Mo/Cl-ZrO$_2$ catalyst. Again the presence of a molybdate (resembling K$_{2+x}$MoO$_4$: JCPDS file [21-0999]) was observed in the sample obtained from the

Cu/K/Mo/Cl-ZrO$_2$ catalyst. Potassium and copper tungstates are less volatile, and therefore not present in the sublimed product of the KCl/CuWO$_4$ mixture.
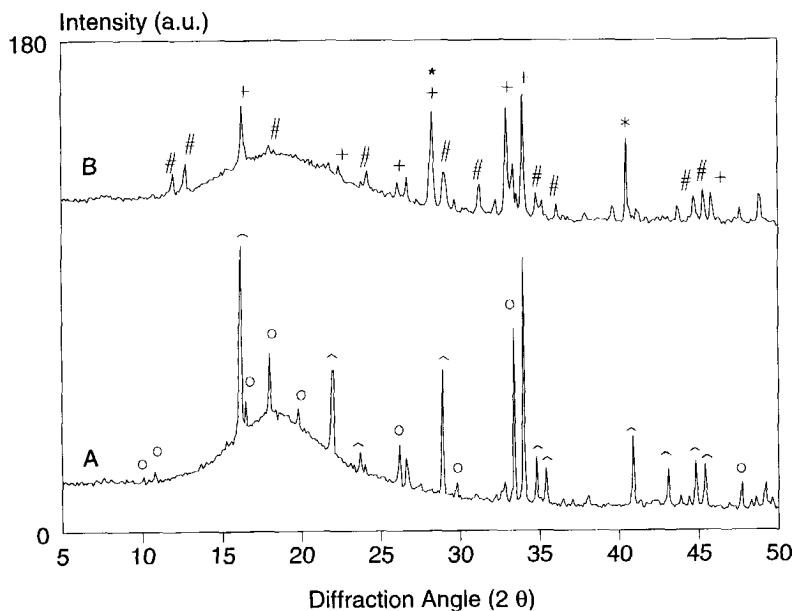

***Figure* 5.** *XRD spectra of the volatile compounds formed by calcination at 925 K of a Cu/K/Mo/Cl-ZrO$_2$ catalyst (A) and a non-supported KCl/CuWO$_4$ mixture (B). Identification: CuCl$_2$.2 H$_2$O (^), K$_{(2+x)}$MoO$_4$ (o), KCuCl$_3$ (#), KCl (*), K$_2$CuCl$_4$.2H$_2$O (+).*

3.3.2. Oxidation Activity

Soot oxidation profiles as obtained for K$_2$MoO$_4$ in 'tight contact' and 'loose contact' are shown in figure 6. The maximum of the exothermic heat effect is located at 685 K (T1) for the ball milled sample ('tight contact') and 790 K (T2) for the spatula mixture ('loose contact'). So, the milling procedure lowers the catalytic soot oxidation temperature by approximately 100 K. Non-catalytic soot oxidation occurs at 875 K. 'Tight contact' between an oxidic catalyst and soot is often required to obtain considerable oxidation activity. Neeft *et al.* [2] and v. Doorn *et al.* [16] reported earlier on the effect of contact on the catalytic performance of metal oxides. They found considerable differences in soot oxidation temperatures depending on the mixing procedure between the catalyst and soot. Combustion temperatures of the molybdates (in 'tight contact'), are given in figure 7. They all show a reasonable catalytic activity.
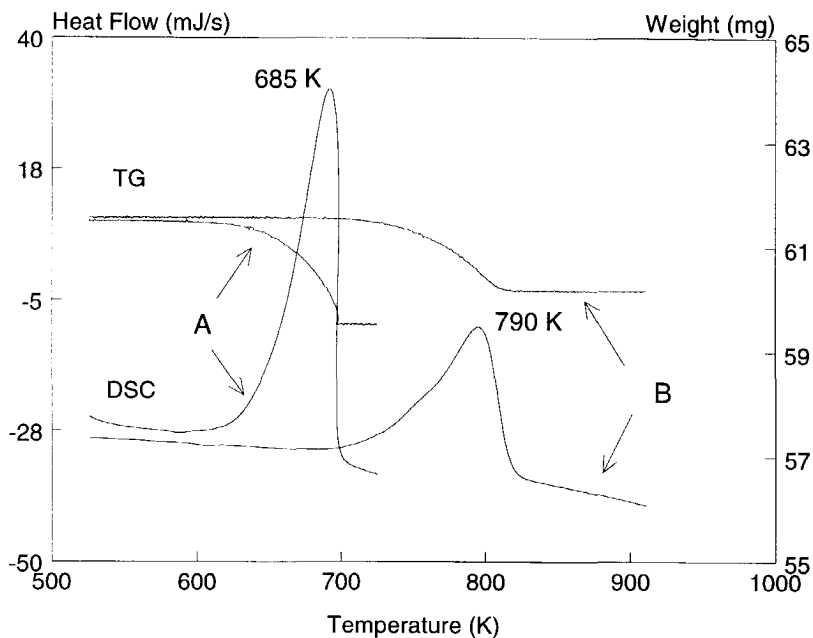
Figure 6. *TG and DSC profiles for soot oxidation catalyzed by K_2MoO_4 in "tight" (A) and "loose contact" (B) in the presence of synthetic air. Heating rate: 10 K/min.*
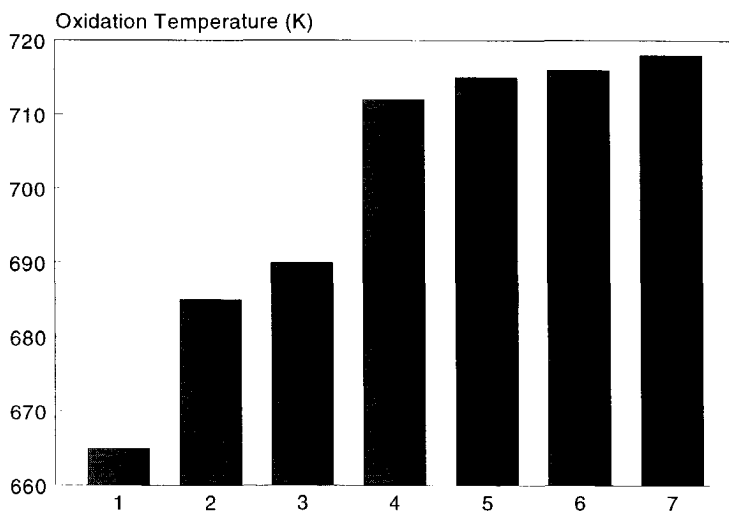
Figure 7. *Soot oxidation temperatures as determined by DSC for the individual molybdates present in the Cu/K/Mo/Cl catalyst in tight contact. 1. $K_2Cu_2(MoO_4)_3$, 2. K_2MoO_4, 3. $K_2Mo_2O_7$, 4. $K_2Mo_3O_{10}$, 5. $K_2Mo_4O_{13}$, 6. $CuMoO_4$, and 7. $Cu_3Mo_2O_9$.*

43

The best results are obtained with the mixed potassium copper molybdate, although the activity is not as high as the activity of the Cu/K/Mo/Cl-ZrO$_2$ catalyst. It should be emphasized that the molybdates have the presented activity only after ball milling, whereas the activity of the Cu/K/Mo/Cl-ZrO$_2$ catalyst reported in figure 7, has been determined without such a procedure. So, the high 'loose contact' activity of the supported Cu/K/Mo/Cl catalyst cannot be caused by the molybdates, which are present in this catalyst.
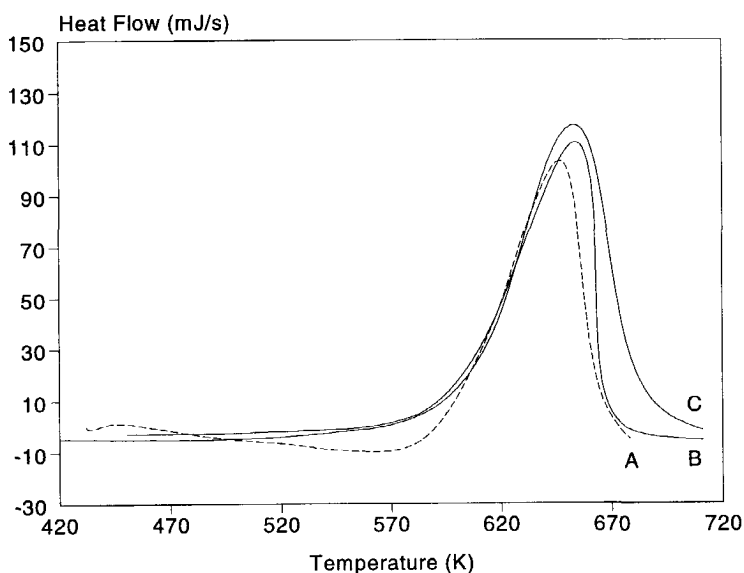
Figure 8. DSC profiles for the catalytic soot oxidation of the KCl/CuMoO$_4$ mixture (2:1 wt%) (A), the volatile fraction thereof (B), and K$_2$CuCl$_4$.2 H$_2$O (C).

The activities of the chloride containing compounds and mixtures described in the experimental part, were determined in 'loose contact'. DSC profiles for the catalytic soot oxidation of the KCl/CuMoO$_4$ mixture, the sublimed material, and K$_2$CuCl$_4$.2H$_2$O are given in figure 8. Obviously, all these catalytic systems have a similar activity in 'loose contact' (around 650 K). The activities of other copper and chlorine containing compounds (determined in 'loose contact') are given in figure 9. CuCl and Cu$_2$OCl$_2$ are even more active 'in loose contact' than the Cu/K/Mo/Cl-ZrO$_2$ catalyst. Addition of KCl to CuCl or Cu$_2$OCl$_2$ has a negative effect on the catalytic performance of these compounds. The application of MoCl$_5$ in 'loose contact' resulted in a soot oxidation temperature of about 730 K and KCl is only slightly active in soot oxidation, even after ball milling. Oxidation temperatures determined for catalytic mixtures of CuMoO$_4$ with KCl, CsCl, and LiCl (without pre-calcination), were determined to be in the range of 655-665 K.
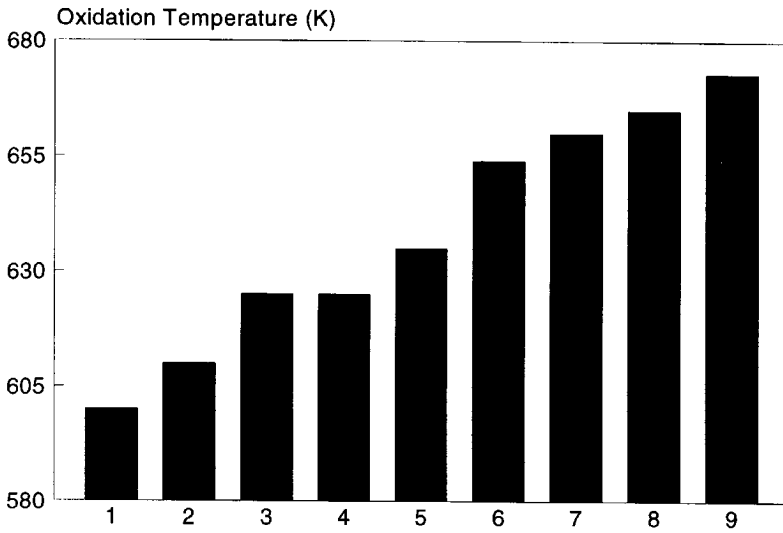
Figure 9. *Soot combustion temperatures for the chlorides present in the Cu/K/Mo/Cl catalyst. 1. CuCl, 2. KCl/CuCl (K_2CuCl_3), 3. Cu_2OCl_2, 4. $CuCl_2/Al_2O_3$, 5. KCl/Cu_2OCl_2 ($K_2Cu_2OCl_4$), 6. KCl/CuMoO_4 (2:1 wt ratio), 7. $KCl/CuCl_2$ ($K_2CuCl_4.2H_2O$), 8. $CuCl_2$, and 9. Cu/K/Mo/Cl-ZrO_2. Temperatures were determined in loose contact.*
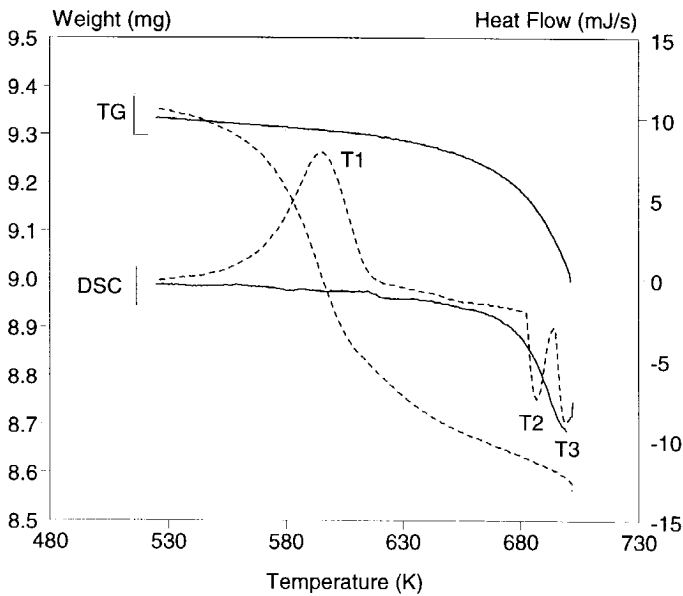
Figure 10. *TG/DSC profiles of Cu_2OCl_2 with (dashed line) and without soot (4:1 wt%). The profiles were recorded in nitrogen, without dilution in SiC.*

Apparently, the application of CsCl or LiCl, instead of KCl, does not result in a change in activity. However, addition of K_2CO_3 to $CuMoO_4$ resulted in a higher oxidation temperature of 750 K. The influence of the counter ion of copper (MoO_4^{2-} or WO_4^{2-}) was tested by comparing the activities of mixtures of KCl with $CuMoO_4$ and $CuWO_4$, respectively. A difference in soot oxidation activity is observed, which can be explained by different reactivities of $CuWO_4$ and $CuMoO_4$ towards KCl.

TG/DSC profiles of Cu_2OCl_2 in nitrogen with and without soot, are shown in figure 10. A weight decrease and a simultaneously generated exothermic effect around 595 K (T1), can be observed for the Cu_2OCl_2/soot sample. Apparently, reduction of Cu_2OCl_2 by soot, yielding CuCl is possible around this temperature. The formation of CuCl is confirmed by the endothermic heat effects at 685 K and 700 K (T2 and T3). These effects are not observed in the DSC-pattern of Cu_2OCl_2 without soot, but are characteristic for pure CuCl [17]. The decrease in weight above approximately 680 K, can be explained by evaporation of Cu_2OCl_2 and CuCl [18].

3.4. *Discussion*

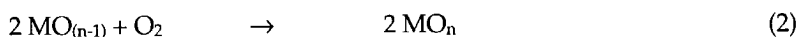Although little is known about the exact nature of the processes occurring when soot (or carbon) is catalytically oxidized by metal oxides, the reaction is often thought to proceed through a Mars & Van Krevelen type redox mechanism, as will be extensively discussed in chapter 7 of this thesis. In a first step the metal oxide is reduced by soot, and in a second step the catalyst is reoxidized by air (reactions 1 and 2, $n \geq 1$):

$$2\,MO_{(n)} + C \qquad \rightarrow \qquad CO_2 + 2\,MO_{(n-1)} \qquad\qquad (1)$$

$$2\,MO_{(n-1)} + O_2 \qquad \rightarrow \qquad 2\,MO_n \qquad\qquad (2)$$

Also Ciambelli *et al.* explain the activity of their Cu/K/V catalyst in soot oxidation in terms of reducibility [7]. In their reduction experiments they used hydrogen as the reducing agent. However, the reduction of metal oxides by hydrogen follows in principle a different mechanism than the reduction by soot. In the former case hydrogen molecule dissociation into atoms is an important factor which largely determines the reduction temperature, while in the latter case the intensity of contact between soot and the metal oxide and the strength of the metal-oxygen bond are important aspects. So, hydrogen reduction temperatures are *a priori* not applicable to explain activities of catalysts in soot oxidation. Moreover, we have demonstrated that none of the individual oxidic compounds in the mixture of the Cu/K/Mo/Cl catalyst is as active as the mixture itself. Therefore, an explanation of the high activity based on a simple reduction/reoxidation cycle of the metal oxides present in the catalytic mixture, is doubtful.

When KCl is added to $CuMoO_4$, the activity of this molybdate is increased considerably, whereas addition of K_2CO_3 hardly results in an increment of activity.

Moreover, it has been demonstrated that copper chlorides are very active in the soot oxidation reaction (figure 9), whereas $MoCl_5$ and KCl have little activity. Considering these results, we conclude that **copper** and **chlorine** are essential for a high 'loose contact' soot oxidation activity. This is in agreement with results of Neeft [10], who found that ZrO_2 supported Cu/K/Mo catalysts prepared from acetates or nitrates are far less active than analogous catalysts based on chlorides.

From the XRD and DRIFT results given in figures 3,4 and 5 it is concluded that (potassium) copper chlorides are formed by reaction between KCl and $CuMoO_4$ (or $CuWO_4$). The following reactions can be proposed:

$$4\,KCl + 7\,CuMoO_4 \quad\rightarrow\quad K_2Mo_3O_{10} + 2\,Cu_3Mo_2O_9 + K_2CuCl_4 \qquad (3)$$

$$2\,KCl + K_2Mo_3O_{10} + 2\,Cu_3Mo_2O_9$$
$$\rightarrow\quad 2\,K_2Cu_2(MoO_4)_3 + CuMoO_4 + CuCl_2 \qquad (4)$$
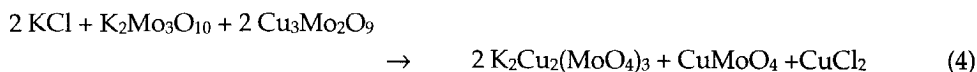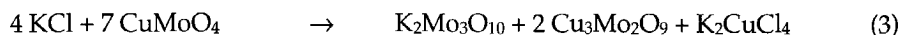
$CuMoO_4$ formed by reaction (4) reacts further with KCl according to reaction (3). Fontana *et al.* [20] have published $KCl-CuCl-CuCl_2$ phase diagrams. Several mixtures of KCl and $CuCl_2$ (*e.g.* K_2CuCl_4) appear to have low melting points (600-700 K). It is, therefore, not surprising that these compounds are identified in the volatile fractions of the $Cu/K/Mo/Cl-ZrO_2$ catalyst and of the $CuWO_4/KCl$ and $CuMoO_4/KCl$ mixtures.

The low melting points of (potassium) copper chlorides, can at least partially explain the high soot oxidation activity of these compounds, compared to molybdates and metal oxides in 'loose contact'. Redistribution of the chlorides over the soot surface occurs, and good contact between the catalyst and soot is established *in situ*. Ciambelli *et al.* [21] have shown that the surface area of their soot, as measured with N_2 at 77 K, increases with catalytic conversion. This can be explained by the (re)distribution of copper chlorides over the soot surface, resulting in the participation of the entire soot surface to the oxidation reaction. If only solid (catalyst) - solid (soot) contact points were involved, the change in specific surface area with conversion would have been negligible [21].

Redistribution of the catalyst can occur *via* a so-called 'wetting' process or *via* gas-phase transport. Xie *et al.* [22] have demonstrated that $CuCl_2$ was able to 'wet' the surface of alumina, and that another metal chloride (Hg_2Cl_2) already lost its crystalline structure when mixed with activated carbon at room temperature, indicating a certain mobility. On the other hand it has been shown in this chapter, that transport of several metal chlorides through the gas phase is also possible. Probably both modes of transport can occur simultaneously.

The activity of the (potassium)-copper chlorides, which are formed within the $Cu/K/Mo/Cl-ZrO_2$ catalyst, is higher than CuO in 'tight contact' [10]. This can be explained in two ways: *i)* the milling procedure results in less intimate contact than 'wetting' or sublimation, or *ii)* the presence of chlorine results in better reduction and reoxidation properties of CuO. Although the first explanation cannot be excluded, the

second one is likely to be more important. The following redox cycle is proposed, in parallel to the oxychlorination reaction [19, 20]:

$$4\ CuCl_2\ (.4\ KCl) + O_2 \quad \rightarrow \quad 2\ Cu_2OCl_2\ (.4\ KCl) + 2\ Cl_2 \qquad (5)$$

$$2\ Cu_2OCl_2 + C \quad \rightarrow \quad 2\ Cu_2Cl_2 + CO_2 \qquad (6)$$

$$2\ Cu_2Cl_2 + O_2 \quad \rightarrow \quad 2\ Cu_2OCl_2 \qquad (7)$$
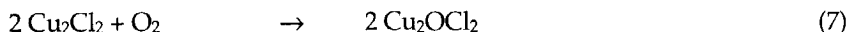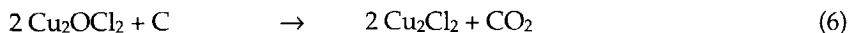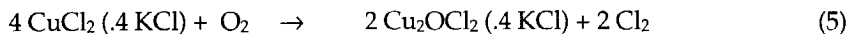
Fontana *et al.* [20] have shown that oxygen adsorption by melts of KCl and $CuCl_2$ at 673 K occurs at a considerable rate. This rate of oxidation increases with the amount of KCl present in the melt. Therefore, it is likely that some Cu_2OCl_2, combined with KCl (*e.g.* $K_2Cu_2OCl_4$), is formed according to reaction 5. This reaction can be regarded as an initiation reaction, and is non-catalytic. From the TGA experiments shown in figure 10, it can be deduced that Cu_2OCl_2 is reduced by soot into CuCl within the temperature range of interest. Therefore, reactions 6 and 7 are likely to describe the active catalytic cycle. The presence of KCl is not essential for the catalytic activity of CuCl and Cu_2OCl_2 (figure 9); it even lowers their activity to some extent. The major role of KCl is to induce the wetting properties of the catalytic system and to provide (part of) the chlorine to enable formation of copper(oxy)-chlorides. A more detailed TG, DSC and DRIFT analysis of copper(oxy)chlorides in the catalytic oxidation of soot will be discussed in chapter 4 of this thesis [17].

A priori, it is to be expected that a major problem of the application of a soot oxidation catalyst based on copper (oxy) chloride will be deactivation by evaporation and/or decomposition of the active compound. The application of a commercially available (oxychlorination) catalyst (30 wt% $CuCl_2$ on alumina), freshly used, yielded a soot oxidation temperature of about 625 K (figure 7). When this catalyst was held for 4 hours at 675 K in air, the activity had decreased significantly: the measured oxidation temperature had increased to approximately 790 K. Although a high stability has been reported [7,8], Neeft has demonstrated that the 'loose contact' activity of the $Cu/K/Mo/Cl$-ZrO_2 catalyst also decreases after treatment in air at 975 K for 24 hours [10]. Moreover, $Cu/K/Mo/Cl$ catalysts supported on ZrO_2 and TiO_2 were tested in the exhaust gas of a diesel engine, and a profound deactivation was observed [10].

Another important aspect of soot oxidation catalyzed by copper chlorides worthwhile mentioning is the possibility that carbon-chlorine bonds are formed (as in the oxychlorination reaction). By further reaction with oxygen, the formation of very toxic compounds, such as chlorobenzenes and chlorophenols, cannot be excluded. Especially chlorophenols are very reactive precursors for the formation of polychlorinated dibenzo-*p*-dioxines at carbon surfaces [23]. In this respect copper and chlorine containing soot oxidation catalysts can be considered to be less attractive for practical applications.

Evaluating the presented data, it is concluded that the ZrO_2 supported $Cu/K/Mo/Cl$ catalyst, and the catalysts prepared by Ciambelli [6, 7, 21] and Watabe

[8] are based on the high 'loose contact' soot oxidation activity of copper and chlorine containing compounds, formed by reactions (3) and (4). The intrinsic 'wetting' properties of these compounds (through the liquid and/or vapor phase), result in the *in-situ* establishment of good contact. The presence of KCl might be promoting for oxygen activation.

Because of their deactivation and the possible formation of polychlorinated dibenzo-*p*-dioxines, catalysts based on copper chlorides are not suitable for the continuous removal (oxidation) of diesel soot particulates. Other possibilities to eliminate the contamination of the environment by diesel soot particulates, like oxidic catalysts with 'loose contact' activity [24], fuel additives [25] or technical developments [1], have to be evaluated.

3.5. *Conclusions*

- Molybdates of copper and potassium have a moderate activity in (diesel) soot oxidation, even in 'tight contact'. The activity of a novel compound, $K_2Cu_2(MoO_4)_3$, is slightly higher than the activity of the individual copper- and potassium molybdates.
- The high soot oxidation activity in loose contact of catalytic systems containing an alkali metal chloride (KCl or CsCl or LiCl) and $CuMoO_4$ (or $CuWO_4$ or copper vanadates) can be ascribed to the formation of volatile copper chlorides or copper oxychlorides.
- The high activity of mixtures containing copper chlorides in 'loose contact' can be partially explained by the mobility and volatility of these compounds, resulting in intimate contact between the catalyst and soot. A catalytic cycle, involving (KCl and) Cu_2OCl_2 and CuCl, may account for the higher oxidation activity than CuO in 'tight contact'.
- Although copper chlorides can be formed by reaction between KCl (which serves as a chlorine supplier) and $CuMoO_4$, the application of the $Cu/K/Mo/Cl-ZrO_2$ catalyst (and analogues) is questionable, because loss of activity due to evaporation and decomposition of the active species will occur eventually.

3.6. *References*

[1] E.S. Lox, B.H. Engler and E. Koberstein, Studies Surf. Sci. Catal., 71 (1991) 291.
[2] J.P.A. Neeft, O.P. v. Pruissen, M. Makkee and J.A. Moulijn, in A. Frennet, and J-M. Bastin, (Editors), Preprints of the Third International Congress on Catalysis and Automotive Pollution Control, April 20-22, 1994, Brussels, Belgium, 1994, p. 355.
[3] A.F. Ahlström and C.U.I. Odenbrand, Appl. Catal., 60 (1990) 157.
[4] Sri Rahayu, W.L. Monceaux, B. Taouk and P. Courtine, in A. Frennet, and J-M Bastin, (Editors), Preprints of the Third International Congress on Catalysis and Automotive Pollution Control, April 20-22, 1994, Brussels, Belgium, 1994, p. 365.
[5] A. Löwe and C. Mendoza-Frohn, Appl. Catal., 66 (1990) L11.

[6]   P. Ciambelli, V. Palma and S. Vaccaro, Studies Surf. Sci. Catal., 71 (1991) 323.

[7]   P. Ciambelli, V. Palma and S. Vaccaro, Catal. Today, 17 (1993) 71.

[8]   Y. Watabe, C. Yamada, K. Irako and Y. Murakami, Catalyst for use in cleaning exhaust gas particulates, European patent application 0092023, (1983).

[9]   S. Yuan, P. Mériaudeau and V. Perrichon, Appl. Catal. B: Env., 3 (1994) 319.

[10] J.P.A. Neeft, 'Catalytic oxidation of soot. Potential for the reduction of diesel particulate emissions', PhD Thesis, TU Delft, 1995, chapter 8.

[11] P. Caillet, Bull. Soc. Chim. France, (1967) 4750.

[12] T. Machej and J. Ziolkowski, J. Solid State Chem. 31 (1980) 135.

[13] A. Goreaud, M. Goreaud and L. Walter-Lévy, Bull. Soc. Chim. France, (1970) 2789.

[14] P. Caillet and P. Saumagne, J. Mol. Structure, 4 (1969) 351.

[15] P.V. Klevtsov, V.G. Kim and R.F. Klevtsova, Sov. Phys. Crystallogr. 25 (1980) 175.

[16] J. v. Doorn, J. Varloud, P. Mériaudeau and V. Perrichon, Appl. Catal. B., Env. 1 (1992) 117.

[17] G. Mul, F. Kapteijn and J.A. Moulijn, Appl. Catal. B: Env. (1997), accepted.

[18] O. Knacke, O. Kubaschewski and K. Hesselmann, Thermochemical properties of inorganic substances, Vol. I and II, Springer-Verlag, Berlin, 1991.

[19] C.M. Fontana, E. Gorin, G.A. Kidder and C.S. Meredith, Ind. Eng. Chem., 44 (1952) 363.

[20] C.M. Fontana, E. Gorin, G.A. Kidder and C.S. Meredith, Ind. Eng. Chem., 44 (1952) 373.

[21] P. Ciambelli, M. D'Amore, V. Palma and S. Vaccaro, Combustion and Flame, 99 (1994) 413.

[22] Y-C Xie and Y-Q Tang, Adv. Catal., 37 (1990) 1.

[23] R. Luijk, D.M. Akkerman, P. Slot, K. Olie and F. Kapteijn, Environ. Sci. Technol., 28 (1994) 312.

[24] J.P.A. Neeft, M. Makkee and J.A. Moulijn, Appl. Catal. B. Env. (1997), accepted.

[25] J.P.A. Neeft, 'Catalytic oxidation of soot. Potential for the reduction of diesel particulate emissions', PhD Thesis, TU Delft, 1995, chapter 9.

4

Catalytic oxidation of model soot by metal chlorides

Abstract

Several metal chlorides were screened on their catalytic activity in the oxidation of model soot (Printex-U) in 'loose contact' by means of TGA/DSC. $HgCl_2$, $CaCl_2$, $BaCl_2$, $CoCl_2$, and $NiCl_2$ show little activity. Hydrated $BiCl_3$ and $FeCl_3$ are converted in air into $BiOCl$ and $FeOCl$, which have a moderate soot oxidation activity. $MoCl_5$ is converted into the corresponding metal oxide and also shows a moderate 'loose contact' activity. $PbCl_2$, $CuCl_2$, and $CuCl$ are very active catalysts; the soot oxidation temperature is lowered by 200-275 K. The activity of metal chlorides is thought to be induced by *in-situ* formation of intimate contact between the soot and the metal chloride *via* 'wetting' and/or gas-phase transport. A correlation between the melting point and the catalytic activity was found. Furthermore, a catalytic cycle is proposed involving activation of oxygen on the surface of the metal (oxy)chloride, followed by transfer of activated oxygen to the soot surface. DRIFT analyses showed that this results in the formation of carbon surface oxygen complexes. Decomposition of those complexes yields CO and CO_2. Practical application of metal chlorides for the removal of soot from diesel exhaust is not recommended, because they suffer from instability or high vapor pressures.

4.1. *Introduction*

Removal of soot and NO_x from diesel exhaust gas is necessary to protect the environment. Although diesel exhaust is rather clean compared to otto engine exhaust, in practice the amount of NO_x and soot emitted by diesel engines is much larger than emitted by otto engines equipped with catalytic converters [1].

Soot emission can be reduced in various ways [1-3]. Collection of soot in a monolithic filter and simultaneous oxidation are considered to be a good option to minimize the contamination of the environment. However, soot oxidation takes place at temperatures of 825 - 875 K, while the temperature of diesel exhaust is typically 500 - 675 K. Hence, a catalytic system is needed to prevent accumulation of soot in the monolithic filter. Several investigators have focused their attention on the application of oxidic materials to lower the oxidation temperature of soot. However the activity of metal oxides is dependent on the intensity of contact between the metal oxide and soot. It has been shown that metal oxides, like Co_3O_4 or Fe_2O_3 can be reasonably active if 'tight contact' between the soot and catalyst has been established mechanically (by ball-milling), but lose their catalytic activity completely when so-called 'loose contact' conditions (after *e.g.* spatula mixing) are present [4,5].

In a previous paper we discussed the catalytic activity of a Cu/K/Mo/Cl catalyst [6]. Copper chlorides are present and formed within this catalyst and it was shown that they are essential for the high soot oxidation activity of a Cu/K/Mo/Cl catalyst in 'loose contact'. Also other authors have shown that $CuCl_2$ is an active catalyst for the carbon oxidation reaction [7]. It was proposed that either the mobility or the volatility of CuCl or $CuCl_2$, or both, results in an *in-situ* establishment of 'tight contact'. Furthermore, the higher activity of copper chlorides compared to copper oxide (even in 'tight contact' conditions) was tentatively explained by favorable redox properties of the copper (oxy) chlorides [6].

Little is known about the catalytic activity in soot oxidation and the stability of other metal chlorides with respect to this reaction. In order to find design rules for an active catalyst in soot oxidation the catalytic activity of several metal chlorides is evaluated with respect to their melting point. The stability of the most active chlorides in air at the temperatures needed to combust the soot, and the necessity of a chloride ion for the activation of oxygen will also be evaluated.

4.2. *Experimental*

The metal chlorides investigated were purchased from Baker ($BaCl_2$, $CaCl_2$, $FeCl_3.6H_2O$, (analytical grade)), Aldrich (CuCl, $BiCl_3$, $HgCl_2$, $CoCl_2.6H_2O$, $MoCl_5$, $NiCl_2.6H_2O$ (analytical grade)), and Merck ($CuCl_2.4H_2O$, $PbCl_2$ (analytical grade)). The corresponding metal oxides were purchased or prepared as described elsewhere [4]. The oxychlorides of copper and lead were prepared by solid-state reactions of $CuCl_2.4H_2O$ and CuO (Merck, *p.a.*) at 525 K for 2 hours [8, 23] and $PbCl_2$ and PbO (Aldrich, > 99%) at 575 K for 2 hours in static air [9].

Since it is difficult to obtain diesel soot with constant properties (the composition depends on the engine load) a model soot was applied (Printex-U, a flame soot purchased from Degussa). This soot has a N_2-BET surface area of 96 m^2g^{-1} and contains approximately 5 wt% of adsorbed hydrocarbons and 0.2-0.4 wt% sulfur [4]. Oxidation temperatures were determined in a thermobalance (STA 1500H) after mixing the soot and the catalyst in a ratio of 1 : 2 by weight with a spatula (*i.e.* 'loose contact') and diluting the sample with SiC in order to prevent thermal runaways [4]. About 4 mg catalyst, 2 mg soot and 54 mg SiC were applied as a sample. In this way, smooth DSC curves could be obtained. A heating rate of 10 K/min and a flow rate of 50 ml/min 21 vol% O_2 in N_2 were used. The maximum of the DSC curve was defined as the oxidation temperature. This temperature coincided with the temperature of the maximum weight loss rate within 10 K. TG analysis of the metal oxides was performed in 'loose' and 'tight contact' mode. Samples referred to as 'tight contact' were intensively milled in a ball mill for one hour, before dilution with SiC and thermal analysis.

A stability test of CuCl was performed by TG/MS in N_2 (50 ml/min) and air (21 vol% O_2 in N_2, 50 ml/min). About 15 mg of the chloride was analyzed without SiC dilution. A quadrupole mass spectrometer (Fisons instruments) was used, which was coupled to the balance with a heated capillary. In this way, products of decomposition could be detected. Carbothermic reduction of Cu_2OCl_2 was recorded in the thermobalance in N_2 (Cu_2OCl_2 : soot = 4 : 1 by weight). A TG/DSC profile of Cu_2OCl_2 without soot was recorded under similar conditions.

Partially converted CuCl, $PbCl_2$, Pb_2OCl_2, FeOCl and BiOCl catalyzed soot samples were prepared (without SiC dilution, and a catalyst:soot ratio of 2:1 by weight) isothermally in the thermobalance at 550 K (CuCl), 610 K ($PbCl_2$, Pb_2OCl_2) and 645 K (FeOCl, BiOCl). The final temperature was reached with 10 K/minute. Approximately 20 minutes were required to obtain soot conversion levels of 20%-60%.

Diffuse Reflectance Infrared Fourier Transformed (DRIFT) spectra were recorded on a Nicolet Magna 550 spectrometer, equipped with a Spectratech DRIFT accessory. Samples were analyzed *in-situ*, after partial conversion of the soot in the thermobalance and dilution with KBr (1:100 by weight). They were recorded against a soot in KBr background (soot : KBr = 1:100 by weight). A resolution of 8 cm^{-1} and 256 scans were applied to obtain the spectra. Spectra are displayed without any further data processing.

4.3. *Results*

4.3.1. Screening of metal chlorides

A typical TG/DSC profile of soot oxidation ($PbCl_2$ is used as a catalyst) is shown in figure 1. The oxidation activity is characterized by the maximum of the exothermic heat effect, located at 683 K (T1). Non-catalytic oxidation of Printex-U (the model soot applied) occurs around 875 K.
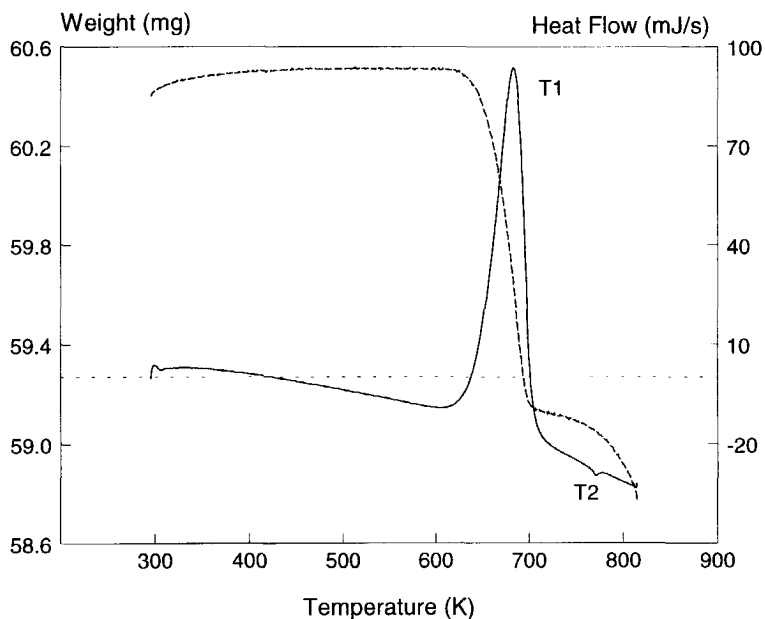
Figure 1. *TG/DSC analysis of PbCl₂ catalyzed soot oxidation. TG: dashed line, DSC: solid line.*

A modest endothermic heat effect (T2) is located at 773 K, due to melting of $PbCl_2$. This is accompanied by a gradually increasing weight loss above this temperature.

Oxidation temperatures for the metal chlorides are given in figure 2. This figure also contains the soot oxidation temperatures for the corresponding metal oxides in 'loose' (without ball milling) and 'tight contact' (with ball milling). Obviously the activity of the metal oxides is strongly contact dependent.

Several metal chlorides have hardly any effect on the soot oxidation temperature. $HgCl_2$ does not lower the soot oxidation temperature. Also $BaCl_2$ and $CaCl_2$ only show a small catalytic effect. Upon heating, $CoCl_2.6H_2O$ and $NiCl_2.6H_2O$ lose crystal water; in air they are (partially) converted into the corresponding oxides [10,11, and references therein]. The soot oxidation activity of partially oxidized nickel and cobalt chlorides lies in between that of 'tight contact' and 'loose contact'. $MoCl_5$ is completely oxidized in air at relatively low temperatures. The activity of oxidized $MoCl_5$ is equal to MoO_3 in 'tight contact'. $FeCl_3.6H_2O$ and hydrated $BiCl_3$ are first converted into the rather stable oxychlorides [12,13] FeOCl and BiOCl, respectively. Also the catalytic activity of those oxychlorides are given in figure 2. FeOCl decomposes into Fe_2O_3 (Hematite) and Cl_2 at approximately 725 K [12]. BiOCl is more stable and does not liberate Cl_2 below 850 K [13]. Both (oxy)chlorides have a somewhat higher activity in the soot oxidation reaction than their corresponding metal oxides in 'tight contact' (*i.e.* after ball milling of the metal oxide and soot).
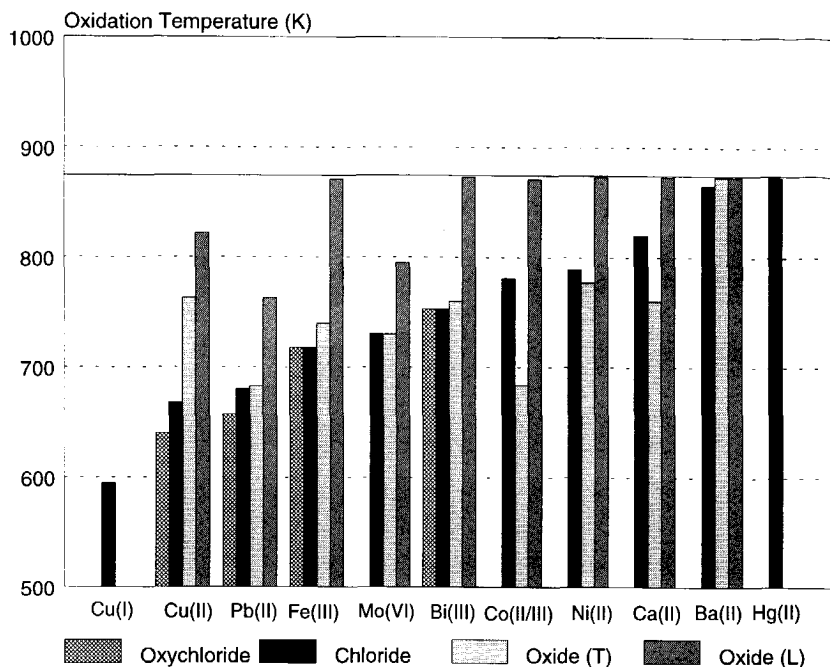
Figure 2. *Soot oxidation temperatures as determined for several metal chlorides ('loose contact') and their corresponding metal oxides ('tight contact' (T), and 'loose contact'(L)).The solid horizontal line indicates the non-catalytic soot oxidation temperature (875 K).*

Also $CuCl_2$ and $PbCl_2$ have higher soot oxidation activities than ball-milled samples of the oxides. The activity of the oxychlorides, Cu_2OCl_2 and Pb_2OCl_2, is even better: maxima in the DSC curves were located at 625 and 660 K, respectively. CuCl is extraordinary active: the soot oxidation temperature is lowered by 285 K. As CuCl is the most active catalyst found, a thorough TG/DSC and DRIFT analysis of CuCl was carried out, in order to reveal the active component and the mechanism by which CuCl is operative. As $PbCl_2$, Pb_2OCl_2, FeOCl and BiOCl have higher activities than their corresponding oxides and a reasonable stability in the temperature range of interest, these compounds were also further investigated.
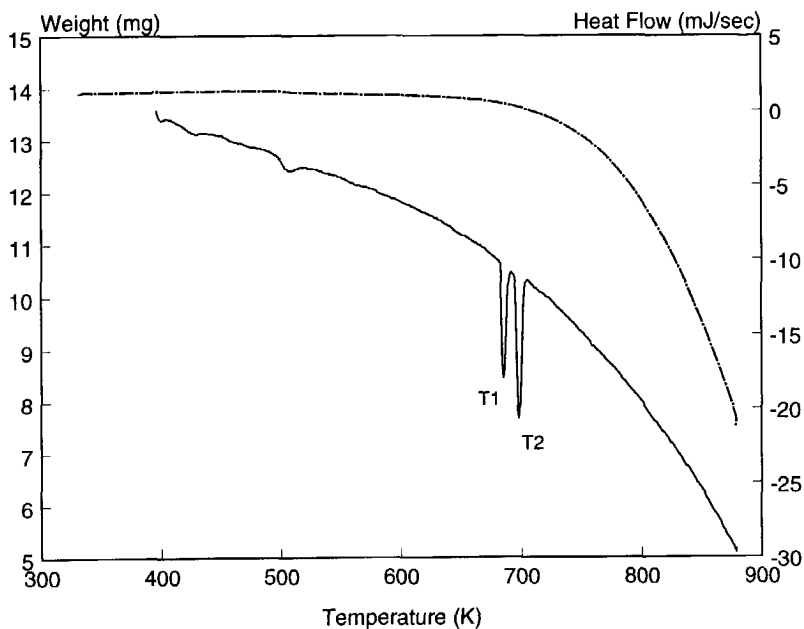
Figure 3. *TG/DSC analysis of CuCl in N₂. TG: dashed line, DSC: solid line.*

4.3.2. Determination of active phases and stability thereof

The TG and DSC profiles of CuCl in a nitrogen atmosphere are shown in figure 3. Two sharp heat effects can be detected at 685 K (T1) and 698 K (T2), characteristic for CuCl, due to a phase transition [14] and melting [15], respectively. A considerable weight loss is observed above 700 K, due to evaporation of CuCl. This compound has an appreciable vapor pressure above this temperature [16].

The TG and DSC profiles of soot oxidation catalyzed by Cu_2OCl_2 (A) and CuCl (C), and the oxidation of CuCl in air (4 mg, without soot, but diluted with SiC (1:15)) (B), are shown in figure 4. The CuCl and Cu_2OCl_2 catalyzed soot oxidation temperatures are located at approximately 595 K (T1) and 625 K (T5), respectively. After 100 % soot conversion, an increase in weight can be observed in the range of 660 K - 690 K, accompanied by two heat effects (T2 and T3): one of which is positive, due to oxidation, and one a superimposed negative heat effect, due to melting. Similar heat effects are observed for pure CuCl. The interpretation is the (re)oxidation of CuCl into Cu_2OCl_2, which is thermally stable in air up to 740 K (T4). At this temperature of 740 K a weight decrease is observed, due to decomposition of the oxychloride, yielding CuO and gaseous chlorine. The formation of chlorine upon Cu_2OCl_2 decomposition was verified by TG/MS analysis of pure CuCl in air (20 mg, without SiC dilution).

Figure 4. *TG/DSC analysis of the Cu_2OCl_2 catalyzed soot oxidation (curves A), the CuCl catalyzed soot oxidation (curves C) and the oxidation of CuCl without soot (curves B).TG: dashed lines, DSC: solid lines.*

Figure 5. *TG/DSC analysis of Cu_2OCl_2, recorded in N_2, with (dashed lines) and without soot (solid lines).*
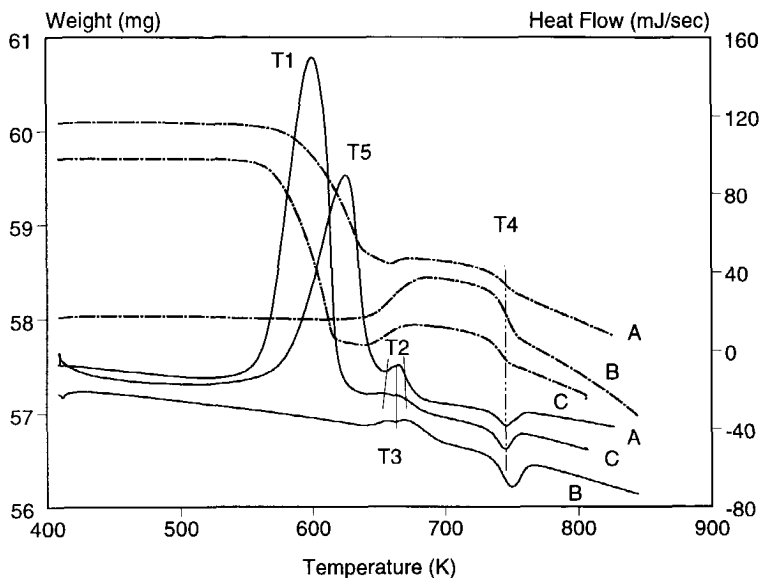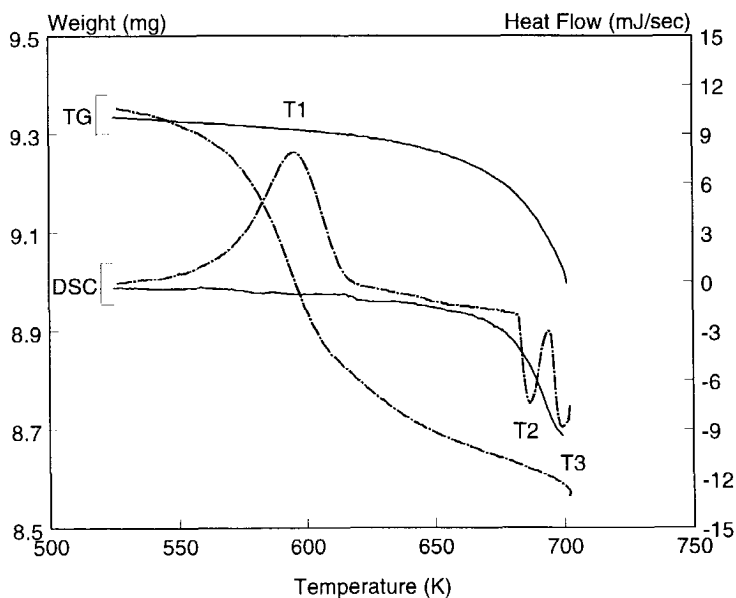
57

The TG/DSC analysis of carbothermic reduction of Cu_2OCl_2 in nitrogen is shown in figure 5. A weight loss, accompanied by an exothermic heat effect is located at approximately 600 K (T1). This weight loss agrees with the formation of CuCl, CO and CO_2. The formation of CuCl is corroborated by the heat effects at 685 K (T2) and 698 K (T3), which are characteristic for CuCl (figure 3). These phenomena are not observed in the TG and DSC patterns of Cu_2OCl_2 without soot. The weight loss above approximately 700 K is ascribed to the volatilization of CuCl and Cu_2OCl_2.

Carbothermic reduction of Pb_2OCl_2 was not observed at the temperatures, where this compound is active in soot oxidation. Oxidation of $PbCl_2$ after 100% soot conversion (figure 1) did not take place either. Hydrated $BiCl_3$ is converted at low temperatures (450-550 K) into BiOCl. Decomposition and carbothermic reduction of the latter compound was not observed. Finally, FeOCl (formed by decomposition of $FeCl_3.6H_2O$) was not carbothermally reduced, but decomposed into Fe_2O_3 and Cl_2 at approximately 720 K.

4.3.3. DRIFT Analysis

DRIFT spectra of a partially converted CuCl/soot mixture (50% conversion), and a BiOCl/soot mixture (20% conversion) are depicted in figure 6. The spectrum of soot after an identical heat treatment is also shown for comparison. The DRIFT spectra contain three main absorptions located at 1738 cm^{-1}, 1607 cm^{-1} and centered around 1257 cm^{-1}. The 1607 cm^{-1} absorption is caused by aromatic stretching vibrations of the soot, which are enhanced by polar functional groups like quinone [17]. The other two absorptions have been assigned to oxygen complexes formed on the soot surface: lactones (1738 cm^{-1}) and ether-like complexes (1257 cm^{-1}), respectively [18,19]. Clearly CuCl causes an enhancement of the amount of surface oxygen complexes. Pure CuCl has no infrared absorptions in the spectral region recorded (400-4000 cm^{-1}). However, the absorptions located at 905, 855 and 810 cm^{-1} can be ascribed to water adsorbed on CuCl [20]. A strong band below 600 cm^{-1} is indicative for Cu_2OCl_2. As this band is not present in the spectrum displayed in figure 6, the DRIFT analysis confirms that transformation of CuCl into Cu_2OCl_2 does not occur during catalytic soot oxidation at 550 K.

The DRIFT spectrum of soot partially converted in the presence of BiOCl is also included in figure 6. BiOCl also catalyzes the formation of surface oxygen complexes. Similar absorptions as for the CuCl sample can be observed. The absorption band at 530 cm^{-1} can be ascribed to BiOCl [21].

DRIFT spectra of partially converted $PbCl_2$ (15%)/-, Pb_2OCl_2 (35%)/- and FeOCl (60%)/soot mixtures are shown in figure 7. Similar absorptions as in figure 6 can be found. Apparently, these (oxy)chlorides also catalyze the formation of surface oxygen complexes. For Pb_2OCl_2, the DRIFT spectrum collected after partial soot conversion, contains a rather large absorption band below 500 cm^{-1}, indicative for the presence of the oxychloride. This band is not observed in the $PbCl_2$ sample.
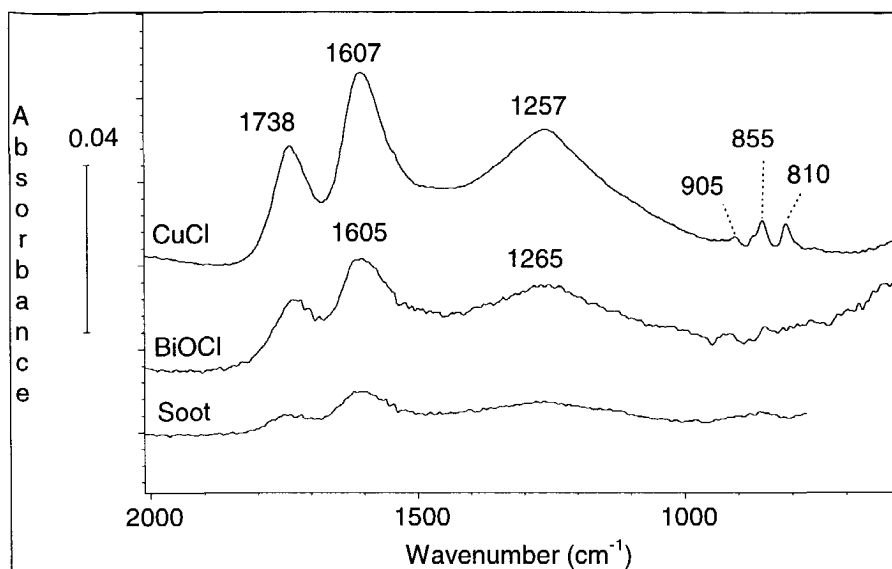
Figure 6. DRIFT analysis of partial converted soot samples. Non-catalytic (3% soot conversion), CuCl catalyzed (50 %), and BiOCl catalyzed (20 %).
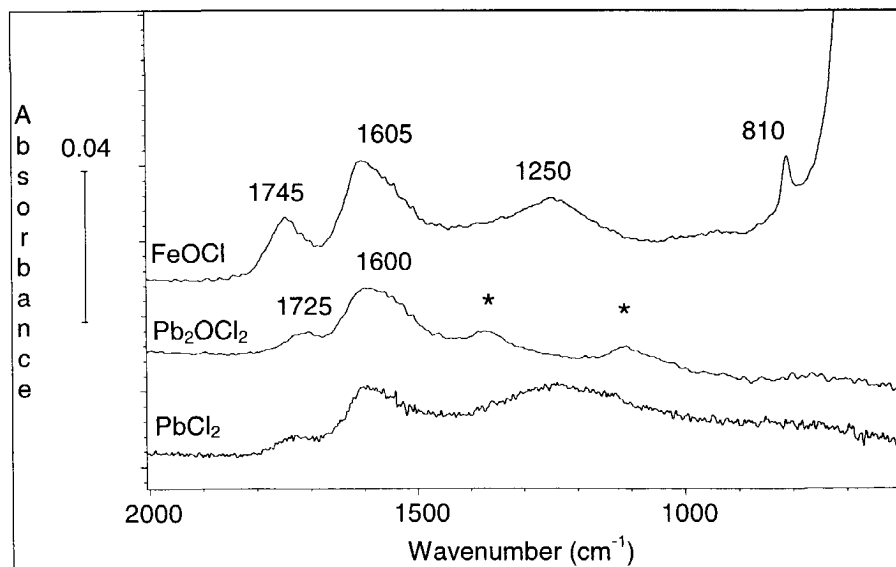

Figure 7. DRIFT analysis of partial converted soot samples. $PbCl_2$ catalyzed (15%), Pb_2OCl_2 catalyzed (35%) and FeOCl catalyzed (60%). Asterisks indicate carbonato vibrations.

The absorptions indicated with an asterisk (at 1375 cm^{-1} and 1113 cm^{-1}) might be due to carbonate formation. Furthermore, the 1250 cm^{-1} band is absent in the Pb$_2$OCl$_2$/soot spectrum. This is still under investigation. Nonetheless, the DRIFT analyses confirm the observations of the TG/DSC analysis, that neither carbothermic reduction of Pb$_2$OCl$_2$, nor (bulk) oxidation of PbCl$_2$ takes place during catalytic soot oxidation. Decomposition of FeOCl into hematite is confirmed by changes in the large band below 800 cm^{-1} (not shown).

4.4. Discussion

4.4.1. Catalytic activity of metal (oxy)chlorides

Metal (oxy)chlorides with high melting points (CaCl$_2$, BaCl$_2$, NiCl$_2$ and CoCl$_2$) are less active in 'loose contact' than metal chlorides with relatively low melting points and high vapor pressures. Milling a metal chloride and soot hardly effects the catalytic soot oxidation temperature. These observations support the conclusion that the high catalytic activity of several metal chlorides in 'loose contact', is due to in-situ distribution of the chlorides over the soot surface (resulting in 'tight contact') and is related to the melting point of the compounds. Neeft [4] found a correlation between the 'loose contact' catalytic activity and the melting point or volatility of metal oxides. The activity of metal chlorides, expressed by the soot oxidation temperature, correlated to their melting point is shown in figure 8. The non-catalytic soot oxidation temperature is indicated by the horizontal solid line. Unfortunately, several metal (oxy) chlorides do not have a well defined melting point in air. They are (partially) transformed before they melt into the corresponding oxide and Cl$_2$ (FeOCl (Hematite), MoCl$_5$, BiOCl, CoCl$_2$, and NiCl$_2$ [16]) or decompose otherwise (CuCl$_2$, yielding CuCl [16]). Therefore, the decomposition temperatures given by Knacke [16] are plotted in the figure, except for Mo, whose melting point of the oxide (MoO$_3$ [16]) was used. These metal chlorides are indicated with an open circle in figure 8, while a solid circle indicates that the metal chlorides (and MoO$_3$) have a well defined melting point. Figure 8 shows that the higher the melting point of the metal chloride, the less 'loose contact' activity it displays. FeOCl, CoCl$_2$, and NiCl$_2$ are partially oxidized around the temperatures, where they display catalytic activity. Nonetheless, these catalysts are more active than the corresponding metal oxides in 'loose contact'. Apparently, a rather intimate contact between the (partially decomposed) chloride and the soot can be established. Although HgCl$_2$ does have a well defined melting temperature, it is not on the curve, obviously because HgCl$_2$ has evaporated before it can exert its catalytic influence.

Whether the in-situ 'tight contact' formation occurs by 'wetting' or gas phase transport has yet to be established. Xie et al. [22] have investigated the spreading (or 'wetting') behavior of many inorganic salts on several carrier materials (like Al$_2$O$_3$, TiO$_2$ and activated carbon), and found that CuCl$_2$ was able to wet the surface of

alumina [22]. Previously, it has been shown that gas phase transport of copper chlorides also occurs [6].

The (oxy)chlorides of Cu, Pb, Fe and Bi are more active than their corresponding oxides in 'tight contact'. This might be the result of an even better contact obtained by 'wetting' or condensation than obtained after ball-milling. However, several experimental observations indicate that chlorine ions also effect the activation of oxygen, as will be discussed in paragraph 4.3.
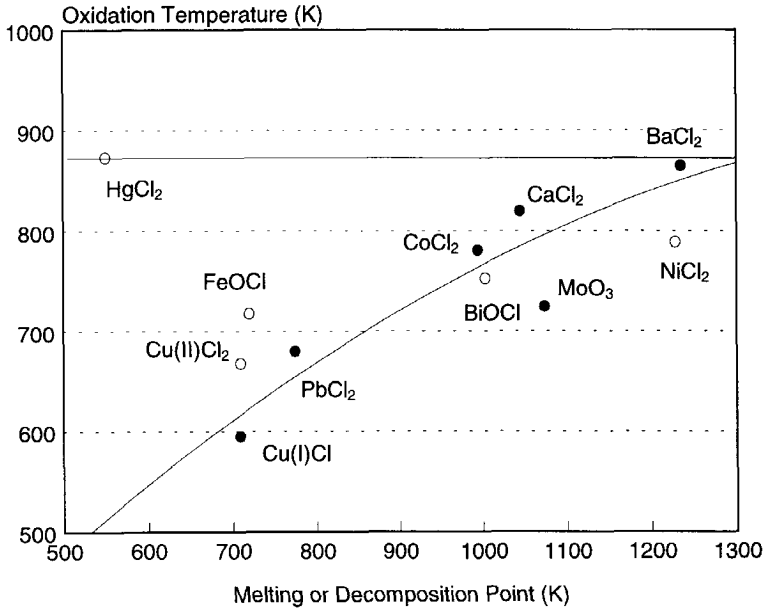
Figure 8. Correlation between the melting point of metal chlorides and the determined soot oxidation temperature. Solid dot: well defined melting point. Open dot : decomposition or oxidation takes place before melting. The horizontal solid line indicates the non-catalytic soot oxidation temperature.

4.4.2. The active phase in metal chloride catalyzed soot oxidation

In the TG profile of soot oxidation catalyzed by Cu_2OCl_2, an increase in weight can be observed after complete soot conversion at 650 K - 680 K. Apparently, even in the presence of 20% O_2 in N_2, an *in-situ* conversion of Cu_2OCl_2 into CuCl during soot oxidation has taken place. This is corroborated by a TG analysis of heating CuCl in air, which revealed a weight increase at the same temperature where the weight increase of the Cu_2OCl_2/soot sample after 100 % soot conversion (figure 4) occurred. Also the heat effects are similar. Furthermore, the TG profile of heating Cu_2OCl_2 and soot in nitrogen showed a weight decrease around 600 K, indicating carbothermic reduction of Cu_2OCl_2

by soot (figure 6). Therefore, we conclude that during soot oxidation Cu_2OCl_2 is reduced to $CuCl$.

The TG/DSC analysis in nitrogen of Pb_2OCl_2 mixed with soot showed that carbothermic reduction does not occur at temperatures below the melting point. On the other hand, figure 1 shows that oxidation of $PbCl_2$ (upon soot oxidation) does not take place either, which is corroborated by the absence of an IR band below 500 cm^{-1} in the DRIFT spectrum of the partially converted soot/$PbCl_2$ mixture. Apparently, the active phase of Pb is determined by the starting compound. This conclusion is confirmed by the activity data: Pb_2OCl_2 is more active than $PbCl_2$.

The DRIFT spectrum of a BiOCl/soot mixture after 20% conversion (figure 6) showed the presence of BiOCl. Furthermore, BiOCl reduction was not observed in a TG/DSC experiment. Hence, during soot oxidation the active phase of Bi is the oxychloride.

FeOCl is rather unstable and decomposes into hematite during soot oxidation. This is confirmed by the DRIFT spectrum of a partially converted soot/FeOCl mixture, which contains the features of Fe_2O_3 [21].

4.4.3. Mechanistic aspects

Soot oxidation, catalyzed by metal oxides, is often thought to proceed through a reduction/oxidation mechanism (Mars & van Krevelen). In a first step the metal oxide is reduced by the soot, and in a second step the catalyst is reoxidized by air. A lot of metal oxides can be reduced by soot at the temperatures at which they catalyze its oxidation (after ball milling) [24]. Another mechanism is based on a spill-over effect: oxygen is activated on the surface of a metal oxide, and subsequently transferred to the soot surface, where it reacts yielding Surface Oxygen Complexes (SOC) and CO and CO_2 [25, 26].

$$(1)$$
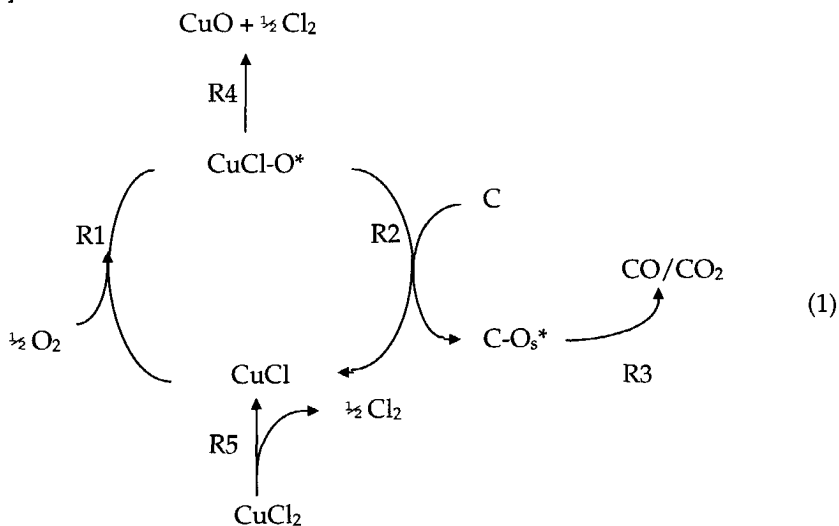
The catalytic activity of CuCl is based on the latter mechanism, which is illustrated in scheme 1. Starting soot oxidation with CuCl, the first step is oxygen activation on the surface of CuCl (R1). Transfer of activated oxygen (indicated by O*) occurs according to reaction R2. DRIFT analysis has shown that this results in the formation of Surface Oxygen Complexes (SOC), indicated by C-O$_s$*. Decomposition of the oxygen complexes results in the formation of CO and CO$_2$. (Surface) oxidation of CuCl has already been proposed in the seventies as an important step in the catalytic conversion of HCl to Cl$_2$, called the Deacon reaction (2), and also in the oxy-chlorination of *e.g.* ethene (3) [27]:

$$4 \, HCl + O_2 \quad \leftrightarrow \quad 2 \, Cl_2 + 2 \, H_2O \tag{2}$$

$$2 \, C_2H_4 + 4 \, HCl + O_2 \quad \leftrightarrow \quad 2 \, C_2H_4Cl_2 + 2 \, H_2O \tag{3}$$

The catalytic activity of CuCl$_2$ in these processes can be explained by reactions 4a (Deacon) or 4b (oxychlorination), followed by reactions 5 and 6:

$$2 \, CuCl_2 \quad \leftrightarrow \quad 2 \, CuCl + Cl_2 \tag{4a}$$

$$CuCl_2 + C_2H_4 \quad \leftrightarrow \quad 2 \, CuCl + Cl_2 \tag{4b}$$

$$4 \, CuCl + O_2 \quad \leftrightarrow \quad 2 \, Cu_2OCl_2 \tag{5}$$

$$Cu_2OCl_2 + 2 \, HCl \quad \leftrightarrow \quad 2 \, CuCl_2 + H_2O \tag{6}$$
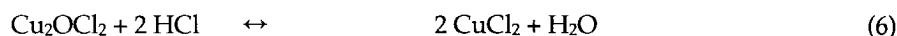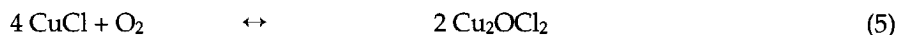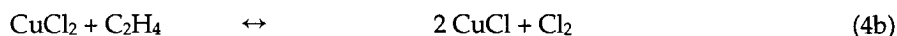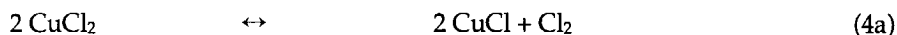
CuCl$_2$ is reduced to CuCl (reactions 4a and 4b) yielding Cl$_2$ or C$_2$H$_4$Cl$_2$, respectively. Subsequently CuCl is oxidized to the oxychloride (Cu$_2$OCl$_2$) under reaction conditions. After the formation of Cu$_2$OCl$_2$ (5), oxygen is transferred to hydrochloric acid (6), yielding water. However, bulk oxidation of CuCl does not occur during soot oxidation, as was discussed in paragraph 4.2. Instead, carbothermic (bulk) reduction of Cu$_2$OCl$_2$ occurs around 600 K (if this compound is applied as the starting material), yielding CuCl and CO and CO$_2$. Cu$_2$OCl$_2$ carbothermally reduces at lower temperatures than CuO (600 K *vs.* 685 K), and even in the presence of oxygen (figure 4). This indicates that a chlorine ligand affects the reducibility of CuO. Once CuCl is formed, it exerts its activity according to scheme (1). Starting soot oxidation with CuCl$_2$ results in a higher soot oxidation temperature, than starting with CuCl or Cu$_2$OCl$_2$, because decomposition of CuCl$_2$ (reaction (4a), *i.e.* reaction R5 in scheme (1)), which is essential for an efficient activation of oxygen (on CuCl), takes place at higher temperatures (>700 K).

Reaction R4 in scheme (1) indicates the possible decomposition of the active (oxy)chloride into the oxide and chlorine by reaction with the activated oxygen. For CuCl this reaction does not occur in the temperature region, where it is catalytically active (550-650 K). However, for other metal chlorides bulk oxidation occurs at

relatively low temperatures, even in the presence of soot, as was observed for $MoCl_5/MoO_3$. At these low temperatures transfer of activated oxygen to the carbon (soot) surface is not fast enough to compensate for reaction R4. $MoCl_5$ does not show an increased activity compared to the corresponding metal oxide in 'tight contact'. This observation indicates that redistribution of metal chlorides does not *per se* result in better contact than ball milling (in that case a higher activity for MoO_3 formed by decomposition of $MoCl_5$ was expected), as was argued in paragraph 4.2.

In the case of lead, the active phase present during soot oxidation (the metal chloride or the metal oxychloride), is dependent on the starting compound. Neither bulk reduction of Pb_2OCl_2, nor oxidation of $PbCl_2$ was observed. Apparently oxygen is activated both on Pb_2OCl_2 and on $PbCl_2$ which are stable at the temperatures where they perform their activity. Hence 'CuCl' in scheme (1) can be replaced either by '$PbCl_2$' or by 'Pb_2OCl_2'. The higher activity of Pb_2OCl_2 suggests better oxygen activation properties. Although surface reduction cannot be excluded, lattice oxygen of the latter compound is not consumed during soot oxidation, as was observed in the case of Cu_2OCl_2.

TG/DSC and DRIFT measurements have shown that BiOCl is not carbothermally reduced upon soot oxidation either. Hence, the catalytic activity might be explained by an activation of oxygen on the surface of BiOCl, followed by reactions R2 and R3.

Interestingly, the application of FeOCl leads to the formation of surface oxygen complexes, whereas catalytic soot oxidation by Fe_2O_3 does not result in the formation of those complexes [19]. This is another indication that chlorine chemically affects the catalytic soot oxidation activity of metal chlorides and that scheme (1) also holds for FeOCl.

Evaluating the experimental results, the high activity of metal (oxy)chlorides in the oxidation of soot is induced by their high mobility or volatility. However, several arguments, previously given, lead to the conclusion that chlorine ions are not only necessary for the establishment of 'tight contact', but also induce oxygen activation and/or facilitate transfer of the activated oxygen to the soot surface.

As can be deduced from this study, a major problem of the application of metal chlorides in soot oxidation is deactivation of the catalyst by evaporation and/or transformation of the active compounds. A detailed deactivation study of the Cu/K/Mo/Cl catalyst, which is based on the activity of CuCl, has confirmed that there is a progressive loss of catalytic material [4].

Another aspect of soot oxidation catalyzed by (copper)chlorides worthwhile mentioning is the possibility that carbon-chlorine bonds are formed by an oxychlorination like reaction. When this reaction is followed by reaction with oxygen, very toxic compounds can be formed. Luijk *et al.* [28] have demonstrated that during oxidation experiments of an activated carbon catalyzed by $CuCl_2$, a relatively small burn-off of the chlorinated carbon surface gives rise to the production of chlorinated compounds such as chlorobenzenes and chlorophenols. Especially chlorophenols are very reactive precursors in the formation of polychlorinated dibenzo-*p*-dioxines at

carbon surfaces. In this respect chlorine containing soot oxidation catalysts are less attractive for practical applications.

This study has shown a relationship between the melting point of catalytic active materials and the soot oxidation activity. In our group eutectic mixtures of several oxidic compounds (which do not contain chlorine) are currently tested for their 'loose contact' soot oxidation activity.

4.5. *Conclusions*

- Several metal (oxy)chlorides appear to be more active in the soot oxidation than their corresponding oxides in 'loose contact'. Especially these of Cu, Pb, Fe, and Bi are very active.
- The high activity of metal chlorides can be partially explained by the *in-situ* formation of intimate contact between the soot and the active metal chloride by 'wetting' or through the gas phase. Metal chlorides which, due to their high melting points, cannot 'wet' the soot surface (like $BaCl_2$, $CaCl_2$, $CoCl_2$, and $NiCl_2$) exhibit little activity. Metal chlorides which have a too high volatility ($HgCl_2$) did not show any catalytic activity.
- The catalytic activity of metal chlorides and metal oxychlorides can be further explained by the activation of oxygen, followed by a transfer of the activated oxygen to the soot surface, resulting in SOC formation. Finally SOC decomposition results in CO and CO_2 evolution.
- The application of metal chlorides as catalysts for diesel soot oxidation is questionable, because loss of activity by evaporation or decomposition of the active species are a severe problem.

4.6. *References*

[1] J.P.A. Neeft, Fuel Proc.Techn., 47 (1996) 1.
[2] T. Inui and A. Miyamoto, Catal.Today, 10 (1991) 45.
[3] E.S. Lox, B.H. Engler and E.Koberstein, Studies Surf. Sci. Catal., 71 (1991) 291.
[4] J.P.A. Neeft, 'Catalytic oxidation of soot-Potential for the reduction of diesel particulate emissions', Ph.D. Thesis TU Delft (1995), chapter 5 (Appl. Catal. B: Env. 8 (1996) 57).
[5] J. van Doorn, J. Varloud, P. Mériaudeau and V. Perrichon, Appl. Catal. B: Env. 1 (1992) 117.
[6] G. Mul, J.P.A. Neeft, F. Kapteijn, M. Makkee and J.A. Moulijn, Appl. Catal. B: Env. 6 (1995) 339.
[7] L. Singoredjo, 'Low temperature selective catalytic reduction (SCR) of nitric oxide with ammonia', Ph.D. Thesis University of Amsterdam (1992).
[8] L. Walter-Levy, A.M. Goreaud and M. Goreaud, Bull.Soc.Chim.France, (1970) 2789.
[9] F.W. Lamb and L.M. Niebylski, Anal.Chem. 23 (1951) 1388.
[10] Gmelins Handbuch der Anorganischen Chemie, 8. Auflage, Verlag Chemie, GMBH., Weinheim, Ni, 57 B (1966) 689.

[11] Gmelins Handbuch der Anorganischen Chemie, 8. Auflage, Verlag Chemie, GMBH., Weinheim, Co, 58 Erg. (1961) 544.

[12] Gmelins Handbuch der Anorganischen Chemie, 8. Auflage, Verlag Chemie, GMBH., Weinheim, Fe, 59 B (1932) 279.

[13] Gmelins Handbuch der Anorganischen Chemie, 8. Auflage, Verlag Chemie, GMBH., Weinheim, Bi, 19 Erg. (1964) 689.

[14] M.R. Lorenz and J.S. Prener, Acta Cryst. 9 (1956) 538.

[15] W. Biltz and W. Fischer, Z. Anorg. Chem. 166 (1927) 290.

[16] O. Knacke, O. Kubachewski and K. Hesselman, Thermochemical Properties of Inorganic Substances, Springer Verlag, Berlin, 1991.

[17] C. Morterra and M.J.D. Low, Spectroscopy Letters, 15(9) (1982) 689.

[18] Q.-L. Zhuang, T. Kyotani and A. Tomita, Energy & Fuels, 8 (1994) 714.

[19] G. Mul, F. Kapteijn and J.A. Moulijn, in Proceedings of 22nd Biennial Conference on Carbon, San Diego, USA, 1995, pp. 554-555.

[20] C.F. Ng, K.S. Leung and C.K. Chan, J. Catal. 78 (1982) 51.

[21] R.A. Nyquist and R.O. Kagel, Infrared Spectra of Inorganic Compounds, Academic Press, New York, 1971.

[22] Y.-G. Xie and Y.-Q. Tang, Adv. Catal. 37 (1990) 1.

[23] L. Walter-Levy and M. Goreaud, Bull. Soc. Chim. France, (1971) 444.

[24] D.W. McKee, J. Catal. 108 (1987) 480.

[25] R.T.K. Baker and J.J. Chludzinski Jr., Carbon 19 (1981) 75.

[26] T. Kyotani, S. Hayashi, A. Tomita, J.A. MacPee and R.R. Martin, Fuel 71 (1992) 655.

[27] J.A. Allen and A.J. Clark, Rev. Pure and Appl. Chem. 21 (1971) 145.

[28] R. Luijk, F. Kapteijn and H.A.J. Govers, Environmental Science & Technology, 28 (1994) 312.

5

A DRIFT spectroscopic study on the interaction of alkali metal oxides with carbonaceous surfaces

Abstract

An extensive DRIFT study on the catalytic oxidation of soot by K_2CO_3, K_2MoO_4, and the nitrates of the alkali metals (Na, K, Rb, and Cs), is described in this chapter. The spectra of potassium benzoate, potassium phenoxide, and catalytically oxidized fullerene C60 were recorded to enable the assignment of the various absorption bands. Alkali benzoate species are likely to be formed upon decomposition of the alkali metal precursors in air, as well as alkali metal oxide species attached to the carbon surface. Absorption bands in the 1100-1150 cm^{-1} region and around 620 cm^{-1} are assigned to CO_2, chemisorbed on the oxidic alkali metal species. A review of literature dealing with alkali catalyzed carbon gasification is presented, to validate this assignment. A strong absorption band around 1140 cm^{-1} has also been observed in the spectra of partially converted CaO/soot samples, which might also be related to chemisorbed CO_2.

5.1. *Introduction*

FT-IR and in particular Diffuse Reflectance Infrared Fourier Trans-formed (DRIFT) spectroscopy are powerful tools for the analysis of oxidic functionalities on carbonaceous materials. Several research groups have successfully analyzed coal using this technique, like *e.g.* [1-3]. Also *in-situ* studies regarding the oxidation of coal have been performed [4-6], as well as DRIFT studies on oxidized soot [7,8] and phenol formaldehyde (PF) resin chars [9]. The observed surface oxygen complexes (SOCs) are generally accepted to play an essential role in the oxidation mechanism.

Interactions between alkali metal oxides and SOCs have been proposed by *e.g.* [10-13]. Mims and Rose [11] used chemical methods to identify potassium containing species on the surface of carbonaceous materials by NMR (Nucleair Magnetic Resonance). The use of a methanation reaction resulted in a proposal for a catalytically active potassium complex, based on potassium phenoxide. Although a similar proposition for the active species has been postulated by Cerfontain and Moulijn [10], based on a spectroscopic study, the observed absorption frequencies are not quite consistent with reference compounds: potassium phenoxide functionalities were assigned to absorption frequencies located around 1100 cm^{-1}, whereas important frequencies of KOC$_6$H$_5$ occur at higher wavenumbers [14]. An exotic compound (C$_6$(OK)$_6$) has been proposed by Freriks *et al.* to explain spectroscopic observations [12]. Finally, various IR frequencies of impregnated potassium salts were assigned to (bi)carbonate species by Yuh and Wolf [13], but mechanistic details were not given. Concluding, an unambiguous interpretation of the spectra of alkali metal catalyzed carbon oxidation has not been presented, and especially the bands in the 1100-1200 cm^{-1} have not been properly assigned.

In this chapter, various spectra of the alkali metal catalyzed soot oxidation will be presented. A detailed description of the various infrared bands visible in the spectra of partially converted soot in the presence of alkali metal oxides, will be given. Assignments will be discussed with reference to spectra of model compounds and literature data. Additionally, several spectra of Ca-catalyzed soot oxidation will be presented and interpreted.

5.2. *Experimental*

Printex-U (a model soot, a gift from Degussa) was used to perform the oxidation studies. This model soot contains approximately 5 wt% of adsorbed hydrocarbons and only 0.2-0.4 wt% sulfur [15]. Sublimed fullerene C60 was purchased from Bucky USA, and used as received. Potassium phenoxide was synthesized by adding phenol (Aldrich, *p.a.*) to a stoichiometric amount of KOH (Baker) in water, followed by drying at 370 K in a rotating evaporator. A white crystalline material was obtained. Potassium benzoate was used as received from Aldrich. Analytical grades of the alkali metal nitrates and Ca(NO$_3$)$_2$.4H$_2$O (Aldrich, used without purification) were used to impregnate the soot. An amount of the nitrate, corresponding to 10 wt% of

the most stable oxide (Me_2O, in which Me is K, Na, Rb, and Cs, and CaO) was dissolved in 200 ml ethanol, followed by addition of 200 mg soot to the solution. Addition of small amounts of distilled water was necessary to entirely dissolve $RbNO_3$ and $NaNO_3$. Ethanol and added water, if any, was removed at 325 K under reduced pressure in a rotating evaporator. The black powder could be recovered by scratching it from the glass wall of the flask with a spatula. The samples will be referred to as alkali impregnated soot. SEM micrographs of the impregnated samples were recorded after preparation on adhesive tape, which is electrical conductive. The BET-surface area of Printex-U, determined by N_2 adsorption at 77 K, before and after impregnation, amounted to approximately 100 $m^2.g^{-1}$.

Physical mixtures were prepared by ball milling various potassium salts with soot or Fullerene C60 in a ratio of 2:1 (wt%) for one hour in an agate ball mill to establish 'tight contact' conditions [16].

Partial conversion of the impregnated samples was accomplished isothermally at 575 K in the so-called six-flow reactor setup [16]. A six-flow experiment was carried out by filling five quartz reactors (one reactor was used as a blank), with approximately 25 mg of the impregnated soot/metal nitrate mixture, sandwiched between two pieces of quartz wool and a small layer of SiC. A controlled flow of 150 ml/min 10 vol% O_2 in Ar was led through the reactors. The alkali metal nitrates were decomposed *in-situ*: calcination after impregnation had not been performed. The amount of soot converted was determined by integration of the CO- and CO_2 concentrations. After reaction SiC was separated from the soot sample before spectroscopic analysis. Ozonation of soot and a K_2MoO_4/soot mixture was performed as described elsewhere [17] (chapter 7 of this thesis).

DRIFT spectra were recorded on a Nicolet Magna 550 spectrometer, equipped with a DTGS detector and a Spectratech DRIFT 'Collector' accessory. *Ex-situ* spectra of the partially converted soot samples were recorded after dilution in KBr by adding 256 scans at a resolution of 8 cm^{-1} against a (*non*-converted) soot in KBr background. *In-situ* spectra were obtained in a compatible Spectratech high temperature cell. The high temperature oxidation studies of model compounds (potassium phenoxide and -benzoate) were performed in KBr, whereas the K_2MoO_4 catalyzed and *non*-catalytic oxidation of fullerene C60 was accomplished without KBr dilution.

The K_2MoO_4/C60 mixture was investigated by *in-situ* X-Ray Diffraction at the Fritz Haber Institut in Berlin. Diffractograms were recorded within two hours on a STOE diffractometer with Cu-$K\alpha$ radiation.
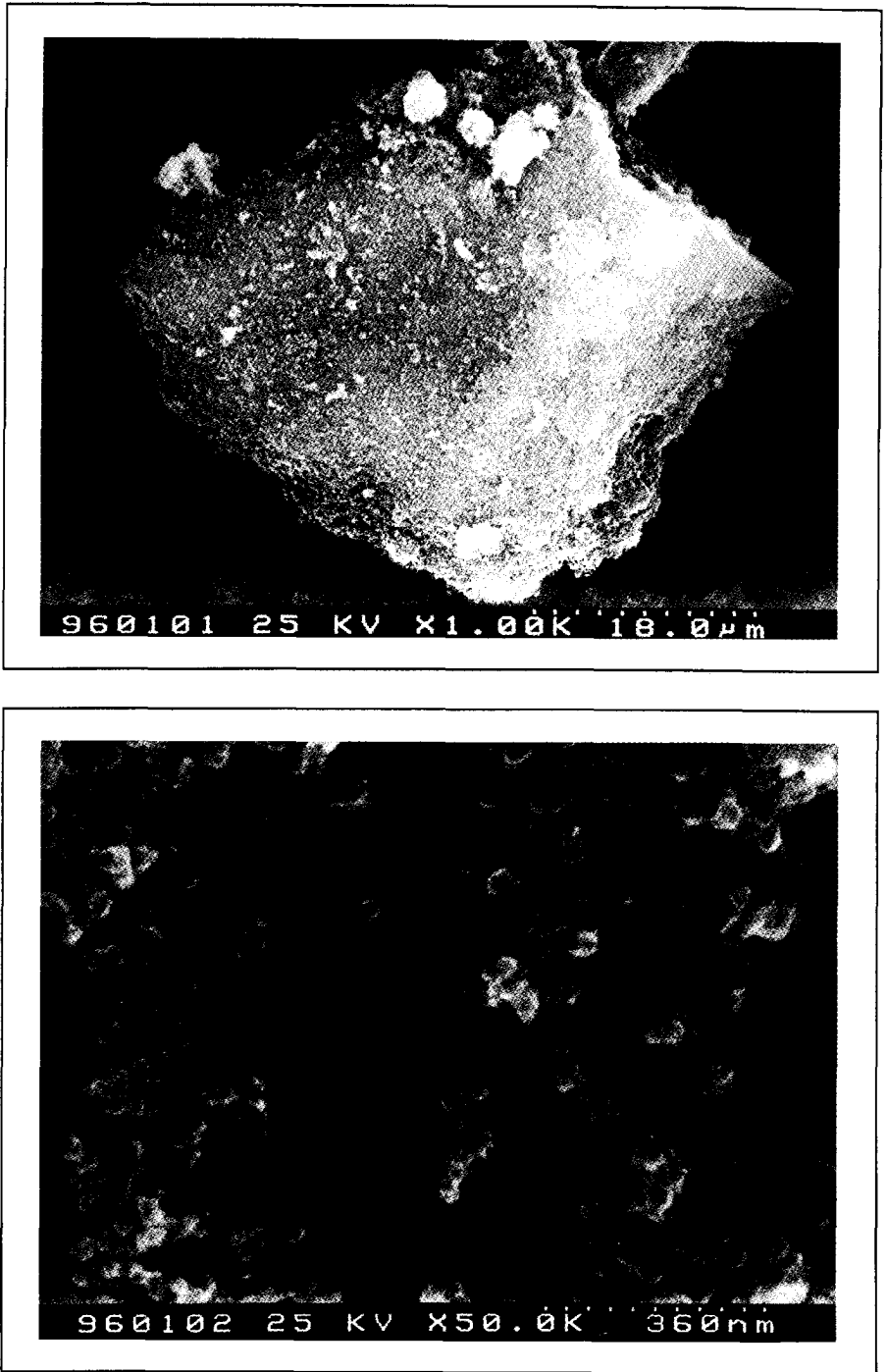
Figure 1. *SEM micrographs of KNO₃ impregnated soot. Magnification as indicated on the micrographs.*

5.3. *Results*

5.3.1. *Morphology of the samples*

SEM micrographs of the K-impregnated soot sample, taken at low and high magnification, are presented in figure 1. The elementary soot particles, clearly visible at high magnification, are encapsulated by crystalline KNO_3 after impregnation and drying: large chunks of sample, containing both KNO_3 and soot are visible at low magnifications. After partial decomposition of KNO_3 in either air or nitrogen, the morphology of the sample hardly changed.

5.3.2. *DRIFT analyses.*

DRIFT spectra of partially converted alkali metal impregnated soot samples are shown in figure 2. Each sample was allowed to react in air up to a soot conversion level of 80 %. An overview of the observed absorption frequencies is given in Table 1.
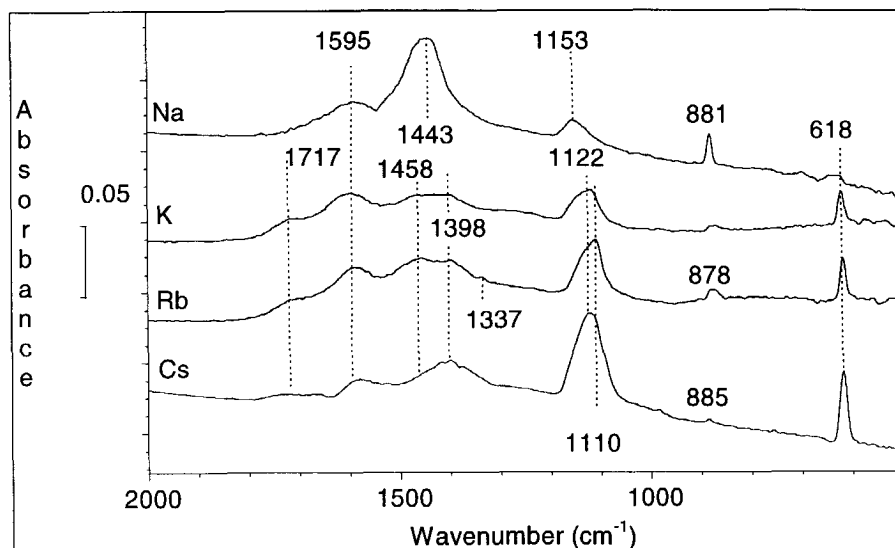
Figure 2. *DRIFT spectra of partially converted Na-, K-, Rb- and Cs-impregnated Printex-U samples at 575 K in 10% O_2 in Ar. The soot conversion level amounts to approximately 90% for all the investigated samples. The spectra have been shifted vertically to enable a better comparison.*

Several absorption frequencies, different from those observed in spectra of non-catalytically oxidized soot (1250, 1605 and 1735 cm^{-1}) [9], can be observed. The relative intensity of the absorption bands in the 1100-1150 cm^{-1} region, located at approximately 1398 cm^{-1}, and located at 620 cm^{-1} seems to increase in the series Na<K<Rb<Cs.

Table 1. *Absorption frequencies observed in the DRIFT spectra of partially converted soot by impregnated alkali metal nitrates.*

Sodium	Potassium	Rubidium	Cesium
--	1717	1717	--
1595	1595	1595	1595
1443	1458	1458	1420
--	1398	1398	1398
--	--	1337	1370
1153	1110	1110	1122
881	880	878	885 (small)
621	618	618	618

The contribution of the 1450 cm^{-1} and 881 cm^{-1} bands seems to decrease in this series. Furthermore, the 1398 cm^{-1} and 1100-1150 cm^{-1} bands seem to be composed of more than one single frequency.

The development of the spectral features of the K-impregnated sample as a function of the carbon conversion level, is shown in figure 3. The spectrum at 0% burn-off corresponds quite well to the spectrum of pure KNO_3: the 1384 cm^{-1} band can be assigned to a nitrato stretching vibration [18]. In the spectrum of the 50% converted sample, the 1384 cm^{-1} vibration is no longer present: the nitrate has decomposed. The increasing absorptions located at 1719 cm^{-1}, 1590 cm^{-1}, and around 1279 cm^{-1} show that SOCs are formed in the presence of potassium (oxide) species. The 1131 cm^{-1} (1119 cm^{-1}) and 620 cm^{-1} bands simultaneously increase with burn-off: they are likely to be induced by the same chemical structure. The spectrum recorded at >90% burn-off shows additional absorptions at 1456, around 1400, and 885 cm^{-1}. Partial conversion of physical K_2CO_3/soot or K_2MoO_4/soot mixtures results, besides the absorptions of the anions, in similar spectral features as shown in figure 3. Apparently, the potassium salts act as precursors for the formation of similar potassium (oxide) species. The spectrum of a K_2MoO_4/soot mixture after ozonation at 355 K for 30 minutes is shown in figure 4 (spectrum A). The spectrum of ozonized soot is shown for comparison (spectrum B). The spectra are significantly different, indicating that interactions between potassium species and SOCs are present. The observed absorption frequencies around 1600 cm^{-1} and 1124 and 623 cm^{-1} correspond quite well to those observed in figure 3. Additionally, a medium absorption band is located at 1381 cm^{-1}, whereas the 1456 cm^{-1} band is not present. The absorptions located at 880 cm^{-1} and 689 cm^{-1} can be assigned to lattice vibrations of K_2MoO_4. The spectral features of ozonized soot (absorptions located at 1726, 1617 and 1232 cm^{-1}) will be extensively discussed in chapter 7.
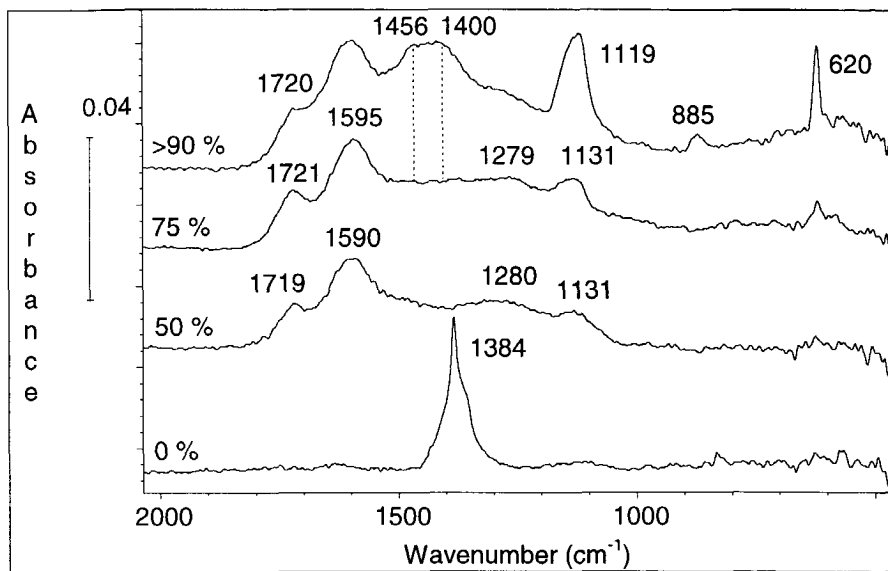
Figure 3. DRIFT spectra of K-impregnated samples at 0 %, 50 %, 75 %, and >90% burn-off, converted at 575 K in 10% O_2 in Ar
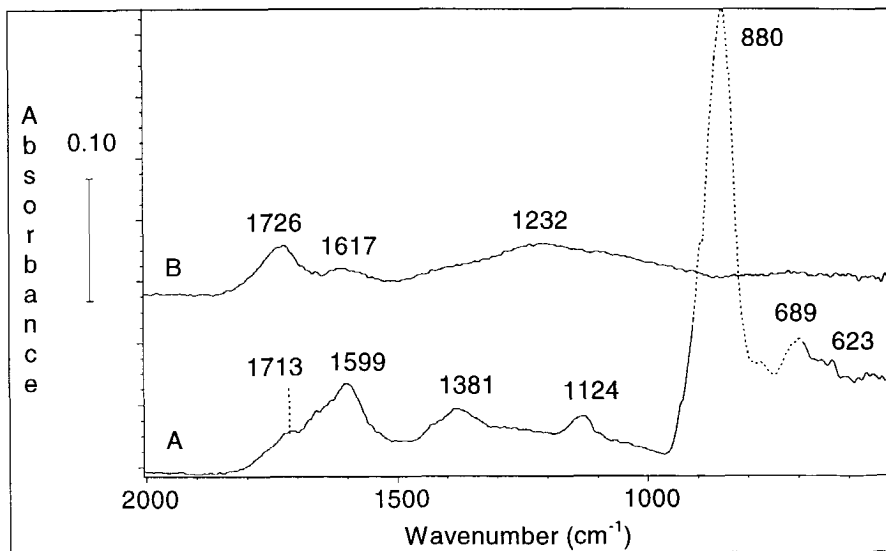

Figure 4. The IR spectrum of a physical K_2MoO_4/soot mixture, ozonized at 355 K for 30 minutes in 10% ozone in oxygen (Spectrum A). The spectrum of soot, treated under similar conditions, is shown for comparison (Spectrum B).

The spectra of partially converted $Ca(NO_3)_2.4H_2O$/soot samples are shown in figure 5. After preparation several absorptions occur in the 500-2000 cm^{-1} region of the spectrum, due to nitrate vibrations (1384, 1046 and 838 cm^{-1}). The broad band located at 1433 cm^{-1} is also present in the DRIFT spectrum of pure $Ca(NO_3)_2.4H_2O$. The absorption band at 1635 cm^{-1} can be assigned to the O-H bending mode of water of crystallization in $Ca(NO_3)_2.4H_2O$ [19]. After 20% soot conversion at 575 K, still some nitrate is present. The 1433 cm^{-1} band has broadened and a new vibration, located at approximately 1579 cm^{-1}, can be observed. At higher conversions (50% and >90% burn-off) the vibrations due to the nitrato groups have disappeared.
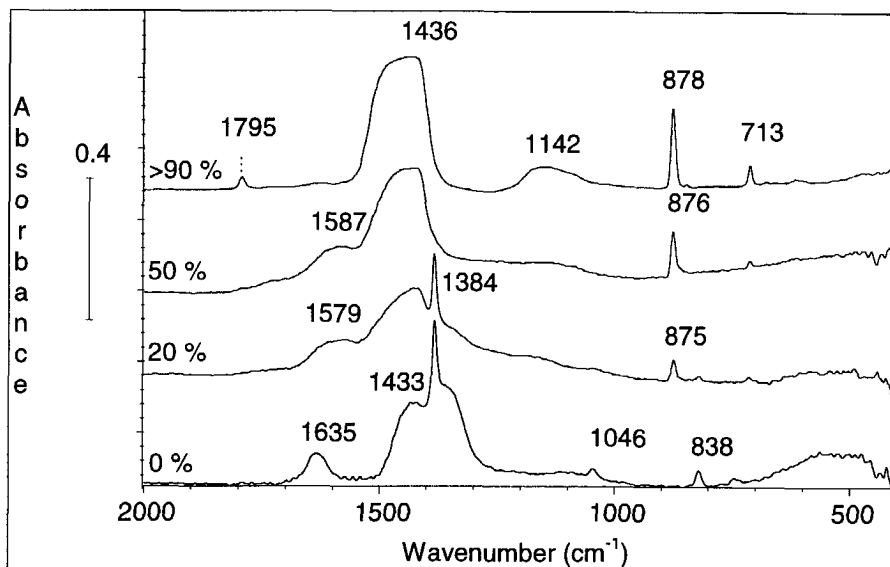
Figure 5. DRIFT spectra of Ca-impregnated soot, at 0%, 50%, 75% and >90% burn-off, converted at 585 K in 10% O_2 in Ar. The spectra were shifted vertically, to enable a better comparison.

Absorptions at 713 cm^{-1}, 875 cm^{-1}, centered at 1436 cm^{-1}, and at 1795 cm^{-1} can be ascribed to $CaCO_3$ [16,19,20]. The 1579 cm^{-1} band is located at 1587 cm^{-1} in the spectrum recorded at 50% burn-off. Also a broad absorption band, which might be composed of two separate ones, starts to develop at 1142 cm^{-1}. This band is clearly visible in the spectrum of >90% soot conversion. In the latter spectrum, the 1587 cm^{-1} vibration is no longer present.

5.3.3. Fullerene C60 oxidation

Fullerene C60 is convenient for spectroscopic analysis, because it has a low overall extinction coefficient, allowing the collection of high quality spectra without KBr dilution.
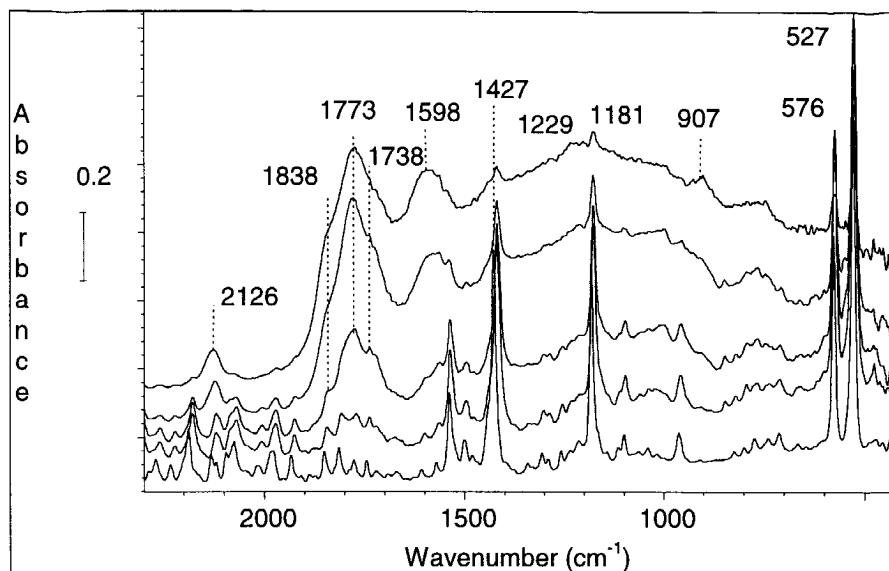
Figure 6. In-situ DRIFT analysis of the non-catalytic oxidation of Fullerene C60 in air at 575 K. Spectra were recorded every 5 minutes (bottom to top): the spectral development was established within 25 minutes.

In chapter 2 it has already been discussed that *in-situ* studies performed in KBr at elevated temperatures might result in interactions between KBr and surface oxygen complexes (SOCs). An *in-situ* DRIFT analysis of the uncatalyzed oxidation of fullerene C60 is shown in figure 6. The spectral development is in close agreement to that reported by Wohlers [21,22]. The four vibrational modes of C60, located at 1427, 1181, 576 and 527 cm^{-1}, are clearly visible. The spectral changes have been ascribed to the formation of several oxygenated species. Typical vibrations are located at 1838, 1773, 1738, 1598, around 1229 and 907 cm^{-1}, which can be assigned to C=O stretching vibrations, C=C ring stretch of (poly)aromatic compounds, and C-O-C stretching modes [22-26].The small absorption band at 2126 cm^{-1} is related to CO intercalated in the fullerene molecule [22]. The spectral observations correspond well to those of ozonized soot: ozone is required to obtain highly oxidized species on the soot surface at relatively low temperatures [27]. To prevent the possible interference of carbonato or nitrato vibrations of either K_2CO_3 or KNO_3, with spectral details of oxidized C60, K_2MoO_4 was used to perform an *in-situ* DRIFT analysis of the catalytic C60 oxidation. The spectra are shown in figures 7a and 7b. Absorption frequencies at 1698 cm^{-1}, 1599 cm^{-1}, 1358 cm^{-1}, 777 cm^{-1} and 709 cm^{-1} are shown to increase with time, and are significantly different from the absorptions shown in figure 6: the 1599 cm^{-1} band has a relatively higher intensity in the K_2MoO_4 catalyzed C60 oxidation than in the uncatalyzed reaction (compare figure 6). The strong 900 cm^{-1} absorption is caused by lattice vibrations of K_2MoO_4. In figure 7b, decomposition of the species

formed at 675 K is witnessed by decreasing intensities at 1590 cm^{-1}, 1362 cm^{-1}, 711 cm^{-1} and 777 cm^{-1}. After reaction, the spectrum shows only minor absorptions at 1138 cm^{-1} and 618 cm^{-1}.
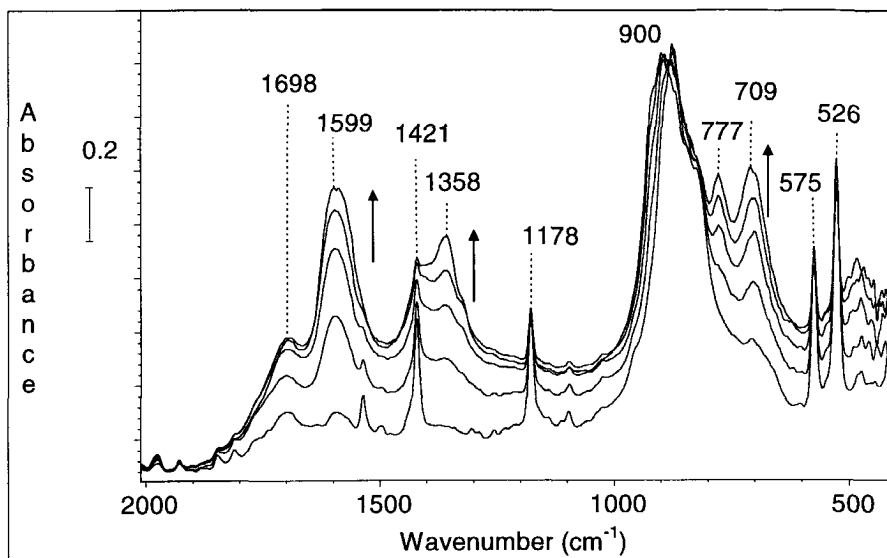
Figure 7a. *Development of the spectral features of fullerene C60 upon oxidation in air, catalyzed by K$_2$MoO$_4$ at 625 K. Spectra were recorded (bottom to top) after 0, 5, 10, 15, and 45 minutes, respectively.*
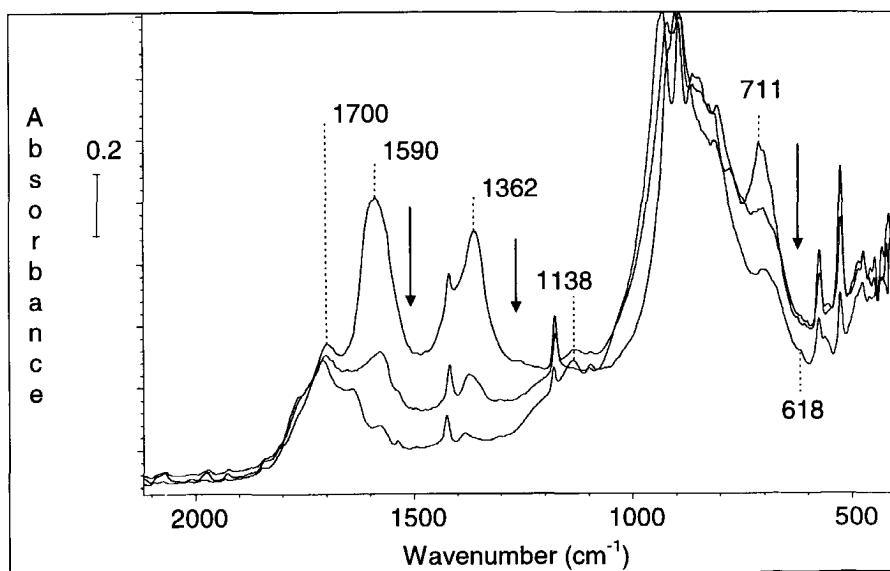
Figure 7b. *Continuation of figure 7a. Spectra were recorded (top to bottom) at 675 K (after 65 minutes), at 725 K (after 85 minutes) and at 475 K (after reaction).*
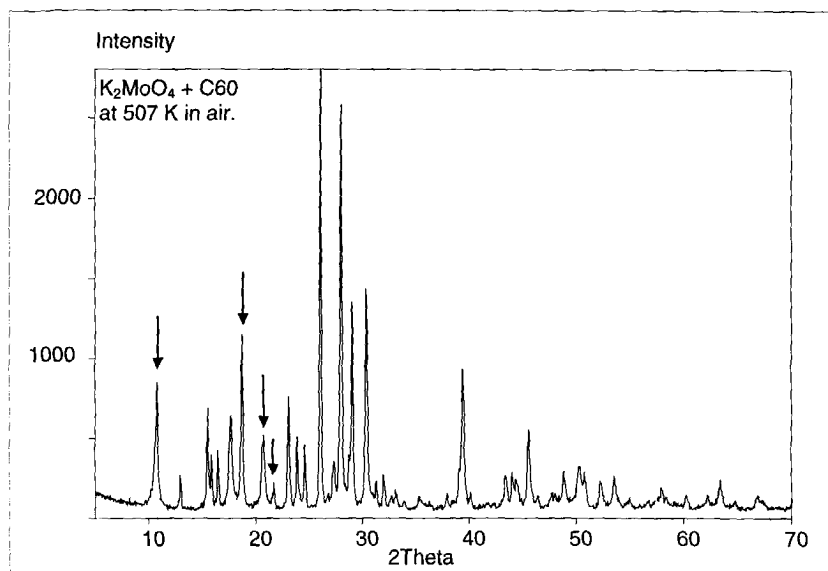
Figure 8a. X-Ray Diffractogram of a mixture of K_2MoO_4 (low temperature modification) and C60 (indicated by the arrows) recorded in air at 507 K.
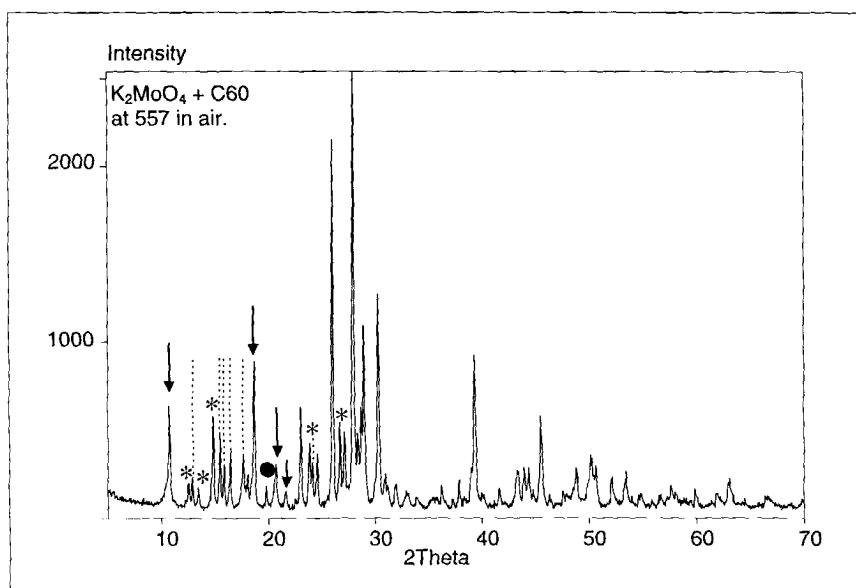
Figure 8b. X-Ray Diffractogram of a mixture of K_2MoO_4 (low temperature modification, and high temperature modification (●)) and C60 (indicated by the arrows), recorded in air at 557 K. $K_2Mo_2O_7$ is indicated with asterisk.
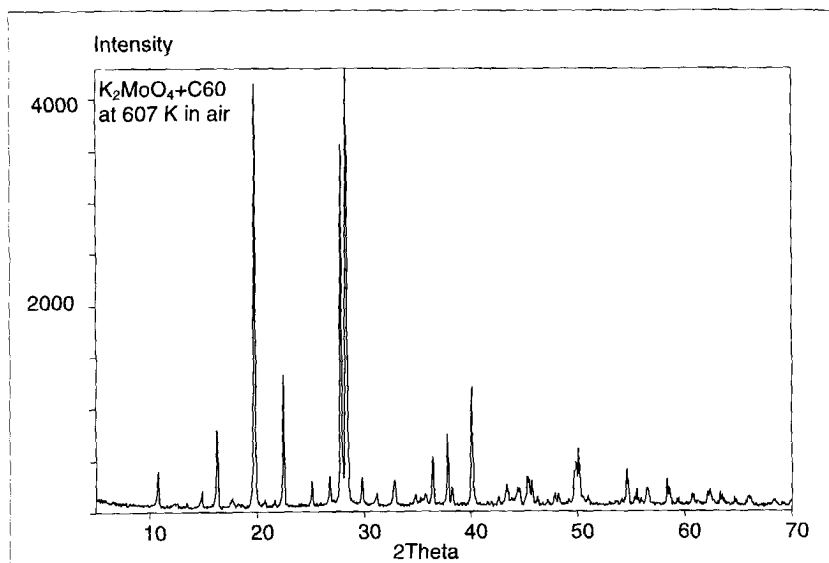
Figure 8c. *X-Ray Diffractogram of the high temperature modification of K_2MoO_4, recorded in air at 607 K.*

Table 2. *XRD data of fullerene C60.*

2 Θ	Intensity (%)
10.8192	100
17.7154	99.3
20.8037	88.2
21.7383	16.9
27.4543	8.8
28.1806	13.6
30.9311	14.6
32.8586	15.7

The K_2MoO_4 catalyzed oxidation of fullerene C60 was also followed by *in-situ* XRD using temperature intervals of 50 K in the range of 507-657 K. The diffractograms are shown in figures 8a-8c. The major diffraction lines of C60 are given in table 2 and indicated with an arrow in figure 8a. Figures 8a-8c show the transformation of the low temperature modification of K_2MoO_4 into the high temperature modification at approximately 600 K. The transition of these phases was also noticed by Caillet [28], who performed thermogravimetric analyses of potassium molybdates. The diffractograms of the low temperature and high temperature modifications correspond excellently with data published in the Joint Committee on

Powder Diffraction Files (JCPDF), files [29-1021] and [23-0489]. The diffractogram shown in figure 8a only contains the lines of the low temperature modification of K_2MoO_4 and C60. The relative intensity of the K_2MoO_4 line at $2\Theta = 26.22$ has increased, compared with JCPDF [29-1021], which might be caused by the presence of C60 or the milling procedure. Major differences can be observed in the diffractogram recorded at 557 K. Several new lines, located at 2Θ values of 12.66, 13.63, 14.97, 24.43, 26.98 and 27.45 (indicated by an asterisk in figure 8b) can be identified, which are assigned to $K_2Mo_2O_7$ (JCPDF [36-0347]). A small amount of the high temperature modification of K_2MoO_4 is also present (indicated with a ● at $2\Theta =$ 19.982). At higher temperatures only the diffraction lines of the high temperature modification of K_2MoO_4 can be observed. $K_2Mo_2O_7$ is no longer observed.

5.3.4. DRIFT analysis of potassium phenoxide and -benzoate.

The DRIFT spectrum of potassium benzoate is shown in figure 9. Major absorptions are located at 1591 (C=C stretch), 1549 (antisymmetric C=O stretch), 1394 (symmetric C=O stretch), 837 cm^{-1} (C-O stretch) and 708 cm^{-1} (-C=C- ring deformation) [29,30]. The spectrum of benzoic acid is shown for comparison. The strong 1686 cm^{-1} (C=O stretch), 1325, 1291 (C-O-C) and 930 cm^{-1} bands are characteristic for aromatic acid dimers (chapter 1) [25].

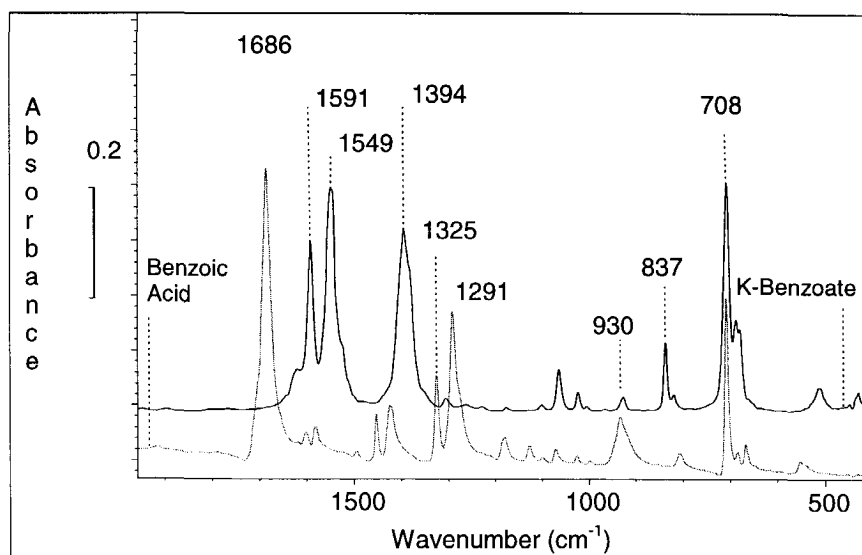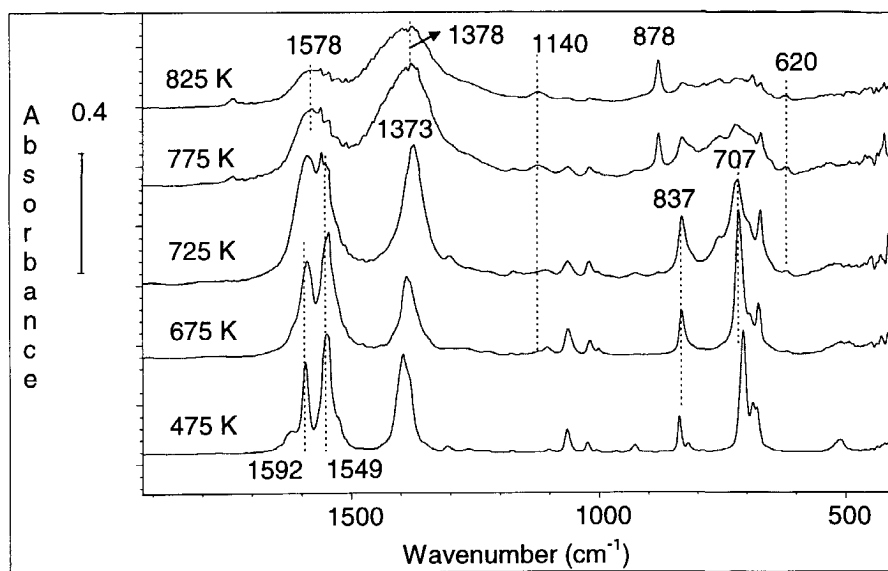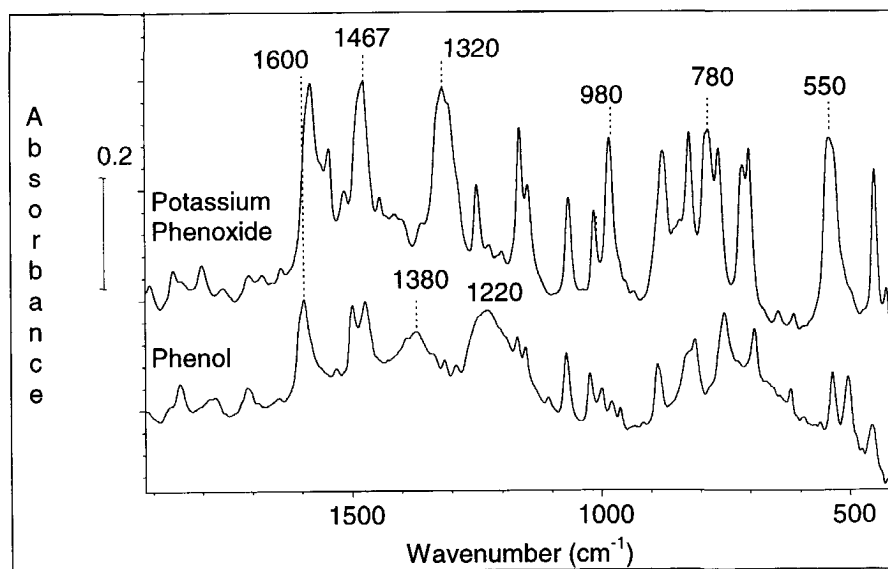*Figure 9.* DRIFT spectra of benzoic acid and potassium benzoate, recorded at 300 K in air.

Figure 10. In-situ DRIFT spectra of potassium benzoate recorded at 475, 675, 725, 775 and 825 K in air (bottom to top). The sample was diluted with KBr.

Figure 11. The IR spectra of phenol and potassium phenoxide, recorded at 325 and 350 K, respectively. The samples were diluted with KBr.

The spectral features of potassium benzoate with increasing temperature are shown in figure 10. The spectra were recorded at 475, 675, 725, 775 and 825 K, respectively. The 1592 and 1549 bands convolute into one broad band centered around 1578 cm^{-1}. The 1394 cm^{-1} band shifts to 1378 cm^{-1} and broadens. After an initial increase, the 707 cm^{-1} band decreases with temperature, as well as the 837 cm^{-1} band. A new absorption frequency at 878 cm^{-1} is visible in the spectra recorded at 775 K and 825 K. Moreover, small absorptions can be found at 1140 cm^{-1} and 620 cm^{-1}. The spectral changes are likely to be caused by carbonization (i.e. the formation of polyaromatic compounds, 1578 cm^{-1}), decomposition of the oxygen functionalities and the formation of K_2CO_3 (878 cm^{-1} and broad band around 1378 cm^{-1}).

The spectrum of potassium phenoxide (350 K) is compared with that of phenol (recorded 325 K) in figure 11. Major bands in the phenoxide spectrum are located at 1467, at 1320, around 980, 780 and 550 cm^{-1}, in agreement with the spectra of Davies and Jones [31]. The 1600 cm^{-1}, 1380 cm^{-1} and 1220 cm^{-1} bands in the spectrum of phenol have been assigned to aromatic C=C stretching, O-H bending, and C-O stretching vibrations, respectively [25].

5.4. *Discussion*

5.4.1. Interpretation of the various DRIFT spectra.

An extended review of IR spectra of oxidized carbon films, including the effects of ion exchange with potassium salts, has been published by Zawadski [30]. A decrease in absorption intensity at 1720 cm^{-1}, an increase at 1590 cm^{-1} and the formation of a 1380 cm^{-1} band have been observed upon ion exchange. These bands were assigned to C=O in carboxylic acids (COOH, 1720), and asymmetric COO$^-$ (1590) and symmetric COO$^-$ (1380) vibrations, respectively [26, 30]. By treatment of the ion exchanged sample with HCl, the original acidic structures were observed (the 1380 cm^{-1} band disappeared and the 1590 cm^{-1} band decreased). Although the studies described by Zawadski were performed to elucidate the acidity of carboxylate groups, and not focused on catalytic phenomena, several spectra presented in this chapter correspond to those published by Zawadski. Partially converted alkali metal impregnated soot samples (figure 2, Table 1), show minor absorptions at 1717, and additional absorptions at 1595 and around 1400 cm^{-1}. These absorptions can be perfectly assigned to potassium benzoate species. The spectra of potassium benzoate and partially converted fullerene C60 in the presence of K_2MoO_4, corroborate the formation of (potassium) benzoate species (compare figures 7b, 9 and 10). The relative low intensity of the benzoate bands in the spectra of partially converted alkali metal containing soot samples might be related to an alkali metal induced decomposition of benzoate species [3,4,33,34]. Otake and Jenkins [35] showed that Na$^+$ exchanged acidic functionalities decomposed at significantly lower temperatures than the original acidic structures.

The broad absorption bands around 1400 cm^{-1} (figure 2) seem to consist of more than a single frequency. Besides benzoate species, carbonato stretching vibrations of

anhydrous alkali metal-carbonates also contribute to the 1400-1480 cm^{-1} absorptions [19,20,36]. Carbonate formation is confirmed by the bending vibrations of the free carbonate ion around 880 cm^{-1} in the spectra of partially converted Na-, Rb- and K-samples. Anhydrous Cs_2CO_3 is hardly formed (figure 2), which is in agreement with the results of Cerfontain, who found a decreasing order in the series Na, K, and Cs for the amount of anhydrous carbonate formed upon CO_2 gasification of carbon. The intensity of the 1110-1153 cm^{-1} band was found to increase in this series [10]. Although the gasification conditions (CO_2, higher temperatures) are quite different from this study, the results of Cerfontain are in excellent agreement with the spectra of figure 2.

An assignment of the 1110-1153 cm^{-1} band to potassium phenoxide species has been proposed [10,12]. However, strong vibrations in the spectrum of potassium phenoxide occur around 1320, 980, 780 and 550 cm^{-1} (figure 11), which are not present in the spectra of alkali catalyzed soot oxidation. Furthermore, Cerfontain [10] and Freriks [12] did not record their spectra below 1000 cm^{-1}, so they were unable to detect the 620 cm^{-1} band. In our opinion this absorption is related to the 1118 cm^{-1} band, because of the simultaneous increase with conversion (figure 3). Although C-O-C (ether like) vibrations occur in the 1100-1200 region [4], the absence of such vibrations in the spectra of non-catalytically oxidized soot [17], disagrees with an assignment to ether functionalities. In fact the 1265 cm^{-1} vibration is ascribed to ether like functionalities [9,37]. Although the spectrum of potassium sulfate contains vibrations in the 1100-1200 cm^{-1} region, formation of this compound is neither likely, as the amount of sulfur initially present in the soot (Printex-U) is low. Moreover, the sulfate-ion has a more complex IR pattern than shown in figure 2 [18].

The interactions between carbon black particles and potassium carbonate in physical mixtures have been studied by Saber [38,39]. Carbonate decomposition already started at 500 K. Using $K_2^{13}CO_3$, Saber concluded that carbon surface oxygen complexes also started to decompose at this temperature. Furthermore, a fast oxygen exchange between gas phase CO_2 and the formed potassium species was observed. The dispersed potassium oxide species are suggested to bind to the surface *via* oxygen linkages [38,39]. Cerfontain [32] noticed that, above 773 K, interaction of CO_2 with the species formed after carbonate decomposition resulted in the formation of the IR band at 1110 cm^{-1}. Meijer [40] also extensively studied impregnated alkali/carbon samples. A strong adsorption of CO_2 on the prepared samples was observed, which could not be removed in an Helium atmosphere below 675 K. However, in the presence of $^{13}CO_2$ or $C^{18}O_2$, exchange of gas-phase CO_2 for chemisorbed CO_2 occurred, as well as oxygen exchange [45]. Knözinger [41], Davydov [42] and Hair [43] describe the IR frequencies of chemisorbed CO_2 and carbonate species, and Ogden those of the alkali metal carbonates isolated in a N_2 matrix [44].

Table 3. *Overview of the vibrational modes of the carbonate ion [47].*

K_2CO_3	Carbonate ion (cm^{-1})	Type [47]	Assignment [47]
1471	1420-1470	v_3	C-O asym. stretching
	1020-1090	v_1	C-O sym. stretching
870	860-880	v_2	CO_3 out of plane deformation
	680-750	v_4	In plane deformation

Table 4. *Overview of the vibrational modes of a covalently bound carbonato group [41-44,47].*

Unidentate CO_3 (cm^{-1})	Bidentate CO_3 (cm^{-1}) [IIIa]	Bidentate CO_3 (cm^{-1}) [IIIb]	Bicarbonate (cm^{-1})	Dimethyl Carbonate (cm^{-1})	Type [47]
1470-1530	1590-1630	1620-1670	1290-1410	1760	v_4
1300-1370	1250-1270	1220-1270	1260-1270	1280	v_1
1040-1080	1020-1030	980-1020	990-1050	969	v_2
			830-840	793	v_6
670-690	660-680	660-680	695-705		v_3 or v_5

Table 5. *Assignment of the vibrational modes of a covalently bound carbonato group [47].*

Type [47]	Assignment [47]
v_4	Asymmetric stretching
v_1	CO_2 symmetric stretching
v_2	CO stretch
v_6	Non-planar rock
v_3	CO_2 bending
v_5	Planar rock
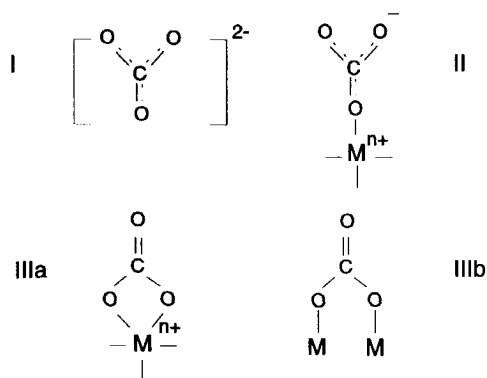
Figure 12. *Chemical forms of CO_2 adsorbed on oxide surfaces [45].*

The 1020-1090 cm^{-1} vibration (symmetric C-O stretch) is IR forbidden in the CO_3^{2-} ion, but becomes IR active in the monodentate or bidentate configuration [42]. The asymmetric C=O stretch and symmetric C=O stretch of chemisorbed CO_2 induce different absorption frequencies [43]: the degree of separation of these frequencies is dependent on the type of ligand formation, and the metal-oxygen bond. The separation is less in the case of a monodentate complex, compared to a bidentate complex. A completely covalent bond, present in dimethyl carbonate, causes an increase in band separation up to 480 cm^{-1}.

Unfortunately, literature dealing with carbonate complexes, is usually focused on transition metal oxides, (carbonates may be important intermediates in the oxidation of CO [42]), whereas alkali metal oxides have not been addressed. Furthermore, the 618 cm^{-1} vibration is usually not observed and/or discussed, as lattice vibrations of transition metal oxides occur in this spectral region. Cerfontain [10,32] and Yuh [13] do not discuss the possible contribution of chemisorbed CO_2 to the spectral features, and, because of experimental limitations, these authors were unable to detect the 618 cm^{-1} band.

After evaluation of the spectral data and mechanistic proposals published in the literature, the 1120 and 620 cm^{-1} absorptions are likely to be the result of chemisorbed CO_2 (formed during soot oxidation [45]), strongly interacting with a potassium oxide (K_2O) cluster attached to the carbon surface (as proposed in [46]). However, the assignment of these absorptions is not straight forward. If a bidentate configuration is considered, a contribution of chemisorbed CO_2 to the 1595 cm^{-1} absorption (v_4), previously assigned to benzoate species, has to be assumed. A large splitting of 440-485 cm^{-1} (1595 (v_4) *vs.* 1153-1110 cm^{-1} (v_1)) can then be calculated. As the broad 1119 cm^{-1} band shown in figure 2 seems to contain an 1140 cm^{-1} contribution, it can be speculated that the higher frequency is caused by configuration IIIa and the lower by configuration IIIb: the two metal atoms concerned in structure IIIb will exert a greater influence on the splitting of vibrations than the single metal atom postulated in IIIa. The relatively low frequency of the bending vibration of bidentate species (620 cm^{-1} vs. 660-680 [41]) might be explained by a strong interaction of the alkali metal ion with chemisorbed CO_2. However, the conspicuous absence of v_2, and a lack in intensity correlation between the 1595 (v_4) and the 1153-1110 cm^{-1} (v_1) band, do not agree with this assignment.

Based on the apparent increase of the 1398 cm^{-1} band in figures 2 and 3, compatible to the 1120 and 620 cm^{-1} bands, this band might be related to chemisorbed CO_2, although it was previously assigned to benzoate species. Based on the location of the bands, an assignment to monodentate CO_2 might be given (v_4 = 1595 cm^{-1}, v_1 = 1398 cm^{-1}, v_2 = 1120 cm^{-1}, and v_3 or v_5 = 620 cm^{-1}). A multiple character of the v_2 vibration has been observed in the spectra of cobalt-carbonato complexes [47]. Unfortunately, the relative intensity of the bands in our spectra is not in agreement with literature data: the v_2 vibration is usually small compared to the v_4 and v_1 vibrations, whereas the opposite is observed in the spectra of figures 2 and 3.

Concluding, the 1120 and 620 cm^{-1} bands are likely to be related to chemisorbed CO_2, but further research is needed to clarify the specific assignment to certain vibrational modes.

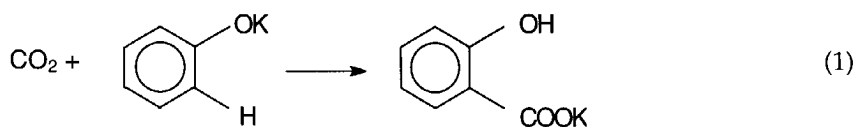It was expected that the compound causing the 1110-1153 cm^{-1} and 618-621 cm^{-1} absorptions, would have been formed upon potassium catalyzed C60 oxidation and potassium benzoate decomposition as well. However the spectra given in figures 7b and 10 hardly show these absorption frequencies: only a small shoulder on the 711 cm^{-1} band and a small absorption at 1138 cm^{-1} can be detected in figure 7b. Apparently a high intensity of these vibrations, *i.e.* a high concentration of chemisorbed CO_2, is related to the presence of soot.

The described interactions between soot, alkali metal catalysts and CO_2, can also be used to explain the spectrum of the ozonized K_2MoO_4/soot sample: benzoate species as well as chemisorbed CO_2 can be observed.

The absorption band around 1142 cm^{-1} in the DRIFT spectrum of the $Ca(NO_3)_2$/soot sample at 90% burn-off, might be related to the 1118 cm^{-1} absorption band observed in the alkali metal oxide spectra: besides carbonate formation, chemisorbed CO_2 on a CaO surface, is proposed to be present. The exact chemical structure of the CaO-species formed, remains to be elucidated.

5.4.2. Interactions of K_2MoO_4 with Fullerene C60.

If the *in-situ* DRIFT spectra of the K_2MoO_4 catalyzed fullerene C60 oxidation are evaluated with respect to the assignments given by Zawadski [30], the spectra of potassium benzoate and the XRD data of figures 8a-8c, the formation of potassium benzoate, and, to a less extent, CO_2, chemisorbed on oxidic potassium clusters, occurs upon K-catalyzed C60 oxidation. $K_2Mo_2O_7$ formation was observed in the X-Ray diffractograms and might explain the absorption band around 770 cm^{-1} in the spectra shown in figures 7a and 7b. The involvement of the so-called Kolbe reaction in the formation of the benzoate species (proposed by Cerfontain [32]), *i.e.* the initial formation of phenoxides, followed by incorporation of CO_2 in the structure (reaction 1), cannot be confirmed by the various spectra presented.

$$CO_2 + \quad \text{(benzene ring with OK and H substituents)} \longrightarrow \text{(benzene ring with OH and COOK substituents)} \qquad (1)$$

$K_2Mo_2O_7$ recrystallizes into K_2MoO_4 after decomposition of the C60-(CO)-OK intermediates (benzoates) into CO_2. CO is less likely to be formed, as intercalation of CO in the C60 cages was not observed [22].

The formation of benzoates and potassium oxide clusters is likely to be related to the relative stability of the potassium salt precursor. Segregation of K_2O from K_2CO_3 (yielding CO_2), from K_2MoO_4 (yielding $K_2Mo_2O_7$) or KNO_3 (yielding NO and NO_2)

are needed to obtain the highly active species. Simultaneously, interaction of potassium ions with surface oxygen complexes and chemisorption of CO_2 on the clusters is likely to occur. This will be further discussed in chapter 6.

5.5. Conclusions.

- Alkali benzoate species are likely to be formed upon conversion of alkali metal-impregnated soot samples in air. Various absorption bands similar to those observed in the spectra of potassium benzoate have been identified in the DRIFT spectra of partially converted, alkali metal impregnated soot.
- CO_2, chemisorbed on alkali metal oxide species, is suggested to cause the absorptions around 1100-1150 cm^{-1} and 620 cm^{-1}. Spectroscopic evidence for the formation of phenoxides was not found.
- $K_2Mo_2O_7$ has been identified in *in-situ* XRD experiments of K_2MoO_4 catalyzed C60 oxidation, corroborating the possible formation of (non-crystalline) oxidic clusters and potassium benzoate species.

5.6. References.

[1] N.R. Smyrl and E.L. Fuller, Appl. Spectrosc. 41 (1987) 1023.
[2] E.L. Fuller and N.R. Smyrl, Appl. Spectrosc. 44 (1990) 451.
[3] B.J. Meldrum and C.H. Rochester, J.Chem.Soc.Faraday Trans. 86 (1990) 1881.
[4] B.J. Meldrum and C.H. Rochester, J.Chem.Soc.Faraday Trans. 86 (1990) 2997.
[5] C.H. Rochester and B.J. Meldrum, J.Chem.Soc.Faraday Trans. 86 (1990) 861.
[6] B.J. Meldrum, J.C. Orr and C.H. Rochester, J. Chem. Soc. Chem. Commun. (1985) 1176.
[7] J.A. Jassim, H.P. Lu, A.R. Chughtai and D.M. Smith, Appl.Spectrosc. 40 (1986) 113.
[8] M.S. Akhter, A.R. Chughtai and D.M. Smith, Appl.Spectrosc. 45 (1991) 653.
[9] Q.-L. Zhuang, T. Kyotani and A. Tomita, Energy & Fuels (1994) 714.
[10] M.B. Cerfontain and J.A. Moulijn, Fuel 62 (1983) 256.
[11] C.A. Mims and K.D. Rose, J.Am.Chem.Soc. 104 (1982) 6886.
[12] I.L.C. Freriks, H.M.H. Wechum, J.C.M. Stuiver and R. Bouwman, Fuel 60 (1981) 463.
[13] J.Y. Yuh and E.E. Wolf, Fuel 62 (1981) 252.
[14] M.B. Cerfontain and J.A. Moulijn, in Proceedings of the International Conference on Coal Science, 1983, pp. 419-422.
[15] F. Kapteijn, L. Singoredjo, A. Andreini and J.A. Moulijn, Appl. Catal. B: Env. 3 (1994) 173.
[16] J.P.A. Neeft, 'Catalytic oxidation of soot-Potential for the reduction of diesel particulate emissions', Ph.D. Thesis TU Delft (1995).
[17] G. Mul, J.P.A. Neeft, F. Kapteijn and J.A. Moulijn, in preparation.
[18] S.D. Ross, Inorganic Infrared and Raman Spectra, McGraw-Hill Book Company, London, 1972.
[19] R.A. Nyquist and R.O. Kagel, Infrared Spectra of Inorganic Compounds, Academic Press, New York, 1971.
[20] W. Sterzel and E. Chorinsky, Spectrochim. Acta, 24A (1968) 353.
[21] M. Wohlers, A. Bauer and R. Schloegl, Microchim. Acta, (1996) submitted.

[22] M. Wohlers, H. Werner, D. Herien, T. Schedel-Niedrig, A. Bauer and R. Schloegl, Synthetic Metals, 77 (1996) 299.

[23] C. Morterra and M.J.D. Low, Spectrosc. Lett., 15 (1982) 689.

[24] G. Cardini, R. Bini, P.R. Salvi, V. Schettino, M.L. Klein, R.M. Strongin, L. Brard and A.B. Smith, J. Phys. Chem. 98 (1994) 9966.

[25] R.T. Conley, Infrared Spectroscopy, Allyn and Bacon, Boston, 1972.

[26] G. Mul, chapter 1 of this thesis.

[27] G. Mul, chapter 2 of this thesis.

[28] P. Caillet, Bull.Soc.Chim.de France, 12 (1967) 4750.

[29] J.H.S. Green, W. Kynaston and A.S. Lindsey, Spectrochim. Acta, 17 (1961) 486.

[30] J. Zawadski, Chem. Phys. Carbon, 21 (1989) 147.

[31] M. Davies and R.L. Jones, J. Chem. Soc. 42 (1954) 121.

[32] M.B. Cerfontain and J.A. Moulijn, Fuel, 65 (1986) 1349.

[33] A.M. Vassallo, Y.L. Liu, L.S.K. Pang and M.A. Wilson, Fuel, 70 (1991) 635.

[34] B.J. Meldrum and C.H. Rochester, Fuel, 70 (1991) 57.

[35] Y. Otake and R.G. Jenkins, Carbon, 31 (1993) 109.

[36] C.J.H. Schutte and K. Buijs, Spectrochim. Acta, 17 (1961) 921.

[37] G. Mul, J.P.A. Neeft, F. Kapteijn, M. Makkee and J.A. Moulijn, in Proceedings of 22nd Biennial Conference on Carbon, San Diego, 1995, pp. 650-651.

[38] J.M. Saber and J.L. Falconer, J. Catal. 90 (1984) 65.

[39] J.M. Saber, J.L. Falconer and L.F. Brown, Fuel, 65 (1986) 1356.

[40] R. Meijer, B. van der Linden, F. Kapteijn and J.A. Moulijn, Fuel, 70 (1991) 205.

[41] H. Knözinger, Adv. Catal. 25 (1976) 234.

[42] A.A. Davydov, Infrared Spectroscopy of Adsorbed Species on the Surface of Transition Metal Oxides, John Wiley & Sons, New York, 1990.

[43] M.L. Hair, Infrared Spectroscopy in Surface Chemistry, Marcel Dekker Inc. New York, 1967.

[44] J.S. Ogden and S.J. Williams, J. Chem. Soc. Dalton Trans. (1981) 456.

[45] R. Meijer, 'Kinetics and Mechanism of Alkali-Catalyzed Gasification of Carbon', PhD Thesis, University of Amsterdam, 1992.

[46] J.A. Moulijn and F. Kapteijn, Carbon, 33 (1995) 1155.

[47] B.M. Gatehouse, S.E. Livingstone, R.S. Nyholm, J. Chem. Soc. (1958) 3137.

Acknowledgement.

6

The feasibility of potassium catalysts for the catalytic oxidation of diesel soot

Abstract

Several isothermal oxidation profiles of the potassium catalyzed soot oxidation are presented. Impregnated samples, as well as physical mixtures have been investigated. The initial oxidation activity was found to depend on the intensity of contact between soot and catalyst, the dispersion of the catalyst and the stability of the potassium anion: in physical mixtures, the soot oxidation activity increases in the series KNO_3 < K_2MoO_4 < K_2CO_3. Decomposition of the precursors is suggested to yield similar active species, which are presumably oxidic clusters. NO_x negatively affects the oxidation rate of potassium impregnated soot at relatively low temperatures (< 600 K), which is explained by chemisorption of NO_2 and KNO_3 formation. Above 675 K, nitrate formation does not occur, and the soot oxidation rate is enhanced by a contribution of the 'C'/NO_2 reaction to the overall reaction rate. CO positively affects the potassium catalyzed soot oxidation rate, irrespective of the reaction temperature. This is tentatively explained by the formation of a slightly lower oxidation state of the active oxidic potassium cluster, which prevents deactivation by NO_2 and/or CO_2 adsorption. Nonetheless, the use of potassium-based catalysts for the catalytic removal of soot from diesel exhaust is not feasible because of (i) a very low 'loose contact' soot oxidation activity, (ii) a low NO and CO oxidation activity, and (iii) a possible deactivation by NO_2 or CO_2 chemisorption at diesel exhaust temperatures.

6.1. *Introduction*

The application of potassium salts in the catalytic gasification of carbonaceous materials has received considerable attention, mainly because of its potential application in commercial coal gasification processes [2]. Especially K_2CO_3 catalyzed carbon gasification has been extensively studied in the 80's and 90's by e.g. Cerfontain and Moulijn [3,4], Meijer *et al.* [5-7], Mims *et al.* [8,9], Saber *et al.* [10,11], and McKee [12].

Several mechanisms have been proposed to explain the action of potassium catalysts in catalytic carbon gasification by CO_2 and H_2O. Mechanisms based on either electronic interactions or a transfer of oxygen have been put forward [13]. The former mechanism is based on the formation of covalent M-C bonds (M is the alkali metal), and weakening of C-C bonds adjacent to C(O) functionalities. The latter facilitates CO desorption [13,14]. However, little experimental results corroborate this mechanism, whereas convincing evidence has been put forward in favour of an oxygen transfer mechanism. The application of isotopically labelled compounds in combination with TPD, TPR, and transient experiments appeared to be very effective. The active species is proposed to be an alkali metal oxide cluster [5-7, 28] attached to the carbon surface, although chemical interactions between potassium and oxygen containing functionalities on carbonaceous materials have also been observed [1,15,16, 28].

This study describes the catalytic activity of potassium salts in the low temperature oxidation of soot in O_2. The activities of impregnated samples and physical mixtures are compared. Furthermore, the effects of CO and NO_x on the oxidation activity (in O_2) are presented, and the observed phenomena will be explained. Finally, the results will be evaluated with respect to the application of potassium catalysts for the removal of soot particulates from diesel exhaust.

6.2. *Experimental*

Printex-U, a model soot kindly provided by Degussa, was used to perform the oxidation studies. This soot contains approximately 5 wt% of adsorbed hydrocarbons and only 0.2-0.4 wt% sulfur [17]. KNO_3 and $RbNO_3$ were used as received from Aldrich and impregnated on Printex-U as described elsewhere [1]. The activity of the impregnated samples was determined either with or without a thermal pretreatment in N_2 at 875 K for 120 min. The BET surface area of the KNO_3 impregnated sample, determined by N_2 adsorption at 77 K, before, and after thermal pretreatment, contributed to about 100 $m^2.g^{-1}$.

Physical mixtures of soot and various potassium salts (K_2MoO_4, KNO_3 (Aldrich) and K_2CO_3 (Baker)) were prepared in a catalyst to soot ratio of 2:1 by weight, by ball milling for one hour in an agate ball-mill. These samples will be referred to as 'tight contact' samples. 'Loose contact' samples were prepared by simply shaking the catalyst and Printex-U in a sample bottle. The oxidation temperatures of the physical

mixtures were determined by TG/DSC analysis [17,18]. The total amount of sample introduced in the thermobalance was adjusted to 2 mg soot each measurement. The sample was diluted with SiC upto 60 mg, to prevent thermal runaways.

The so-called six-flow equipment [17] was used to collect oxidation profiles in 10% O_2/Ar, either with or without 1080 ppm CO and/or 1000 ppm NO, respectively. Introduction of 1000 ppm NO into the 10% O_2/Ar stream resulted in a partial conversion of NO into NO_2. A gas composition of 650 ppm NO and 350 ppm NO_2 was obtained, which will be referred to as 1000 ppm NO_x throughout this paper. Apparently, NO oxidation (yielding NO_2) is catalyzed by the stainless steel tubing used in the six-flow reactor setup. This is schematically shown in figure 1. After interaction of the NO_x/O_2/Ar mixture with soot, the NO concentration increased to about 800 ppm, which will be further discussed in paragraph 6.3.2. A continuous flow of 150 ml/min was led through each reactor. A non dispersive infrared detector (Hartmann & Braun Uras 10 E) was used to measure the CO, CO_2, and NO concentrations alternately every 90 seconds within 12 seconds. A multiposition valve (Valco) selected the reactor for analysis. The experimental results are presented by plotting the reaction rate in $\mu g.g_{initial}^{-1}.s^{-1}$ as a function of soot conversion.
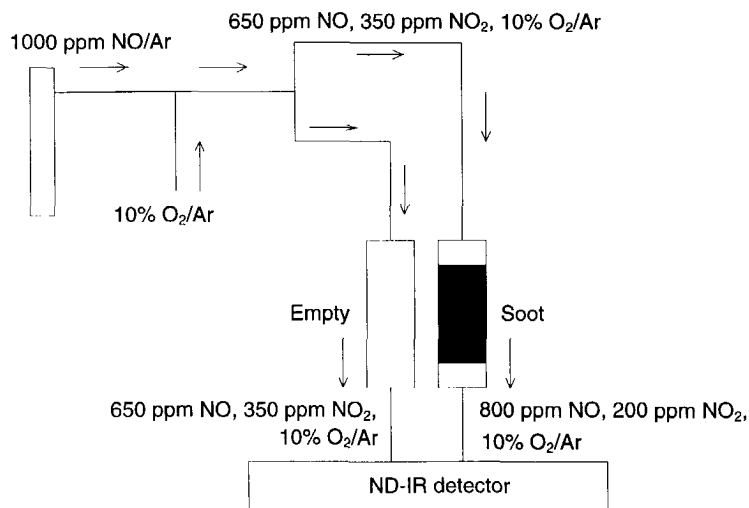
Figure 1. Schematic representation of the various NO/NO$_2$ concentrations in the six-flow reactor setup.

Before every experiment, an initial amount of 20 mg soot was introduced in each reactor. Hence, the total amount of a sample was dependent on the catalyst/soot ratio (22.2 mg for the impregnated samples and 60 mg for the physical mixtures). The impregnated and 'tight contact' catalyst/soot mixtures were homogeneously mixed

with 400 mg SiC and introduced in the reactor, sandwiched between two pieces of quartz wool. The 'loose contact' samples were introduced in the reactor, sandwiched between two layers of 200 mg SiC and two pieces of quartz wool. An overview of the performed isothermal experiments, including temperature and gas composition, is given in table 1. DRIFT spectra of various samples were recorded as described elsewhere [1].

Table 1. Experimental conditions of the measurements performed in the six flow reactor setup.

Catalyst	Contact	Cat./Soot Ratio	Temperature	Gas Comp.
----	----	Only soot	675 K	10% O_2/Ar
----	----	Only soot	675 K	10% O_2/Ar, 1000 ppm CO
----	----	Only soot	675 K	10% O_2/Ar, 1000 ppm NO
----	----	Only soot	675 K	10% O_2/Ar, 1000 ppm CO and NO
KNO_3	Impreg.	10 wt% K_2O	575 K	10% O_2/Ar
$RbNO_3$	Impreg.	10 wt% Rb_2O	575 K	10% O_2/Ar
KNO_3	Impreg.	10 wt% K_2O, Pretr.*	550 K	10% O_2/Ar
KNO_3	Impreg.	10 wt% K_2O, Pretr.*	550 K	10% O_2/Ar, 1000 ppm CO
KNO_3	Impreg.	10 wt% K_2O, Pretr.*	550 K	10% O_2/Ar, 1000 ppm NO
KNO_3	Impreg.	10 wt% K_2O, Pretr.*	550 K	10% O_2/Ar, 1000 ppm CO and NO
K_2CO_3	tight	2:1	550 K	10% O_2/Ar
K_2CO_3	tight	2:1	550 K	10% O_2/Ar, 1000 ppm NO
K_2CO_3	loose	2:1	550 K	10% O_2/Ar, 1000 ppm NO
K_2MoO_4	tight	2:1	550 K	10% O_2/Ar
K_2MoO_4	loose	2:1	675 K	10% O_2/Ar, 1000 ppm NO

*   Pretr. indicates that the measurement was performed after pretreatment of the sample in N_2 at 675 K for 120 minutes.

Soot was non-catalytically converted in 10% O_2 in N_2 at 775 K, 10 % NO_2 in Ar at 575 K, pure N_2O at 825 K and 10% O_3 in O_2 at 360 K [19]. DRIFT analyses of the partially converted soot samples was performed as described elsewhere [1]. Impregnated KNO_3/soot samples, before and after partial conversion in N_2, in 10% O_2/Ar, or in 10% O_2/Ar containing 1000 ppm NO_x (Table I), were also analyzed.

6.3. Results

6.3.1. Activity measurements in air

Metal oxide catalyzed soot oxidation profiles have been divided into three catogories [17,32], which are schematically shown in figure 2. An <u>exponential decay-type profile</u> is defined by a rapidly decreasing reaction rate as a function of soot conversion in the intial stage of the reaction, followed by a relatively low oxidation rate at higher conversion levels. If the reaction rate is less rapidly declining, and a monotonically decreasing reaction rate as a function of soot conversion is obtained,

the oxidation profile is defined as a <u>constant-type profile</u>. Also profiles which are distinguished by a clear plateau in the reaction rate, as indicated in figure 2C, are classified as a <u>constant-type profile.</u> Finally, <u>rising-type profiles</u> are characterized by an increasing reaction rate at a certain soot conversion level. This classification will be used throughout this chapter, as well as in chapters 9 and 10 of this thesis.

Reaction
Rate
$(\mu g.g_{initial}^{-1}.s^{-1})$
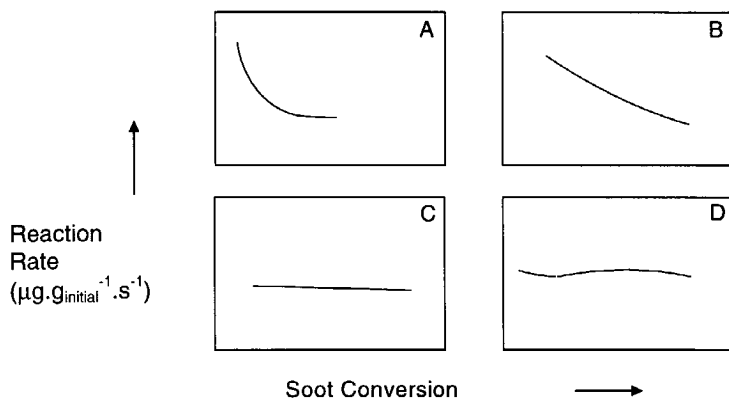
Soot Conversion

Figure 2. Schematic representation of the classi-fication of soot oxidation profiles [32]: Exponential decay-type (A), Constant-type (B and C) and Rising-type (D) profiles.
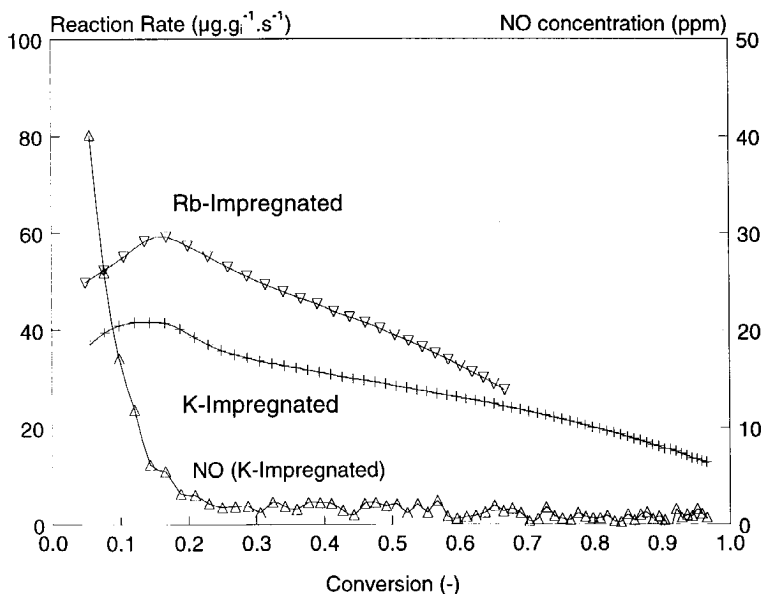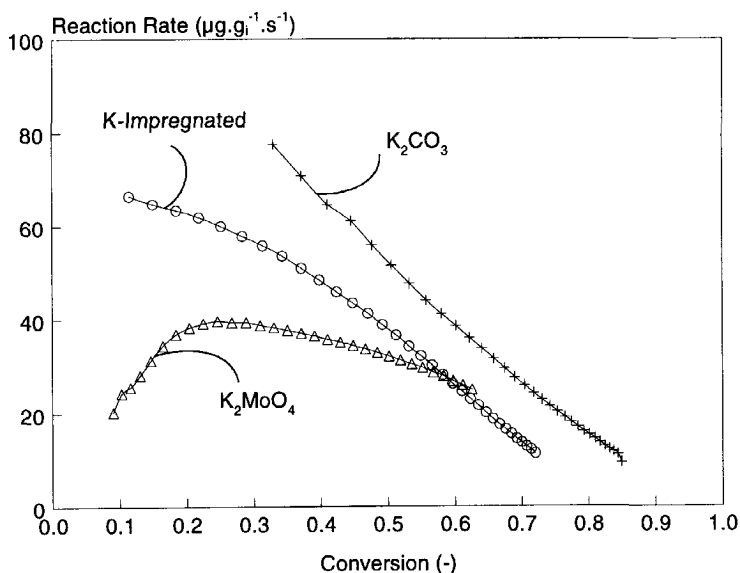

Figure 3. The soot oxidation profiles of K-impregnated and Rb-impregnated samples, without pretreatment in 10% O₂/Ar at 575 K. The concentration of NO, formed by decomposition of KNO₃, is also shown.

Figure 4. *Isothermal oxidation profiles of K-impregnated soot after pretreatment in N_2 at 675 K for 120 min, and of 'tight contact' K_2MoO_4/soot and K_2CO_3/soot mixtures at 550 K in 10% O_2 in Ar.*

The oxidation profiles of impregnated KNO_3/soot and $RbNO_3$/soot samples (without pretreatment) in 10% O_2/Ar are shown in figure 3. Decomposition of KNO_3 is witnessed by the evolution of NO. The NO concentration rapidly decreases as a function of soot conversion, accompanied by a slowly increasing reaction rate. As soon as nitrate decomposition has been completed, the reaction rate linearly decreases as a function of soot conversion. $RbNO_3$ and the other alkali metal nitrates show similar profiles. Decomposed $RbNO_3$ shows a higher catalytic activity than decomposed KNO_3 despite of its lower molar loading.

The oxidation profiles of pretreated KNO_3-impregnated soot, and 'tight contact' physical mixtures of K_2CO_3 and K_2MoO_4 with soot are compared in figure 4. The activity of KNO_3-impregnated soot is increased by the thermal treatment, as can be deduced from the oxidation profiles shown in figures 3 and 4: a higher initial reaction rate (65 *vs* 40 $\mu g.g_{initial}^{-1}.s^{-1}$) is obtained after pretreatment. The reaction rate of the K_2CO_3/soot sample shows a linear decay with conversion (*i.e.* a constant-type profile), whereas the oxidation profile of the K_2MoO_4/soot sample exhibits a rising-type profile.

The effect of the anion on the initial catalytic activity of potassium salts was also investigated by TG/DSC analyses, of which the results are summarized in figure 5.
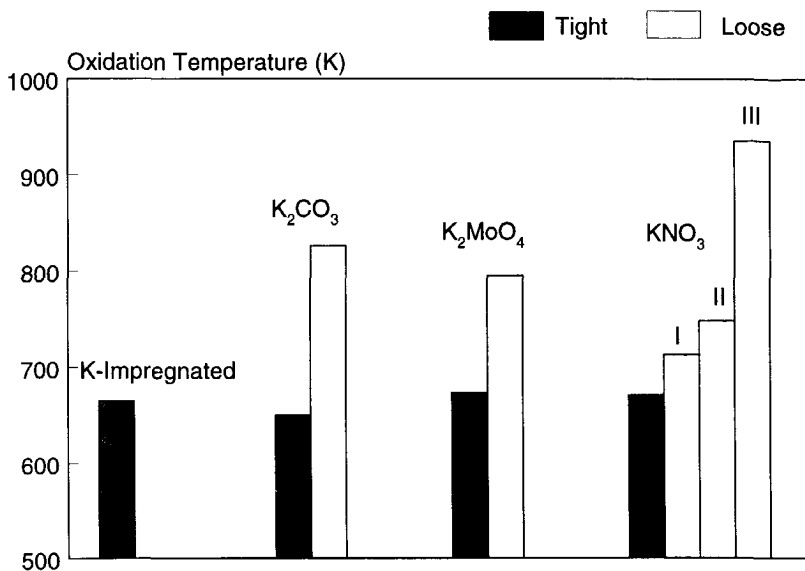
Figure 5. Oxidation temperatures in air of various potassium salts in tight and 'loose contact' as determined by TG/DSC analysis [17]. Legend as indicated. For the KNO₃/soot mixture, three DSC maxima were observed (I, II and III).

The TG/DSC results agree with the activity profiles shown in figure 4: decreasing 'tight contact' activities in the series K_2CO_3 > K-impregnated (after pretreatment) > K_2MoO_4 > KNO_3 are found. Another activity order is found in 'loose contact'. The carbonate and molybdate catalysts loose their activity, whereas the nitrate remains reasonably active. Three maxima were found in the DSC profile of the 'loose contact' KNO_3/soot mixture. The third exothermal heat effect, located at 940 K, indicates thermal decomposition of bulk KNO_3.

6.3.2. The effects of NO_x and CO on the non-catalysed soot oxidation rate

The effect of the gas composition (see table I) on the non-catalyzed soot oxidation rate has been studied at 675 K. The isothermal oxidation profiles are shown in figure 6. The oxidation profile in 10% O_2 in Ar shows a rather fast decay in reaction rate up to a conversion level of 0.2, after which it levels off to approximately 2 $\mu g.g_{initial}.s^{-1}$. The oxidation rate is considerably increased by the presence of 1000 ppm NO_x in the oxidizing medium. An initial decrease is followed by a constant reaction rate of 12 $\mu g.g_{initial}.s^{-1}$ up to a conversion level of 0.9, after which it rapidly declines to zero.
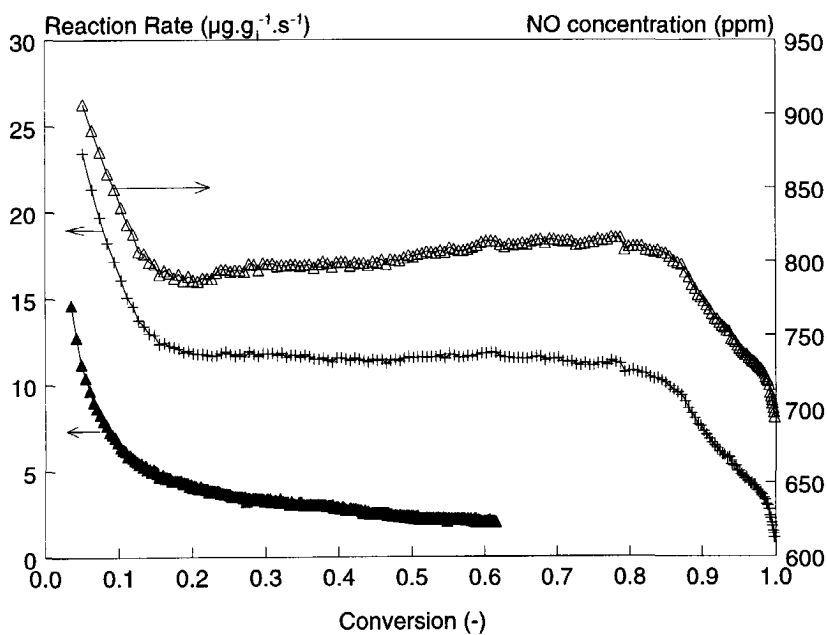
Figure 6. Non catalytic soot oxidation at 675 K in the absence (▲) and in the presence of NO_x (+). The NO concentration is indicated with an (Δ).
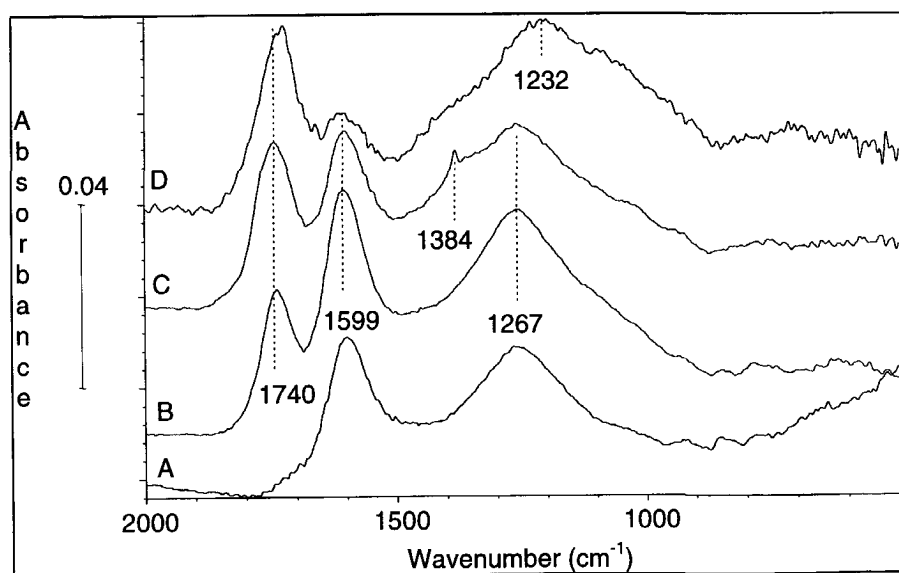
Figure 7. DRIFT spectra (8 cm^{-1}, 256 scans) of partially converted soot samples in pure N_2O (900 minutes at 825 K) [A], 10% O_2 in N_2 (60 min at 775 K) [B], 10 % NO_2 in Ar (60 min at 575 K) [C] and 10% O_3 in O_2 (30 minutes at 360 K) [D].

Addition of 1000 ppm CO did not affect the oxidation profile, nor the overall oxidation rate. The effect of the oxidizing medium on the formation of oxygen complexes on the soot surface (SOC), is shown in figure 7. Absorption bands around 1740, 1599 and 1267 cm^{-1} (1230 cm^{-1} for the ozonized sample) are clearly visible. The intensity of the 1740 cm^{-1} band increases relative to the 1600 cm^{-1} band (with decreasing pretreatment temperature), in the series $N_2O < O_2/N_2 < NO_2/Ar < O_3/O_2$. The spectrum of the sample treated in 10% NO_2 in Ar, contains a small band at 1384 cm^{-1}, which was not observed in the other spectra.

6.3.3. The effects of NO_x and CO on the oxidation rate of KNO_3 impregnated soot

The effects of NO_x and CO on the oxidation rate of KNO_3 impregnated soot (after pretreatment) are shown in figure 8a. NO_x negatively affects the oxidation rate. The activity is somewhat enhanced by the presence of 1000 ppm CO. The oxidation profile is significantly altered by the addition of CO <u>and</u> NO_x to the oxidizing medium: a high oxidation rate is observed in the beginning of the reaction, which is rapidly decreasing up to a soot conversion level of approximately 0.2. A slowly diminishing oxidation rate is observed at higher conversions. The corresponding development of the NO and CO concentrations is shown in figure 8b.
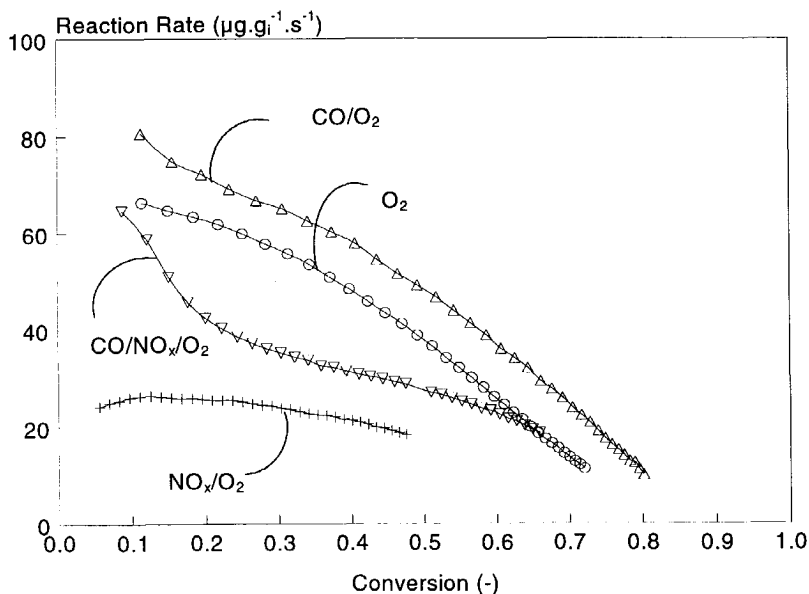
Figure 8a. *Effects of 1000 ppm NO_x and 1080 ppm CO on the oxidation rate of KNO_3 impregnated soot in 10% O_2 in Ar at 550 K. Gas composition as indicated.*
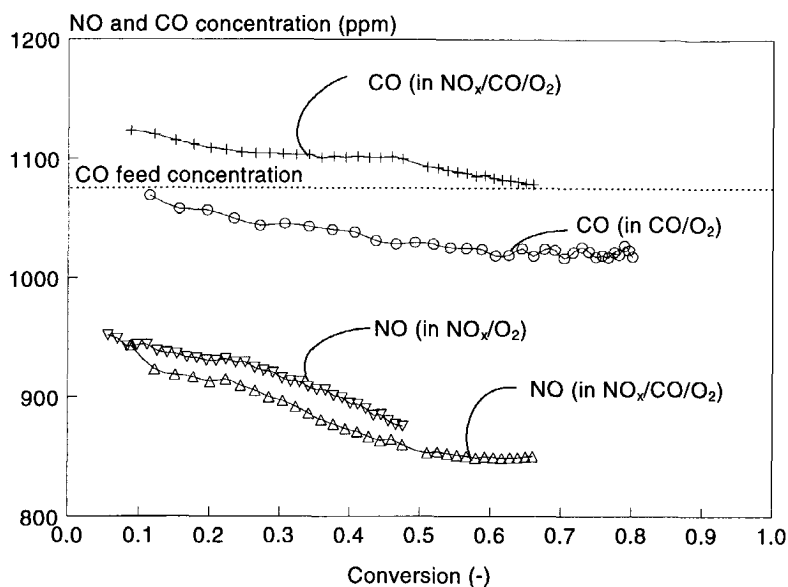
Figure 8b. *The development of the NO and CO concentrations in the KNO₃ impregnated soot oxidation at 550 K under the conditions as indicated. The CO feed concentration (1080 ppm) is indicated by the dashed horizontal line. The NO feed concentration amounted to 1000 ppm.*
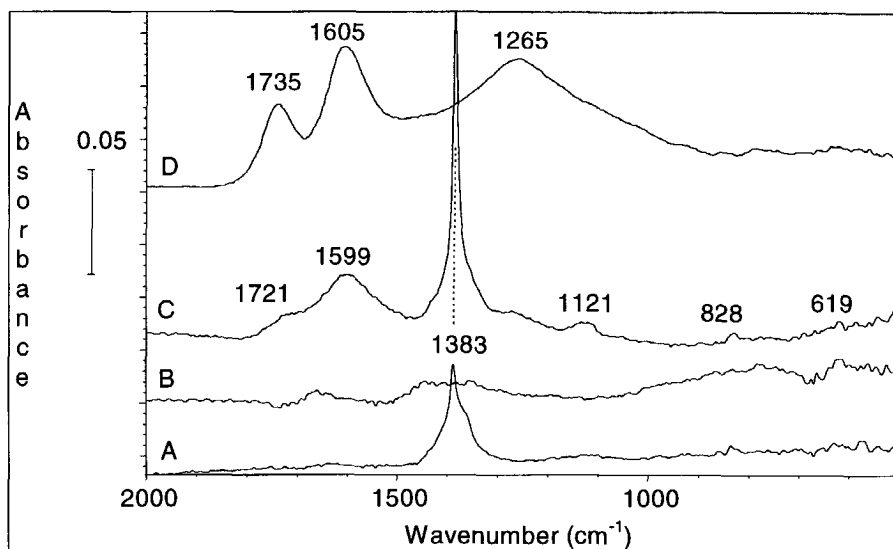
Figure 9. *DRIFT spectra of K-loaded soot directly after impregnation [A], after thermal treatment in N₂ (120 min, 675 K) [B], and after reaction in 1000 ppm NOₓ /10% O₂ in Ar at 550 K up to 65 % conversion [C]. The spectrum of non-catalytically converted soot at 775 K (up to 30 % burn-off) is shown for comparison [D].*

In 10 % O_2 in Ar, the CO concentration is slightly lower than the CO feed concentration. This is not observed in the presence of NO_x, where the CO concentration remains higher than the CO feed concentration up to 70% soot conversion. The NO concentration seems to be fairly independent of the presence of CO. Only a slightly lower NO concentration (± 20 ppm) is observed in the presence of CO. The DRIFT spectra of K-impregnated soot, after various treatments, are shown in figure 9.

After pretreatment at 675 K in N_2, the absorption pattern around 1383 cm^{-1}, clearly visible in spectrum A, is no longer present. After reaction at 550 K in $NO_x/O_2/Ar$, absorptions can be observed at 1721 cm^{-1}, 1599 cm^{-1}, 1121 cm^{-1}, 828 cm^{-1} and 619 cm^{-1}. Furthermore, a very strong absorption band is observed at 1383 cm^{-1}. The band positions are significantly different from the absorptions obtained after non-catalytic oxidation (spectrum D): 1735, 1605 and 1265 cm^{-1}.

6.3.4. The effect of NO_x on the oxidation rate of physical mixtures

The effect of NO_x on the K_2CO_3 catalyzed soot oxidation, in 'tight' and 'loose contact', is shown in figure 10. A small promoting effect of NO_x on the oxidation rate is observed in 'tight' contact. However, NO_x does not alter the shape of the oxidation profile.
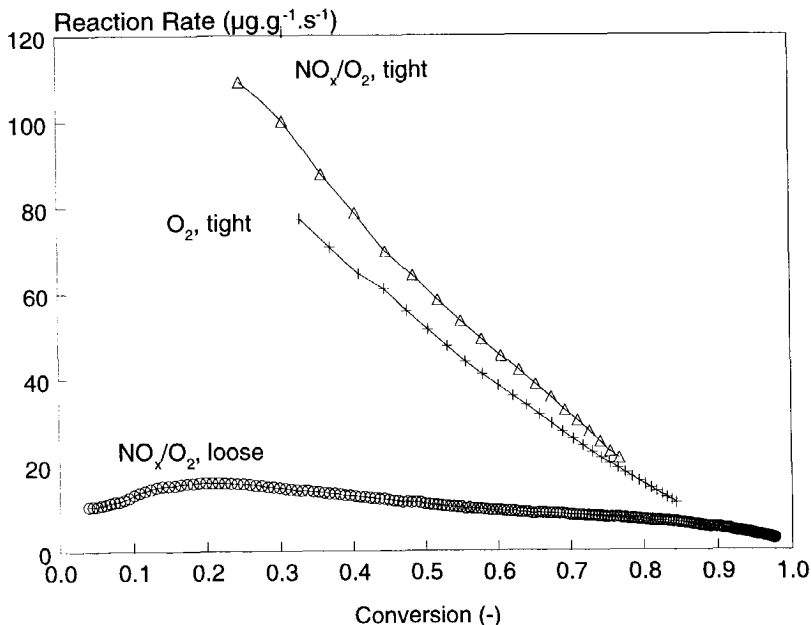
Figure 10. The effect of NO_x on the 'tight' and 'loose' contact activities of K_2CO_3 at 550 K. Experimental conditions as indicated in Table 1.

The 'loose' contact activity of K_2CO_3, in the presence NO_x is quite low: the oxidation rate is only slightly higher than the non-catalyzed oxidation rate in NO_x (figure 5).

The effect of K_2MoO_4 on the soot reactivity in NO_x is shown in figure 11. At 675 K, the presence of K_2MoO_4 enhances the oxidation rate of soot. A fairly linear decrease in reaction rate is found as a function of soot conversion, whereas non-catalytic soot oxidation shows a zero order behaviour.
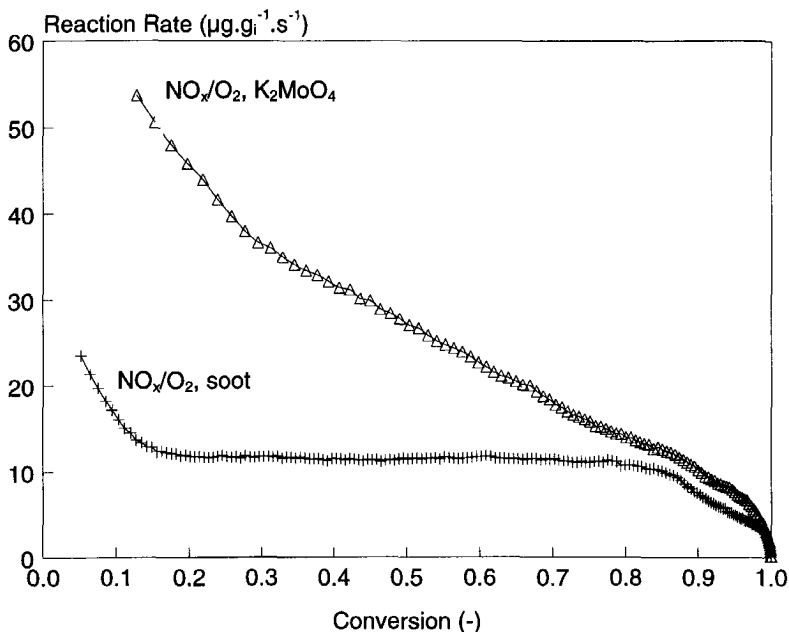
Figure 11. *The reactivity of soot in 1000 ppm $NO_x/10\%$ O_2 in Ar in the absence and presence of K_2MoO_4 ('loose contact') at 675 K. Experimental conditions as indicated in Table I.*

6.4. *Discussion*

6.4.1. Activity measurements in 10 % O_2 in Ar

Impregnation of soot with an alkali metal nitrate considerably enhances the soot oxidation rate. $RbNO_3$ is even more effective than KNO_3, which is in agreement with the observations of other authors [4,7,17]. At first sight, the initial activity of KNO_3 impregnated soot, determined by TG/DSC analysis, seems to be lower than that of a K_2CO_3/soot 'tight contact' physical mixture (figure 3). However, the amount of KNO_3 in the impregnated sample is much smaller than the amount of K_2CO_3 in the physical mixture (3.8 wt% K *vs.* 113 wt% K). So, the activity *per* K-atom is significantly higher in the impregnated sample. The N_2-BET surface area of the

impregnated sample amounts to approximately 100 $m^2.g^{-1}$, which is almost identical to the surface area of soot without catalyst. This confirms a high dispersion of the active potassium species after impregnation and thermal pretreatment, which is advantageous for a high soot oxidation rate.

The initial activity of various potassium salts, as determined by TG/DSC analysis (figure 3), is affected by the stability of the potassium anion. In 'tight contact' K_2CO_3 shows a higher activity than K_2MoO_4, followed by KNO_3. Apparently, K_2CO_3 decomposition and K_2MoO_4 disproportionation (chapter 5), yielding the active alkali oxide species, occurs at lower temperatures than KNO_3 decomposition.

Potassium catalysts show a considerably lower soot oxidation activity in 'loose contact' than in 'tight contact'. Apparently, decomposition of the precursor and redistribution of the active species is a function of contact with soot. The relatively high 'loose contact' activity of KNO_3 can be explained by NO_x formation upon decomposition of KNO_3 or a high mobility of KNO_3 relative to the other potassium precursors. The effect of NO_x on the oxidation rate is evaluated in paragraphs 4.3 and 4.4.

As was already indicated in paragraph 3.1 of this chapter, activity profiles of the catalyzed soot oxidation can divided into three groups: exponential decay-type curves, constant-type curves, and rising-type curves. Neeft obtained a rising-type curve for the K_2CO_3 catalyzed soot oxidation in 'tight contact' at 552 K [17]. Such a rising-type profile was explained by a high mobility of the alkali metal oxides formed upon decomposition of the carbonate precursor: redistribution of the active species increases the reactivity. Several authors already observed that the decomposition temperature of K_2CO_3 was strongly affected by the presence of a carbonaceous support. The reactivity of soot is such, that decomposition of K_2CO_3 into the active oxidic species [5-7], already occurs at 550 K, whereas bulk K_2CO_3 does not decompose below ± 1280 K [7]. In this study, a rising-type curve was obtained for the K_2MoO_4 catalyzed soot oxidation, which can be explained, in analogy to K_2CO_3 [17], by the formation and simultaneous redistribution of the active oxidic species. A slow decay in the reaction rate with conversion, was found for the 'tight contact' K_2CO_3/soot sample (figure 3) in this study, as well as for the alkali metal loaded soot samples. Generally, such a profile can be explained by a moderate loss of contact between the catalyst and soot as a function of soot conversion. An exponential-type curve, as observed by Neeft for *e.g.* Fe_2O_3, is not obtained, because the formation and decomposition of SOC, shown in figure 9 and extensively discussed in chapter 5 of this thesis, contributes to the oxidation profile [17]. A rising-type profile is not obtained for the impregnated sample, obviously because a relatively high dispersion of the active potassium species is already obtained by the impregnation procedure and after pretreatment in N_2 (compare figure 1 of chapter 5). The relatively low activity and absence of a maximum in the oxidation profile of K_2CO_3 in this study, is likely to be caused by a poor contact between K_2CO_3 and soot. This results in a small amount of sites available for K_2CO_3 decomposition: the soot oxidation rate is not

increased by a fast formation and redistribution of the active species. Obviously, the bulk of K_2CO_3 is not participating in the reaction.

Concluding, the presence of a highly dispersed, presumably oxidic potassium phase is essential for a high soot oxidation activity. The rate of formation of the oxidic phase is dependent on the stability of the potassium precursor and the intensity of contact between the precursor and soot.

6.4.2. The effects of NO_x and CO on the uncatalysed soot oxidation rate

The soot oxidation profiles obtained at 675 K in 10% O_2 in Ar, either with or without NO_x, are quite similar to the ones obtained by Neeft for the oxidation of soot in 10% O_2 in Ar [17]. The rapid decay in reaction rate at low conversion levels, is likely to be explained by the presence of reactive hydrocarbons. These are easily oxidized and contribute to the reaction rate in the initial stage of the reaction.

An apparent reaction order of 0.73 ($\pm$ 0.04) in carbon was found for the non-catalyzed Printex-U oxidation [17] in 10% O_2 in Ar. In contrast, the profiles given in figure 6, show an apparent zero order behaviour. In the final stage of the reaction, the available surface area decreases, causing a rapid decay in the reaction rate. The formation of NO_2 out of NO and O_2 is described by reaction (1):

$$2\,NO + O_2 \quad \leftrightarrow \quad 2\,NO_2 \tag{1}$$

In the experimental setup (figure 1), reaction (1) is not at thermodynamic equilibrium, which predicts an NO conversion into NO_2 of at least 70% at 675 K [31]. The increase in the oxidation rate after the addition of NO_x to the oxidizing medium can be explained by reaction of NO_2 with soot:

$$2\,NO_2 + \text{'C' (soot)} \quad \rightarrow \quad CO_2 + 2\,NO \tag{2}$$

This reaction is corroborated by a relatively high NO concentration (800 ppm) measured at the exit of the soot containing reactor (figures 1 and 6). If the reaction would be stoichiometric, the amount of NO_2 converted yields a soot oxidation rate of 6 $\mu g \cdot g_{initial}^{-1} \cdot s^{-1}$, whereas the measured overall soot oxidation rate amounts to 12 $\mu g \cdot g_{initial}^{-1} \cdot s^{-1}$. Apparently, stoichiometric NO_2 conversion cannot entirely account for the measured soot oxidation rate. The uncatalyzed reaction of soot with O_2 only contributes 2-3 $\mu g \cdot g_{initial}^{-1} \cdot s^{-1}$ to the overall reaction rate. To explain a soot oxidation rate of 12 $\mu g \cdot g_{initial}^{-1} \cdot s^{-1}$, it is suggested that NO_2 is reformed by collision of NO and O_2 with a soot particle. In other words, NO acts as a soot oxidation catalyst. Since the supply of NO_2 now determines the soot oxidation rate, the zero order in soot is at least partly explained. It is, however, not excluded that the reactivity of soot towards O_2 is enhanced by a single interaction of soot with NO_2. The increased soot reactivity might be related to the formation of surface oxygen containing complexes (SOCs),

which have been identified by DRIFT spectroscopy (figure 7). Cooper [21] states that in the soot/NO_2 reaction, CO_2 is produced as a secondary product *via* reactions (2) and (3):
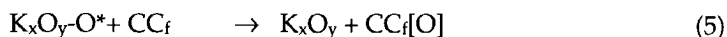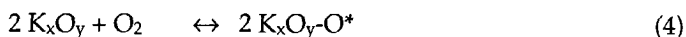
$$CO + NO_2 \quad \rightarrow \quad CO_2 + NO \tag{3}$$
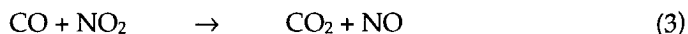
However, addition of CO to an NO_x/O_2 atmosphere did not result in a higher NO_2 conversion, and did not show a considerable oxidation of CO: the measured amount of CO was even higher than the feed concentration (explained by reaction (2)). Therefore, it is proposed that CO_2 is produced by decomposition of oxygen intermediates formed on the soot surface. The DRIFT spectra shown in figure 7, reveal that reaction of soot with NO_2 yields various surface oxygen complexes (SOCs). The 1740, 1600 and 1265 cm^{-1} (1232 cm^{-1}) bands can be assigned to lactones, quinones and ether like functionalities, respectively [22,23]. The relative intensities of the lactone, quinone and ether absorptions are dependent on the ratio of the rate of formation and decomposition of these complexes. The spectra show that lactones are less stable than quinones and ethers, as the lactone/quinone ratio rapidly increases with decreasing reaction temperature (and increasing reactivity of the oxidant). This is in agreement with the experiments performed by Zhuang [23]. After reaction of soot with NO_2 at 298 K, Chughtai *et al.* [24,25] identified various nitrogen containing complexes on the surface of soot, such as C-NO_2, C-ONO and C-N-NO_2, in addition to oxygen containing functionalities. The spectrum shown in figure 7, only contains a minor absorption band at 1384 cm^{-1}, which can be assigned to adsorbed NO_2. The absence of other NO_2 containing functionalities is likely to be explained by a rapid decomposition of these functionalities at temperatures above 298 K, yielding NO and oxygen containing functionalities. The non-catalyzed oxidation of soot and other carbonaceous materials has been extensively described by *e.g.* Neeft [17], Walker *et al.* [26], and Moulijn and Kapteijn [27]. Dissociation of the oxidant, yielding activated oxygen species and the formation and decomposition of carbon surface oxygen complexes (SOCs) are considered to be important steps in the oxidation mechanism. The formation of the oxygen containing complexes is corroborated by the IR spectra shown in figure 7.

Concluding, the results of non-catalyzed soot oxidation indicate that a contribution of the uncatalyzed NO_2/soot reaction to the overall potassium catalyzed soot oxidation rate (in NO_x) can be expected. As CO did not affect the non-catalytic soot oxidation rate, a possible effect of CO on the catalytic oxidation rate is exclusively caused by interactions of CO with the catalyst.

6.4.3. The effects of NO and CO on the oxidation rate of K-impregnated soot
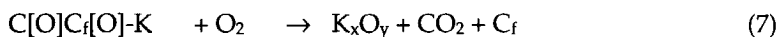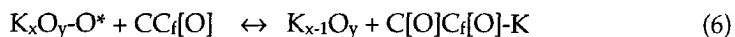
As was already mentioned in the introduction of this chapter, the activity of potassium catalysts in the oxidation of soot can be explained by an oxygen transfer mechanism. Usually a redox mechanism [12,28,29] is used to describe catalytic

carbon oxidation. A plausible mechanism for the potassium catalyzed carbon oxidation in CO_2, is described by Meijer *et al.* [5] and Moulijn and Kapteijn [27] and consists of the formation of potassium oxide clusters, followed by the interaction of CO_2 with these species. Subsequently, activated oxygen and CO are formed by CO_2 dissociation. Activated oxygen is transported to the carbon surface and reacts with a free carbon site. In paragraph 4.1. and chapter 5, the formation of the alkali metal oxide clusters was already discussed. It can be suggested that, just like CO_2, oxygen is chemisorbed and dissociated on the alkali metal oxide clusters, followed by reaction with the carbon surface. This is represented by reactions (4) and (5). Activated oxygen is indicated by O^*, a free carbon site by CC_f, and an oxidized site by $CC_f[O]$.

$$2\,K_xO_y + O_2 \quad \leftrightarrow \quad 2\,K_xO_y\text{-}O^* \tag{4}$$

$$K_xO_y\text{-}O^* + CC_f \quad \rightarrow \quad K_xO_y + CC_f[O] \tag{5}$$

Reaction (5) represents the oxidation of a free carbon site. Thermal decomposition of the oxidized sites yields CO and CO_2. Oxidation experiments in $^{18}O_2$ have shown that gas phase oxygen is not directly incorporated in the products. A so-called push-pull mechanism, as has been proposed for ZnO-catalyzed CO oxidation [34], will be used to describe K_2MoO_4-catalysis, as reported in chapter 8 of this thesis. The high activity of K-based catalysts is likely to be due to an acceleration of the activation of oxygen. Transport of the activated oxygen to the carbon surface is related to the mobility of lattice oxygen atoms, as will be further discussed in chapter 8.

However, activation of oxygen might not be the only reason for the catalytic effect of alkali metals in carbon oxidation. The formation of potassium benzoate species cannot be excluded [1]. An absorption band around 1600 cm^{-1} (figure 9, spectrum C), can be assigned to these species, assuming that the accompanying 1395 cm^{-1} absorption is obscured by the large vibration at 1383 cm^{-1} [1]. The formation and decomposition of benzoate species is indicated schematically by reactions (6) and (7).

$$K_xO_y\text{-}O^* + CC_f[O] \quad \leftrightarrow \quad K_{x\text{-}1}O_y + C[O]C_f[O]\text{-}K \tag{6}$$

$$C[O]C_f[O]\text{-}K \ + O_2 \quad \rightarrow \quad K_xO_y + CO_2 + C_f \tag{7}$$

Otake and Jenkins have shown that alkali metal benzoate functionalities thermally decompose at lower temperatures than other surface oxygen complexes (SOCs) [33]. Hence, besides oxygen activation, the alkali metal catalyst might promote decomposition of SOCs. Decomposition of the benzoate species explains the high CO_2/CO ratio observed in K-catalyzed soot oxidation. The 1721 cm^{-1} absorption (figure 9, spectrum C) is related to remaining lactone and/or acidic functionalities. The 1121 and 619 cm^{-1} bands, often observed in the DRIFT spectra of partially

converted K-impregnated soot samples, were assigned to CO_2 chemisorbed on oxidized potassium clusters [1]:

$$K_xO_y\text{-}O + CO_2 \quad \leftrightarrow \quad K_xO_y\text{-}O\text{-}CO_2 \tag{8}$$
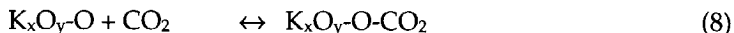
CO_2 chemisorption was found to negatively affect the catalytic oxidation activity of the oxidic potassium clusters [30]. Analogous to CO_2, the relatively low oxidation rate of K-loaded soot at 550 K in the presence of NO_x (figure 7), can be explained by chemisorption of NO_2 on the oxidic potassium species, decreasing the overall oxidation rate: less sites are available for oxygen activation. NO_2 chemisorption on the oxidic clusters is represented by reaction (9), which was witnessed by the very strong absorption band at 1384 cm^{-1} (nitrato stretch), accompanied by a weak band at 828 cm^{-1} (nitrato bending vibration) in spectrum C of figure 9.

$$K_xO_y\text{-}O + NO_2 \quad \leftrightarrow \quad K_xO_y\text{-}O\text{-}NO_2 \tag{9}$$
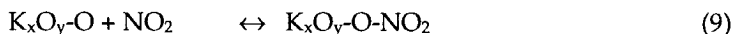
It is interesting that higher NO concentrations were observed in K-impregnated soot oxidation than in non-catalyzed soot oxidation. Apparently, the NO_2 conversion is enhanced by the presence of potassium. It can be speculated that NO_2 reacts similarly to reaction (4), yielding NO and an activated O*-species on the potassium oxide cluster.

CO addition was shown to slightly increase the K-catalyzed soot oxidation rate. Moreover, CO oxidation over the potassium oxide clusters was observed, which is represented by reaction (10):

$$K_xO_y\text{-}O + CO \quad \rightarrow \quad K_xO_y + CO_2 \tag{10}$$

Two plausible reasons can be proposed for the enhancement of the soot oxidation rate by the addition of CO: i) exothermal CO oxidation causes a localized increase in the temperature of the catalyst particles or ii) CO slightly reduces the oxidation state of the potassium oxide clusters, thereby inhibiting carbonate formation and blocking of active sites. The experimental observation, that CO addition decreases the soot oxidation activity of Co_3O_4, whilst 100% CO conversion was obtained [29], excludes a considerable heat effect. Abbel [30] indicated that the N_2O gasification rate of K_2CO_3 impregnated Norit RX extra, was inhibited by carbonate formation (compare reaction (8)). Saber indicated that the K:O ratio is variable between 2 and 1, depending on the experimental conditions [10,11], and Meijer *et al.* have shown that reduction of the oxidic clusters reduces CO_2 chemisorption [7]. Hence, the second proposition seems to be plausible. Addition of CO to the NO_x containing reaction medium also enhances the reaction rate and changes the oxidation profile. The phenomena can be explained by assuming that at low carbon conversions (*i.e.* in the beginning of the reaction) the reduction of the active cluster by CO prevents the chemisorption NO_2,

analogous to CO_2. At higher conversions, NO_2 chemisorption prevails, which decreases both the soot and CO oxidation rate.

Addition of 1000 ppm NO_x to the oxidizing medium slightly enhanced the activity of K_2CO_3 at 550 K in 'tight contact', whereas it decreased the oxidation rate of K-loaded soot at 550 K (compare figures 7 and 10). This controversy can be explained by the relatively high potassium concentration in the K_2CO_3/soot mixture: NO_2 might chemisorb on K_2CO_3, but apparently does not block all the active sites. The slightly enhanced oxidation rate is likely to be explained by the soot/NO_2 reaction. A 'loose contact' K_2CO_3/soot mixture shows a much lower reaction rate in the presence of NO_x, than a 'tight contact' mixture either with or without NO_x, whereas figure 11 shows that addition of K_2MoO_4 considerably increases the soot oxidation rate in 10% O_2 and 1000 ppm NO_x at 675 K. This is explained by the fact that chemisorption of NO_2 does not inhibit the catalytic activity at 675 K. Moreover, the stoechiometric NO_2/soot reaction (350 ppm NO_2 is converted) can only account for a soot oxidation rate of 12 $\mu g.g_i^{-1}.s^{-1}$. whereas the observed increment of the soot oxidation rate contributes to 50 $\mu g.g_i^{-1}.s^{-1}$. This is explained by K_2MoO_4-catalyzed NO oxidation, *i.e.* NO_2 reformation.

6.4.4. The feasibility of potassium catalysts for the catalytic removal of soot from diesel exhaust.

Based on the high activity in 'tight contact' conditions, the practical application of K-based catalysts for the removal of soot might be considered. However, figure 5 shows that potassium catalysts have a low catalytic activity in air in 'loose contact', which unfortunately is the type of contact under practical conditions.

A practical application of the oxidation of soot by NO_2 has been proposed by Cooper and Thoss using a Pt-catalyst [21]. The Pt-catalyst accelerates NO_2 formation, which acts as the transport medium for activated oxygen. This way, the contact problem might be solved. Unfortunately K-based catalysts possess a low activity for the oxidation for the oxidation of NO into NO_2. Moreover, the activity of potassium oxide clusters is negatively affected by chemisorption of NO_2, which readily occurs at the diesel exhaust temperatures (550-675 K). Furthermore, K-based catalysts show a very low CO oxidation activity, compared to transition metal oxides. Although water vapor, which is also present in diesel exhaust, might positively influence the characteristics of K-based catalysts with respect to deactivation by NO_2 or CO_2, it can be anticipated that, due to the high volatility of the formed potassium hydroxides and peroxides, deactivation of K-based catalysts occurs under these conditions. Moreover, hydroxides and peroxides are highly corrosive. Evaluating these observations, it can be concluded that a practical application of alkali metal oxides for catalytic soot oxidation, is not feasible. The application of the NO_2/soot reaction will be further discussed in chapter 10 of this thesis.

6.5. *Conclusions*

- The initial activity of potassium catalysts is strongly dependent on the stability of the potassium precursor: formation of oxidic clusters is necessary to obtain a high soot oxidation rate.
- After thermal treatment, K-impregnated soot shows a higher oxidation rate at 550 K than 'tight' and 'loose' contact physical mixtures of soot and potassium salt precursors.
- Addition of NO to 10% O_2 in Ar, enhances the uncatalyzed soot oxidation rate, which is explained by the soot/NO_2 reaction.
- DRIFT analyses show that several SOC are formed upon oxidation of soot. The relative intensity of the IR bands assigned to lactones, quinones and ethers, is dependent on the oxidizing capacity of N_2O, O_2, NO_2 or O_3 and the oxidation temperature.
- Addition of NO to the oxidizing medium has a negative effect on the oxidation rate of K-loaded soot at 550 K, which is explained by chemisorption of NO_2 on active sites.
- Above 675 K, nitrate formation does not occur, and the soot oxidation rate is enhanced by the contribution of the 'C'/NO_2 reaction.
- CO addition slightly increased the oxidation rate of K-loaded soot, which is tentatively explained by a reduction of the active species, preventing CO_2 and NO_2 chemisorption.
- Potassium salts have little practical potential as diesel soot oxidation catalysts.

6.6. *References.*

[1] G. Mul, chapter 5 of this thesis.
[2] H. Kubiak, H.J. Schroter, A. Sulimma and K.H. van Heek, Fuel, 62 (1983) 242.
[3] M.B. Cerfontain and J.A. Moulijn, Fuel, 62 (1983) 256.
[4] M.B. Cerfontain and J.A. Moulijn, Fuel, 65 (1986) 1349.
[5] R. Meijer, F. Kapteijn and J.A. Moulijn, Fuel, 73 (1994) 723.
[6] F. Kapteijn, R. Meijer, J.A. Moulijn and D. Cazorla-Amoros, Carbon, 32 (1994) 1223.
[7] R. Meijer, B. van der Linden, F. Kapteijn and J.A. Moulijn,. Fuel, 70 (1991) 205.
[8] C.A. Mims and J.K. Pabst, J. Catal. 107 (1987) 209.
[9] C.A. Mims and K.D. Rose, J.Am.Chem.Soc. 104 (1982) 6886.
[10] J.M. Saber and J.L. Falconer, J. Catal. 90 (1984) 65.
[11] J.M. Saber, J.L. Falconer and L.F. Brown, Fuel, 65 (1986) 1356.
[12] D.W. McKee, Fuel, 62 (1983) 170.
[13] B.J. Wood and M. Sancier, Catal.Rev.-Sci.Eng. 26.(2) (1984) 233.
[14] F.J. Long and K.W. Sykes, Proc. Roy. Soc. (London) Series A, 215 (1952) 100.
[15] Z.J. Pan and R.T. Yang, J. Catal. 130 (1991) 161.
[16] A.M. Vassallo, Y.L. Liu, L.S.K. Pang and M.A. Wilson, Fuel, 70 (1991) 635.
[17] J.P.A. Neeft, 'Catalytic oxidation of soot-Potential for the reduction of diesel particulate emissions', Ph.D. Thesis TU Delft (1995), chapter 10.

[18] J.P.A. Neeft, M. Makkee and J.A. Moulijn,. Appl. Catal. B: Env. 8 (1996) 57.

[19] G. Mul, F. Kapteijn and J.A. Moulijn, in Proceedings of 22nd Biennial Conference on Carbon, San Diego, USA, 1995, pp. 554-555.

[20] G. Mul, F. Kapteijn and J.A. Moulijn,. Prepr. Pap. -Am. Chem. Soc. Div. Fuel Chem. 41 (1996) 230.

[21] B.J. Cooper and J.E. Thoss, SAE Paper 890404, (1989) 171.

[22] C. Morterra and M.J.D. Low, Spectroscopy Letters, 15 (1982) 689.

[23] Q.-L. Zhuang, T. Kyotani and A. Tomita, Energy & Fuels, (1994) 714.

[24] M.S. Akhter, A.R. Chughtai and D.M. Smith, Appl.Spectrosc. 45 (1991) 653.

[25] A.R. Chughtai, W.F. Welch and D.M. Smith, Carbon, 28 (1990) 411.

[26] P.L. Walker, R.L. Taylor and J.M. Ranish, Carbon, 29 (1991) 411.

[27] J.A. Moulijn and F. Kapteijn, in: H. Marsh, P. Ehrburger, B. McEnaney and I. Mochida (Editors), The science of carbon materials, Elsevier, Amsterdam, 1995.

[28] S.G. Chen and R.T. Yang, J. Catal., 141 (1993) 102.

[29] G. Mul, Chapter 10 of this thesis.

[30] G. Abbel, 'Kolenvergassing, een onderzoek naar de van belang zijn de parameters.', M.Sc. report, University of Amsterdam, 1984.

[31] E. Ito, R.J. Hultermans, P.M. Lugt, M.H.W. Burgers, M.S. Rigutto, H. van Bekkum, and C.M. vd Bleek, Appl. Catal. B: Env. 4 (1994) 95.

[32] J.P.A. Neeft, M. Makkee, and J.A. Moulijn, Fuel, in preparation.

[33] Y. Otake and R.G. Jenkins, Carbon, 31 (1993) 109.

[34] V.D. Sokolovskii, Catal. Rev. - Sci. Eng. 32 (1990) 1.

7

The effect of metal oxides on the formation of carbon surface oxygen complexes in air and ozone

Abstract

Various surface oxygen complexes (SOCs) have been identified by DRIFT spectroscopy on the surface of soot (Printex-U) after partial non-catalytic conversion in 10% O_2 in Ar and ozone. An *in-situ* DRIFT analysis of the oxidation of fullerene C60 showed the formation of similar functionalities and validated the use of C60 as a soot model compound for DRIFT spectroscopic studies. *Ex-situ* DRIFT analyses of partially converted catalyst/soot mixtures and *in-situ* analyses of catalytic fullerene C60 oxidation, revealed that several transition metal oxides (Cr_2O_3, MoO_3, V_2O_5, and CuO) promote the formation of carbon surface oxygen complexes (SOCs). Fe_2O_3 and Co_3O_4 do not enhance the formation of SOCs in 10% O_2 in Ar and prevent the formation of SOCs in ozone. This prevention is tentatively explained by recombination of activated oxygen species on the catalyst surfaces. Reaction of soot with oxygen associated with metal oxides (carbothermic reduction) does not yield SOCs. Apparently, lattice oxygen is not directly involved in the catalytic formation of these complexes. Indications for chemical interactions between metal oxides and either soot or C60, such as M-O-C bonds, have not been found. Spill-over of activated oxygen from the Cr_2O_3, MoO_3, V_2O_5, and CuO surfaces onto the soot surface is likely to explain the catalytic formation of SOCs.

7.1. *Introduction*

Elucidation of the mechanism of catalytic oxidation reactions of carbonaceous materials has been the subject of many researchers over the last decades [1-6]. It has been generally accepted that non-catalytic oxidation yields Surface Oxygen Complexes (SOCs), which play an essential role in the oxidation mechanism. These complexes are formed in the presence of different oxidizing agents, such as CO_2, H_2O or O_2. Researchers involved in the catalytic oxidation of graphite, chars and/or soot by metal oxides, usually describe a redox mechanism to explain experimental phenomena: in a first step the catalyst is reduced by carbon ('carbothermic reduction'), followed by re-oxidation of the oxide by molecular oxygen [1,2]. Apparently, the formation of SOCs does not play an essential role in this mechanistic proposition. The importance of SOCs has only been discussed in mechanistic studies of potassium and calcium catalyzed (activated) carbon oxidation [3-6].

A powerful tool for the analysis of oxygen complexes on carbonaceous materials is Fourier Transformed Infrared spectroscopy and in particular Diffuse Reflectance Infrared Fourier Transformed (DRIFT) spectroscopy. Several research groups analyzed coal of different ranks using this technique, *e.g.* [7-9]. Also *in-situ* studies towards the oxidation of carbonaceous materials have been performed [10-14] as well as DRIFT studies on oxidized soot [15] and phenol formaldehyde (PF) chars [16]. As far as catalyst/oxygen/carbon interactions are concerned, only the alkali carbonate catalyzed carbon gasification by CO_2 has been studied by means of FT-IR [17-19]. IR, and more specifically, DRIFT spectroscopy has never been used to elucidate the mechanism of the catalytic oxidation of carbonaceous materials by transition metal oxides.

In the first publication of a series of papers describing several phenomena of the catalytic oxidation of soot [20], results are presented, which show that isothermal oxidation profiles of soot in the presence of various catalysts, can be classified into three categories: exponential decay-type, constant-type and rising-type profiles [20]. In this chapter it will be demonstrated by *ex-situ* DRIFT spectroscopic analyses of catalyst/soot mixtures, and *in-situ* catalyst/fullerene C60 mixtures, that the formation of SOCs is promoted in the presence of several transition metal oxides. Some preliminary conclusions regarding the oxidation mechanism will be drawn. Furthermore, the use of C60 as a soot model compound for spectroscopic studies will be evaluated.

7.2. *Experimental*

Printex-U (a soot, kindly provided by Degussa) was used to perform the oxidation studies. This soot has a BET surface area of 96 $m^2.g^{-1}$ and contains approximately 5 wt-% of adsorbed hydrocarbons and only 0.2-0.4 wt-% sulfur [22]. Neeft [22] and van Doorn *et al.* [23] have shown that the activity of (transition) metal oxides in soot oxidation is very much dependent on the intensity of contact between

the metal oxide and soot. In this paper we describe phenomena which were observed for catalyst/soot interactions obtained by ball-milling of physical mixtures ('tight contact') and by impregnation of the soot with transition metal nitrates. 'Tight contact' catalyst-soot mixtures of 2:1 wt-% were prepared in one hour in an agate ball mill in such a way that heating of the sample was prevented as much as possible. Increasing the milling time did not result in a higher soot oxidation activity [20]. Analytical grades of the transition metal nitrates were used to impregnate the soot. An amount of the nitrate, corresponding to 10 wt-% of the most stable oxide of the element (Fe_2O_3, Co_3O_4, Cr_2O_3), was dissolved in 200 ml ethanol, followed by addition of 200 mg soot to the solution. The ethanol was removed at 325 K under reduced pressure in a rotating evaporator. The black powder could be recovered by scratching it from the glass wall of the flask with a spatula.

Partial conversion of the ball-milled catalyst/soot samples was accomplished in a Thermal Sciences STA-1500H balance (TGA/DSC). Approximately 10 mg of a catalyst/soot mixture was placed in an alumina sample cup and treated in 10% O_2 in N_2 at a temperature of 100 K below the oxidation temperature (determined by DSC analysis [24]) to prevent thermal runaways. A conversion of approximately 50% could be achieved (as determined from the weight loss) within 30 minutes. Carbothermic reduction of several metal oxides, leading to 50% carbon burn off, was also performed in the thermobalance, as described elsewhere [25]. Besides the thermobalance, the so-called six-flow reactor setup was also used to prepare batches of partially converted soot and impregnated soot samples [22]. A six-flow experiment was carried out by packing five quartz reactors (one reactor was used as a reference) with 25 mg of the impregnated soot/metal nitrate mixture, sandwiched between two pieces of quartz wool and two layers of SiC. A controlled flow of 150 ml/min (10 vol% O_2 in Ar) was led through each reactor. A non-dispersive infrared detector (Hartmann & Braun Uras 10 E) was used to measure the CO, CO_2, and NO concentrations every 90 seconds in each reactor. A multiposition valve (Valco) selected the reactor for analysis. The partial conversions were obtained isothermally at 575 K (Co) and at 585 K (Fe, Cr). The isothermal temperature was reached with a ramp of 5 K/min. The amount of soot converted was determined by integration of the CO and CO_2 concentrations.

Ozonized soot was prepared in a closed quartz tube, with a porcelain crucible containing the sample placed inside, and an ozonizer which produced approximately 10% ozone in oxygen. Catalyst/soot samples with a total weight of 100 mg, physically mixed in a ratio of 2:1 in the ball mill, were allowed to react for 60 minutes in an oxygen/ozone flow of approximately 10 ml/min at 313 K. Soot was treated under similar conditions, and also at 400 K for three hours, to induce the formation of a highly oxidized sample.

Sublimed fullerene C60 was used as received from Bucky USA. Catalyst/C60 (2:1 wt-%) 'tight contact' mixtures were prepared by ball milling, as described previously. DRIFT spectra of catalyst/soot mixtures were recorded by collection of 256 scans at 8 cm^{-1} resolution on a Nicolet Magna 550 spectrometer equipped with a DTGS detector

and a Spectratech DRIFT accessory. KBr was used as a diluent. Room temperature spectra are displayed in absorbance reflectance mode against an unreacted soot in KBr background. *In situ* spectra of the decomposition of ozonized soot and C60 oxidation, either in the presence or the absence of a catalyst, were recorded in a Spectratech environmental cell, which was compatible with the DRIFT accessory. Undiluted samples were used for the *in-situ* analyses, to prevent the interference of KBr. Chemical interactions between transition metal oxides and KBr, and SOCs and KBr have been observed at elevated temperatures in a previous study [21], whereas they did not occur at room temperature. Ozonized soot was decomposed in a N_2 flow of 30 ml/min, whereas *in-situ* oxidation of C60 and catalyst/C60 mixtures was performed in 50 ml/min 20% O_2 in N_2.

7.3. *Results*

7.3.1. *Non-catalytic formation of SOCs in ozone and 10%O_2 in Ar*

The amount and nature of the oxygenated species formed on the soot surface by oxidation in ozone is related to the time and temperature of this treatment. A treatment of three hours at 400 K yields a yellowish brown material, which contains an enormous amount of oxygen containing functionalities (figure 1). Absorption bands are located at 1857, 1793, 1763, 1617, 1423, 1214 and 926 cm^{-1}. In figure 1a, showing the spectral development up to 575 K, which was established within 30 minutes, a reduction in the intensities of the 1763 cm^{-1} and 1423 cm^{-1} bands is accompanied by increasing 1857 cm^{-1} and 926 cm^{-1} bands. Furthermore, the broad absorptions in the 2300-4000 cm^{-1} range decrease in intensity. In the temperature range of 625-900 K two bands appear at 3085 and 731 cm^{-1}. In figure 1b, a further decomposition of the oxygen containing functionalities is observed with increasing temperature: the bands located at 3400, 3085, 1849, 1780, 914, and 731 cm^{-1} are reduced in intensity. The 1617 cm^{-1} band is shifted to 1594 cm^{-1}, but the intensity is not drastically diminished. The latter is also valid for a band located at 1217 cm^{-1}.
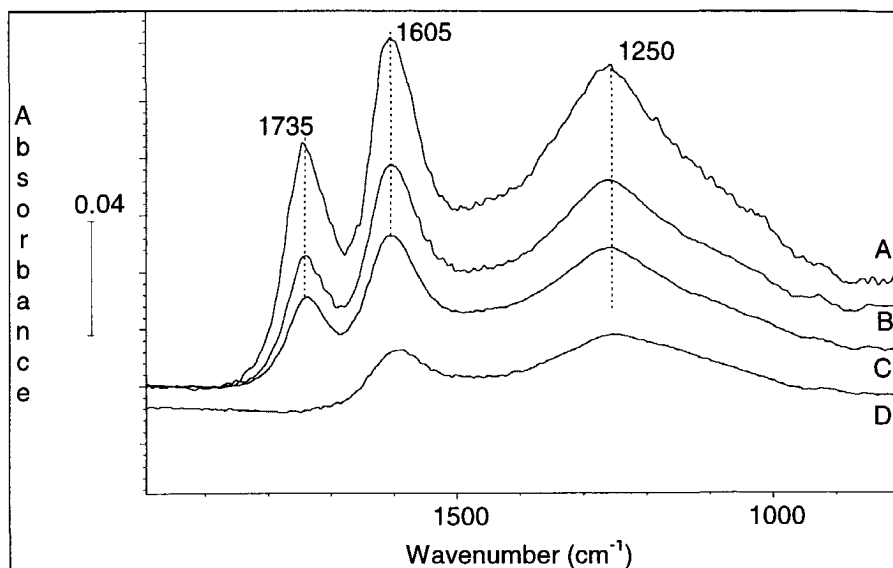
Ex-situ DRIFT spectra of partially converted soot in the six-flow apparatus up to conversion levels of 30%, 40% and 60% are shown in figure 2. Only three broad bands can be identified in the spectra, located at 1250 cm^{-1}, 1605 cm^{-1}, and 1735 cm^{-1}. The intensity of the IR bands, *i.e.* the concentration of SOCs, is found to increase with conversion. The spectrum of oxidized soot after treatment in N_2 at 975 K for 10 minutes, only shows the 1605 and 1250 cm^{-1} bands (figure 2, spectrum D), which are obviously reduced in intensity.
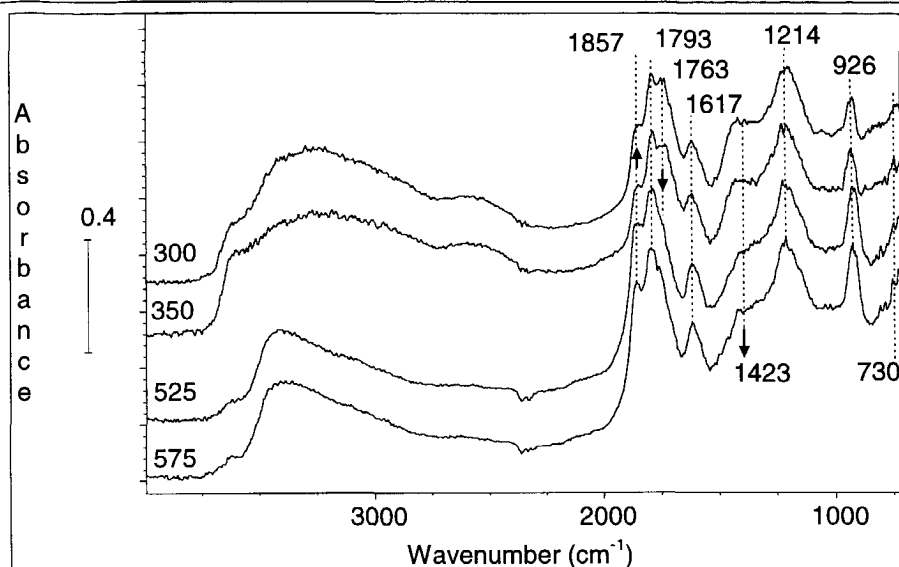
Figure 1a. In-situ DRIFT spectra (8 cm^{-1}, 256 scans) of the decomposition of ozonized soot in N$_2$ (3 h at 400 K). Spectra were recorded at 300, 350, 525 K and 575 K (top to bottom). Spectral development as indicated. Pure sample (i.e. no KBr dilution), background KBr.
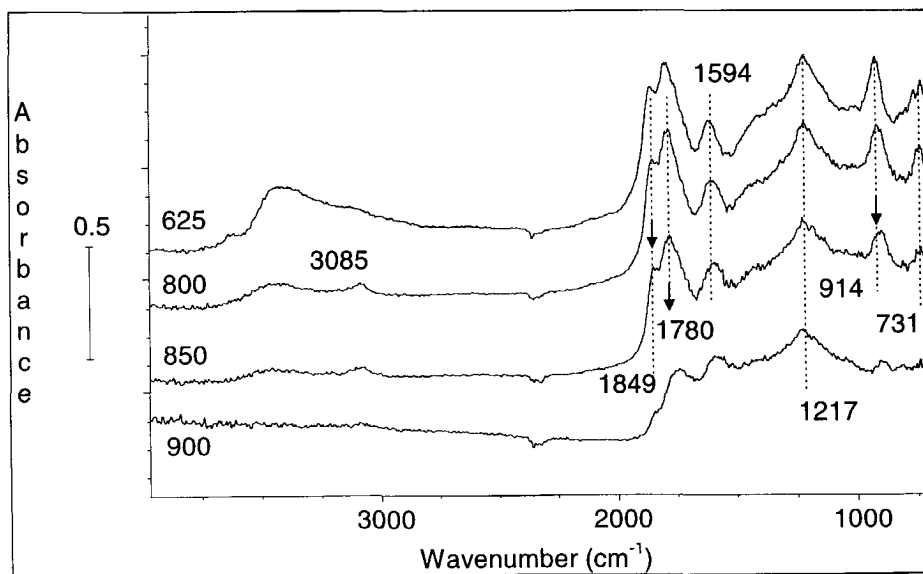
Figure 1b. The decomposition of ozonized soot (continued). Spectra were recorded at 625, 800, 850, and 900 K (top to bottom). Pure sample (i.e. no KBr dilution), background KBr.

Figure 2. Ex-situ DRIFT spectra (in KBr) of partially converted soot in 10% O₂ in Ar at 775 K in the six-flow apparatus. A. 60% conversion, B. 40% conversion, C. 30% conversion, D. after partial decomposition of the complexes (present after 30 % conversion) at 975 K for 10 minutes, in nitrogen.

An *in-situ* DRIFT analysis of the non-catalytic oxidation of fullerene C60 is shown in figure 3. The spectral development is in close agreement to that reported by Wohlers [26,27]. The four vibrational modes of C60, located at 1427, 1181, 576, and 527 cm⁻¹, are clearly visible. Typical vibrations after partial oxidation are located at 1838, 1773, 1738, 1598, around 1229 cm⁻¹, and 907 cm⁻¹, and are increasing with conversion. A minor absorption band can be observed at 2126 cm⁻¹.

The spectrum of oxidized fullerene C60 is compared with that of ozonized soot in figure 4. Quite similar features can be observed in the two spectra, especially in the 1700-1850 cm⁻¹ region. The 730 cm⁻¹ band is less clearly resolved in the spectrum of oxidized fullerene C60 than in the spectra ozonized soot, as illustrated in figure 4.

7.3.2. Formation of SOCs on Printex-U in the presence of transition metal oxide catalysts.

DRIFT spectra of 'tight contact' catalyst/soot samples, treated at elevated temperatures in 10% O₂ in Ar in the thermobalance, are shown in figure 5. The experimental data are summarized in Table 1.
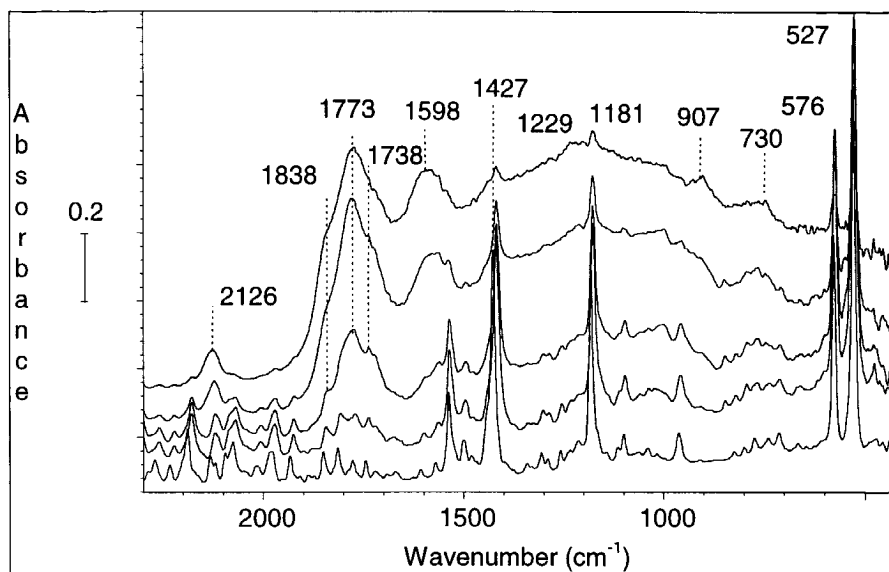
Figure 3. *In situ DRIFT spectra of the non catalytic oxidation of Fullerene C60 in 10% O_2 in Ar at 575 K. Spectra were recorded every 5 minutes (bottom to top). The spectral development was established within 25 minutes.*
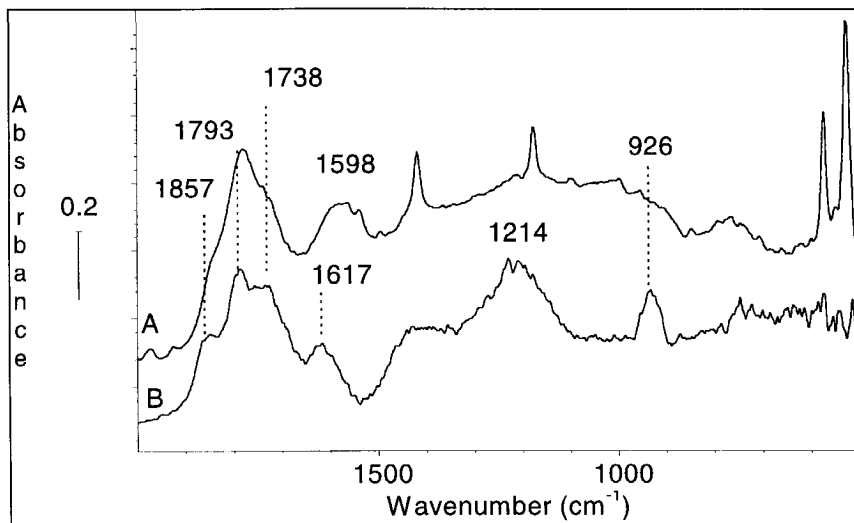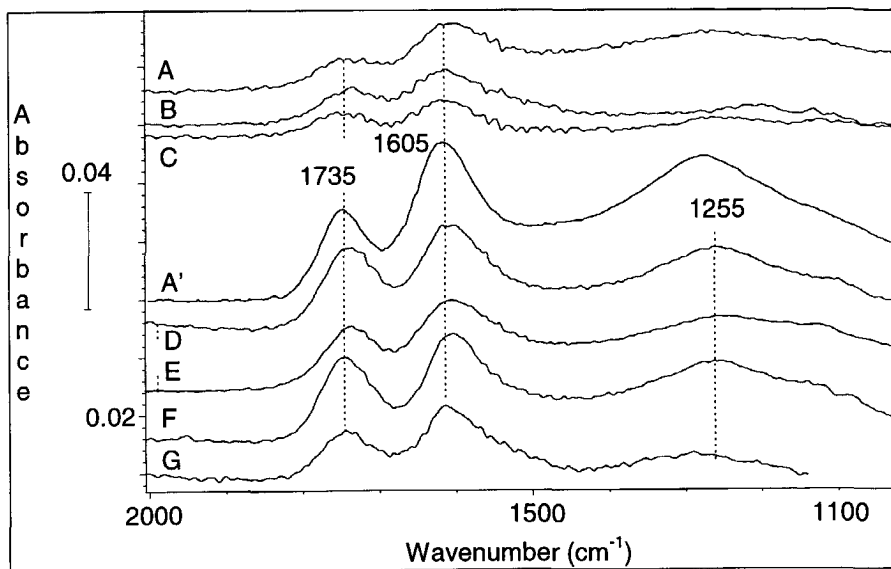

Figure 4. *In situ DRIFT spectra in 10% O_2 in Ar (256 scans, 8 cm^{-1} resolution) of oxidized C60 (figure 3) and ozonized soot (figure 1a).*

Figure 5. Ex situ DRIFT spectra (recorded in KBr) of oxidized 'tight contact' catalyst/soot mixtures (for further details see Table 1). *A.* Soot, *B.* Co_3O_4/soot, *C.* Fe_2O_3/soot, *A'.* Soot converted to 30 % (figure 2), *D.* Cr_2O_3/soot, *E.* CuO/soot, *F.* MoO_3/soot, *G.* V_2O_5/soot.

The 1265, 1605, and 1735 cm^{-1} bands have similar intensities after non-catalytic oxidation (spectrum A) and after catalytic oxidation in the presence of Fe_2O_3 and Co_3O_4 (spectra B and C) although the obtained soot conversion level in the presence of these catalysts is much higher. Cr_2O_3, CuO, MoO_3, and V_2O_5 (spectra D-G) clearly cause an enhancement of the intensity of the IR bands ascribed to SOCs, relative to soot prepared at similar conditions. The spectrum of soot, pretreated at 775 K up to 30% conversion in the six-flow apparatus (spectrum A'), is shown for comparison. Apparently, the presence of a catalyst hardly affects the band positions for the oxygen functionalities.

Table 1. *Experimental data for pretreatment in the thermobalance of several soot/catalyst mixtures in 10% O_2 in Ar.*

Catalyst	Temperature (K)	Time (min)	Conversion (%)	Complexes*
MoO_3	675	15	35	++
V_2O_5	650	20	50	+
Cr_2O_3	685	35	30	+
CuO	695	20	25	++
Fe_2O_3	700	15	40	--
Co_3O_4	635	25	45	--

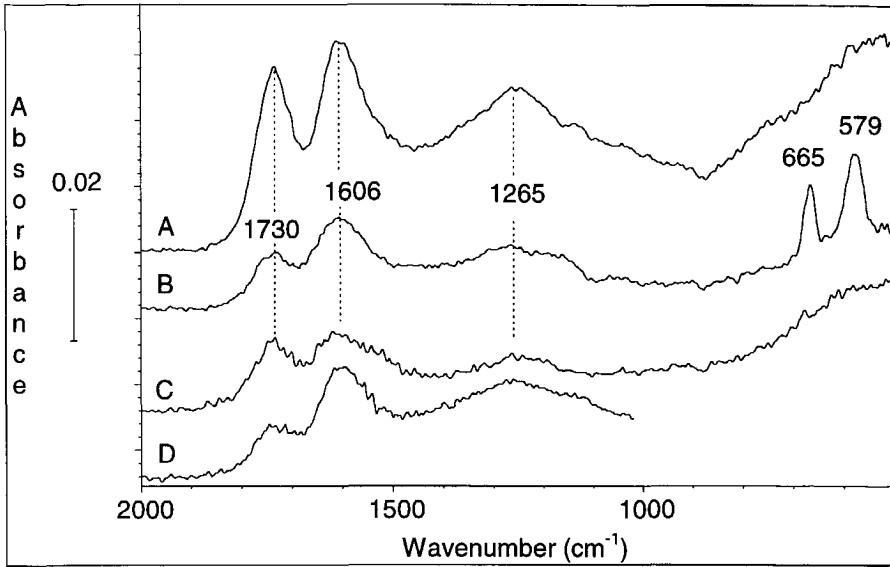*   Relative to soot, pretreated at 675 K for 30 minutes in a thermobalance, leading to a conversion of only 1-2%.

*Figure 6. Ex-situ DRIFT spectra (recorded in KBr) of partially oxidized catalyst/soot mixtures, prepared by impregnation. **A.** Cr_2O_3/soot (40% burn off)), **B.** Co_3O_4/soot (50% burn off), **C.** Fe_2O_3/soot (20% burn off), **D.** Soot, pretreated in the thermobalance at 675 K for 30 minutes.*
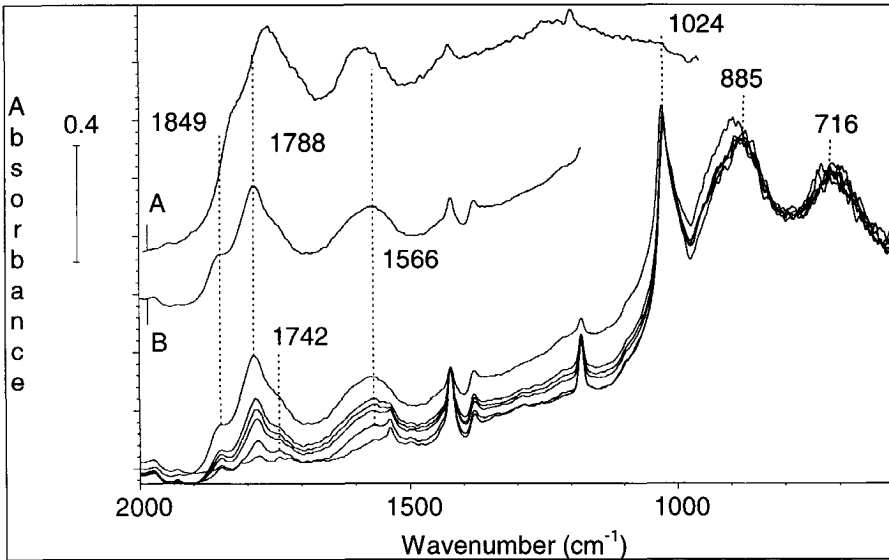

*Figure 7. In-situ DRIFT spectra of the V_2O_5 catalyzed oxidation of fullerene C60. Spectra were recorded at 575 K in 10% O_2 in Ar, every 3 minutes (bottom to top). The spectral development was established within 15 minutes. A copy of the last spectrum of the series is shifted vertically (**B**) to enable a comparison with the last spectrum in the series of non-catalytic C60 oxidation (figure 3), (**A**).*

The intensity of the absorption bands is somewhat higher than the intensity after catalytic conversion to similar or even higher conversion levels, at lower temperatures in the presence of Cr_2O_3, CuO, MoO_3 or V_2O_5.

Ex-situ DRIFT spectra of partially converted catalyst/soot samples, prepared by impregnation and reaction in the six-flow apparatus, are shown in figure 6. The spectral observations are in good agreement with those of figure 5 and appear to be independent on the preparation method of the catalyst/soot mixture: Cr_2O_3 promotes the formation of SOCs, while Fe_2O_3 and Co_3O_4 do not. The absorption bands located at 665 cm^{-1} and 579 cm^{-1} can be assigned to lattice vibrations of Co_3O_4 [29].

The formation of SOCs was also observed upon the V_2O_5-catalyzed fullerene C60 oxidation. *In-situ* DRIFT spectra of a V_2O_5/C60 'tight contact' mixture in 10% O_2 in N_2, are shown in figure 7. The bands at 1024 cm^{-1}, 885 cm^{-1}, and 716 cm^{-1} can be ascribed to V_2O_5. The development of the bands upon catalytic oxidation, corresponds to that in the *non*-catalytic oxidation in 10% O_2 in Ar (spectrum A), although the frequencies have shifted somewhat (1849 *vs.* 1838 cm^{-1}, 1788 *vs.* 1773 cm^{-1}, and 1566 *vs.* 1598 cm^{-1}). The intensities of the oxygen functionalities formed after catalytic and non-catalytic oxidation of C60 cannot be compared, since there is a considerable effect of 'dilution' of C60 with V_2O_5.
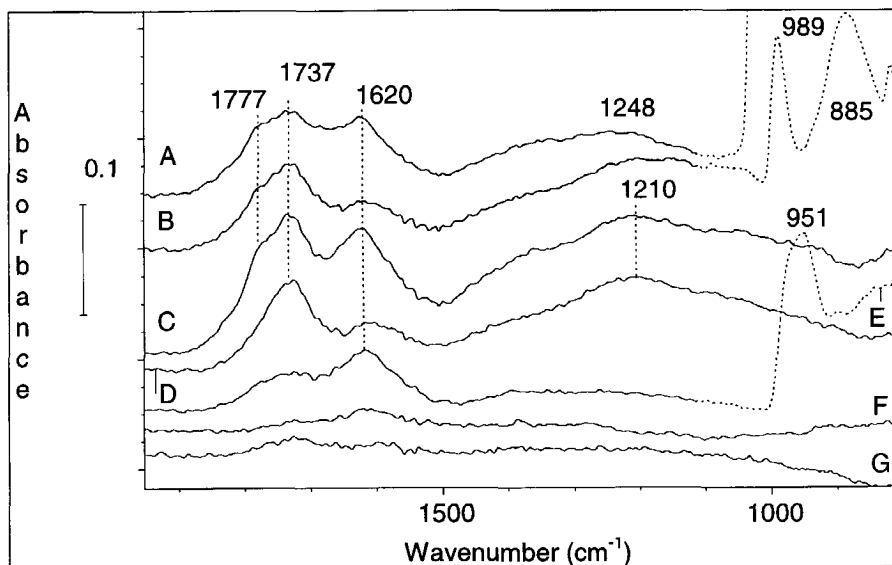
Figure 8. Ex-situ DRIFT spectra of ozonized catalyst/soot 'tight contact' physical mixtures recorded at room temperature in KBr. A. V_2O_5/soot, B. MoO_3/soot, C. CuO/soot, D. Soot, E. Cr_2O_3/soot, F. Co_3O_4/soot, G. Fe_2O_3/soot.
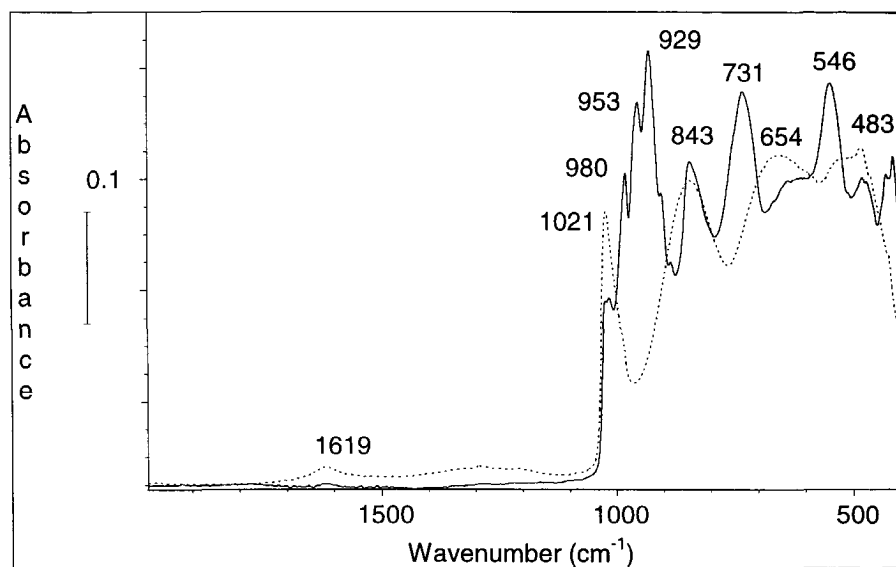
Figure 9. *Ex-situ DRIFT spectra (recorded in KBr) of a V_2O_5/soot mixture before (dashed line) and after (solid line) carbothermic reduction up to 725 K in N_2. A catalyst to soot ratio of 8:1 wt% ('tight contact') was used, to obtain a soot conversion level of 50%.*
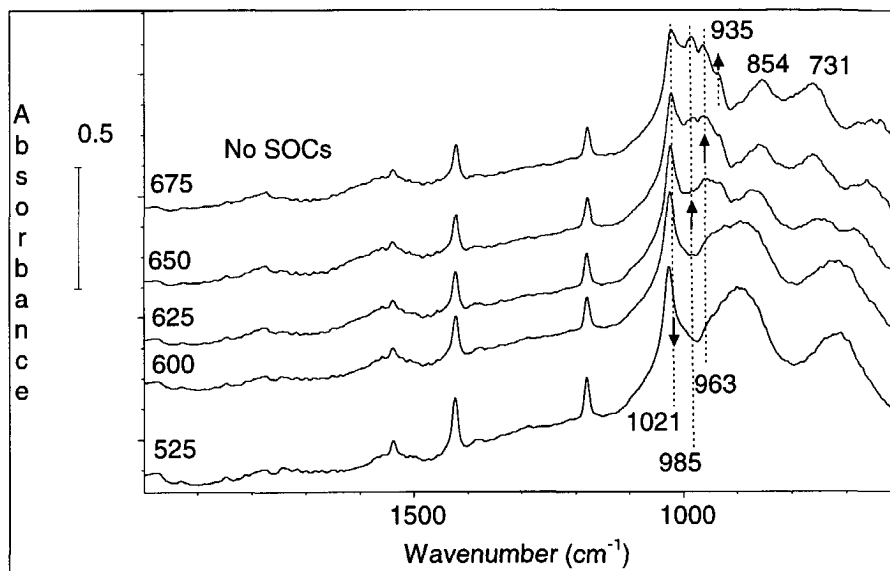
Ex-situ DRIFT spectra of catalyst/soot mixtures reacted in ozone (350 K, 30 minutes) are shown in figure 8. In the presence of Fe_2O_3 and Co_3O_4, soot ozonation does not result in the formation of SOCs, while in the presence of other catalysts (CuO, Cr_2O_3, MoO_3 and V_2O_5) SOCs can be observed. Absorption bands are located at 1777, 1737, 1620, and 1210-1248 cm^{-1}, whereas the 1857 cm^{-1} band is not present (compare figure 1a). The relative intensity of the 1737 and 1620 cm^{-1} bands is catalyst dependent. Furthermore, several absorptions (indicated with a dashed line) can be assigned to vibrational modes of MoO_3 (989 cm^{-1} and 885 cm^{-1}) and CrO_3 (951 cm^{-1}) [30]. Apparently, CrO_3 is formed by oxidation of Cr_2O_3.

An *ex-situ* DRIFT spectrum of carbothermally reduced V_2O_5 is shown in figure 9. The spectrum of the unreacted sample is shown for comparison. After reduction, reduced vanadium species are formed, such as V_6O_{13} and/or V_2O_4, identified by absorption bands at 980 cm^{-1}, 953 cm^{-1}, 929 cm^{-1}, 731 cm^{-1}, and 546 cm^{-1} [31-33].

A small band in the unreacted sample at 1619 cm^{-1} can be assigned to adsorbed water on V_2O_5. Note that the absorptions assigned to SOCs do not appear. Apparently, surface oxygen complexes are not formed by reaction of soot with lattice oxygen of V_2O_5.

In-situ DRIFT spectra of the reduction of V_2O_5 induced by fullerene C60 are shown in figure 10. Dilution with KBr was not necessary to obtain a high quality spectrum. Increasing absorptions can be observed in the range of 920-970 cm^{-1}. Absorption bands at 985 cm^{-1} and 963 cm^{-1} are very well resolved. The absorption

band at 1021 cm^{-1} shows a slightly decreasing intensity. The spectral changes can be assigned to the formation of reduced vanadium species [31-33]. In agreement with the results obtained for soot, reduction of V_2O_5 does not yield any oxygen containing functionalities. Reduction of MoO_3 and CuO, induced by soot or fullerene C60, did not result in the formation of SOCs either (not shown).

Figure 10. In-situ DRIFT spectra of an undiluted V_2O_5/C60 (2:1 wt%) mixture with increasing temperature (bottom to top). Temperatures and spectral development as indicated.

7.4. *Discussion.*

7.4.1. Non-catalytic soot and fullerene C60 oxidation.

The uncatalyzed oxidation and ozonation of soot and fullerene C60, is shown to result in the formation of several surface oxygen complexes (SOCs). Upon decomposition of the complexes formed by ozonation of soot (figures 1a and 1b), initially the 1763 cm^{-1} and 1423 cm^{-1} bands are decreasing, accompanied by a simultaneous increase of the bands located at 1857 cm^{-1} and 926 cm^{-1}. This might be explained by the condensation of two carboxylic acid groups, yielding cyclic acid anhydride species. Ozonation studies of poly aromatic hydrocarbons [35] have shown that hydroxyls are formed in a first stage, followed by a transformation into carboxylic acid functionalities. Furthermore, formation of quinones and carbonyls is possible. Very broad absorptions occur in the 2300-4000 cm^{-1} region of the DRIFT spectra presented in figures 1a and 1b, which can be assigned to carboxylic acid and hydroxylic functionalities. Band positions at 1857 cm^{-1}, 1793 cm^{-1}, and 1763 cm^{-1} (anhydrides, acids), 1617 cm^{-1} (C=O, quinones / C=C carbon framework), 1300-1500

cm^{-1} (carbonates, (dimeric) acids), 1214 cm^{-1} (COC, ethers), and 926 cm^{-1} (dimeric acids, epoxides) relate perfectly to the compounds formed upon ozonation of polyaromatic hydrocarbons and literature on the oxidation of soot in ozone [36]. In the temperature range of 350-800 K two bands appear at 3085 and 731 cm^{-1}. These bands can be assigned to stretching and bending modes of aromatic C-H species, respectively [36, 37]. The molecular structure of the various functionalities, including the corresponding absorption frequencies, is presented in chapter 1 of this thesis.

The *ex-situ* DRIFT spectra of partially oxidized soot in 10% O_2 in Ar only show three major absorption bands, which can be assigned to (*i*) ethers (1250 cm^{-1}), (*ii*) quinones (1605 cm^{-1}), and (*iii*) lactones (1735 cm^{-1}) [16]. Oxygen containing functionalities have been proposed as important intermediates in the formation of CO and CO_2 [16]. Lactones are shown to be less stable than quinones and ethers: the 1735 cm^{-1} is not observed in the spectrum of oxidized soot after treatment at 975 K in N_2 (figure 2, spectrum D), in agreement with the observations of Zhuang *et al.* [16].

The absorptions of several oxygen containing functionalities, observed in the spectra of ozonized soot, are also found in the spectra of oxidized fullerene C60 (figures 3 and 4), although the frequencies have shifted somewhat to lower wavenumbers. The absorptions at 1838 cm^{-1} and 1773 cm^{-1} can be assigned to cyclic acid anhydrides [27]. The band located at 1738 cm^{-1} can be assigned to lactones. The absorption band at 1500-1630 cm^{-1} is due to carbonaceous C=C vibrations, induced by oxygenated species [38], such as quinones. The broad absorption band ranging from 1000 to 1350 cm^{-1}, is related to aliphatic and aromatic ether functionalities. The absorption band at 907 cm^{-1} has been assigned to epoxidic functionalities [39], but might also be related to dimeric acidic functionalities. Finally, the small absorption band at 2126 cm^{-1} is caused by CO, intercalated in the fullerene molecule [27].

By evaluating the DRIFT spectra of oxidized soot (at 775 K), oxidized C60 (at 575 K) and ozonized soot (at 350 K), it is clear that the composition of the oxygen containing functionalities on carbonaceous materials is related to the carbon conversion level, the oxidation temperature, and the reactivity of the oxidant. Although small differences in wavenumbers of oxidized fullerene C60 and ozonized soot have been observed (which are likely to be caused by differences in oxidation and ozonation temperatures), the nature of the carbonaceous material appears to be less important: the use of fullerene C60 as a model compound for *in-situ* DRIFT analyses of catalytic soot oxidation, seems to be quite feasible. Fullerene C60 enables an accurate *in-situ* analysis without the need of KBr as a diluent.

7.4.2. Catalytic soot oxidation.

Important differences in the amounts of SOCs, formed upon catalytic oxidation of soot, have been observed: Fe_2O_3 and Co_3O_4 hardly promote the formation of these complexes, whereas the presence of other oxides (CuO, MoO_3, V_2O_5, and Cr_2O_3) significantly increases the amount of lactones, quinones and ethers, relative to non-catalytic oxidation at similar conditions. However, catalysts hardly affect the

absorption frequencies of the SOCs: indications for metal oxide/soot interactions, such as M-O-C bonds (M is the transition metal), have not been found. This is corroborated by *in-situ* DRIFT spectra of V_2O_5-catalyzed C60 oxidation: V_2O_5 only slightly affects the absorption frequencies, relative to non-catalytic C60 oxidation. The latter might be attributed to a spectroscopic effect of 'dilution' of C60 with V_2O_5 or a slightly different composition of the oxygen containing functionalities.

Strikingly, catalysts that do not promote the formation of SOCs in 10% O_2 in Ar at elevated temperatures (Fe_2O_3 and Co_3O_4), neither promote the formation of SOCs by ozone at relatively low temperatures (273-373 K). Accordingly, catalysts, which cause the formation of SOCs in 10% O_2 in Ar, also show the formation of SOCs at relatively low temperatures in ozone. Reaction of ozone with catalyst/soot mixtures is likely to yield CO_2, which is subsequently chemisorbed on the CuO, Cr_2O_3 (CrO_3) or V_2O_5 surfaces. The formed carboxylate species are known to be quite stable and have a vibration frequency of 1560-1630 cm^{-1} [40]. Hence, the apparent increased quinone/lactone ratio in the spectra of ozonized mixtures of CuO/soot, Cr_2O_3/soot and V_2O_5/soot, might be caused by superposition of carboxylate absorptions on the 1605 cm^{-1} band.

Ozone can be regarded as an activated oxygen species. Apparently ozone is decomposed into oxygen on the Fe_2O_3 and Co_3O_4 surfaces, before it can react with soot at low temperatures. The interaction of ozone with certain metal oxides is described by Horvath [41]. The metal oxides, which are claimed to be good catalysts for ozone decomposition, correlate with the catalysts which do not promote the formation of SOCs. Furthermore, SOCs were not formed upon carbothermic reduction of metal oxides either, even if these promote the formation of SOCs in oxygen and ozone (figures 9 and 10). Considering this promoting effect, the formation of SOCs might be explained by the migration of activated oxygen species from the catalyst surface to the carbonaceous substrate: catalysts, increasing the rate of SOCs formation, act as donors of activated oxygen. The latter reacts with the carbon surface yielding SOCs. Only very few authors have mentioned spill-over as a possible mechanism for the oxidation of carbon. Baker explained his CAEM (Controlled Atmosphere Electron Microscopy) observations for a Cr_2O_3 catalyst on graphite by a spill-over mechanism [42]. This is in agreement with the observed formation of carbon oxygen complexes in the presence of Cr_2O_3 in this study.

Oxidation of benzoate ions, bound to an alumina substrate, was claimed to be enhanced by the presence of a Pt-catalyst, without intimate contact between the catalyst and the substrate [43]. Benzoic acid adsorbed on alumina was used as a model for a coked catalyst. Baumgarten and Schuck conclude from their experiments that oxygen spill-over has to be involved in the oxidation of coked catalysts [43]. Also V_2O_5, WO_3, and Fe_2O_3 were described as being active for the benzoate oxidation via spill-over. In this study, an increase in the SOCs concentration upon soot oxidation in the presence of V_2O_5 was observed, but not in the presence of Fe_2O_3. The fact that Fe_2O_3 is a good ozone decomposition catalyst, also does not seem to correlate with the results of Baumgarten and Schuck.

Spill-over of activated oxygen has been proposed by Delmon and his coworkers [44-47] in explaining synergetic effects of physical mixtures of metal oxides in selective oxidation reactions. MoO_3 was dealt with in those studies. Combined with $BiPO_4$ and other oxides, MoO_3 was suggested to be an acceptor of activated oxygen. It was shown that removal of carbon from coked MoO_3 (MoO_3C) was enhanced by the presence of Sb_2O_4 [47]. To explain this phenomenon, spill-over of activated oxygen from Sb_2O_4 onto MoO_3 was suggested. It is likely that activated oxygen species can migrate over the MoO_3 surface and subsequently react with MoO_3C. Concerning the MoO_3 catalyzed formation of SOCs, this catalyst is suggested to act as a donor of activated oxygen in our study, instead of an acceptor. According to the donor/acceptor scale Delmon proposed [45], carbon has to be a strong acceptor of spill-over oxygen.

Another mechanism for the MoO_3 catalyzed carbon oxidation was proposed by Silva and Lobo [48]. Carbon was claimed to migrate through the MoO_3 catalyst. However, evidence for strong Mo-O-C interactions was not found in the DRIFT spectra presented here, and such an oxidation mechanism is therefore unlikely to occur under our experimental conditions.

To the best of my knowledge, CuO has never been claimed to be a donor of activated oxygen in catalytic reactions. However, oxygen, activated on Cu-surfaces covered with Pb particles, was found to spill-over (on)to the Pb surface, yielding PbO [47]. In view of the observed formation of SOCs in this study, the activation of oxygen, followed by spill-over, seems very well possible on CuO surfaces.

Considering the results of the oxidation and ozonation studies presented here, and data published in the literature, the promotion of the formation of SOCs on the surface of carbonaceous materials by the presence of V_2O_5, Cr_2O_3, MoO_3, and CuO, is proposed to be explained by spill-over of activated oxygen. The fundamental reason for the fact that some catalysts stimulate, and others do not promote the formation of SOCs, remains to be elucidated.

7.5. *Conclusions.*

- Oxidation of soot in oxygen yields several oxygen complexes (SOCs). The amount of SOCs increases with soot conversion.
- Ozone is a very strong oxidant, and SOCs with a high oxygen content are formed at relatively low temperatures. Decomposition of these complexes starts at 525 K: acid anhydrides and lactone functionalities are less stable than quinones and ethers.
- Fullerene C60 seems to be a useful model compound for soot, suited for *in-situ* DRIFT spectroscopic studies: the DRIFT spectra of ozonized soot and air-oxidized C60 are quite similar. Moreover, the use of fullerene C60 allows a DRIFT analysis without the use of a diluent.

- The presence of several metal oxide catalysts (MoO_3, Cr_2O_3, V_2O_5, and CuO) is found to enhance the formation of SOCs, while others (Fe_2O_3 and Co_3O_4) do not promote the formation of those complexes.
- Metal oxides which do not promote the formation of SOCs in oxygen at elevated temperatures, neither promote the formation of SOCs in ozone at relatively low temperatures.
- Oxygen from the metal oxide lattice does not contribute to SOCs formation.
- Catalytic formation of SOCs is proposed to be related to spill-over of activated oxygen.

7.6. *References.*

[1] D.W. McKee, Fuel, 62 (1983) 170.
[2] D.W. McKee, J. Catal., 108 (1987) 480.
[3] R. Meijer, F. Kapteijn and J.A. Moulijn, Fuel, 73 (1994) 723.
[4] F. Kapteijn, R. Meijer, J.A. Moulijn and D. Cazorla-Amoros, Carbon, 32 (1994) 1223.
[5] T. Kyotani, S. Hayashi and A. Tomita, Energy Fuels, 5 (1991) 683.
[6] T. Kyotani, S. Hayashi, A. Tomita, J.A. MacPhee and R.R. Martin, Fuel, 71 (1991) 655.
[7] E.L. Fuller and N.R. Smyrl, Fuel, 64 (1985) 1143.
[8] N.R. Smyrl and E.L. Fuller, Appl. Spectrosc., 41 (1987) 1023.
[9] E.L. Fuller and N.R. Smyrl, Appl. Spectrosc., 44 (1990) 451.
[10] B.J. Meldrum, J.C. Orr and C.H. Rochester, J.Chem.Soc.Chem.Commun., (1985) 1176.
[11] B.J. Meldrum and C.H. Rochester, Fuel, 70 (1991) 57.
[12] B.J. Meldrum and C.H. Rochester, J.Chem.Soc.Faraday Trans., 86 (1990) 2997.
[13] B.J. Meldrum and H. Rochester, J.Chem.Soc.Faraday Trans., 86 (1990) 1881.
[14] C.H. Rochester and B.J. Meldrum, J.Chem.Soc.Faraday Trans., 86 (1990) 861.
[15] M.S. Akhter, A.R. Chughtai and D.M. Smith, Appl.Spectrosc., 45 (1991) 653.
[16] Q.-L. Zhuang, T. Kyotani and A. Tomita, Energy Fuels, (1994) 714.
[17] M.B. Cerfontain and J.A. Moulijn, Fuel, 62 (1983) 256.
[18] I.L.C. Freriks, H.M.H. Wechum, J.C.M. Stuiver and R. Bouwman, Fuel, 60 (1981) 463.
[19] J.Y. Yuh and E.E. Wolf, Fuel, 62 (1981) 252.
[20] J.P.A. Neeft, M. Makkee and J.A. Moulijn, Fuel, in preparation.
[21] G. Mul, F. Kapteijn and J.A. Moulijn, in preparation.
[22] J.P.A. Neeft, 'Catalytic oxidation of soot-Potential for the reduction of diesel particulate emissions', Ph.D. Thesis TU Delft (1995).
[23] J. van Doorn, J. Varloud, P. Meriaudeau and V. Perrichon, Appl. Catal. B: 1 (1992) 117.
[24] J.P.A. Neeft, M. Makkee and J.A. Moulijn, Appl. Catal. B: 8 (1996) 57.
[25] J.A. Neeft, L. Boellaard, M. Makkee, A.M. van der Kraan and J.A. Moulijn, in preparation.
[26] M. Wohlers, A. Bauer and R. Schloegl, Microchim. Acta, submitted.
[27] M. Wohlers, H. Werner, D. Herien, T. Schedel-Niedrig, A. Bauer and R. Schlögl, Synthetic Metals, 77 (1996) 299.
[28] G. Mul, F. Kapteijn and J.A. Moulijn, Prepr. Pap. -Am. Chem. Soc. Div. Fuel Chem., 41 (1996) 230.

[29] R.A. Nyquist and R.O. Kagel, Infrared Spectra of Inorganic Compounds, Academic Press, New York, 1971.

[30] M.A. Vuurman, D.J. Stufkens, A. Oskam and J.A. Moulijn, J. Mol. Catal., 60 (1990) 83.

[31] L.D. Frederickson and D.M. Hausen, Anal. Chem., 35 (1963) 818.

[32] K. Mori, A. Miyamoto and Y. Murakami, J.Chem.Soc. Faraday Trans., 82 (1986) 13.

[33] M. Akimoto, M. Usami and E. Echigoya, Bull.Chem.Soc.Japan, 51 (1978) 2195.

[34] G. Mul, C. Doornkamp, F. Kapteijn and J.A. Moulijn, in preparation.

[35] P.S. Baily, Ozonation in Organic Chemistry II: Non-olefinic Compounds, Academic Press, New York, 1982.

[36] P.E. Fanning and M.A. Vannice, Carbon, 31 (1993) 721.

[37] C.A. Sergides, J.A. Jassim, A.R. Chughtai and D.M. Smith, Appl.Spectrosc., 41 (1987) 482.

[38] C. Morterra and M.J.D. Low, Spectrosc. Lett., 15 (1982) 689.

[39] G. Cardini, R. Bini, P.R. Salvi, V. Schettino, M.L. Klein, R.M. Strongin, L. Brard and A.B. Smith, J. Phys. Chem., 98 (1994) 9966.

[40] J. Bijsterbosch, 'Copper based catalysts for CO oxidation and NO reduction', PhD Thesis, University of Amsterdam, (1993)

[41] M. Horvath, L. Bilitzky and J. Huettner, Ozone, Elsevier, Amsterdam, 1985.

[42] R.T.K. Baker and J.J. Chludzinski, Carbon, 19 (1981) 75.

[43] E. Baumgarten and A. Schuck, Appl. Catal., 37 (1988) 247.

[44] L.T. Weng, P. Ruiz, Y. Ma and B. Delmon, J. Mol. Catal., 61 (1990) 99.

[45] L.T. Weng, P. Ruiz and B. Delmon, Stud.Surf.Science and Catal., 72 (1992) 399.

[46] L.T. Weng, P. Ruiz and B. Delmon, J. Mol. Catal., 52 (1989) 349.

[47] B. Zhou and B. Delmon, in Proceedings of 2nd conf. on Spillover, Leipzig, 1989, pp. 87-95.

[48] I.F. Silva and L.S. Lobo, J.Catal., 126 (1990) 489.

8

Catalytic Soot Oxidation by Transition Metal Oxides: An $^{18}O_2$ study

Abstract

Physical mixtures of soot and several transition metal oxides (Cr_2O_3, Co_3O_4, Fe_2O_3, MoO_3, V_2O_5, and K_2MoO_4) were treated in $^{18}O_2$ at 625-675 K in a high vacuum batch reactor. By analysis of the reaction products ($C^{16}O$, $C^{18}O$, $C^{16}O_2$, $C^{16}O^{18}O$ and $C^{18}O_2$) for experiments in which $^{18}O_2$ and $^{16}O_2$ were fed alternately, it was shown that the amount of gas-phase oxygen incorporated in the gaseous products, increases in the series $K_2MoO_4 < V_2O_5 < MoO_3 < Co_3O_4 = Fe_2O_3 < Cr_2O_3$. The experimental results agree well with oxygen exchange data given in the literature: less than one monolayer is exchangeable for Co_3O_4, a monolayer for Fe_2O_3 and Cr_2O_3 and the entire bulk for MoO_3, V_2O_5, and K_2MoO_4. Relatively large amounts of $C^{16}O$ were formed in the presence of MoO_3, which is explained by carbothermic reduction of volatile MoO_3 species with soot, yielding MoO_2 and CO. An adapted redox mechanism is proposed for Fe_2O_3 and Co_3O_4 catalyzed soot oxidation in which only a small fraction of lattice oxygen (located in the surface layer, defined as surface oxygen) is available. Surface oxygen of Cr_2O_3 is also found to be involved in the oxidation mechanism. However, based on the relatively high fraction of ^{18}O labeled products and experimental results of other publications, a spill-over mechanism, involving so-called *super* surface oxygen, is also proposed for Cr_2O_3 catalysis. A combination of a spill-over mechanism and a redox mechanism, including oxygen from the bulk, is proposed for MoO_3 and V_2O_5. A similar mechanism is proposed for K_2MoO_4, with the exception that gas-phase oxygen is needed to keep the reaction going ('push-pull mechanism), whereas carbothermic reduction of MoO_3 and V_2O_5 was also observed in the absence of gas-phase oxygen.

8.1. *Introduction*

Mechanistic studies on transition metal oxide catalyzed oxidation reactions have been performed extensively. Generally four (!) oxidation mechanisms have been proposed within a range of 625-750 K, the temperature range where diesel soot oxidation catalysts should be operative: a redox (Mars and van Krevelen [1,2,3]), a push-pull *e.g.* [4,5], an associative (Langmuir-Hinselwood) [6,7], and a spill-over mechanism [8-10]. The redox mechanism can be illustrated as follows:
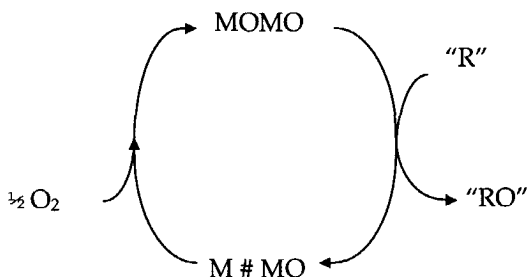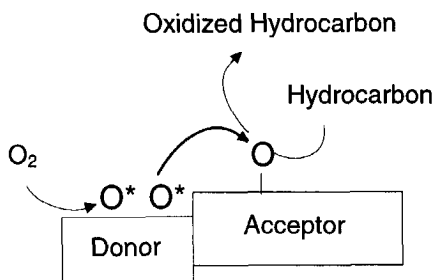

Scheme 1. *Representation of the redox mechanism for oxidative reactions over transition metal oxides.*

In scheme 1 M is the transition metal, O oxygen, R the reactant, and # an oxygen vacancy. For example, in the sixties Winter found evidence for such a redox mechanism in the catalytic oxidation of CO by transition metal oxides, using labeled oxygen ($^{18}O_2$) [11-13]. In the seventies Boreskov and coworkers used $^{18}O_2$ to study the oxygen exchange of gaseous oxygen with the lattice for a large number of transition metal oxides and found a correlation between the oxygen exchange activity and the activity in the oxidation of carbon monoxide, hydrogen, and methane of several metal oxides [14-16]. Keulks [17] demonstrated that lattice oxygen of bismuth molybdate was incorporated in acrolein formed by propene oxidation. Recently, Iizuka and coworkers [18-20] studied the mechanism of the MoO_3 catalyzed oxidation of CO by $^{18}O_2$ and also found evidence for a redox mechanism.

The push-pull mechanism is a variant of the redox mechanism and has been proposed for catalytic CO oxidation on ZnO [4]: CO is adsorbed on the ZnO surface, followed by CO_2 formation (with the incorporation of lattice oxygen) in combination with a simultaneous reoxidation of the active site. CO_2 is only formed in the presence of gaseous oxygen, while ZnO is not reduced by CO at temperatures where catalytic oxidation takes place.

The associative mechanism involves the adsorption of both the reactant (*e.g.* CO) and oxygen on the surface of a transition metal oxide. Recombination of dissociated oxygen and CO results in CO_2 formation. The oxidized product only contains gas-phase oxygen, while lattice oxygen is not consumed.

Finally, oxidation reactions on combinations of two metal oxides have been explained by a so-called spill-over mechanism. Oxygen is adsorbed and activated on one metal oxide (the donor) and transferred to the second metal oxide (the acceptor). The reactant (*e.g.* a hydrocarbon) reacts with the oxygen adsorbed on the acceptor [8-10] (Scheme 2, O* indicates activated oxygen).

Scheme 2. *Representation of the 'spill-over' mechanism, proposed to explain synergetic effects of metal oxides in selective oxidation reactions.*

Although catalytic carbon oxidation has been studied extensively, only few studies describe details such as the mechanistic steps given above. The use of $^{18}O_2$ is limited to a study on CaO catalyzed carbon oxidation [21-23]. Nonetheless, several authors have proposed a redox mechanism for the catalytic oxidation of carbonaceous materials by transition metal oxides such as activated carbon, single crystal graphite, and model soot particulate [24-26]. McKee *et al.* [24-26] state that only if carbothermic reduction (*i.e.* reduction of the metal oxide by carbon) is thermodynamically feasible, a metal oxide can catalyze the oxidation of carbon. This tendency to generalize the behavior of transition metal oxides in the oxidation of carbon is not compatible with the that different soot oxidation profiles were found, strongly depending on the transition metal oxide involved [27]. The formation of surface oxygen complexes (SOCs) was held responsible for those differences [27,28]. SOCs are proposed to be generated by oxygen spill-over (the carbon or soot surface acts as the acceptor). In order to explain several microscopic observations, Baker [29] proposed such a spill-over mechanism for the Cr_2O_3 catalyzed soot oxidation, but this is one of the few transition metal oxides whose activity cannot be explained by a redox mechanism.

The objective of this chapter is to reveal the mechanism of catalytic soot oxidation by various metal oxides, which are relevant for soot oxidation. Some of these do not enhance the amount of SOCs on the soot surface (Fe_2O_3, Co_3O_4), while others promote SOCs formation (Cr_2O_3, V_2O_5, MoO_3, and K_2MoO_4) [28]. $^{18}O_2$ has been used for this purpose. The results are evaluated and compared with carbothermic reduction experiments [37].

8.2. *Experimental*

Fe_2O_3 and Co_3O_4 were prepared by thermal decomposition of the corresponding nitrates (Aldrich, 99%) in air at 775 and 875 K, respectively. Cr_2O_3 was prepared by calcination of CrO_3 at 775 K, and V_2O_5 by thermal decomposition of NH_4VO_3 at 675 K in air. MoO_3 (Merck, *p.a.*) and K_2MoO_4 (Fluka >98%) were used as received. The BET surface area of the pure metal oxides, determined by N_2 adsorption at 77 K, was as follows: Fe_2O_3, 19 m^2g^{-1}, Cr_2O_3, 24 m^2g^{-1}, Co_3O_4, 22 m^2g^{-1}, V_2O_5, 6 m^2g^{-1}, MoO_3, ≈ 1 m^2g^{-1}, and K_2MoO_4, < 1 m^2g^{-1}. Printex-U, kindly provided by Degussa, was used as a model soot (BET-surface area: 96 m^2g^{-1}). Soot was mixed with the transition metal oxides in a weight ratio of 1:2 by milling in a ball-mill (1 h) in order to obtain 'tight contact' conditions, needed for a reproducible soot oxidation activity [30,31].

A high-vacuum system was used for the oxidation experiments, which was connected to a mass-spectrometer (VG Instruments MM8-80s) [32]. Molecular masses in the range of 10-60 $g.mol^{-1}$ were analyzed every two minutes. Sample sizes of 30-70 mg (soot and metal oxide) were used and reacted in a quartz batch reactor of about 910 ml. The experimental procedure is outlined in figure 1.
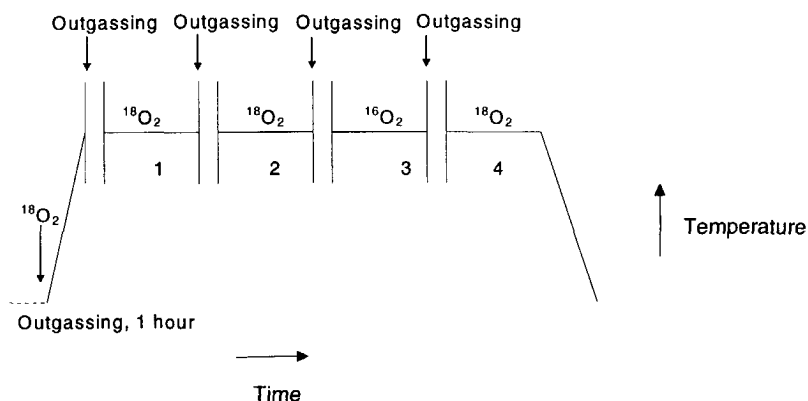

Figure 1. *Outline of the experimental procedure.*

Outgassing of the sample was accomplished in about one hour at room temperature in vacuum. Subsequently, $^{18}O_2$ was introduced in the reactor, followed by heating to the desired reaction temperature (625-700 K) with 5 K/min. $^{18}O_2$ and several reaction products (labeled and unlabelled CO and CO_2, formed by decomposition of SOCs and reaction with $^{18}O_2$) were removed by outgassing of the reactor for 15 minutes. Then, the first isothermal experiment was started by introduction of 0.3 mbar $^{18}O_2$ in the reactor, which amount was consumed isothermally (depending on the catalytic activity) in about 30-60 minutes. After every

experiment the reactor was outgassed for another 15 minutes to remove reaction products, before introduction of a new batch of $^{18}O_2$ (or $^{16}O_2$). Generally, two isothermal experiments were performed in $^{18}O_2$, followed by one in $^{16}O_2$ and one in $^{18}O_2$, as indicated in figure 1. The masses have not been corrected for fragmentation. The product ratio ($C^{18}O_{out}/C^{16}O_{out}$) is defined in (1) as:

$$\frac{2\,C^{18}O_2 + C^{18}O + C^{18}O^{16}O}{2\,C^{16}O_2 + C^{16}O + C^{18}O^{16}O} \tag{1}$$

The amount of oxygen introduced in the batch reactor was relatively small: a soot conversion level of only 1-2% was reached after 4 sequential runs.

8.3. Results

8.3.1. Uncatalyzed soot oxidation

In general, labeled/unlabelled product distributions obtained in the metal oxide catalyzed soot oxidation, might be affected by the uncatalyzed soot oxidation and carbon oxygen complexes already present on the soot surface before the experiment. The oxidation pattern of soot at 650 K, without any catalyst, is shown in figure 2.
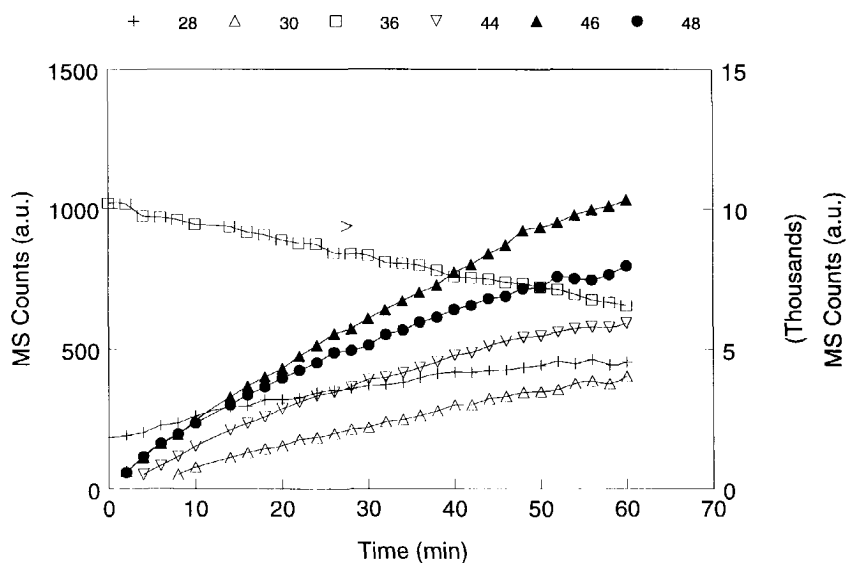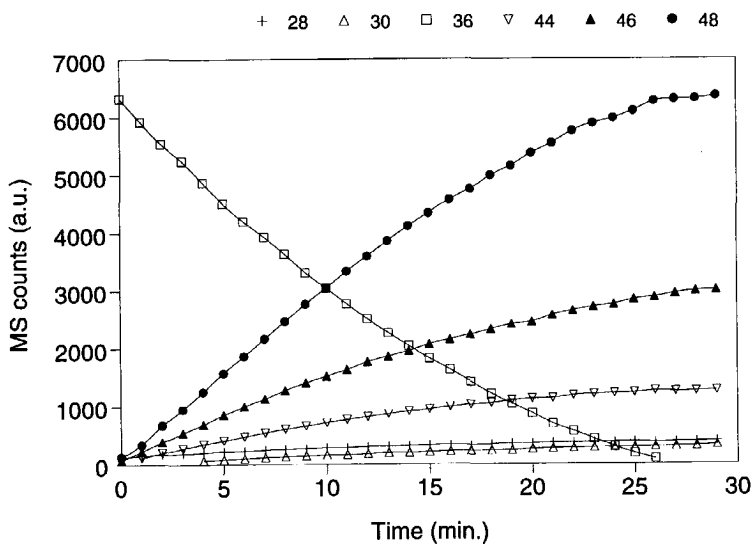

Figure 2. *First isothermal measurement performed with 25 mg pure soot in 0.3 mbar $^{18}O_2$. The development of the $C^{16}O$ (28), $C^{18}O$ (30), $^{18}O_2$ (36, right y-axis), $^{16}O_2$ (44), $C^{16}O^{18}O$ (46) and $C^{18}O_2$ (48) concentrations at 650 K as a function of time are shown.*

The oxidation rate is rather low (compare *e.g.* figure 3): only 30-40% of the introduced amount of $^{18}O_2$ is converted within 1 hour. Although only $^{18}O_2$ and soot are brought into the batch reactor, several ^{16}O labeled products (predominantly $C^{18}O^{16}O$) are formed, obviously due to decomposition of surface oxygen complexes (SOCs) originally present on the surface of Printex-U. In view of the low reaction rate, and low amount of oxygen functionalities on the soot surface [30], the contribution of the uncatalyzed soot oxidation to product distributions obtained in isothermal catalytic soot oxidation experiments, is limited.

8.3.2. Cr_2O_3 and Fe_2O_3 catalyzed soot oxidation

A typical development of the product concentrations by reaction of a Cr_2O_3/soot sample at 675 K in $^{18}O_2$ is shown in figure 3.

*Figure 3*. Development of the $C^{16}O$ (28), $C^{18}O$ (30), $^{18}O_2$ (36), $C^{16}O_2$ (44), $C^{16}O^{18}O$ (46) and $C^{18}O_2$ (48) concentrations with time at 675 K. First isothermal measurement, performed on 70 mg of a Cr_2O_3/soot mixture (2:1 wt-%).

It takes about 30 minutes to consume 0.3 mbar $^{18}O_2$ at 675 K. Besides $C^{18}O_2$ and $C^{18}O$, ^{16}O labeled compounds are also formed, of which the highest quantity is $C^{16}O^{18}O$. Once $^{18}O_2$ has completely reacted, CO and CO_2 are no longer produced: carbothermic reduction is not observed. Exchange of $C^{18}O_2$ and $C^{18}O^{16}O$ with lattice oxygen is slow compared to the oxidation rate (figure 3): only a minor contribution

of the exchange reaction to the product distribution (obtained in the presence of $^{18}O_2$) is expected.

Figure 4 shows the product ratio ($C^{18}O_{out}/C^{16}O_{out}$) of the isothermal experiments performed with the Cr_2O_3/soot mixture in $^{18}O_2$. The product ratio is shown to increase with the number of times $^{18}O_2$ has been introduced. A relatively small amount of ^{18}O labeled products was produced in the third experiment, which was performed in $^{16}O_2$. The development of the product concentrations, after the introduction of $^{16}O_2$, is shown in figure 5.
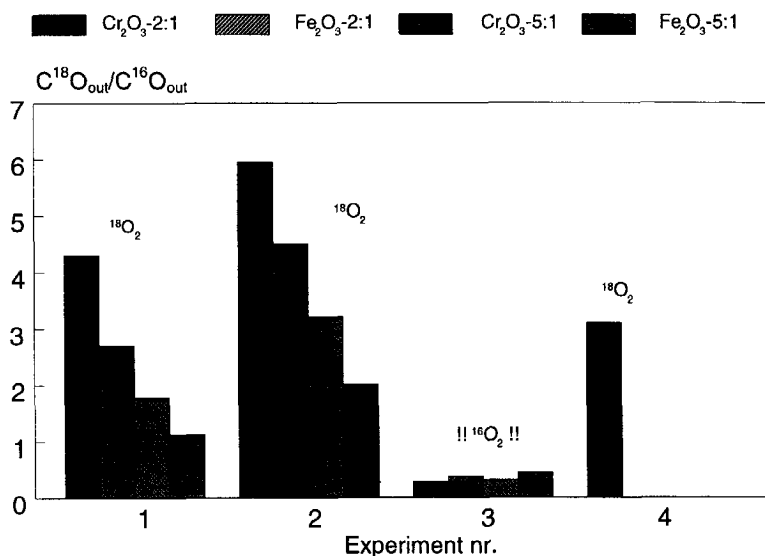
Figure 4. *Product distributions for Cr_2O_3 and Fe_2O_3 catalyzed soot oxidation. Catalyst to soot ratio's of 2:1 and 5:1 (wt%) were applied. The ratio obtained after experiments performed in $^{16}O_2$ are also shown.*

The development of the $C^{16}O_2$ concentration shows an S-shaped curve, which indicates that a sequential reaction takes place. At the end of the fourth part of the experiment $C^{16}O_2$ is the main product, followed by $C^{18}O^{16}O$ and $C^{16}O$. Figures 4 and 5 show that at least some ^{18}O is stored in the sample, either on the soot surface, or in the Cr_2O_3 catalyst. The product ratio calculated after the fourth part of the experiment, which was performed in $^{18}O_2$, is also included in figure 4. This time, the development of the $C^{18}O_2$ concentration yields an S-shaped curve (not shown). The obtained $C^{18}O_{out}/C^{16}O_{out}$ ratio is somewhat lower than the ratio of the first part of the experiment 1, obviously because the sample had already been heated in $^{18}O_2$, before this part of the experiment was performed. The product ratio's will be further evaluated in paragraph 4.1 of this chapter.
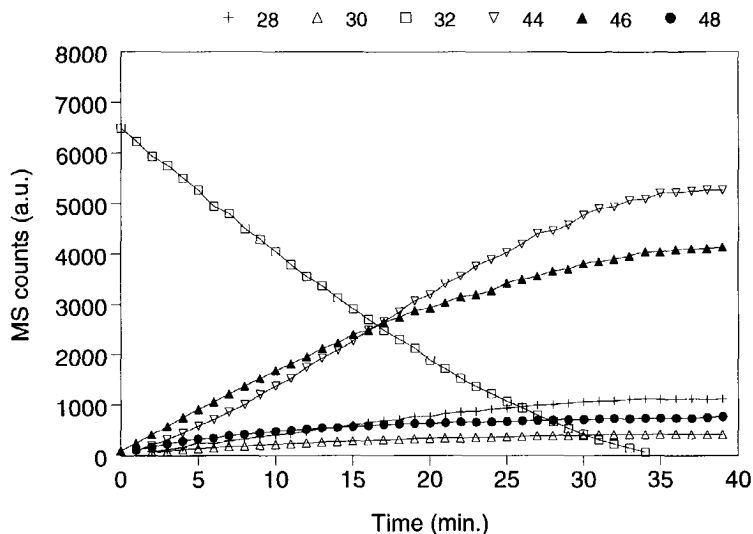
Figure 5. *Development of the $C^{16}O$ (28), $C^{18}O$ (30), $^{16}O_2$ (32), $C^{16}O_2$ (44), $C^{16}O^{18}O$ (46) and $C^{18}O_2$ (48) concentrations in $^{16}O_2$ with time at 675 K. The measurement was performed on a Cr_2O_3/soot mixture after treatment of 70 mg sample in $^{18}O_2$ three times.*

Although unexpected, the oxidation patterns obtained for the Fe_2O_3 catalyst are qualitatively very similar to those presented for the Cr_2O_3 catalyst. However, the Fe_2O_3 catalyst is less active than Cr_2O_3, resulting in longer reaction times: 60 minutes are required to convert 0.3 mbar $^{18}O_2$ at 675 K. The Fe_2O_3 sample was reacted isothermally in $^{18}O_2$ two consecutive times: the product distributions are included in figure 4. The $C^{18}O_{out}/C^{16}O_{out}$ ratio is somewhat lower than that obtained for the Cr_2O_3 catalyst, but still relatively high. Oxidation of soot in the absence of oxygen was not observed: carbothermic reduction of the catalyst does not take place under the experimental conditions. This indicates that surface and/or lattice oxygen are not easily removed from the Fe_2O_3 catalyst.

The isothermal experiment performed in $^{16}O_2$ (experiment 3 in figure 4), yielded a similar S-shaped curve for the $C^{16}O_2$ production as was observed for Cr_2O_3 (within an identical time range). Apparently, the Fe_2O_3 and Cr_2O_3 catalysts behave quite similarly.

Oxidation experiments with samples containing a Cr_2O_3/soot and Fe_2O_3/soot ratio of 5:1, resulted in lower $C^{18}O_{out}/C^{16}O_{out}$ ratio's (figure 4) than samples containing a 2:1 catalyst/soot ratio. Apparently a higher amount of oxygen initially associated with the metal oxide, is incorporated in the products. The results obtained

by switching $^{18}O_2$ for $^{16}O_2$ agree with this observation: in $^{16}O_2$ a higher $C^{18}O_{out}/C^{16}O_{out}$ ratio is obtained for the 5:1 samples than for the 2:1 samples. Again, the shape of the oxidation profiles in $^{16}O_2$ is quite similar for the 5:1 Cr_2O_3/soot and Fe_2O_3/soot samples: an S-shaped $C^{16}O_2$ concentration profile was obtained for both catalysts.

8.3.3. Co_3O_4-catalyzed soot oxidation

The activity of Co_3O_4 in soot oxidation was shown to be highly dependent on the preparation temperature of the catalyst. Calcination of $Co(NO_3)_2$ at 675 K yields a very active Co_3O_4 catalyst, whereas calcination at higher temperatures (875 K or 1075 K) diminishes the activity [30].
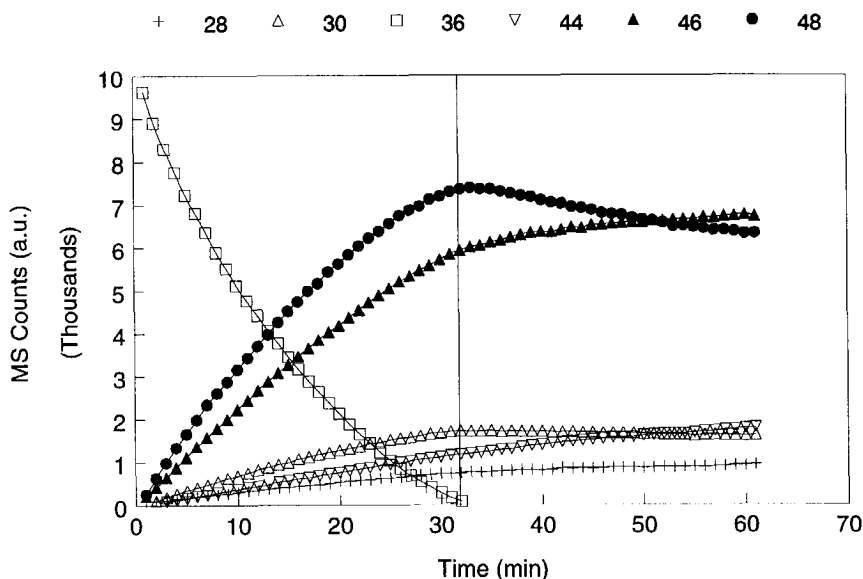
Figure 6. Development of the $C^{16}O$ (28), $C^{18}O$ (30), $^{18}O_2$ (36), $C^{16}O_2$ (44), $C^{16}O^{18}O$ (46) and $C^{18}O_2$ (48) concentrations in $^{18}O_2$ with time. The measurement was performed on a Co_3O_4/soot mixture (2:1) after heating 70 mg sample in $^{18}O_2$ to 625 K.

In this study, Co_3O_4 prepared by calcination at 875 K was used, because the activity of this catalyst is comparable with the activity of the other catalysts tested, although at a 50 K lower temperature. The development of the products formed in $^{18}O_2$ at 625 K, is shown in figure 6. The main product is $C^{18}O_2$, followed by $C^{18}O^{16}O$ and $C^{18}O$. However, changes in the product distribution are observed after complete conversion of $^{18}O_2$: exchange of $C^{18}O_2$ with lattice oxygen yields $C^{16}O^{18}O$ and $C^{16}O_2$, while some $C^{18}O$ is also converted into $C^{16}O$. Although the exchange reaction is slow

compared to the oxidation reaction, the influence of this reaction on the calculated $C^{18}O_{out}/C^{16}O_{out}$ ratio is higher for the Co_3O_4 catalyst than for the Cr_2O_3 and Fe_2O_3 catalysts.

Besides $C^{18}O_2$ exchange, oxygen exchange was observed during the Co_3O_4 catalyzed soot oxidation reaction, predominantly yielding $^{18}O^{16}O$. A very small amount of $^{16}O_2$ was detected, probably formed by a consecutive exchange of $^{18}O^{16}O$ with lattice oxygen. $^{18}O_2$ exchange reactions with lattice oxygen of unsupported transition metal oxides have been reviewed by Novakova [33] and Boreskov [14], and will not be discussed here.

Switching from $^{18}O_2$ to $^{16}O_2$ results in the instant formation of large amounts of ^{16}O-labeled CO and CO_2. However, an S-shaped curve is not obtained. So only a small amount of ^{18}O, stored in the Co_3O_4/soot sample during the experiments performed in $^{18}O_2$, is supposed to be available for soot oxidation. Some of the ^{18}O atoms incorporated in the Co_3O_4 catalyst are exchanged for ^{16}O by reaction with $^{16}O_2$, as gaseous $^{18}O^{16}O$ was detected during the experiment.
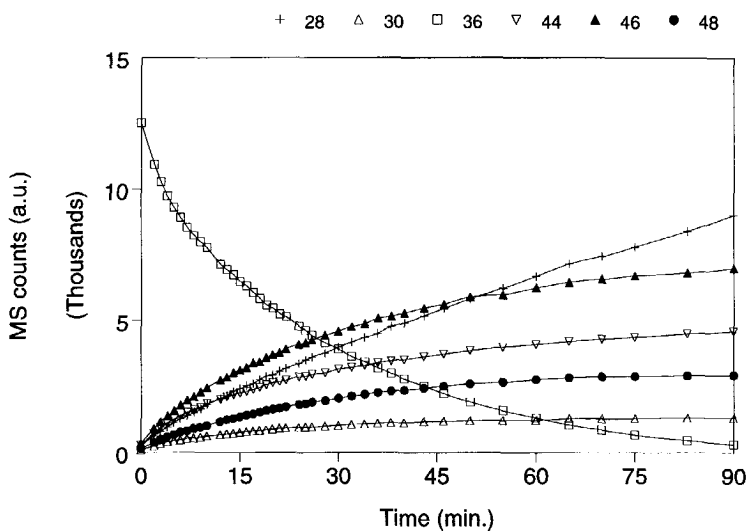
Figure 7. *Development of the $C^{16}O$ (28), $C^{18}O$ (30), $^{18}O_2$ (36), $C^{16}O_2$ (44), $C^{16}O^{18}O$ (46) and $C^{18}O_2$ (48) concentrations in $^{18}O_2$ with time at 625 K. The measurement was performed after heating 70 mg of the MoO_3/soot sample in $^{18}O_2$.*

8.3.4. MoO_3, V_2O_5, and K_2MoO_4 catalyzed soot oxidation

The result obtained for a MoO_3/soot sample (2:1 wt-%) in $^{18}O_2$ at 625 K is shown in figure 7. A relatively high amount of ^{16}O is incorporated in the products: $C^{18}O^{16}O$ is the main product, followed by $C^{16}O_2$ and $C^{18}O_2$. Hence, lattice oxygen is involved in the MoO_3 catalyzed soot oxidation. Striking is the continuous production of $C^{16}O$, independent of the decreasing oxygen partial pressure.
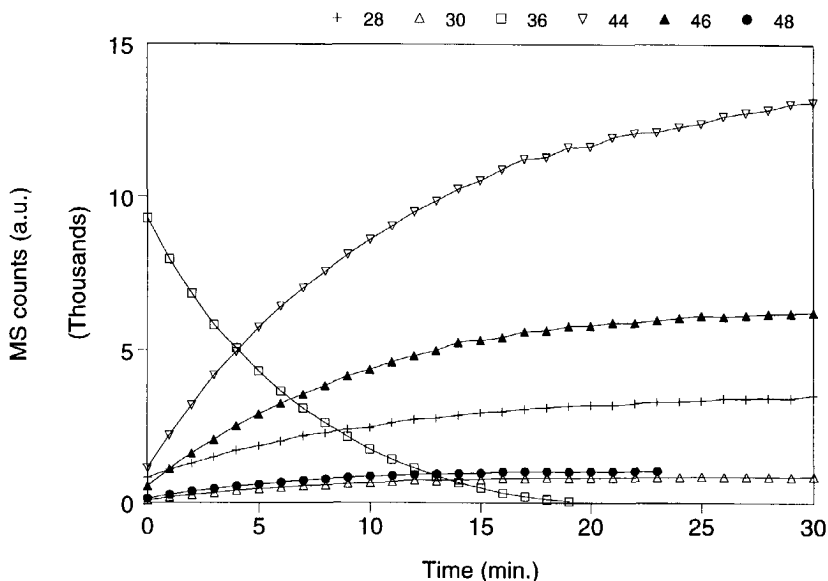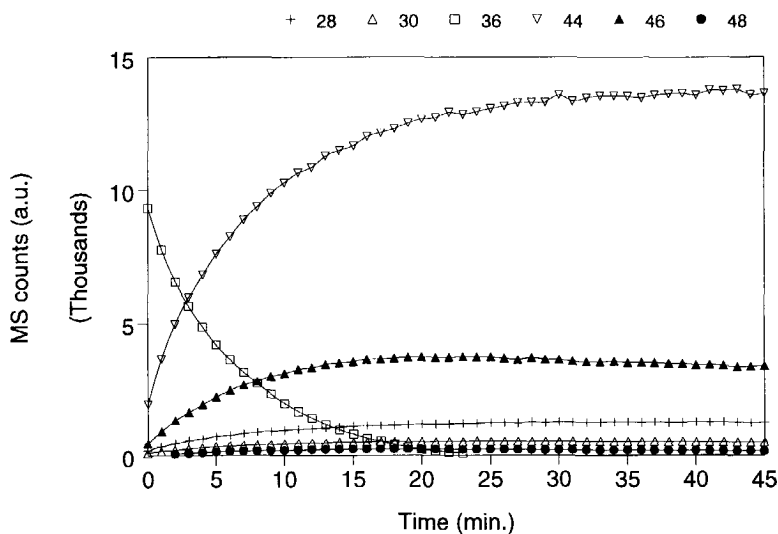

Figure 8. Development of the $C^{16}O$ (28), $C^{18}O$ (30), $^{18}O_2$ (36), $C^{16}O_2$ (44), $C^{16}O^{18}O$ (46) and $C^{18}O_2$ (48) concentrations in $^{18}O_2$ with time at 625 K, after heating 70 mg of the V_2O_5/soot sample in $^{18}O_2$.

The results for the V_2O_5-catalyzed soot oxidation are shown in figure 8. Compared to MoO_3, an even higher amount of $C^{16}O_2$ is formed, indicating the participation of lattice oxygen. Although some $C^{16}O_2$ and $C^{16}O$ is produced after 100 % $^{18}O_2$ conversion, formation of CO was not as extended for V_2O_5 as for MoO_3. The $C^{18}O_2$ concentration remained constant after 100% conversion of labeled oxygen: it is therefore concluded that $C^{18}O_2$ exchange on V_2O_5 does not occur.

The measurement with the K_2MoO_4/soot sample is shown in figure 9. Hardly any CO is formed. Of the amount of CO_2 produced, the main product is $C^{16}O_2$, followed by $C^{18}O^{16}O$, and a very low amount of $C^{18}O_2$. After 100% conversion of gas-phase oxygen, the product distribution does not change and CO and CO_2 are no longer formed.

Figure 9. Development of the $C^{16}O$ (28), $C^{18}O$ (30), $^{18}O_2$ (36), $C^{16}O_2$ (44), $C^{16}O^{18}O$ (46) and $C^{18}O_2$ (48) concentrations in $^{18}O_2$ with time at 625 K, after heating 70 mg of the K_2MoO_4/soot sample in $^{18}O_2$.
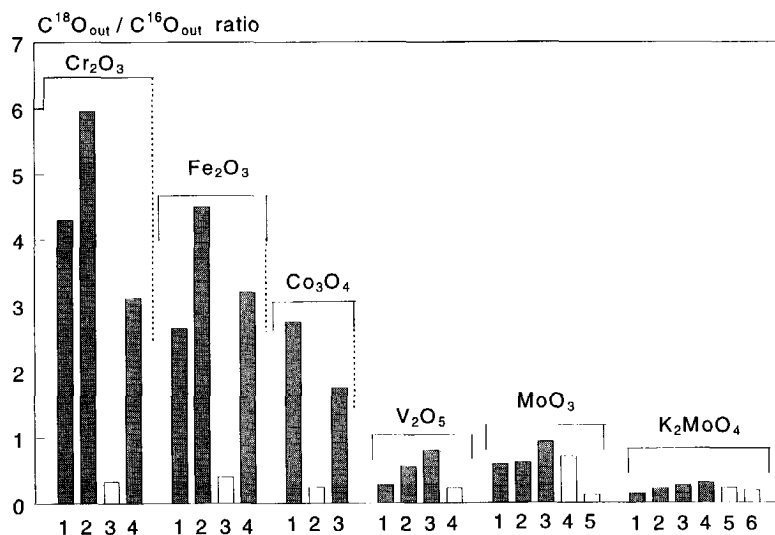
Figure 10. Development of the $C^{18}O_{out}/C^{16}O_{out}$ ratio with the experiment number for the MoO_3, V_2O_5 and K_2MoO_4 catalysts. The ratio of Cr_2O_3, Fe_2O_3, and Co_3O_4 are also shown. A catalyst to soot ratio of 2:1 was used in all cases. Experiments in $^{16}O_2$ are indicated by an open bar and in $^{18}O_2$ by a solid bar.

This is in agreement with TG/DSC experiments [34], which indicate that carbothermic (bulk) reduction of K_2MoO_4 is not possible. Furthermore, oxygen exchange of $C^{18}O^{16}O$ with lattice oxygen occurs at a slow rate, as is witnessed by the concentration development of $C^{18}O^{16}O$ after 100% $^{18}O_2$ conversion. Measurement 4 shows a relatively high $C^{18}O_{out}/C^{16}O_{out}$ ratio: apparently, during the former three experiments, quite some ^{18}O was incorporated in the MoO_3 lattice, available for soot oxidation in measurement 4 (in $^{16}O_2$). A much lower $C^{18}O_{out}/C^{16}O_{out}$ ratio is obtained in a consecutive experiment in $^{16}O_2$.

An overview of the relative amounts of gas phase oxygen and lattice oxygen involved in the catalytic oxidation of soot, expressed by the $C^{18}O_{out}/C^{16}O_{out}$ ratio, is shown in figure 10. The V_2O_5/soot sample was treated three sequential times in $^{18}O_2$, followed by two times in $^{16}O_2$. A gradually increasing $C^{18}O_{out}/C^{16}O_{out}$ ratio is observed. In the fourth measurement $^{16}O_2$ was used as the oxidizing agent: several ^{18}O-labeled products could be detected, yielding the $C^{18}O_{out}/C^{16}O_{out}$ ratio shown in figure 10. The product ratio of the MoO_3/soot sample was calculated directly after 100% conversion of gas phase oxygen. Measurement 4 (in $^{16}O_2$) shows a relatively high $C^{18}O_{out}/C^{16}O_{out}$ ratio: apparently, during the former three experiments, quite some ^{18}O was incorporated in the MoO_3 lattice, available for soot oxidation in measurement 4 (in $^{16}O_2$). A much lower $C^{18}O_{out}/C^{16}O_{out}$ ratio is obtained in a consecutive experiment in $^{16}O_2$.

The isothermal reaction of the K_2MoO_4/soot mixture was performed three sequential times in $^{18}O_2$. In a fourth experiment $^{16}O_2$ was used as the oxidant. A very low amount of ^{18}O labeled products was obtained. Reaction of a second batch of $^{16}O_2$ yielded an amount of ^{18}O labeled products equal to the amount obtained in the second experiment, which was performed in $^{18}O_2$. A fast interconversion of the product distributions, as was observed for the Cr_2O_3, Fe_2O_3, and Co_3O_4 catalysts, does not occur for K_2MoO_4 catalysis.

8.4. Discussion

8.4.1. An overview of the tested catalysts

IR and isothermal soot oxidation studies revealed that Cr_2O_3 behaves quite differently from Fe_2O_3 with respect to the formation of surface oxygen complexes (SOCs) and the shape of the isothermal oxidation profile (rate *vs.* carbon conversion) [30,35]. Cr_2O_3 promotes the formation of SOCs, explained by oxygen spill-over, whereas Fe_2O_3 does not. Based on these results, a higher $C^{18}O_{out}/C^{16}O_{out}$ ratio was expected for Cr_2O_3 than for Fe_2O_3. Indeed, a higher $C^{18}O_{out}/C^{16}O_{out}$ ratio was found for the Cr_2O_3 catalyst, which rapidly increased with the experiment number. Assuming that some oxygen is associated with and incorporated in the carbon surface, the product distributions might be explained by a spill-over mechanism. The calculation of the product distributions of the Fe_2O_3 and Cr_2O_3 samples is slightly affected by differences in activity: the lower activity of Fe_2O_3 results in longer

reaction times, and, as a consequence, in a higher contribution of exchange reactions to the final product distribution. Exchange of labeled CO_2 with lattice oxygen of Fe_2O_3 was observed. Taking this and the results shown in figure 4 into account, it is concluded that Cr_2O_3 and Fe_2O_3 behave quite similarly with respect to the oxidation of soot in $^{18}O_2$. As spill-over of oxygen results in the formation of surface oxygen complexes (SOCs) and they are not formed in Fe_2O_3 catalysis [28], the spill-over mechanism cannot explain the results for the Fe_2O_3 catalyst. Moreover, if spill-over played a predominant role in Cr_2O_3- and Fe_2O_3-catalyzed soot oxidation, a higher catalyst/soot ratio should not have lead to a decreasing $C^{18}O_{out}/C^{16}O_{out}$ ratio. The results indicate that ^{18}O stored in the Cr_2O_3/soot and Fe_2O_3/soot sample is located in the catalyst and not on the soot surface. The results obtained by switching from $^{18}O_2$ to $^{16}O_2$, are in agreement with these considerations: the 5:1 catalyst/soot samples show higher $C^{18}O_{out}/C^{16}O_{out}$ ratio's than the 2:1 catalyst/soot samples. This indicates that a higher amount of ^{18}O was incorporated in the transition metal oxide surface during the oxidation experiments in $^{18}O_2$, induced by a higher amount of available active sites. It was considered that the change in product ratio for a catalyst/soot ratio of 5:1, might also be caused by a higher $C^{18}O_2$ exchange rate, as more metal oxide surface is available. However, this explanation is not supported by the minor change in product distribution after 100% $^{18}O_2$ conversion. Apparently, oxygen associated with the surface of the catalyst, is involved in the oxidation of soot both by Fe_2O_3 and Cr_2O_3, although the bulk of the latter compound cannot be carbothermally reduced below 1000 K [37].

Co_3O_4 does not promote the formation of surface oxygen complexes and does not react according to a spill-over mechanism. This indicates that the high amount of $C^{18}O_2$ is due to ^{18}O reacting *via* the Co_3O_4 surface. Actually, the $C^{18}O_{out}/C^{16}O_{out}$ ratio would have been higher than the ratio shown in figure 10, if di-oxygen and CO_2 exchange would not have affected the product distribution.

MoO_3 shows a different oxidation behavior than Fe_2O_3, Co_3O_4 and Cr_2O_3. The $C^{18}O_{out}/C^{16}O_{out}$ ratio's are much smaller than those of the Cr_2O_3/soot Fe_2O_3/soot, and Co_3O_4/soot samples. A lot of lattice oxygen is available for reaction with soot. The formation of CO is probably caused by evaporation and sublimation processes occurring under the reaction conditions (675 K, high vacuum). MoO_3 is known to have a rather high vapor pressure at relatively low temperatures [36]. The reaction of the subliming oxide with soot yields CO and MoO_2: as the reaction is stoichiometric and MoO_2 is not carbothermically reduced at 675 K, CO_2 is not formed. Oxygen exchange was observed (results not shown): $^{16}O_2$ was formed by reaction of $^{18}O_2$ with lattice oxygen, whereas $^{16}O^{18}O$ was not observed. Iizuki *et al.* [18-20] did not mention oxygen exchange, suggesting that the exchange is related to the presence of soot. Although (slightly) affected by exchange of $^{18}O_2$ with bulk oxygen, the results indicate that besides a spill-over mechanism, witnessed by SOCs formation in DRIFT spectroscopic observations [28], lattice oxygen of MoO_3 is participating in the catalytic oxidation of soot.

Although some $C^{16}O_2$ and $C^{16}O$ are produced after 100 % $^{18}O_2$ conversion, formation of CO was not as obvious for V_2O_5 as for MoO_3. However, a DRIFT spectrum of the V_2O_5/soot sample, recorded after the oxidation experiments (not shown) revealed the formation of reduced vanadium species. Hence, carbothermic reduction of V_2O_5 did occur and lattice oxygen of V_2O_5 is participating in the catalytic oxidation of soot.

The catalysis by K_2MoO_4 is rather unique in the sense that hardly any gas-phase oxygen is directly incorporated in the oxidation products. Although $^{18}O_2$ exchange rates are not available for this compound, a very fast and efficient oxygen exchange with the bulk is likely to be possible at the reaction conditions applied. Thus, activated $^{18}O_2$ is incorporated in the K_2MoO_4 lattice, and ^{16}O labeled products are released. The exchange of $C^{18}O_2$ with lattice oxygen of K_2MoO_4 has also been considered. However, this exchange reaction was hardly observed in the absence of $^{18}O_2$ (figure 9). This study and a TG/DSC analysis have shown that carbothermic reduction of K_2MoO_4 is not possible. Apparently, gas-phase oxygen is needed to stimulate the desorption of carbon oxides.

In general the results obtained for the metal oxides investigated can be correlated to the reducibility and mobility (or exchangeability) of lattice oxygen. The amount of lattice oxygen incorporated in the oxidation products decreases in the series K_2MoO_4 > MoO_3 > V_2O_5 > Co_3O_4 = Fe_2O_3 > Cr_2O_3. This range corresponds quite well with literature dealing with $^{18}O_2$ exchange reactions: less than one monolayer is exchangeable for Co_3O_4, a monolayer for γ-Fe_2O_3 and α-Cr_2O_3 and the entire bulk for MoO_3 and V_2O_5 [14-16]. The mobility of lattice oxygen ions in MoO_3 and V_2O_5 is rather high. Therefore, a high amount of $^{18}O_2$ can be absorbed by these metal oxides, yielding ^{16}O labeled carbon oxide species. The observed low $C^{18}O_{out}/C^{16}O_{out}$ ratio for V_2O_5 and MoO_3 can thus be explained. The results for K_2MoO_4 suggest an even higher mobility of lattice oxygen.

8.4.2. Oxidation mechanism

The main goal of the investigations described here, was to elucidate the mechanism, by which metal oxides are active in the catalytic oxidation of soot and if there is a correlation between the formation of surface oxygen complexes (SOCs), as described in a previous publication on the catalytic oxidation of soot [28], and a spill-over mechanism. Neeft *et al.* [27] already discussed propositions for carbon oxidation mechanisms: a subdivision of so-called oxygen transfer mechanisms was made, based on different roles of gas-phase and lattice oxygen [37]. A correlation was found between the carbothermic reduction temperatures of certain transition metal oxides, determined in a thermobalance, and the catalytic activity. In general, the temperatures of carbothermic reduction are somewhat higher than the catalytic oxidation temperatures. This can be explained by the fact that only bulk reduction (by carbon) results in a measurable weight decrease, whereas only surface reduction and reoxidation is needed for carbon oxidation. This is corroborated by Mössbauer

measurements [37], which showed that Fe_2O_3 is not reduced during catalytic soot oxidation. As Mössbauer is a bulk technique, surface reduction of Fe_2O_3 cannot be observed.

The experimental results presented here and in a separate paper [28], can be explained if three types of oxygen are defined: *super*-surface oxygen, surface oxygen, and lattice oxygen. *Super* surface oxygen is defined as activated oxygen located **on** the surface of a metal oxide (it is not incorporated in the surface layer). These oxygen species might spill-over to other oxides or soot. Surface oxygen is activated oxygen which is incorporated in the surface (*i.e.* first) layer and transported *via* this surface layer to the catalyst/soot interface. Lattice oxygen is defined as oxygen associated with the bulk of the metal oxide, below surface oxygen. As was already discussed in paragraph 4.1, exchange of one oxygen atom for another, is very well possible, but largely dependent on the metal oxide. An overview of the interactions of oxygen species with metal oxides is given in figure 11.

Model A in figure 11 represents a modified Mars & van Krevelen mechanism for Fe_2O_3 and Co_3O_4 catalysis: $^{18}O_2$ is activated on sites in the direct vicinity of a soot particle, yielding ^{18}O labeled products. Furthermore, activation might occur on sites remote from a soot particle. Activation is proposed to yield surface oxygen, which is transported through the surface metal oxide surface layer to the catalyst soot interface. First, ^{16}O atoms, initially present in the surface layer of Fe_2O_3 and Co_3O_4 react and are replaced by ^{18}O atoms. Subsequently, the ^{18}O atoms react at the surface/soot interface. The experimental results suggest that reaction of surface oxygen with soot is only possible, if gas-phase oxygen is present: apparently gas-phase oxygen is needed to activate surface oxygen, *i.e.* to 'push the chain of surface oxygen atoms' forward to the metal oxide/ soot interface. A slight surface reduction causes a stagnation of this chain, as residual oxygen is more strongly bonded due to oxygen deficiency in this layer. A more complicated description of the processes occurring on the Cr_2O_3 surface is needed to explain all the experimental observations (figure 11, model B). Besides surface oxygen, several ^{18}O atoms are not incorporated into the Cr_2O_3 surface layer, but present as *super* surface oxygen species, which move in an activated state over the surface (indicated by an asterisk) to a soot particle, followed by spill-over and the formation of surface oxygen complexes (SOCs). These complexes slowly decompose yielding ^{18}O labeled carbon oxides. Whether exchange of $^{18}O^*$ with surface ^{16}O can occur before SOCs are formed, remains to be elucidated. Oxygen, activated on the surfaces of Co_3O_4 and Fe_2O_3, either recombines into O_2 or is directly transformed in surface oxygen. Adding the exchange of bulk oxygen with surface oxygen to the Cr_2O_3 model, yields the proposed oxidation model for V_2O_5 and MoO_3 (figure 11, model C). Also for these oxides, *super* surface oxygen might spill-over onto the carbon surface, yielding SOCs. Furthermore, surface oxygen is exchanged with bulk oxygen, explaining the low $C^{18}O_{out}/C^{16}O_{out}$ ratio for these catalysts. Gas-phase oxygen is not needed to 'push the chain forward': transport of bulk oxygen atoms to the catalyst/soot interface occurs in the absence of gas-phase oxygen, as is witnessed by carbothermic reduction.

The reaction of potassium containing catalysts with carbon has been extensively studied by Cerfontain *et al.* [38,39] and Meijer *et al.* [40,41]. A potassium oxide cluster is proposed as being the active species. In chapter 5 it was shown by DRIFT spectroscopy and X-Ray diffraction, that these potassium oxide clusters might very well be formed by disproportionation of K_2MoO_4, yielding $K_2Mo_2O_7$ [34]. Furthermore, a rather strong interaction of potassium ions with carbon oxygen complexes has been found [34]. From the observations made here, the so-called push-pull mechanism (see introduction of this paper) can be proposed for K_2MoO_4: a simultaneous reduction and reoxidation of an active site, followed by oxygen exchange with the bulk, can explain the experimental results. In fact this mechanism is quite similar to scheme C of figure 11, with the exception that bulk oxygen does not react in the absence of gas-phase oxygen: the 'oxygen chain', including the bulk, can only be pushed forward in the presence of oxygen.
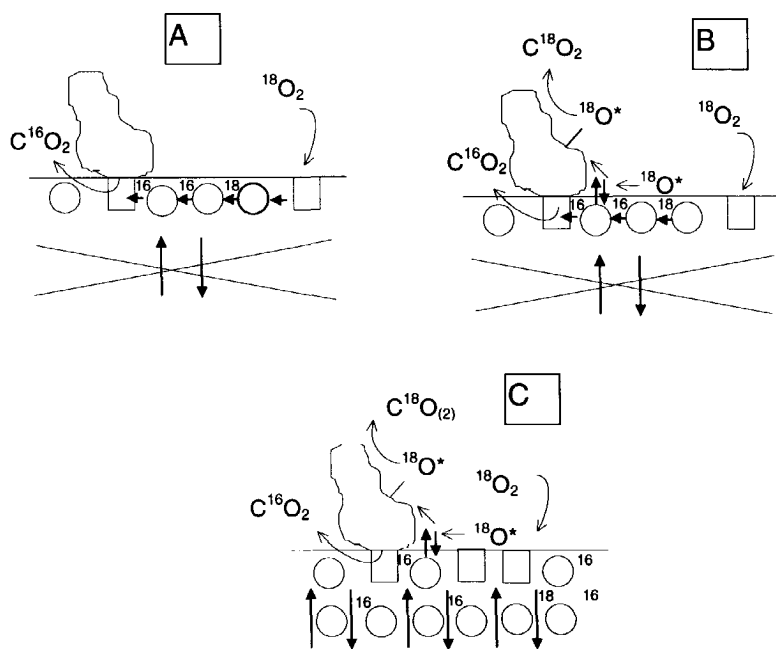
Figure 11. *Overview of the processes occurring on the surfaces of different transition metal oxides: A. Co_3O_4, and Fe_2O_3; B. Cr_2O_3; C. MoO_3, V_2O_5, and K_2MoO_4: active sites (vacancies) are indicated by squares, and lattice oxygen ions by circles. Charge transfers are not considered.*

Although several mechanistic details were not elucidated in this study, such as the sequence of reactions leading to $C^{16}O^{18}O$ formation (*e.g.* catalytic oxidation of $C^{16}O$ with $^{18}O_2$), it is obvious that an interplay between surface and lattice oxygen

determines to a great extent the final product distributions: the higher the exchange rate, the lower the amount of $^{18}O_2$ incorporated in the products.

8.5. *Conclusions*

- In view of the results, it is useful to distinguish lattice (*i.e.* bulk) oxygen, surface oxygen and *super* surface oxygen.
- To explain the presented phenomena on catalytic soot oxidation, two mechanisms are proposed to occur simultaneously: a redox, involving surface or lattice oxygen associated with the metal oxide, and a spill-over mechanism, involving so-called *super* surface oxygen yielding carbon surface oxygen complexes.
- Lattice oxygen of Cr_2O_3, Fe_2O_3, and Co_3O_4 is hardly involved in the catalytic oxidation of soot. Only reduction and reoxidation of the surface layer is likely to occur.
- In the case of V_2O_5 and MoO_3, quite some lattice oxygen is incorporated in the carbon oxides produced. Moreover, V_2O_5 and MoO_3 are evidently carbothermally reduced in the absence of $^{18}O_2$, yielding $C^{16}O_2$ and $C^{16}O$.
- A simultaneous reduction and reoxidation (a push-pull mechanism) followed by a fast exchange with bulk oxygen is likely to explain the observations made for the K_2MoO_4 catalyzed soot oxidation.
- MoO_3 yields relatively high amounts of $C^{16}O$, formed by carbothermic reduction of evaporated MoO_3 species.

8.6. *References*

[1] F. van Looij, 'The Catalytic Partial Oxidation of Methane to Synthesis Gas', Ph.D. Thesis, Utrecht University, (1994), chapter 2.
[2] C. Kröger, Z. Anorg. u. Allg. Chem. 206 (1932) 289.
[3] P. Mars and D.W. van Krevelen,. Chem. Eng. Sci. 3 (1954) 41.
[4] V.D. Sokolovskii, Catal.Rev.-Sci.Eng. 32 (1&2) (1990) 1.
[5] M. Bielanski and J. Haber, Oxygen in Catalysis, M. Dekker Inc. New York, 1991.
[6] G.I. Golodets, Stud. Surf. Sci. Catal. 15 (1983) 438.
[7] A. Maltha, S.C. van Wermeskerken, T.L.F. Favre, P.A.J.M. Angevaare, E.J. Grootendorst, C.A. Koutstaal, A.P. Zuur and V. Ponec, Catal. Today, 10 (1991) 387.
[8] L.T. Weng, P. Ruiz, Y. Ma and B. Delmon, J.Mol.Catal. 61 (1990) 99.
[9] L.T. Weng, P. Ruiz and B. Delmon, Stud.Surf.Science and Catal. 72 (1992) 399.
[10] L.T. Weng, P. Ruiz and B. Delmon, J.Mol.Catal., 52 (1989) 349.
[11] E.R.S. Winter,. J. Chem. Soc. (1955) 2726.
[12] E.R.S. Winter,. J. Chem. Soc. (1964) 5781.
[13] E.R.S. Winter,. J. Chem. Soc. A. (1968) 2889.
[14] G.K. Boreskov, Adv. Catal. 15 (1964) 285.
[15] V.V. Popovskii, G.K. Boreskov, V.S. Muzykantov, V.A. Sazonov and S.G. Shubnikov, Kinet.Katal. 10 (1969) 643.
[16] V.S. Muzykantov, T. Cheshkova and G.K. Boreskov, Kinet. Katal. 14 (1973) 365.

[17] G.N. Keulks, J. Catal. 19 (1970) 232.

[18] Y. Iizuka, J. Chem. Soc. Faraday Trans. 90 (1994) 1301.

[19] Y. Iizuka, H. Tanigaki, M. Sanada, J. Tsunetoshi, N. Yamauchi and S. Aral, J. Chem. Soc. Faraday Trans. 90 (1994) 1307.

[20] Y. Iizuka, J. Chem. Soc. Faraday Trans. 90 (1994) 3449.

[21] T. Kyotani, S. Hayashi and A. Tomita, Energy and Fuels, 5 (1991) 683.

[22] T. Kyotani, S. Hayashi, A. Tomita, J.A. MacPhee and R.R. Martin, Fuel, 71 (1991) 655.

[23] R.R. Martin, J.A. MacPhee, T. Kyotani, S. Hayashi and A. Tomita, Carbon, 29 (1991) 475.

[24] D.W. McKee, Carbon, 8 (1970) 623.

[25] D.W. McKee, Fuel, 62 (1983) 170.

[26] D.W. McKee, J. Catal. 108 (1987) 480.

[27] J.P.A. Neeft, G. Mul, M. Makkee and J.A. Moulijn, in preparation.

[28] G. Mul, J.P.A. Neeft, F. Kapteijn and J.A. Moulijn, in preparation.

[29] R.T.K. Baker and J.J. Chludzinski, Carbon, 19 (1981) 75.

[30] J.P.A. Neeft, 'Catalytic oxidation of soot-Potential for the reduction of diesel particulate emissions', Ph.D. Thesis TU Delft (1995), chapter 7.

[31] J. van Doorn, J. Varloud, P. Meriaudeau and V. Perrichon, Appl. Catal. B: Env. 1 (1992) 117.

[32] E.J. Grootendorst, 'Selective Reduction Reactions on Oxidic Catalysts', Ph.D. Thesis Leiden University (1994).

[33] J. Novakova, Catal. Rev. 4 (1970) 77.

[34] G. Mul, Chapter 5 of this thesis.

[35] G. Mul, F. Kapteijn and J.A. Moulijn, in Proceedings of 22nd Biennial Conference on Carbon, San Diego, 1995, pp. 554-555.

[36] O. Knacke, O. Kubachewski and K. Hesselman, Thermochemical Properties of Inorganic Substances, Springer Verlag, Berlin, 1991.

[37] J.A. Neeft, L. Boellaard, M. Makkee, A.M. van der Kraan and J.A. Moulijn,. in preparation.

[38] M.B. Cerfontain and J.A. Moulijn, Fuel, 62 (1983) 256.

[39] M.B. Cerfontain and J.A. Moulijn, in Proceedings of International Conference on Coal Science (1983) p. 419.

[40] R. Meijer, B. van der Linden, F. Kapteijn and J.A. Moulijn, Fuel, 70 (1991) 205.

[41] R. Meijer, F. Kapteijn and J.A. Moulijn, Fuel, 73 (1994) 723.

9

The catalytic activity of transition metal oxides and their Ag- or Au-promoted analogues in the catalytic oxidation of soot and CO

Abstract

An order in catalytic CO oxidation activity of $Co_3O_4 > CuO > MnO_x$ was found. An associative mechanism might explain the CO oxidation over MnO_x catalysts at relatively low temperatures, as a step in the oxidation profile was observed. A redox mechanism is proposed for the Co_3O_4 and CuO catalyzed CO oxidation, and for MnO_x at higher temperatures. Addition of Ag to Co_3O_4 or CuO hardly affected the CO oxidation activity, whereas a positive effect was found for MnO_x. Addition of Au increased the low temperature CO oxidation activity of Co_3O_4 and CuO, but negatively affected the activity of these metal oxides at higher temperatures (> 365 K). An enormous positive effect was found for MnO_x, which is not yet understood.

Furthermore, several isothermal profiles of the Co_3O_4, CuO, V_2O_5, and MnO_x catalyzed soot oxidation are presented. The catalytic activity of transition metal oxides in the oxidation of soot appears to be largely determined by the surface area of the catalyst, *i.e.* the number of catalyst/soot contact points. Furthermore, the similarity in activity order found in the oxidation of CO as well as soot, *i.e.* $Co_3O_4 > CuO > MnO_x$, suggests an effect of the metal-oxygen bond strength on the oxidation activity and the involvement of a redox mechanism. A positive effect of the addition of Ag to Co_3O_4, CuO, and MnO_x on the soot oxidation activity was observed, ascribed to a high intrinsic activity of Ag_2O species, which are reoxidized by the transition metal oxides. Au modification of the investigated metal oxides negatively affected the soot oxidation activity, which is tentatively explained by a partial coverage of the metal oxide surface with Au particles. The addition of K, Ag or Cu to V_2O_5 also negatively affected the soot oxidation activity, ascribed to a diminished mobility and reducibility of oxygen anions in vanadium bronzes.

9.1. *Introduction*

The collection of soot in a monolithic filter and simultaneous oxidation at diesel exhaust gas temperatures (600 K) is considered to be feasible in the abatement of the emission of diesel soot. A catalyst is needed for this purpose, since soot non-catalytically oxidizes into CO_2 and CO at approximately 875 K, whereas diesel exhaust temperatures are in the range of 475 - 675 K [1].

The catalytic activity of transition metal oxides in the oxidation of soot has been extensively investigated by *e.g.* Ahlstrom and Odenbrand [2,3], Neeft *et al.* [4] and van Doorn *et al.* [5]. In the publications cited, supported as well as unsupported oxides were used. The catalytic effect appeared to be strongly dependent on the intensity of contact between the soot and the transition metal oxide.

The role of surface and lattice oxygen and the spill-over capability of the oxidic catalysts in the oxidation of soot have been discussed in chapter 8 of this thesis. However, this mechanistic study, in which $^{18}O_2$ was used, encompassed only the initial few percent of soot conversion. In this chapter isothermal soot oxidation profiles over the entire conversion range are presented, to further evaluate the properties of certain transition metal oxides. Furthermore, the catalytic activity in soot oxidation is related to the activity of the metal oxides in CO oxidation.

Although several papers describe multi component catalysts for the catalytic oxidation of soot [6-12], such as Pt/Co/La catalysts [6,8-9], Cu/K/Mo catalysts, and Cu/K/V catalysts [13], Ag- or Au-promotion of transition metal oxides to improve the catalytic activity in the oxidation of soot has hardly been reported. Since the addition of Ag or Au has been shown to be very effective in the (low temperature) oxidation of CO [14-20], the effect of Ag- or Au-modification on the activity of Co_3O_4, CuO and MnO_x in the oxidation of soot is reported in this chapter and related to the CO oxidation activity. Since additions of silver, copper or potassium to V_2O_5-based catalysts have been reported to enhance the activity in the oxidation of CO, due to the formation of so-called vanadium bronzes [21,22], the soot oxidation activity of vanadium bronzes is also described in this chapter.

9.2. *Experimental*

9.2.1. Synthesis of the catalysts

9.2.1.1. Vanadium pentoxide

Vanadium pentoxide was prepared by decomposition of ammonium metavanadate (NH_4VO_3, 'Baker Analyzed'). Decomposition was performed in an oven in air, under static conditions at 623 K, during 15 hours. The color of the powder changed from white to cinnabar-red. The product was analyzed by DRIFT spectroscopy (compare chapters 2 and 7 for experimental procedures). Absorptions at 1022 and 835 cm^{-1} were observed, which are attributed to symmetrical stretching

vibrations of vanadyl oxygen (V=O) and V-O-V bridges, respectively. A small shoulder at 980 cm^{-1} reveals the formation of V^{4+}=O species. Broad absorptions, located at 625 and 495 cm^{-1}, can also be observed in the spectrum, attributed to VO$_3$, and V-O-V bending vibrations, respectively [21,23].

High purity grade V$_2$O$_5$ was purchased from Aldrich, and used as received. The DRIFT spectrum corresponded to the V$_2$O$_5$ (*ex* vanadate) spectrum. However, the 625 cm^{-1} band was located at 590 cm^{-1}, indicating a smaller concentration of V^{4+} ions. A relatively smaller intensity of the 980 cm^{-1} vibration is in agreement with this observation [21].

9.2.1.2. Vanadium bronzes

A bronze is a non-stoichiometric solid solution of a metal and a transition metal oxide, characterized by the general formula M$_x$TO$_m$, in which M is a metal or alkali metal and T is one of the early transition metals. Vanadium bronzes can be described by M^+_xV$^{4+}_x$V$^{5+}_{(2-x)}$O$_5$, in which vanadium has two different oxidation states: V^{4+} and V^{5+}. The fraction of tetravalent vanadium is equal to the fraction of M$^+$. During the synthesis of the bronze V^{5+} is reduced by the inserted metal to V^{4+}, thereby forming M$^+$. In the case of alkali metals, a non-stoichiometric vanadium bronze can also be prepared by heating vanadium pentoxide with M$_2$O, M$_2$CO$_3$ or MVO$_3$ (M is the alkali metal), causing evolution of CO$_2$ and/or oxygen. The β-sodium vanadium bronze was synthesized by treatment of a thoroughly mortared mixture of 0.096 g Na$_2$CO$_3$ and 1 g V$_2$O$_5$ ex NH$_3$VO$_4$ at 823 K for 15 hours under a nitrogen atmosphere [24]. The sample quickly changed color from yellow to brown, due to sodium vanadate formation. Subsequently, the temperature was raised to 900 K and maintained for 20 hours. The sample color changed to dark blue, indicating bronze formation. The bronze was analyzed by DRIFT spectroscopy: the spectrum contains a strong band at 996 cm^{-1}.

The ß-phase of the potassium bronze with the stoichiometry K$_{0.23}$V$_2$O$_5$, was synthesized by mixing V$_2$O$_5$ *ex* NH$_3$VO$_4$ and K$_2$CO$_3$ (Baker analyzed) and treatment at 773 K for 15 hours in a nitrogen atmosphere. Subsequently, the sample allowed to react at 900 K for 8 hours. The products were cooled to room temperature and crushed with a pestle and mortar and treated at 900 K for another 15 hours. The color of the sample changed from dark brown to dark blue metallic. XRD analysis confirmed that K$_{0.23}$V$_2$O$_5$ had been formed. However, a small amount of remaining V$_2$O$_5$ was observed in the DRIFT spectrum of the product, in agreement with the findings of Van den Berg [21].

A copper vanadium bronze with the stoichiometry Cu$_{0.35}$V$_2$O$_5$ was prepared by solid state reaction of a stoichiometric mixture of metallic copper (Aldrich >99%) and vanadium pentoxide ex NH$_3$VO$_4$ during 45 hours at 883 K in a nitrogen atmosphere. A dark blue material with a metallic luster was obtained. The IR spectrum showed a V^{4+}=O stretching vibration at 983 cm^{-1}. Some residual V$_2$O$_5$ was also present, witnessed by a small 1021 cm^{-1} band. The spectrum corresponds to that of Van den Berg [21].

Ag$_{0.35}$V$_2$O$_5$ was prepared by solid state reaction of a mixture of 0.83 g V$_2$O$_5$ ex NH$_3$VO$_4$ with 0.17 g Ag (Aldrich >99%). The formation of the bronze is a slow process

and the mixture was allowed to react for 45 hours at 900 K. A grayish product was obtained and FTIR and XRD analyses showed the formation of the silver vanadium bonze. V_2O_5 was not detected and an IR absorption band around 1000 cm^{-1} was split in three smaller ones due to the heterogeneity of the V=O species in $Ag_{0.35}V_2O_5$ [21].

The BET-surface areas of the bronzes, obtained by N_2 adsorption at 77 K, are given in Table 1.

9.2.1.3. Ag based catalysts

Several Ag based transition metal oxide catalysts were prepared by the coprecipitation method. A solution containing a (hydrated) transition metal nitrate ($Co(NO_3)_2$, $Cu(NO_3)_2$, or $Mn(NO_3)_2$) and $AgNO_3$ was added dropwise to a NaOH solution of pH 8 under vigorous stirring [14]. The precipitates were filtered, washed, dried at 363 K overnight, and calcined at 673 K for 4 hours. The pure metal oxides and Ag_2O were also prepared, following the same procedure. After drying in air at 363 K overnight a part of the samples was calcined at 873 K and another part at 1073 K. Ag/MnO_x catalysts were prepared with a different Ag loading of 10, 30, 50, 70 and 90 wt%. Combined with Co_3O_4 and CuO, a Ag loading of 10 wt% were applied. An overview of the surface areas of the various unsupported metal oxides and Ag-based catalysts, is given in Table 1. The precipitated metal oxides were analyzed by means of DRIFT spectroscopy and XRD. The DRIFT spectra of Co_3O_4 and CuO agree perfectly well with those presented by Nyquist [23] and ourselves (chapter 2). Addition of Ag hardly affected the spectra. XRD analysis of the MnO_x sample revealed the presence of Mn_3O_4 and Mn_5O_8, in agreement with the spinel-like DRIFT spectrum [27]. Due to the high surface area of the Ag/MnO_x catalysts, XRD analyses did not reveal any crystalline identity. It has been proposed that Ag is predominantly in the Ag^+ state and silver manganates might be formed ($AgMn_2O_4$) [15]. The silver catalyst without MnO_x consists of Ag_2O after precipitation and drying, and is transformed into metallic Ag upon calcination at 675 K. In view of the XRD line broadening, the surface area of Ag_2O is estimated to be 20 m^2.g^{-1}, whereas a surface area smaller than 1 m^2.g^{-1} is obtained for metallic Ag after calcination.

9.2.1.4. Au based catalysts.

The transition metal oxide supported Au catalysts were prepared according to the method described by Haruta *et al.* [17]. An aqueous solution containing $HAuCl_4$ and the desired transition metal nitrate was added dropwise to a NaOH solution (pH 8) under vigorous stirring. After coprecipitation, the solution was kept at pH 8 for another hour, followed by filtration and washing with water until it was free of chloride ions. The catalysts were dried in air at 363 K overnight and calcined at 673 K. Au-loadings of approximately 10 wt-% were obtained after preparation [17]. The BET surface areas of the Au-based catalysts are shown in Table 1.

Table 1. *The N_2-BET surface areas of the bronzes, the unsupported metal oxides, and their Au- and Ag-based analogues.*

CATALYST	BET- Surface area ($m^2.g^{-1}$)
V_2O_5 (*ex* NH_4VO_3)	6.4 ± 0.1
$K_{0.23}V_2O_5$	< 1
$Cu_{0.35}V_2O_5$	≈ 2
$Ag_{0.35}V_2O_5$	< 1
CuO (*ex* nitrate)	< 1
CuO (675 K)	19 ± 1
CuO (Merck)	25 ± 1
Ag/CuO (10 wt-% Ag) (675 K)	26 ± 1
Au/CuO (10 wt-% Au) (675 K)	14 ± 1
Co_3O_4 (675 K)	52 ± 1
Co_3O_4 (875 K)	22 ± 1
Co_3O_4 (1075 K)	9 ± 1
Ag/Co_3O_4 (10 wt-% Ag) (675 K)	40 ± 2
Au/Co_3O_4 (10 wt-% Au) (675 K)	39 ± 2
MnO_x (675 K)	30 ± 1
Ag/MnO_x (30 wt-% Ag) (675 K)	41 ± 1
Ag/MnO_x (50 wt-% Ag) (675 K)	47 ± 1
Ag/MnO_x (70 wt-% Ag) (675 K)	46 ± 2
Au/MnO_x (10 wt-% Au) (675 K)	68 ± 2

9.2.2. CO oxidation experiments

CO oxidation experiments concerning Ag- and Au-based catalysts, and pure metal oxides (Co_3O_4, CuO and MnO_x), were performed using the so-called six-flow reactor setup. A total flow of 150 ml.min^{-1} *per* reactor and a gas composition of 1000 ppm CO in 10 % O_2 in Ar were applied, which is comparable with the amounts present in diesel exhaust. An amount of 40 mg catalyst was diluted with 400 mg SiC (400 μm) and introduced in the reactor, sandwiched between two pieces of quartz wool. The oxidation experiments were performed with a temperature ramp of 0.5 K.min^{-1}, to approach steady state and allow the collection of a high density of data points per time unit. The measurements were performed up to 520 K. In all cases an increasing ramp was followed by a decreasing ramp, and at least one more experiment with an increasing ramp. Extensive data analyses, like the calculation of activation energies and pre exponential factors were not considered: only relative activities will be presented.

9.2.3. Soot oxidation experiments

9.2.3.1. Six-flow experiments

Soot oxidation experiments were performed in the six-flow apparatus. An amount of 60 mg sample, containing 40 mg catalyst and 20 mg soot, was homogeneously mixed with 400 mg SiC and introduced in a quartz tube reactor, fitted with a quartz frit and a piece of quartz wool. SiC (average particle size 400 μm) was used to prevent thermal runaways and to reduce the pressure drop over the sample. A second piece of quartz wool was placed on top of the sample to prevent swirling up during the experiment. The flow per reactor amounted to 150 ml.min^{-1} of 10% O_2 in Ar. A non-dispersive infrared detector (Hartmann & Braun Uras 10 E) was used to measure the CO and CO_2 concentrations alternately every 90 seconds within 12 seconds in each reactor. A multiposition valve (Valco) selected the reactor for analysis.

9.2.3.2. TG/DSC analyses

A Polymer Laboratories STA 1500 H TGA/DSC (Thermo Gravimetrical Analysis/ Differential Scanning Calorimetry) apparatus was used to perform the thermogravimetric and calorimetric analyses. The experimental procedures and heat transport phenomena in the sample cup have been extensively described by Neeft *et al.* [26]. Catalyst/soot samples of 6 mg, containing 4 mg catalyst and 2 mg soot, were diluted with 54 mg SiC, to ensure a proper heat transport and to prevent thermal runaways. The oxidation temperature was defined as the maximum in the heat flow curve, obtained in a 50 ml.min^{-1} flow of 10% O_2 in Ar with a temperature ramp of 10 K.min^{-1}.

9.3. Results

9.3.1 CO oxidation catalyzed by transition metal oxides modified by Ag and Au

The CO oxidation activities of precipitated Co_3O_4 calcined at 675 K and 875 K, respectively, are shown in figure 1. Clearly Co_3O_4 (675 K) shows a higher CO oxidation activity than Co_3O_4 (875). For the primer, a conversion level of 100 % is already obtained at 400 K. A very high CO oxidation activity is maintained in subsequent runs. A hysteresis is observed for the two catalysts between the CO oxidation profiles recorded for increasing or decreasing temperature in the first run, which is less pronounced in subsequent runs.

The activity of MnO_x at 500 K is found to decrease as a function of time during temperature cycling between 350 and 500 K (figure 2). Furthermore, a peculiar shoulder is present in the CO oxidation profile, which is reproducible every run and located at a somewhat lower conversion and temperature level in the curves recorded by decreasing the temperature.
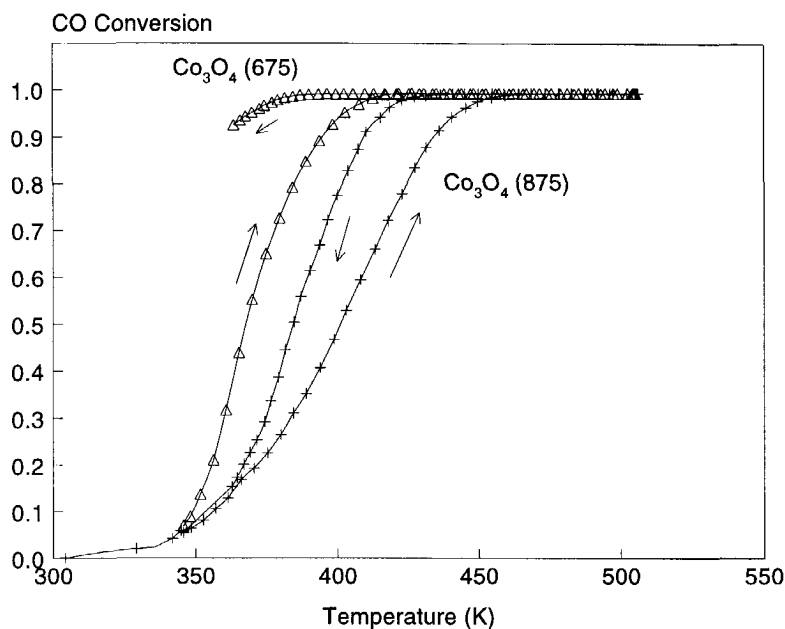
Figure 1. *CO oxidation curves of Co3O4 in 1000 ppm CO and 10% O2 in Ar: The activities of Co3O4 (675 K) [Δ] and Co3O4 (875) [+] are compared. The curves recorded for an increasing or decreasing temperature respectively, are indicated by the arrows.*
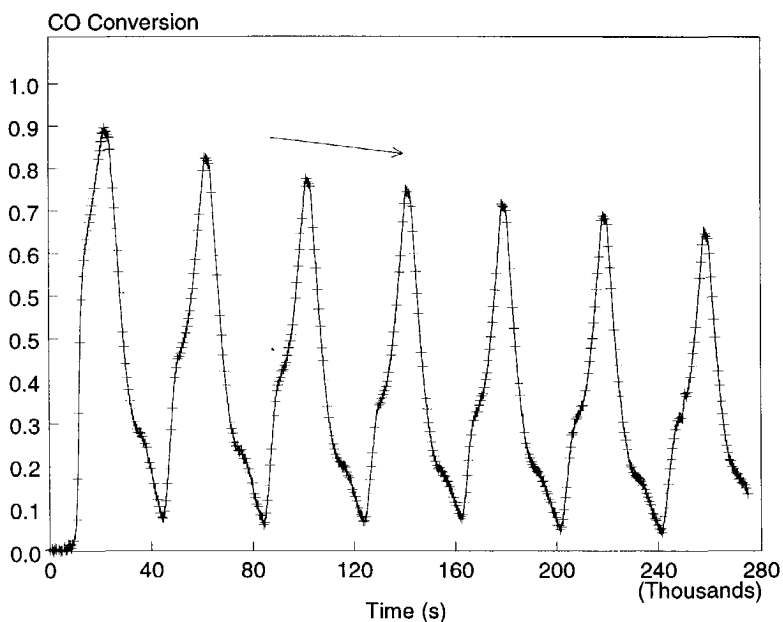

Figure 2. *CO oxidation pattern of MnOx in 1000 ppm CO and 10% O2 in Ar upon temperature cycling between 350 K and 500 K.*

The first and fifth run activity profiles of unsupported Co_3O_4, CuO and MnO_x are compared in figures 3a and 3b. The activity of Co_3O_4 is much lower in the first run than in the subsequent runs, as was already observed in figure 1. The activity of CuO is almost identical in the first and fifth runs. The CO oxidation profiles of MnO_x are quite different: a higher low temperature activity (360-410 K) and lower high temperature activity (410-510 K) is obtained in the first run compared to the fifth run.

The reactivity of the Au- and Ag-based catalysts in the oxidation of CO, relatively to the oxidation activity of the single component catalysts, is shown in figures 4a and 4b (CuO, first and second run), 5a and 5b (Co_3O_4, first and second run) and 6a and 6b (MnO_x, first and second run).

Addition of Au is shown to slightly enhance the activity of CuO at low temperatures (< 380 K) and decrease the activity at higher temperatures. Addition of Ag decreases the activity of CuO above 365 K. CuO and Au/CuO are slightly activated in the first run, whereas the activity of Ag/CuO is identical in the first and second runs (figure 4b).
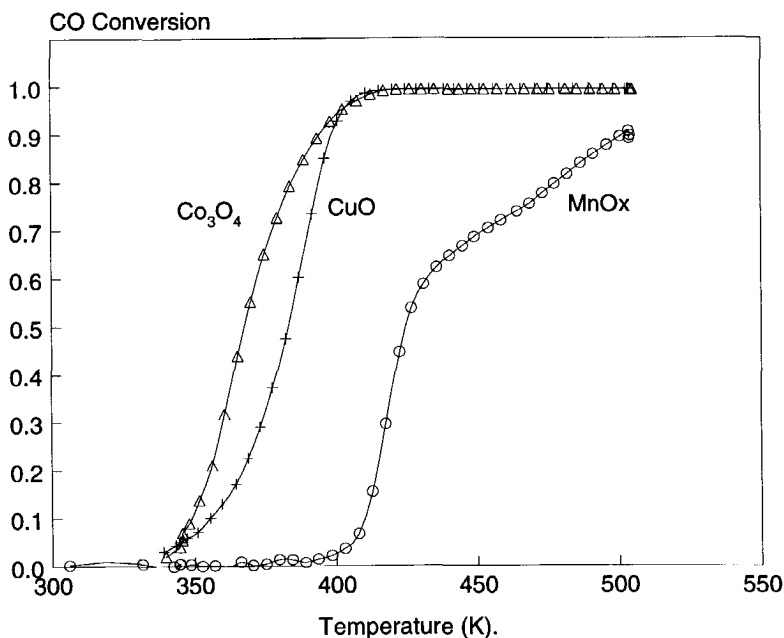
Figure 3a. *CO oxidation curves of Co_3O_4, CuO, and MnO_x, recorded in 1000 ppm CO and 10% O_2 in Ar. First run, freshly calcined catalysts at 675 K, increasing temperature.*

Figure 3b. *CO oxidation curves of Co₃O₄, CuO, and MnOₓ, recorded in 1000 ppm CO and 10% O₂ in Ar. Fifth run, increasing temperature.*
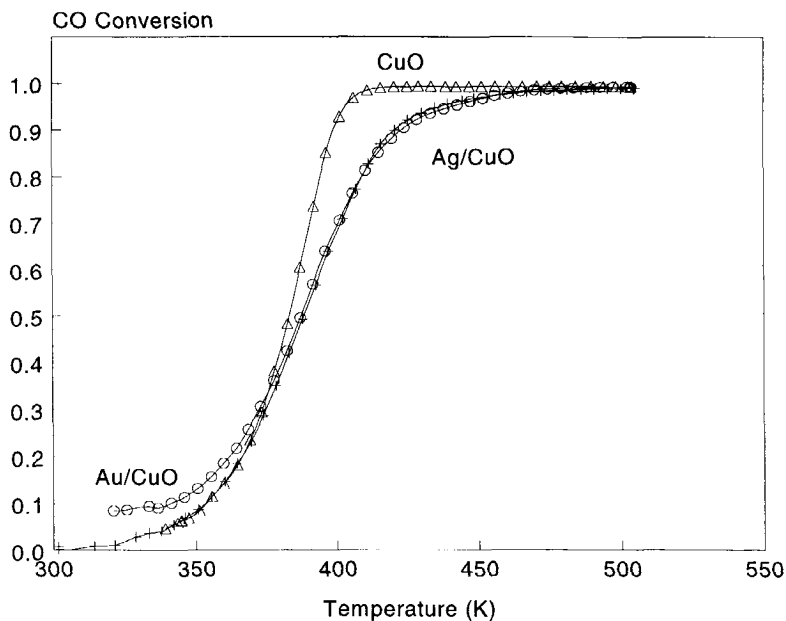
Figure 4a. *CO oxidation curves of CuO, (10wt-%)Ag/CuO and (10wt-%)Au/CuO recorded in 1000 ppm CO and 10% O₂ in Ar. **a.** First run, freshly calcined catalysts at 675 K, increasing temperature.*

CO Conversion
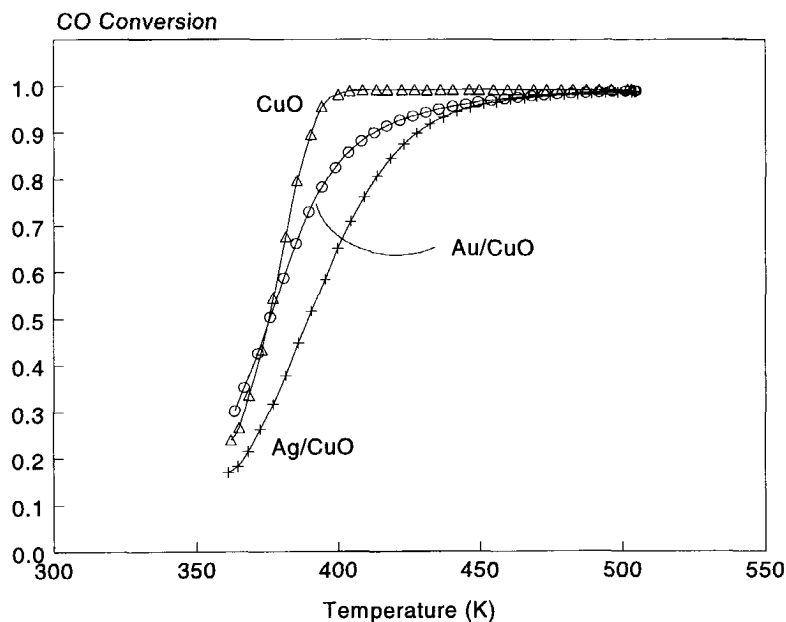
Figure 4b. *CO oxidation curves of CuO, (10wt-%)Ag/CuO and (10wt-%)Au/CuO recorded in 1000 ppm CO and 10% O_2 in Ar. Second run, increasing temperature.*

CO Conversion
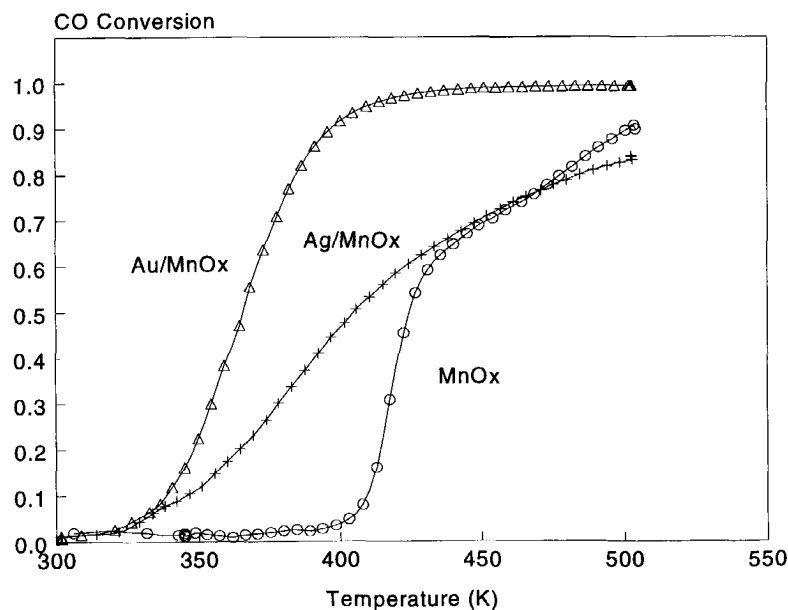
Figure 5a. *CO oxidation curves of MnO_x, (10wt-%)Ag/MnO_x, and (10 wt-%)Au/MnO_x, recorded in 1000 ppm CO and 10% O_2 in Ar. First run, freshly calcined catalysts at 675 K, increasing temperature.*

CO Conversion

Figure 5b. *CO oxidation curves of MnO$_x$, (10wt-%)Ag/MnO$_x$, and (10 wt-%)Au/MnO$_x$, recorded in 1000 ppm CO and 10% O$_2$ in Ar. Second run, increasing temperature.*

CO Conversion
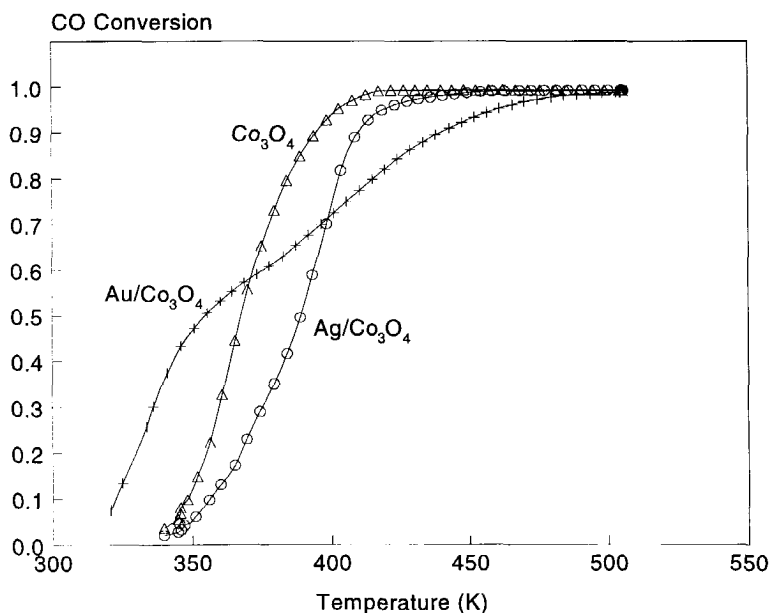
Figure 6a. *CO oxidation curves of Co$_3$O$_4$, (10wt-%)Ag/Co$_3$O$_4$ and (10 wt-%) Au/Co$_3$O$_4$, recorded in 1000 ppm CO and 10% O$_2$ in Ar. **a**. First run, freshly calcined catalysts at 675 K, increasing temperature.*

CO Conversion

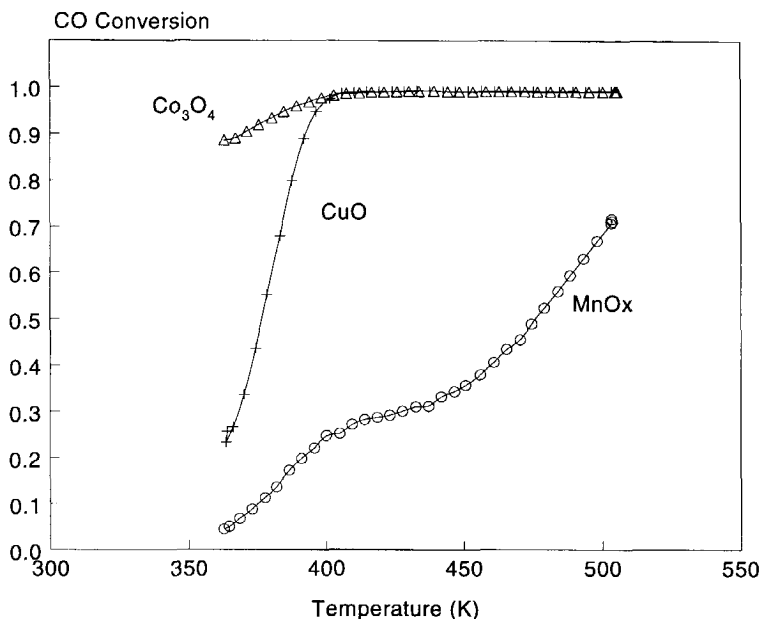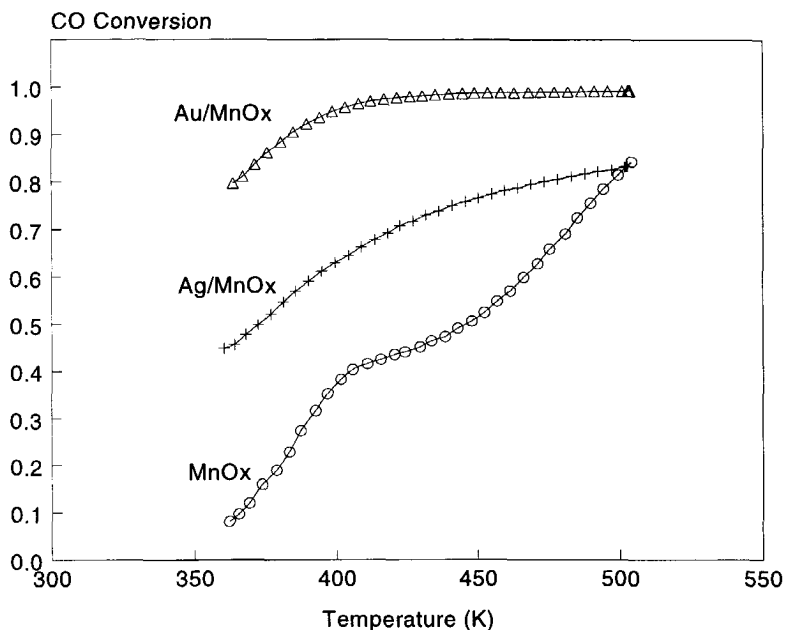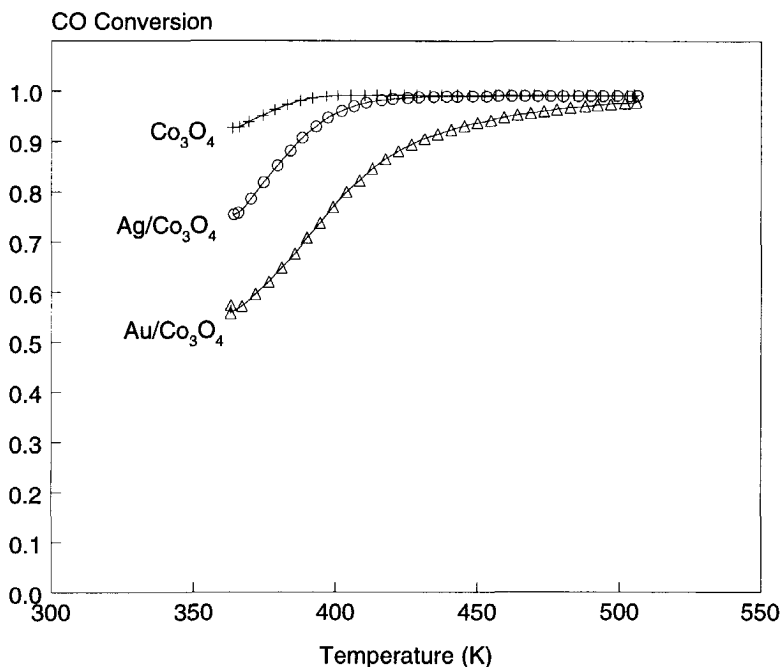*Figure 6b. CO oxidation curves of Co_3O_4, (10wt-%)Ag/Co_3O_4 and (10 wt-%) Au/Co_3O_4, recorded in 1000 ppm CO and 10% O_2 in Ar. Second run, increasing temperature.*

The addition of Au to MnO_x has a strong positive effect on the CO oxidation activity. The activity is even higher in the second run with increasing temperature (figure 5b). A higher activity for (50wt-%)Ag/MnO_x than that of MnO_x is also found, although the beneficial effect of Ag on the CO oxidation activity is less pronounced than the effect of Au.

The addition of Ag decreases the CO oxidation activity of Co_3O_4 (figures 6a and 6b). Despite the lower specific surface area (Table 1), Au addition to Co_3O_4 has a promoting effect at low temperatures. Above approximately 360 K, the opposite effect is observed. In the second run (figure 6b) addition of Au is found to decrease the CO oxidation activity of Co_3O_4 in the temperature range of 360-500 K.

9.3.2. Soot oxidation.

9.3.2.1. Vanadium bronzes.

Generally, soot oxidation profiles of transition metal oxides can be divided into three types: an 'exponential decay-type profile', a 'constant-type profile' and a 'rising-type profile' [26], as was already discussed in chapter 6 of this thesis. The soot oxidation profiles of the vanadium bronzes are shown in figure 7. $K_{0.23}V_2O_5$ shows

the highest activity, although differences are small. 'Constant-type' profiles are observed for all the bronzes. The activity of V_2O_5, either with or without an oxidative high temperature pretreatment for 15 hours at 775 K, is shown for comparison. The high temperature pretreatment does not affect the activity. V_2O_5 possesses a much higher soot oxidation activity than the vanadium bronzes, and also displays a constant-type soot oxidation profile.
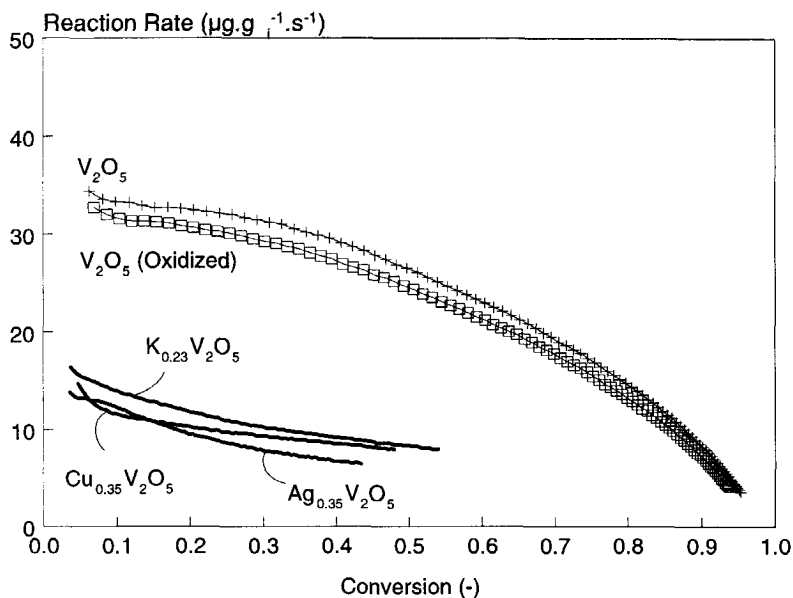
Figure 7. Isothermal soot oxidation rates of 'tight contact' soot containing samples of V_2O_5(Aldrich), V_2O_5(Aldrich, oxidized), $K_{0.23}V_2O_5$, $Cu_{0.35}V_2O_5$, and $Ag_{0.35}V_2O_5$ physical mixtures as a function of soot conversion at 675 K.

9.3.2.2. Ag- and Au-modified transition metal oxides.

The soot oxidation activities of various copper oxides, determined at 600 K, are shown in figure 8. The following order in activity is found: CuO (Merck) > CuO (675 K) > CuO (875 K) > CuO (ex nitrate). CuO (Merck) is very effective in oxidizing soot. CuO prepared by nitrate decomposition has a low surface area (< 1 $m^2.g^{-1}$) and a relatively low soot oxidation activity. So-called constant-type oxidation profiles are obtained for the different CuO catalysts.
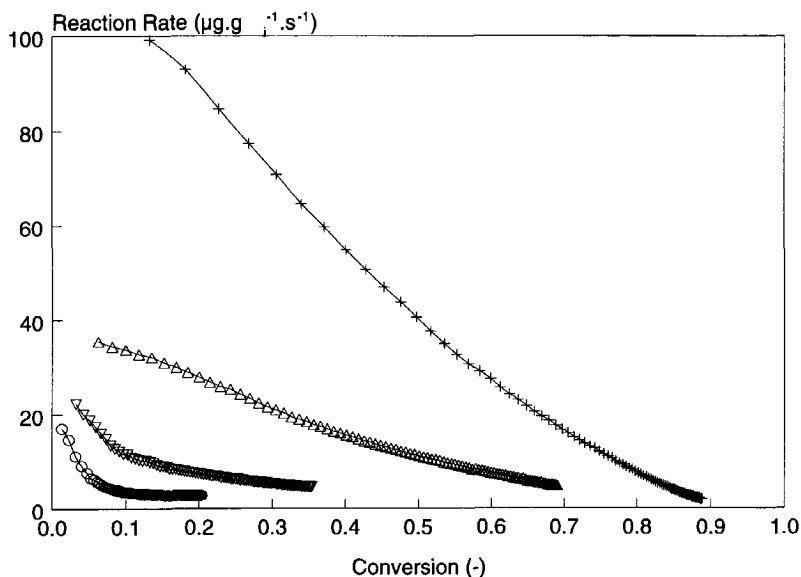
Figure 8. Soot oxidation rates of 'tight contact' CuO/soot physical mixtures at 600 K in 150 ml.min⁻¹ 10% O_2 in Ar, as a function of soot conversion: CuO[Merck] (+), CuO [675] (Δ), CuO[875] (∇) and CuO(ex nitrate) (o).

The activities of the CuO, and Co_3O_4 catalysts, determined by DSC analysis and defined by the oxidation temperature, and the catalyst' surface areas are related to the calcination temperature of the hydroxylic precursors. This is shown in figure 9. A higher calcination temperature results in a lower BET surface area and in a higher soot oxidation temperature.

The activity of the Ag/MnO_x catalysts in soot oxidation appears to be related to the amount of Ag incorporated in the MnO_x lattice. This is shown in figure 10. A synergetic effect is observed by adding 10-70 wt% Ag to the MnO_x catalysts, only slightly depending on the preparation conditions (drying or calcination at 675 K). The activity of the Ag_2O catalyst is much lower after calcination, due to sintering and metallic Ag formation [15]. The soot oxidation temperature determined for MnO_x is lower than the temperature determined by Neeft [26] for MnO_2.

The 'tight contact' soot oxidation activities of Co_3O_4, CuO and MnO_x modified by (10 wt-%)Ag or (10 wt-%)Au, as determined by TG/DSC analysis, are compared in figure 11. Ag is a promoter for the soot oxidation activity of the transition metal oxides tested, but Au only shows a slightly positive effect on the soot oxidation activity of Co_3O_4, whereas a negative effect is found for CuO and MnO_x.
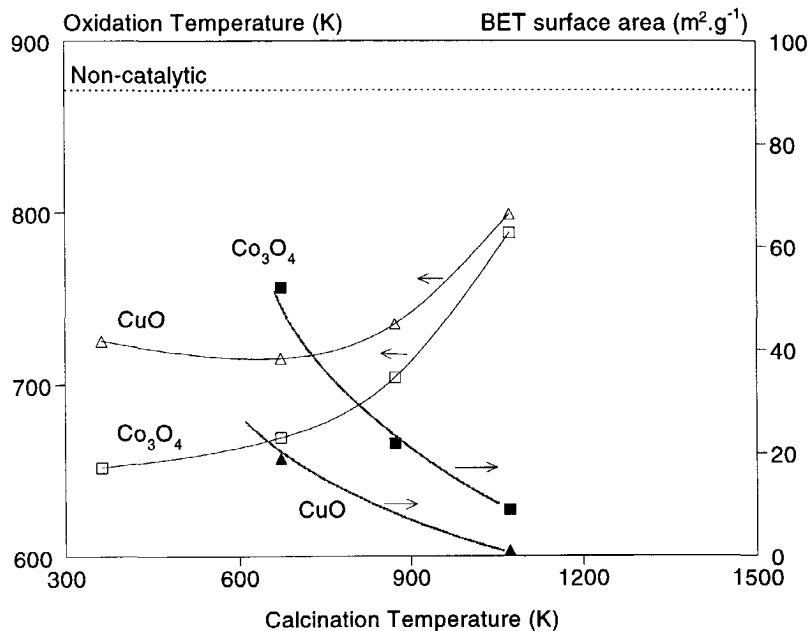
Figure 9. *'Tight contact' soot oxidation temperature and specific surface area of the oxides as a function of the decomposition temperature of the hydroxylic precursors, formed by precipitation: CuO (Δ) and Co_3O_4 (□). The specific surface areas of the samples are indicated with solid symbols: CuO (▲) and Co_3O_4 (■).*
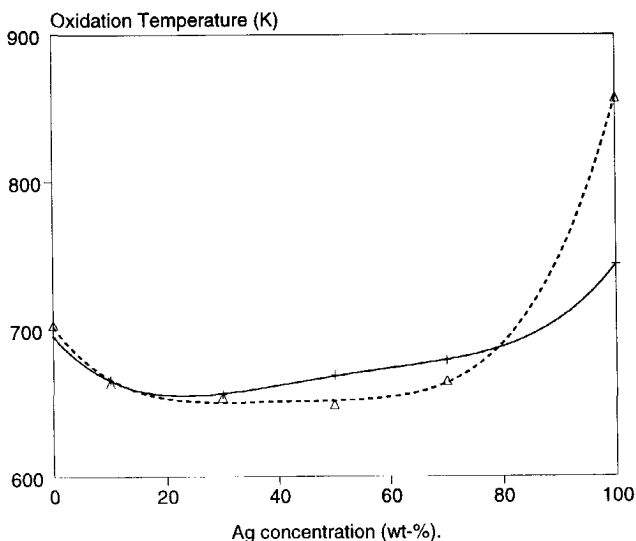
Figure 10. *The 'tight contact' soot oxidation temperatures of Ag/MnO_x mixtures (determined by TG/DSC analysis [26]) as a function of Ag loading, determined after drying (dotted line) and after calcination at 675 K (solid line).*
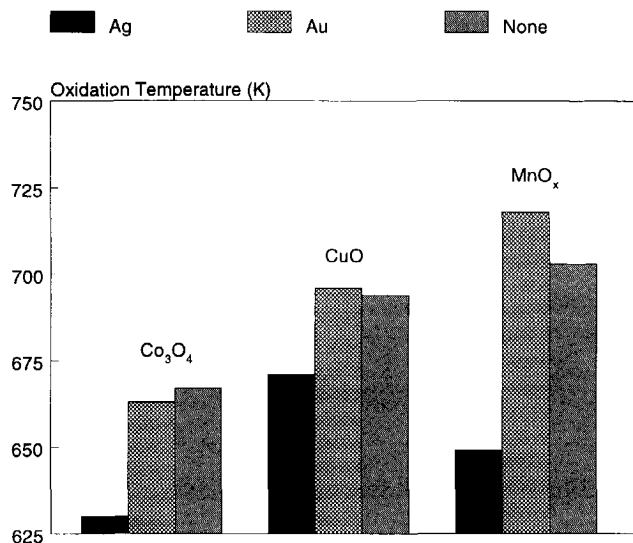
Figure 11. *The 'tight contact' soot oxidation temperatures (determined by TG/DSC analysis) of Co3O4, CuO and MnOx, compared with their (10 wt-%)Au and (10 wt-%)Ag analogues.*

The effect of Ag on the isothermal soot oxidation profiles of Co_3O_4 and CuO is also shown in figure 12. The (10 wt-%)Ag/Co_3O_4 catalyst shows a much higher activity than the Co_3O_4 catalyst, but the shape of the oxidation profile is not affected: an exponential decay in reaction rate as a function of soot conversion can be observed. The activity of CuO is also enhanced by Ag addition, but the development of the oxidation profile is not affected: a constant-type curve is obtained for the Ag/CuO catalyst. The activity of Co_3O_4 calcined at 875 K is shown for comparison.

The activity patterns of the Ag based manganese catalysts are shown in figure 13. The activity of the catalyst containing 50 wt% Ag shows the highest activity. The activity differences are more pronounced than indicated in figure 10.

The isothermal soot oxidation profiles of Au/Co_3O_4 and Au/CuO catalysts are shown in figure 14. Clearly, the Au-modified catalysts are less effective for the oxidation of soot than the pure oxides. The shape of the oxidation profiles is not affected by addition of Au. The results of the isothermal experiments slightly deviate from the results obtained by TG/DSC analysis (figure 11): Au addition was found to enhance the oxidation activity of Co_3O_4.
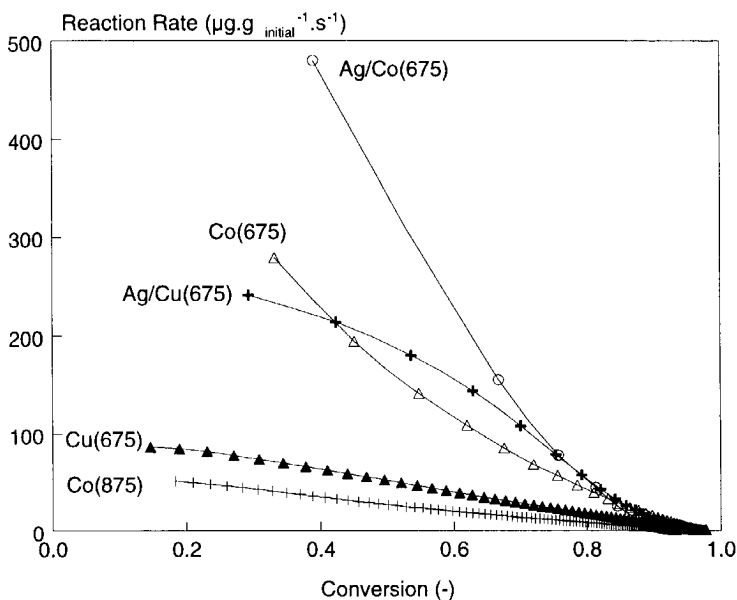
Figure 12. *'Tight contact' isothermal soot oxidation rates of Ag-based CuO and Ag-based Co_3O_4 catalysts as a function of soot conversion at 600 K in 150 ml.min^{-1} 10% O_2 in Ar. The rates of the pure metal oxides, determined at 600 K, are shown for comparison.*
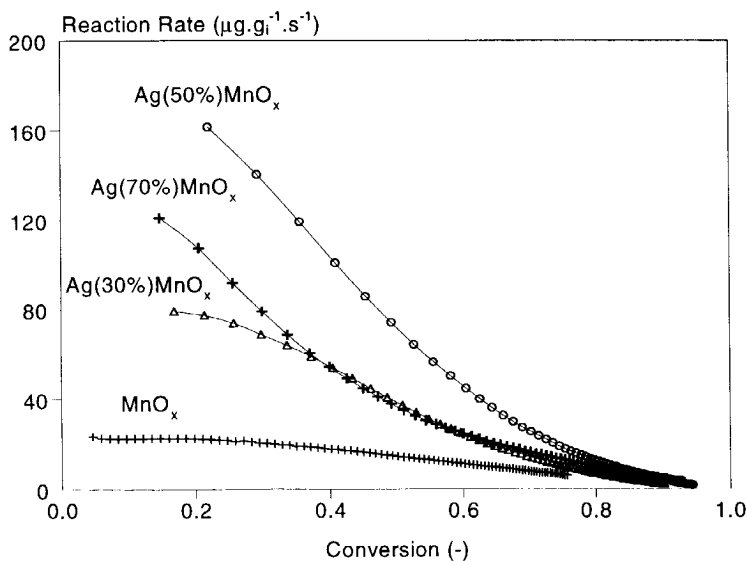
Figure 13. *'Tight contact' isothermal soot oxidation rate of Ag-based MnO_x/soot physical mixtures as a function of soot conversion at 575 K in 150 ml.min^{-1} 10% O_2 in Ar. The soot oxidation profile MnO_x is shown for comparison.*
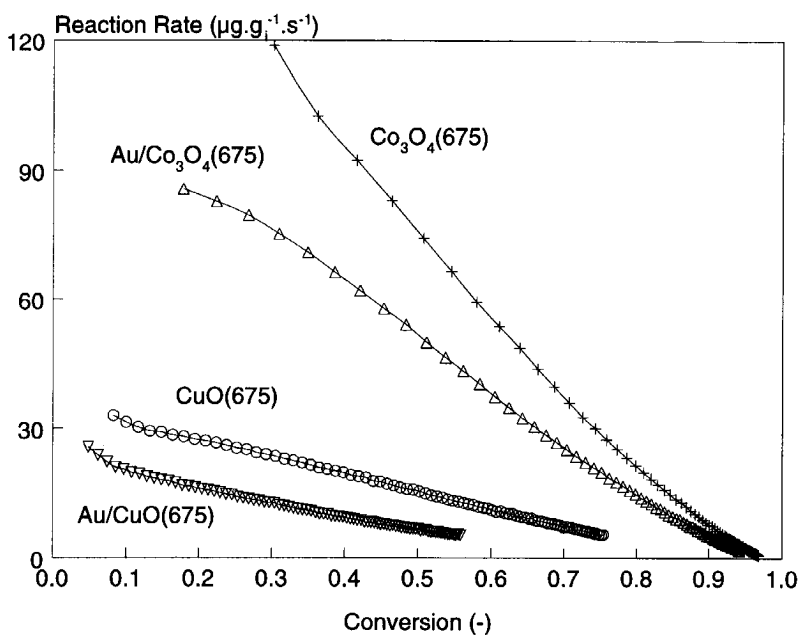
Figure 14. 'Tight contact' isothermal soot oxidation rate of Au-based Co_3O_4/- and CuO/soot physical mixtures as a function of soot conversion at 575 K. The rates of the pure metal oxide analogues, determined at 600 K, are shown for comparison.

9.4. *Discussion.*

9.4.1. CO oxidation.

The oxidation of CO by transition metal oxides has been investigated in the sixties by Winter and coworkers. A redox mechanism has been proposed, based on experiments with labeled oxygen ($^{18}O_2$) [28-30]. In the seventies Boreskov and coworkers found a correlation between the oxygen exchange activity between gas phase and lattice oxygen of several metal oxides, and their activity in the oxidation of carbon monoxide, hydrogen and methane [31-33]. In the eighties Stegenga used transition metal oxides as alternatives for Pt-based automotive three way catalysts and tested the CO oxidation activity. The CO oxidation activity was correlated to the metal-oxygen bond strength [34], and explained by a redox mechanism. Van den Berg [21] found evidence for another, so-called associative mechanism for CO oxidation catalyzed by vanadium bronzes at relatively low temperatures. Gas phase oxygen is activated on lattice defects and reacts directly with CO, yielding CO_2. Lattice oxygen is not involved in this mechanism (chapter 8). A transition of the associative to the redox mechanism was observed at a certain defined temperature by a change in activation

energy. A low activation energy and number of active sites is involved in the associative mechanism, whereas the opposite is true for the redox mechanism [21].

The activity of the metal oxides, tested in this study, is lower in the first run than in subsequent runs: apparently the system is initially not in a stable state. This is likely to be caused by adsorbed water and hydroxyls initially present on the metal oxide surfaces, which inhibit the oxidation of CO.

The activity order of the metal oxides ($Co_3O_4 > CuO > MnO_x$) found in this study, is in agreement with the results of Stegenga, Winter and Boreskov, although the O_2/CO ratio (100) was much higher. Based on literature data [28-34] a redox mechanism is suggested for CO oxidation over Co_3O_4 and CuO. A peculiar shoulder is found in the CO oxidation pattern of the MnO_x catalyst. Van de Kleut [15] found similar phenomena in the CO oxidation profiles of unsupported MnO_2 and Al_2O_3-supported MnO_x catalysts. Additionally, it was show in this study, that the effect is reversible. An explanation of the phenomena, similar to that proposed for the vanadium bronzes, is suggested [15, 21]. An associative mechanism is operative at low temperatures. At relatively high temperatures (440 K) the contribution of the redox mechanism gradually increases: lattice oxygen of MnO_x starts to participate in the CO oxidation process. Initially, the latter results in a less rapid increase in CO conversion as a function of temperature. For a more detailed discussion on the mechanism of CO oxidation over pure metal oxides the reader is referred to Van de Kleut [15], Bielanski [35] or Mergler [36].

Addition of Ag to MnO_x appeared to enhance the CO oxidation activity, whereas a positive effect was not observed for Co_3O_4 and CuO. Ag induces sintering of bulk Co_3O_4 and CuO (Table 1), in agreement with the data presented by Srivannavit [19]. The lower active surface area of the Ag-based Co_3O_4 and CuO catalysts explains the low activity of the Ag-based catalysts relative to the pure metal oxides. The high CO oxidation activity of Ag/MnO_x, relative to MnO_x (figure 5), can only be partially explained by the 50% higher specific surface area (Table 1). Van de Kleut showed that the Ag/MnO_x catalysts consist of Ag_2O, MnO_x and a mixed Ag/MnO_x phase, probably $AgMn_2O_4$. Hence, the activity enhancement might also be related to the formation of $AgMn_2O_4$, or to a cooperative effect of Ag and MnO_x. The latter has been proposed by Imamura [14]. The Ag surface is claimed to be reoxidized by lattice oxygen of a MnO_x phase: this phase maintains silver in the oxidized state [14]. Whether $AgMn_2O_4$ (and Co [19] and Cu- analogues) or a combination of Ag_2O and a transition metal oxide causes the synergetic effect (Ag_2O is hardly active in CO oxidation [14]), cannot be deduced from the results presented here.

Recently, various papers have been published that report on a positive effect of Au-modification of transition metal oxides on the CO oxidation activity [16-18,20]. In this study, Au addition to Co_3O_4, and CuO is shown to be only beneficial at low temperatures. At higher temperatures, Au addition even decreased the activity somewhat. Hence, Au modification of either Co_3O_4 or CuO is of little use to improve the CO oxidation activity at diesel exhaust temperatures (600 K). On the other hand, Au addition to MnO_x increased the CO oxidation activity enormously, and over the

entire temperature range (350-500 K). The synergetic effect of Au-modified oxidic catalysts (metallic Au has a low CO oxidation activity) in the oxidation of CO has been suggested to be caused by a modification of the surface properties of Au by the transition metal oxides, thus enhancing the adsorption of CO on the Au surface [17]. Also a bifunctional mechanism was suggested, in which CO adsorbed on Au particles migrates towards the perimeter and reacts with oxygen adsorbed on the transition metal oxides, yielding carbonate intermediates. Decomposition of these intermediates is considered to be rate determining [18]. The latter mechanism has recently been corroborated by DRIFT measurements [20]. The very high activity of the Au/MnO$_x$ catalyst, relative to MnO$_x$, found in this study, might be partially explained by a higher specific surface area, but is not yet completely elucidated.

9.4.2. Soot oxidation

Vanadium pentoxide (V$_2$O$_5$) is a powerful catalyst for many reactions, such as the oxidation of aromatic compounds. Although several details of the mechanism of oxidation reactions over V$_2$O$_5$ are still under discussion, the activity of V$_2$O$_5$ is often claimed to be enhanced by an increase in the concentration of lattice-defects. These defects consist of oxygen vacancies, which are related to the amount of V^{4+} ions. A high concentration of V^{4+} facilitates the reduction of V$_2$O$_5$ to V$_2$O$_3$ and the oxidation of CO to CO$_2$ [21]. Therefore, a higher activity of the bronzes was expected in the catalytic oxidation of soot. However, an opposite effect was found. Besides the relatively low surface area of the bronzes, the following argument might also explain the low soot oxidation activity of the bronzes. In contrast to CO, soot does not migrate over the catalyst' surface to active sites: activated oxygen has to migrate to the soot particles, either *super*-surface (spill-over), yielding surface oxygen complexes, or *via* surface oxygen, or *via* lattice oxygen. In chapter 8 lattice oxygen of V$_2$O$_5$ was shown to be involved in the oxidation of soot. Addition of Cu, Ag and K is likely to diminish the mobility of lattice oxygen. This is corroborated by carbothermic reduction experiments, which show that the bronzes reduce at higher temperatures than bulk V$_2$O$_5$. Moreover, Van den Berg [21] found a correlation between the onset temperature of the redox mechanism, and (bulk) CO reduction temperatures. Assuming that the mobility of lattice oxygen (and surface oxygen) affects the soot oxidation rate and that the contribution of the spill-over mechanism to the activity is relatively low (chapters 7 and 8), the low activity of the bronzes can thus be explained.

The catalytic activity of several transition metal oxides in soot oxidation was shown to be very much dependent on the calcination temperature of the sample after precipitation. Neeft [4,26] found significant differences in the 'tight contact' activity of Co$_3$O$_4$. Similar observations were made for CuO in this study. A high calcination temperature results in a low specific surface area (Table 1) and a decreased 'tight contact' soot oxidation activity (figure 9). Apparently, the soot oxidation activity is related to the available surface area. Moreover, the shape of the CuO and Co$_3$O$_4$ catalyzed soot oxidation profiles is affected by the surface area: a continuously

decreasing reaction rate as a function of soot conversion was found for $CuO(675)$, $CuO(Merck)$ and $Co_3O_4(675 K)$ in this study, whereas a rising-type curve was found for $CuO(ex nitrate)$ and an exponential decay-type curve for $Co_3O_4(ex nitrate)$ by Neeft [26]. Generally, soot oxidation profiles of transition metal oxides can be divided into three types: an 'exponential decay-type profile', a 'constant type-profile' and a 'rising-type profile' [26] (compare chapter 6). The shape of the profile is proposed to be related to *i)*. the mobility and volatility of the metal oxide, *ii)*. the formation of carbon surface oxygen complexes (SOCs), *iii)*. the redox properties of the metal oxide, and *iv)*. the number of contact points between the catalyst and soot [26]. A redox mechanism, *i.e.* reaction of 'surface oxygen' (chapter 8), at the catalyst-soot interface, yields oxygen vacancies, CO and CO_2, and a considerably reduced amount of catalyst/soot contact points. The latter results in a decreasing oxidation activity with conversion, and is reflected by an 'exponential decay-type' oxidation profile. A constant type profile can be explained by a considerable contribution of *super* surface oxygen' to the reaction rate (spill-over mechanism), which does not cause a rapid decrease of the number of catalyst/soot contact points. A rising-type profile, as found for $CuO(ex nitrate)$ by Neeft [26], was explained by a more or less equal participation of *super* surface oxygen' and 'surface oxygen' to the oxidation mechanism: the formation of surface oxygen complexes (SOCs) was shown to enhance the reactivity of soot in the redox mechanism [26], which explains an increasing reaction rate as a function of conversion.

The enhanced activity of CuO and Co_3O_4 with increasing surface area, is explained by an increased amount of catalyst-soot contact points. Apparently, the initial amount of Co_3O_4/soot contact points is high enough to prevent a rapid decay of the reaction rate as a function of soot conversion. Furthermore, the contribution of oxygen spill-over to the oxidation profile of CuO is suggested to be decreased, as a rising-type curve is not obtained.

Regardless of the lower surface area (Table 1), a higher soot oxidation activity is observed for Ag/Co_3O_4 than for pure Co_3O_4. The oxidation profile is hardly affected by Ag addition. Ag/CuO also shows a much higher activity than its pure metal oxide analogue. Finally, the addition of Ag to MnO_x was shown to affect the shape of the oxidation profile and to yield a high soot oxidation activity: a change from a constant-type oxidation profile to a monotonically decreasing reaction rate as a function of soot conversion was observed with increasing Ag content (compare $(30wt-\%)Ag/MnO_x$ and $(70wt-\%)Ag/MnO_x$). Evaluating literature data and the results presented here, the relatively high activity of the Ag/Co_3O_4, Ag/CuO and Ag/MnO_x mixtures is likely to be explained by an enhanced activity of Ag_2O, which is maintained in the oxidized state by lattice oxygen of the transition metal oxide. This is corroborated by experiments performed by Imamura [14], who showed that oxygen reacting with CO was originally associated with the active Ag-species. The presence of oxidized Ag species apparently is a prerequisite, as addition of Ag to V_2O_5, yielding a Ag vanadium bronze in which Ag is virtually in the metallic state, was shown to yield a lower activity than bulk V_2O_5. Increasing the amount of silver

enhances the activity of Ag/MnO_x catalysts up to a value of 50 wt-% Ag. Higher silver contents are no longer beneficial, because the amount of MnO_x is not sufficient to perform a fast reoxidation of the (reduced) Ag surface [19]. The relative activities of the Ag-based catalysts are caused by the capability of the transition metal oxide to reoxidize the Ag surface. Apparently Co_3O_4 is more effective than CuO and MnO_x, in agreement with an increasing metal-oxygen bond strength in the series $Co_3O_4 <$ CuO $< MnO_x$, as determined by Boreskov *et al.* [31-33]. The oxidation activity is not entirely determined by the Ag_2O species: the relative amount of soot in contact with the transition metal oxide or $Ag(_2O)$, the available surface area, and the contribution of mixed phases, like *e.g.* $AgMn_2O_4$, is also likely to affect the activity and the oxidation profile.

Au addition to Co_3O_4 and CuO is shown to lower the soot oxidation activity and not to affect the shape of the oxidation profiles. Au addition enhances the CO oxidation activity of MnO_x, whereas it hardly influences the soot oxidation activity. According to the CO oxidation mechanisms proposed by Imamura for Ag-based catalysts [19] and Haruta for Au-based catalysts [18], Ag and Au affect the activity of transition metal oxides quite differently: Ag provides activated oxygen, which might react with a substrate (CO, CH_4 or soot), whereas Au provides a strong CO adsorption capability and/or CO activation. Au_2O_3 hardly shows any catalytic soot oxidation activity. Considering these observations, partial Au coverage of the oxide surface is likely to diminish the amount of oxide/soot contact points, thus yielding a lower overall activity. Ag_2O provides an (additional) high soot oxidation activity, whereas Au does not.

9.4.3. Evaluation

The order in activity found for the oxidation of CO ($Co_3O_4 >$ CuO $> MnO_x$) in this study corresponds quite well to order found for the catalytic oxidation of soot. The similarity in activity orders in CO and soot oxidation might be related to the strength of the metal-oxygen (M-O) bond. A redox mechanism has often been proposed for (high surface area) Co_3O_4, CuO and MnO_x in the oxidation of CO, and was suggested for Co_3O_4, in a slightly modified form, in chapter 8 for the oxidation of soot. Obviously, reduction of a metal oxide by CO is facilitated by a weaker M-O bond. Also the transport of oxygen from an active site to the catalyst/soot interface, *via* the surface layer, is likely to be related to the M-O bond strength, as was visualized and discussed in chapter 8.

Based on the presented oxidation profiles and the discussed dependence on the surface area of the catalysts, the contribution of the 'spill-over' mechanism to the overall reaction mechanism, if possible (chapter 7), is suggested to decreases as a function of increasing catalyst surface area. Apparently, the redox mechanism benefits more extensively from an increased amount of catalyst/soot contact points than the spill-over mechanism.

Although an associative mechanism might be applicable for MnO_x catalysts in the oxidation of CO, depending on the temperature of operation, an associative mechanism cannot explain a high soot oxidation activity. Obviously, CO can migrate towards active sites involved in the associative mechanism, whereas soot cannot.

The small (negative) effect of Ag on the activities of transition metal catalysts in the oxidation of CO is not compatible with the positive effect found in the catalytic oxidation of soot. This might be related to the activity of Ag_2O in the oxidation of CO and soot. Apparently, the intrinsic activity of Ag_2O (at relatively low temperatures) for soot oxidation, is higher than the activity of the investigated pure transition metal oxides, whereas the activity in the oxidation of CO is not much different than the activity of the CuO-, Co_3O_4-, and MnO_x catalysts. Furthermore, it can be speculated that the introduction of Ag_2O in the metal oxide lattice, facilitates transport of oxygen through the metal oxide surface layer to the catalyst/soot interface, which does not affect the CO oxidation activity.

With respect to the practical application of the catalysts dealt with in this chapter, Ag based catalysts seem to be promising, but a high surface area and 'tight contact' conditions are necessary to induce and maintain high activities. The application of Ag based fuel additives might result in the formation of small oxidic particles intimately mixed with soot. Although in this way, due to the high price of Ag, only very low concentrations of the oxidic species can be used, the high surface area might provide enough activity at low Ag concentrations to oxidize the soot particulate to a large extent. Coating of a monolithic filter with *e.g.* CuO, MnO_x or Co_3O_4 provides the necessary CO oxidation activity, which might even be positively affected by deposition of Ag particles. Further research should be focused on the assessment of the effects of other constituents of diesel exhaust, such as NO, SO_x and hydrocarbons, on the catalytic activity.

9.5. *Conclusions*

- The catalytic activity of transition metal oxides in soot oxidation is largely determined by the available surface area and the number of catalyst/soot contact points.
- The similarity in activity order found for Co_3O_4, CuO, and MnO_x in the oxidation of CO and soot, suggests a redox mechanism for the oxidation of soot and CO and an effect of the metal-oxygen bond strength on the activity.
- An associative mechanism might be involved in CO oxidation over MnO_x catalysts at relatively low temperatures.
- An associative mechanism cannot explain a high soot oxidation activity: soot is immobile and cannot migrate to the active sites.
- The addition of K, Ag or Cu to V_2O_5 negatively affects the soot oxidation activity, ascribed to a reduced mobility and reducibility of oxygen anions in the vanadium bronzes.

- A negative effect of the addition of Au on the soot oxidation activity was observed, which is tentatively explained by a partial coverage of the active oxide surface by inactive Au particles, emphasizing the importance of a large number of transition metal oxide/soot contact points.
- A positive effect of the addition of Ag to Co_3O_4, CuO, and MnO_x on the soot oxidation activity was observed, ascribed to a high intrinsic activity of transition metal supported Ag_2O species, which are reoxidized by the transition metal oxides.
- Addition of Ag to Co_3O_4 and CuO hardly affects the CO oxidation activity, whereas a positive effect was found for MnO_x. Au addition was found to largely increase the CO oxidation activity of MnO_x, whereas it only slightly promoted the activity of Co_3O_4 and CuO at low temperatures.

9.6. *References*

[1] E.S. Lox, B.H. Engler and E.Koberstein, in Proceedings of Catalysis and Automotive Polution Control, Amsterdam, 1991, pp. 291-321.
[2] A.F. Ahlstrom and C.U.I. Odenbrand, Appl. Catal. 60 (1990) 143.
[3] A.F. Ahlstrom and C.U.I. Odenbrand, Appl. Catal. 60 (1990) 157.
[4] J.P.A. Neeft, M. Makkee and J.A. Moulijn,. Appl. Catal. B: Env. 8 (1996) 57.
[5] J. van Doorn, J. Varloud, P. Meriaudeau and V. Perrichon, Appl. Catal. B: Env. 1 (1992) 117.
[6] T. Inui, T. Otowa and Y. Takegami, J. Catal. 76 (1982) 84.
[7] A. Bellaloui, J. Varloud, P. Meriaudeau, V. Perrichon, E. Lox, M. Chevrier, C. Gauthier and F. Mathis, Catal. Today, 29 (1996) 421.
[8] C. Mendoza-Frohn, 'Entwicklung und Charakterisierung eines Katalysators für die Russverbrennung mit hilfe Temperatur-programmierter Desorption, Oxidation und Reduktion.', Ph.D. Thesis Technischen Universität Braunschweig, (1990).
[9] T. Inui, T. Otowa, K. Tsutchihashi and Y. Takegami, Carbon, (1982) 213.
[10] P. Ciambelli, M. D'Amore, V. Palma, and S. Vaccaro, Combust.Flame, 99 (1994) 413.
[11] P. Ciambelli, V. Palma, and S. Vaccaro, Catal.Today, 17 (1993) 71.
[12] P. Ciambelli, V. Palma and S. Vaccaro, Combust. Sci. and Techn. 103 (1994) 337.
[13] G. Mul, J.P.A. Neeft, F. Kapteijn, M. Makkee and J.A. Moulijn, Appl. Catal. B: Env. 6 (1995) 339.
[14] S. Imamura, H. Sawada, K. Uemura and S. Ishida, J. Catal. 109 (1988) 198.
[15] D. Van de Kleut, 'On the preparation and properties of manganese oxide based combustion catalysts.', Ph.D. Thesis, Utrecht University, (1994).
[16] D.G. Steven and G.B. Hoflund, Langmuir, 7 (1991) 2135.
[17] M. Haruta, N. Yamada, T. Kobayashi and S. Iijima, J. Catal. 115 (1989) 301.
[18] M. Haruta, S. Tsubota, T. Kobayashi, H. Kageyama, M.J. Genet and B. Delmon, J. Catal. 144 (1993) 175.
[19] O. Srivannavit, S. Osuwan and E. Gulari, in Proceedings of The 5th World Congress of Chemical Engineering, San Diego, 1996, pp. 507-512.
[20] M.A. Bollinger and M.A. Vannice, Appl. Catal. B: Env. 8 (1996) 417.

[21] J. van den Berg, 'Stoichiometry and Catalytic Activity of Vanadia Based Oxides for the Oxidation of CO and H_2', Ph.D. Thesis, Utrecht University (1984).

[22] J. van den Berg, J.H.L.M. Brans-Brabant, A.J. van Dillen, J.C. Flach and J.W. Geus, Ber. Bunsenges. Phys. Chem. 87 (1983) 1204.

[23] R.A. Nyquist and R.O. Kagel, Infrared Spectra of Inorganic Compounds, Academic Press, New York, 1971.

[24] M. Pouchard, A. Casalot and J.B. Goodenough, Bull.Soc.Chim.de France, 11 (1967) 4343.

[25] J.R. Pels, 'Nitrous oxide in coal combustion.', Ph.D. Thesis, TU Delft (1995).

[26] J.P.A. Neeft, 'Catalytic oxidation of soot-potential for the reduction of diesel particulate emissions', Ph.D. Thesis, TU Delft (1995).

[27] K. Nakamoto, Infrared spectra of inorganic and coordination compounds. Wiley, New York, 1978.

[28] E.R.S. Winter, J. Chem. Soc. (1955) 2726.

[29] E.R.S. Winter, J. Chem. Soc. (1964) 5781.

[30] E.R.S. Winter, J. Chem. Soc. (1968) 2889.

[31] G.K. Boreskov, Adv. Catal. 15 (1964) 285.

[32] V.V. Popovskii, G.K. Boreskov, V.S. Muzykantov, V.A. Sazonov and S.G. Shubnikov, Kinet.Katal. 10 (1969) 643.

[33] V.S. Muzykantov, T. Cheshkova and G.K. Boreskov, Kinet. Katal. 14 (1973) 365.

[34] S. Stegenga, 'Automotive Exhaust Catalysis without Noble Metals', Ph.D. Thesis, University of Amsterdam (1991), chapter 1.

[35] M. Bielanski and J. Haber, Oxygen in Catalysis, M. Dekker Inc., New York, 1991.

[36] Y. Mergler, 'Rh-free Automotive Catalysts', Ph.D. Thesis, Leiden University (1995), chapter 5.

10

The effect of NO_x and CO on the rate of the transition metal oxide catalyzed soot oxidation: an exploratory study

Abstract

The catalytic activity of Cr_2O_3, Co_3O_4, and CuO in the oxidation of soot has been investigated. Impregnated samples were found to show a higher activity than 'tight contact' and 'loose contact' physical mixtures of soot and the corresponding transition metal oxides (TMO) in 10% O_2 in Ar. Addition of NO_x enhances the oxidation rate, in 'tight', as well as in 'loose contact', which is attributed to the reaction of NO_2 with soot, yielding NO, CO, and CO_2. It is concluded that NO is reoxidized over the catalyst and performs a catalytic cycle. The NO/TMO combination provides a bifunctional catalyst, where the role of NO is to improve the efficiency of the TMO by transporting activated oxygen. In 'loose contact', the primary function of the catalyst is to promote the oxidation of NO, whereas in 'tight contact' the NO_2/soot reaction is also likely to be catalyzed.

The effect of CO is strongly dependent on the catalyst: CO promotes the CuO catalyzed soot oxidation, it hardly affects the Cr_2O_3 activity, and suppresses the Co_3O_4 activity. Furthermore, impregnated CuO catalyzes the oxidation of CO in the presence of NO_x, and Co_3O_4 the oxidation of CO in O_2. Several tentative explanations for the observed phenomena are presented, and implications for the practical use of the investigated catalysts given.

10.1. *Introduction*

Catalytic oxidation of soot by transition metal oxides has recently been investigated by several research groups because: *(i)* diesel engines can, in the long term, no longer meet the requirements of the particulate (soot) emission standards, and *(ii)* collection of soot in a monolithic filter and simultaneous oxidation at diesel exhaust gas temperatures (600 K) is considered to be the best option for the removal of soot from diesel exhaust [1]. Various metal oxides have been tested on their catalytic activity for the oxidation of soot in air [2-6]. However, the effects of NO_x and CO (other constituents of diesel exhaust gas) on the catalytic oxidation rate is usually not addressed.

In chapters 5 and 6 of this thesis, the activity of alkali metal oxides in the oxidation of soot has been dealt with, including the effects of CO and NO_x on the catalytic performance. CO was found to have a positive effect, and NO_x a negative effect on the oxidation rate of K-impregnated soot. CO was suggested to slightly reduce the active alkali oxide clusters, thereby preventing the irreversible chemisorption of CO_2, formed upon soot oxidation in the 10% O_2 in Ar stream. The latter is likely to deactivate the catalyst.

Chemisorption of NO_2 on the active oxidic clusters and nitrate formation also decreases the number of available active sites and the overall oxidation rate. If soot oxidation is carried out at higher temperatures (above 670 K), where chemisorption of NO_2 cannot occur, a slightly positive effect on the soot oxidation rate was found, which can be explained by the soot/NO_2 reaction. Finally, it was concluded that K-based catalysts have little value for the removal of diesel soot particulate in practice.

In chapters 7 and 8 of this thesis, a DRIFT spectroscopic study, and a mechanistic study on the oxidation of soot by transition metal oxides, using labeled oxygen ($^{18}O_2$), have been presented. Several oxidation phenomena were found to be dependent on the metal oxide used, and explained by differences in the mobility of lattice oxygen and the oxygen spill-over capability.

In the present chapter, the effects of CO and NO_x on the activities of transition metal oxides are presented. Co_3O_4, Cr_2O_3 and CuO were applied as catalysts, as they represent catalysts that exhibit three different oxidation profiles [7]: Co_3O_4 shows an exponential decay-type profile, Cr_2O_3 a constant-type, and CuO a rising-type profile. Moreover, insight in the oxidation mechanism of Co_3O_4 and Cr_2O_3 was obtained using $^{18}O_2$ [8]. The soot oxidation rates of impregnated and physical mixtures ('tight' and 'loose' contact) will be discussed. The impregnated samples were prepared to simulate the catalyst/soot interaction which is likely to be obtained by conversion of a diesel fuel additive in a diesel engine [9]. Several mechanistic considerations to explain the observed phenomena will be presented. Finally, the practical application of the investigated catalysts for the removal of soot from diesel exhaust, is evaluated.

10.2. *Experimental*

Printex-U (a model soot, a gift of Degussa) was used to perform the oxidation studies. This flame soot has a BET surface area of 96 m^2.g^{-1} and contains approximately 5 wt% of adsorbed hydrocarbons and only 0.2-0.4 wt% sulfur [10]. Soot was impregnated by dissolving an amount of the nitrate (analytical grade) in ethanol, corresponding to 10 wt% of the most stable oxide (CuO, Co$_3$O$_4$, and Cr$_2$O$_3$). A fairly good suspension of soot in the transition metal nitrate solution could be obtained. The ethanol was removed by treatment of the suspension in a rotating evaporator at 325 K. The black powder could be recovered by scratching it from the glass wall of the flask with a spatula. Subsequently, 200 mg of the samples was pretreated at 675 K in a N$_2$ flow of 200 ml.min^{-1} for 2 hours, to transform the nitrates into the corresponding oxides. The samples will be referred to as Cu-impregnated, Co-impregnated and Cr-impregnated soot.

Unsupported transition metal oxides were prepared according to the procedures given by Neeft. The corresponding nitrate was treated at 875 K for 2 hours in an oven in static air [7]. These oxides will be referred to as '*ex* nitrate'. CuO and Co$_3$O$_4$ were also prepared by precipitation at pH 8 in a NaOH solution, followed by calcination at 875 K for two hours [11]. These samples will be referred to as CuO(875) and Co$_3$O$_4$(875), respectively.

'Tight contact' mixtures of the oxidic catalysts and soot were prepared by ball-milling in a catalyst to soot ratio of 2:1 [7]. The effects of NO$_x$ and CO on the oxidation rate were determined in the so-called six-flow reactor setup [7]. A six-flow experiment was carried out by filling five quartz reactors (one reactor was used as a reference), with a metal oxide/soot mixture. An initial amount of 20 mg soot was introduced in the reactor every experiment. Hence, the total amount of sample was dependent on the catalyst/soot ratio (approximately 25 mg for the impregnated samples and 60 mg for the physical mixtures). The impregnated and 'tight contact' physical mixtures were homogeneously mixed with 400 mg SiC and introduced in the reactor, sandwiched between two pieces of quartz-wool. The 'loose contact' mixtures were packed in the reactor between two layers of SiC (each layer amounted to approximately 200 mg) and two pieces of quartz wool. NO (1000 ppm) and/or CO (1000 ppm) were added to a controlled flow of 150 ml.min^{-1} 10 vol% O$_2$ in Ar, which was led through each reactor. Introduction of 1000 ppm NO into the 10% O$_2$/Ar stream, led to the formation of NO$_2$ at ambient temperatures in the presence of stainless steel tubing, as was already discussed in chapter 6 of this thesis. The terminology 1000 ppm NO$_x$ will be used to describe a gas composition of 650 ppm NO and 350 ppm NO$_2$. A non-dispersive infrared detector (Hartmann & Braun Uras 10 E) was used to measure the CO, CO$_2$ and NO concentrations alternately every 90 seconds within 12 seconds. A multiposition valve (Valco) selected the reactor for analysis. The experimental results are presented by plotting the reaction rate in μg.g$_{initial}^{-1}$.s^{-1} as a function of soot conversion. Oxidation temperatures, used to

express the activity of the various catalysts, were determined by TG/DSC analysis, as described elsewhere [7].

10.3. *Results.*

10.3.1. *CuO-catalyzed soot oxidation.*

The effect of NO_x and CO on the soot oxidation profile of Cu-impregnated soot at 575 K is shown in figure 1. In all cases, up to a soot conversion level of approximately 0.05-0.1, the reaction rate rapidly decreases as a function of soot conversion. Obviously, NO_x and CO enhance the oxidation rate. The reaction rate shows a fairly linear decay as a function of soot conversion in the presence of NO_x, whereas a slight increase in the reaction rate is observed in the presence of CO. The reaction rate in the presence of both NO_x <u>and</u> CO is lower than in the presence of NO_x: CO negatively affects the soot oxidation rate in the presence of NO_x. The non-catalyzed oxidation rate appears to be almost constant as a function of soot conversion in the presence of NO_x, and is even higher than the Cu-catalyzed reaction in O_2/Ar.
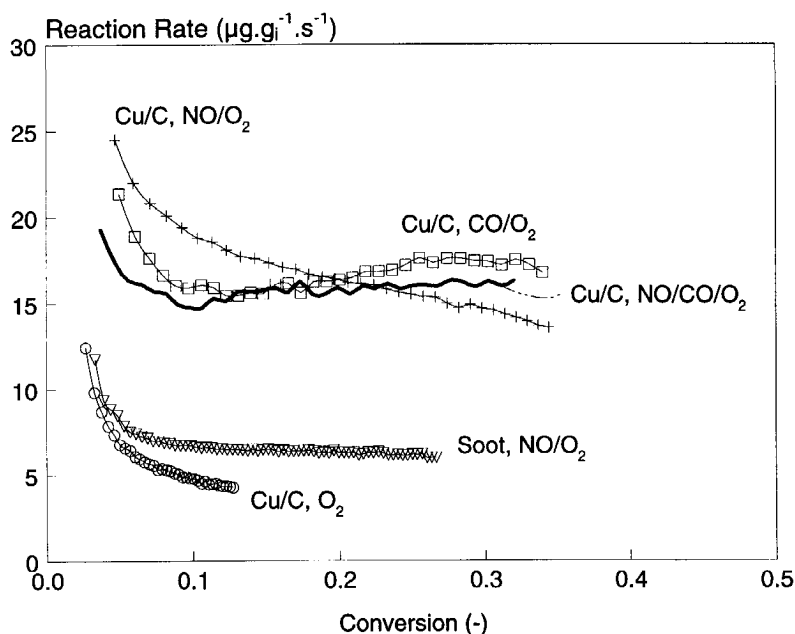
Figure 1. *Oxidation rate of Cu-impregnated soot at 575 K as a function of soot conversion for different gas compositions (10% O_2/Ar, with and without 1000 ppm CO and/or 1000 ppm NO_x). The non-catalyzed soot oxidation profile in NO_x/O_2 is shown for comparison.*

The development of the CO and NO$_x$ concentrations as a function of conversion is shown in figure 2. The NO$_x$ concentration in an empty reactor amounted to approximately 650 ppm: 350 ppm was converted into NO$_2$. By interaction of the gas mixture with Cu-impregnated soot, the NO concentration increases to 900-950 ppm. Apparently NO$_2$ is converted back into NO. An even higher NO concentration was obtained in the presence of CO. Over almost the entire conversion range the NO concentration amounted to 1000 ppm.

In a NO$_x$(1000 ppm)/CO(1000 ppm)/O$_2$ mixture, CO oxidation (yielding only CO$_2$) is observed. At low soot conversion levels, the CO conversion is essentially 100%. The CO conversion gradually decreases as a function of increasing soot conversion. CO oxidation over Cu-impregnated soot was not observed in the absence of NO$_x$ (not shown): the CO concentration amounted to the feed concentration.
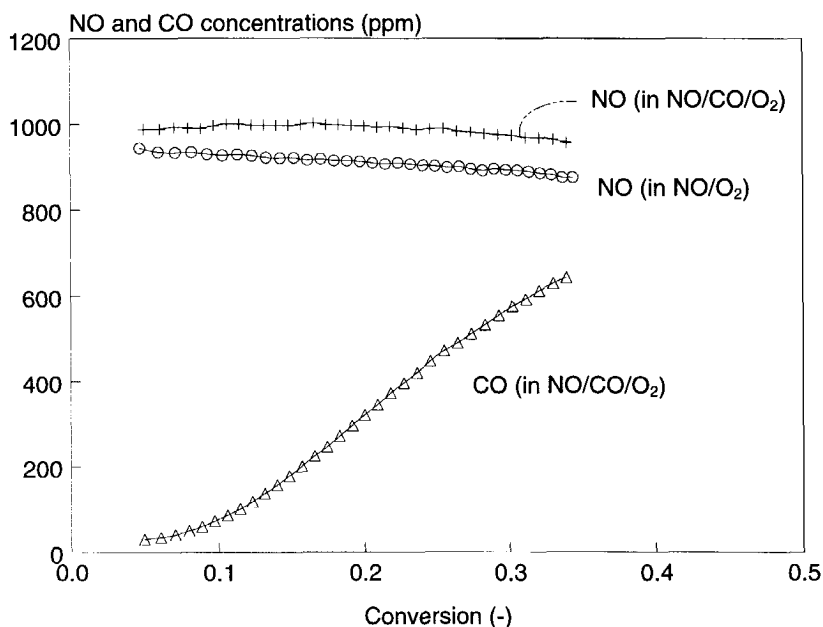
Figure 2. Development of the CO and NO concentrations as a function of soot conversion in the Cu-impregnated soot oxidation at 575 K. Corresponding reaction rates are shown in figure 1. Gas mixtures as indicated.

The effects of NO$_x$ and CO on the oxidation rate are more pronounced in the oxidation profiles of physical mixtures ('tight contact'). This is shown in figure 3. CuO(*ex* nitrate) shows a so-called rising-type oxidation profile at 675 K [7]. Addition of CO increases the oxidation rate over the entire conversion range and yields a more pronounced rising-type profile. In the presence of NO$_x$, initially a higher oxidation rate than in the presence of CO is observed.
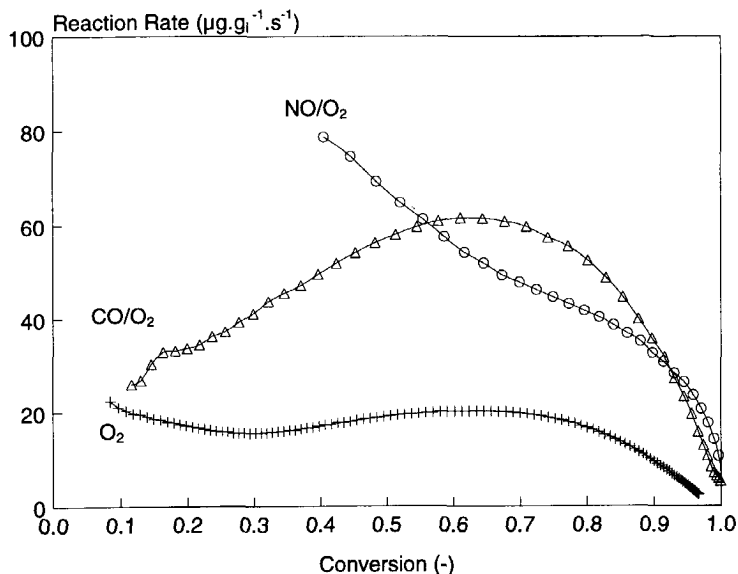
Figure 3. The oxidation rate of a 'tight contact' CuO(ex nitrate)/soot mixture at 675 K as a function of soot conversion for different gas compositions (10% O_2/Ar, with and without 1000 ppm CO or 1000 ppm NO_x).
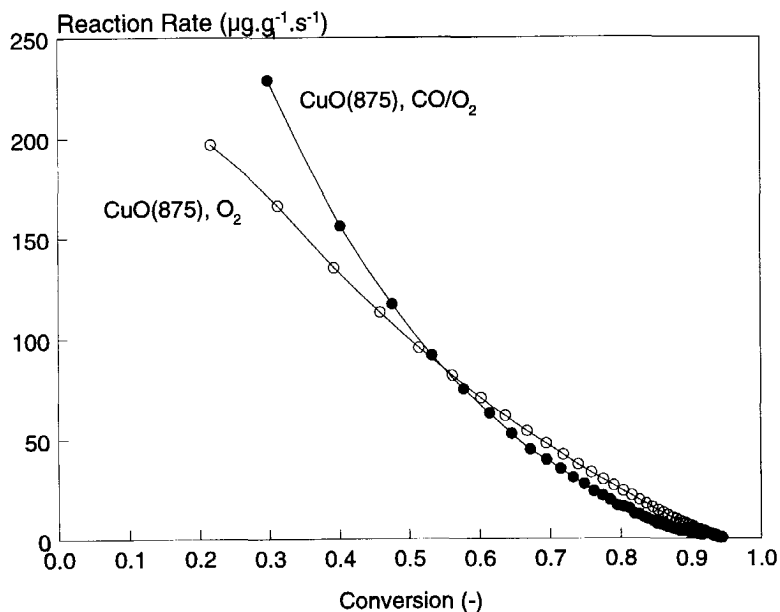
Figure 4. The oxidation rate of a 'tight contact' CuO(875)/soot physical mixture at 650 K as a function of soot conversion for different gas compositions (10% O_2/Ar, with and without 1000 ppm CO).

As the reaction rate decreases linearly as a function of soot conversion, above a soot conversion level of approximately 0.6, the reaction rate attains the same order of magnitude in the presence of NO$_x$, as in the presence of CO. The effect of CO on the oxidation rate of CuO(875) is shown in figure 4. CuO(875) shows a much higher activity than CuO(*ex* nitrate). Moreover, a monotone decrease in the reaction rate as a function of soot conversion is observed. CO addition has a positive effect on the oxidation rate up to a soot conversion level of approximately 0.5. It also affects the oxidation profile: a more or less exponential decay-type oxidation profile is obtained. The effect of NO on the catalytic oxidation rate of CuO(875) was not determined.

10.3.2. Cr$_2$O$_3$-catalyzed soot oxidation.

Oxidation profiles of Cr-impregnated soot are shown in figure 5. The corresponding CO and NO$_x$ concentrations are shown in figure 6.
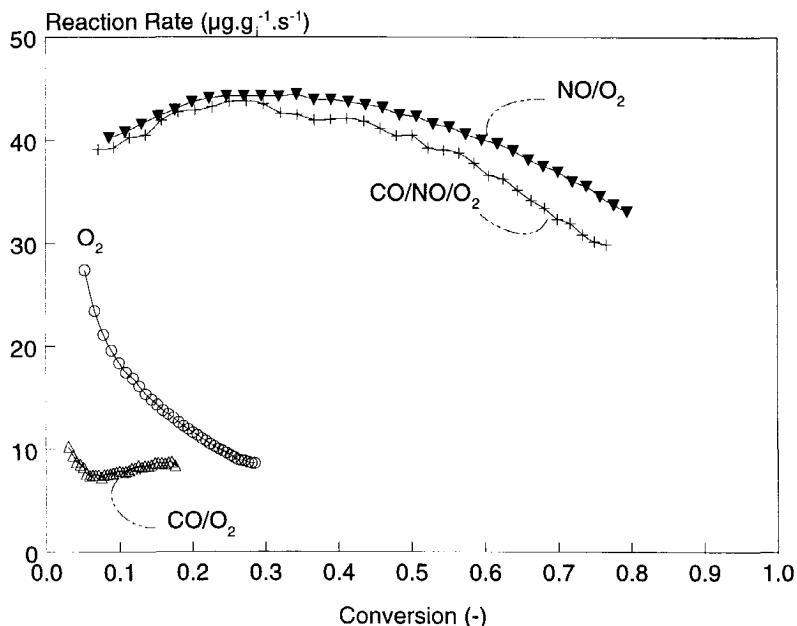
Figure 5. Oxidation rate of Cr-impregnated soot at 675 K as a function of soot conversion for different gas compositions (10% O$_2$/Ar, with and without 1000 ppm CO and/or 1000 ppm NO$_x$).

A rapidly decreasing oxidation rate is found for Cr-impregnated soot in 10% O$_2$ in Ar. The oxidation profile is significantly altered by the presence of NO$_x$, which positively affects the rate. A slight increase in the reaction rate up to a conversion level of 0.3 is found.
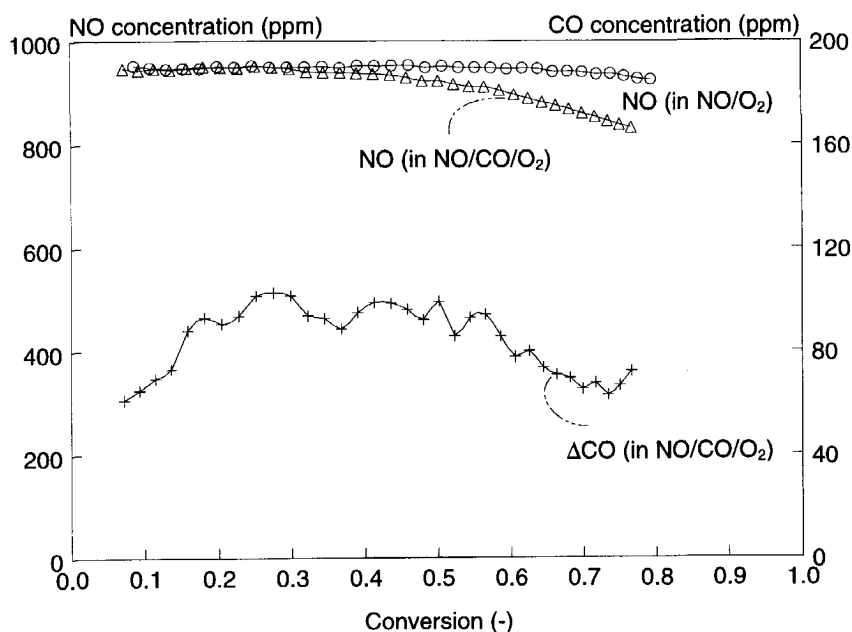
Figure 6. Development of the CO and NO_x concentrations as a function of soot conversion in Cr-impregnated soot oxidation (compare figure 5). The CO feed concentration (1000 ppm) was subtracted from the measured CO concentration.

The oxidation profile of Cr-impregnated soot in the presence of CO was only recorded up to a conversion level of 0.18. The reaction rate is low, but seems to slightly increase as a function of soot conversion. CO is shown to have a negative effect on the soot oxidation rate. Furthermore, CO slightly decreases the positive effect of NO_x.

As can be observed in figure 6, NO is formed by interaction of NO_2 with the Cr-impregnated soot sample: the NO concentration amounted to about 950 ppm. Addition of CO slightly affects the NO concentration at high conversion levels. The CO concentration, corrected for the CO feed concentration, follows a similar pattern as the oxidation rate (compare figure 5). Considerable CO oxidation was not observed in O_2 nor in NO_x/O_2 (not shown).

The effect of NO_x and CO on the oxidation rate of 'tight contact' Cr_2O_3/soot physical mixtures, is shown in figure 7. A constant-type oxidation profile is obtained in 10% O_2/Ar, which is not affected by the presence of 1000 ppm CO. NO_x significantly increases the oxidation rate. A monotonically decreasing reaction rate is obtained.

Figure 7. *Oxidation rate of a Cr_2O_3/soot 'tight contact' physical mixture at 675 K as a function of soot conversion for different gas compositions (10% O_2/Ar, with and without 1000 ppm CO or 1000 ppm NO_x).*

Figure 8. *Oxidation rate of $Co_3O_4(875)$/soot 'tight contact' physical mixtures at 650 K as a function of soot conversion for different gas compositions (10% O_2/Ar, with and without 1000 ppm CO).*

10.3.3. Co₃O₄ -catalyzed soot oxidation.

Co$_3$O$_4$ (875) shows a high catalytic activity (figure 8): a nearly linear decay of the reaction rate as a function of soot conversion is observed. Obviously, CO negatively affects the Co$_3$O$_4$(875) catalyzed soot oxidation rate, although the shape of the oxidation profile has not changed. Co$_3$O$_4$(875) shows a high activity for CO oxidation: CO is completely converted over the entire soot conversion range. The reaction rate of soot oxidation was calculated after correction for the oxidation of CO.

Co$_3$O$_4$(*ex* nitrate) is less active than Co$_3$O$_4$(875). The activity profile of a 'tight contact' Co$_3$O$_4$(*ex* nitrate)/soot mixture is presented in figure 9. A rapidly decreasing reaction rate is obtained up to a soot conversion level of 0.5. In the final stage of the reaction, Co$_3$O$_4$(*ex* nitrate) hardly affects the soot oxidation rate.

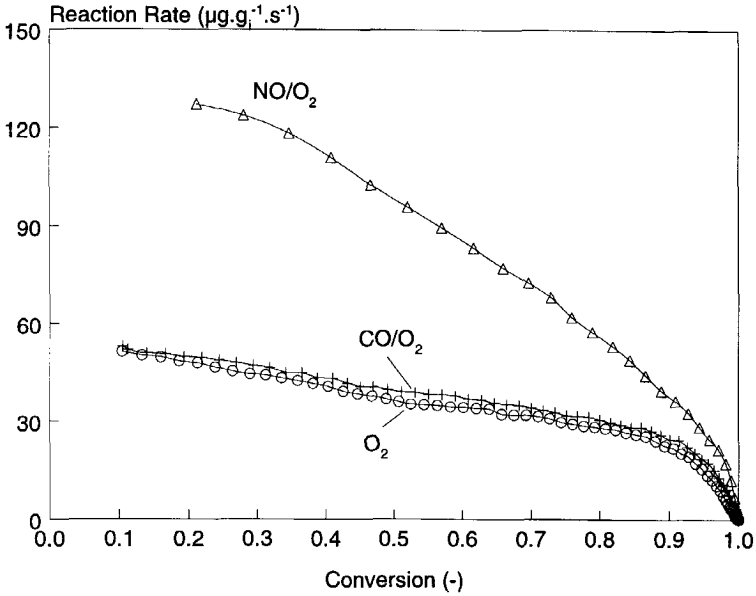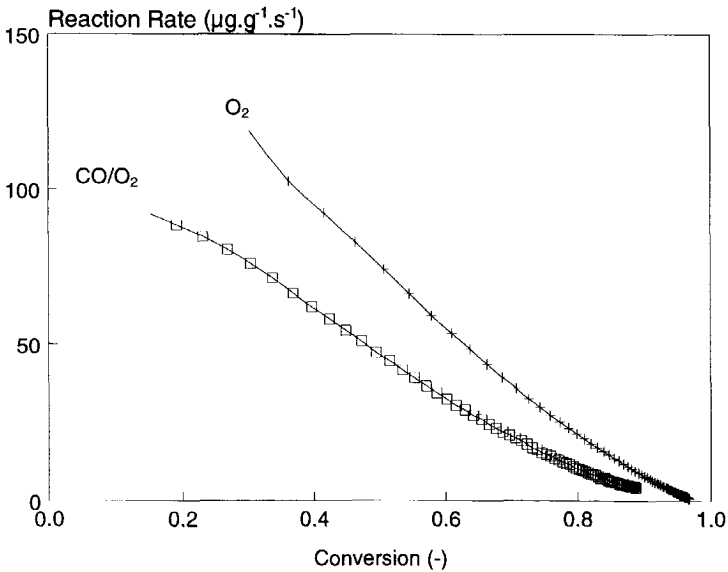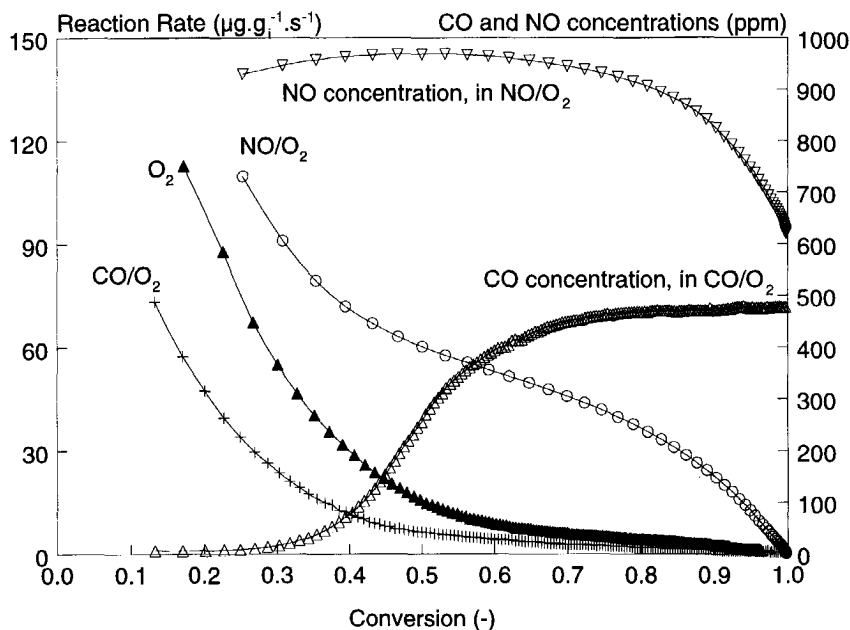*Figure 9. Oxidation rate of Co₃O₄(ex nitrate)/soot 'tight contact' physical mixtures at 675 K as a function of soot conversion for different gas compositions (10% O₂/Ar, with and without 1000 ppm CO or 1000 ppm NOₓ). The corresponding CO and NOₓ concentration are also shown.*

The observed effect of CO is in close agreement with figure 8: it decreases the soot oxidation rate, but does not affect the shape of the oxidation profile. The CO concentration is shown to strongly increase in the soot conversion range of 0.3 to 0.6.

NO$_x$ positively affects the activity of Co$_3$O$_4$(*ex* nitrate) over the entire soot conversion range. A monotone decrease in the reaction rate as a function of soot conversion is observed up to a soot conversion level of 0.8. The observed NO

concentration amounted to about 1000 ppm, indicating that NO$_2$ conversion occurred in the reactor. The NO concentration decreased to the level of 650 ppm upon reaching a complete conversion of soot.

10.3.4. The effect of NO$_x$ on the loose contact activity of the transition metal oxides.

The oxidation temperatures of the metal oxide impregnated samples, determined by TG/DSC analysis in air [7], are compared with the 'tight contact' and 'loose contact' oxidation temperatures of the corresponding oxides (ex nitrate) in figure 10.
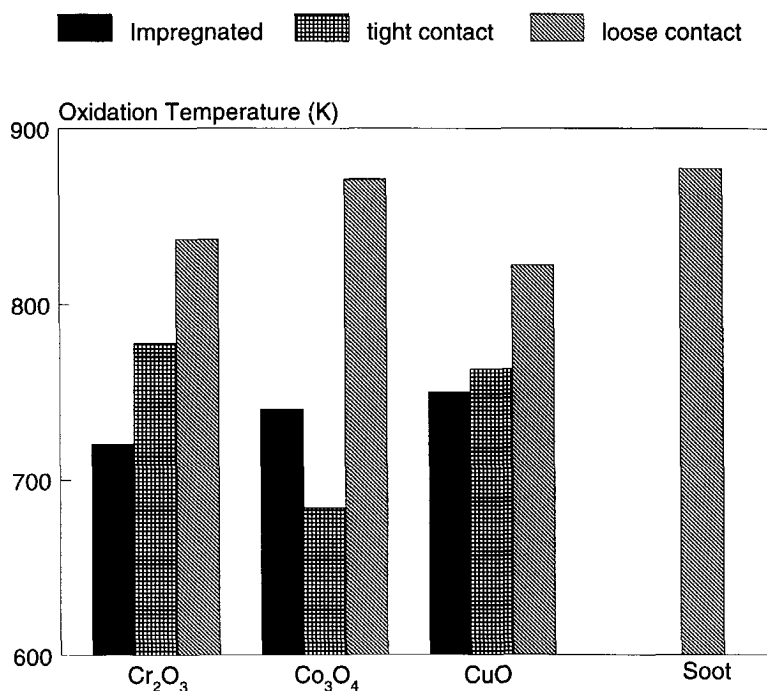
Figure 10. The oxidation activities of Cr$_2$O$_3$-, Co$_3$O$_4$- and CuO impregnated soot, compared with the corresponding 'tight contact' and 'loose contact' activities of the oxides (ex-nitrate). The non-catalytic soot oxidation temperature is shown for comparison.

The oxidation activity of the metal oxides is shown to be strongly dependent on the intensity of contact between the metal oxides and soot. Co$_3$O$_4$(*ex* nitrate) shows a fairly high soot oxidation activity in 'tight contact', but does not show any catalytic activity in 'loose contact'. Although much less than in 'tight contact', some 'loose contact' activity is obtained for Cr$_2$O$_3$ and CuO. The activity of the impregnated samples is higher than the activity of the physical mixtures, except for Co$_3$O$_4$ in 'tight contact'. It should be noted that the loading of the catalyst in the impregnated samples is much lower than in the physical mixtures, whereas the dispersion is expected to be higher.
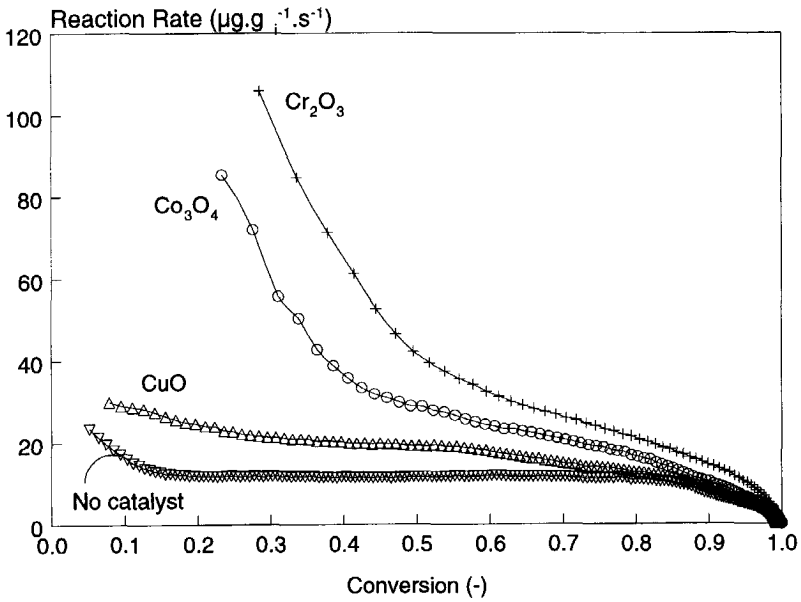
Figure 11. *The oxidation rate of 'loose contact' physical mixtures (catalysts (ex nitrate)) at 675 K as a function of soot conversion in 10% O_2/Ar with 1000 ppm NO_x. The uncatalyzed soot oxidation profile is shown for comparison.*
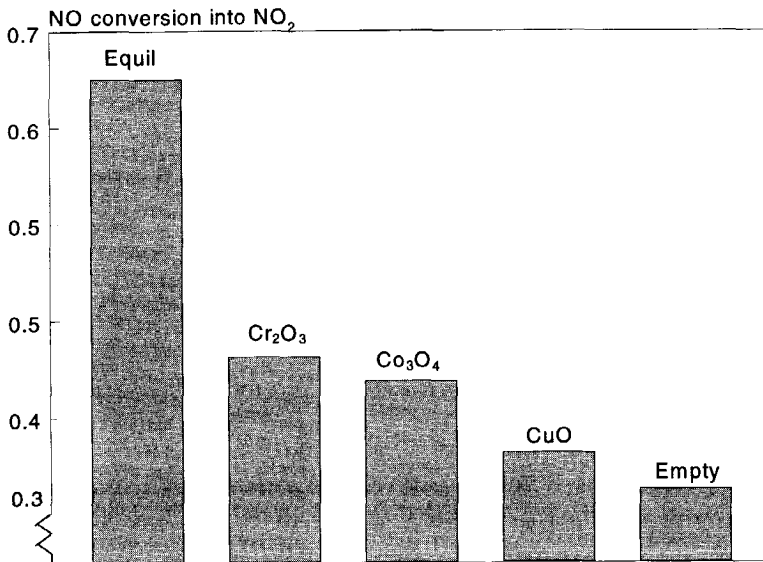
Figure 12. *Catalytic conversion of NO into NO_2 as determined for Cr_2O_3, Co_3O_4, and CuO. Reaction conditions : T=675 K, 40 mg sample in 400 mg SiC, 1000 ppm NO in 10% O_2 in Ar. The thermodynamic equilibrium (Equil [20]) and the NO conversion in an empty reactor are shown for comparison.*

The effect of NO$_x$ on the 'loose contact' activity of transition metal oxides is shown in figure 11. The 'loose contact' activity of Co$_3$O$_4$ is increased enormously by the presence of NO$_x$, since Co$_3$O$_4$ showed an insignificant 'loose contact' activity in 10% O$_2$ in Ar (compare figure 10). A considerable positive effect of NO$_x$ on the 'loose contact' activity of Cr$_2$O$_3$ was also observed. The positive effect of NO$_x$ is less pronounced for CuO. The 'loose contact' activity in NO$_x$ decreases in the series Cr$_2$O$_3$ > Co$_3$O$_4$ > CuO, which is different from the order found in 10% O$_2$ in Ar: CuO > Cr$_2$O$_3$ > Co$_3$O$_4$ (figure 10).

The catalytic activity of the transition metal oxides (ex nitrate) for the oxidation of NO into NO$_2$ is shown in figure 12. Obviously the order in catalytic activity for the oxidation of NO (Cr$_2$O$_3$ > Co$_3$O$_4$ > CuO) corresponds to the order found for the 'loose contact' soot oxidation activity in NO$_x$.

10.4. *Discussion*

10.4.1. General observations

The effects of CO and NO$_x$ on the non-catalyzed soot oxidation rate have been extensively discussed in chapter 6 of this thesis. CO was found not to affect the oxidation rate of soot in 10% O$_2$ in Ar. An enhancement of the oxidation rate was found after the addition of NO$_x$ to the oxidizing medium, explained by the NO$_2$/soot reaction. The NO$_2$ conversion could not entirely account for the measured soot oxidation rate: apparently NO$_2$ can be reformed by collision of NO and O$_2$ with soot particles, *i.e.* NO acts as a catalyst. The soot may also become more reactive towards O$_2$ after interaction with NO$_2$. The results indicate that the effect of CO on the catalytic oxidation rate is solely caused by interactions of CO with the catalyst surface, while a contribution of the NO$_2$/soot reaction to the overall catalytic soot oxidation rate can be expected.

An overview of the effect of the gas composition on the activity of impregnated and 'tight' and 'loose contact' mixtures of CuO, Cr$_2$O$_3$, and Co$_3$O$_4$ with soot, is shown in table 1. Qualitatively, the observed effects are independent on the intensity of contact between the catalyst and soot.

The impregnated catalysts, although present in lower concentrations, were found to be more active in the oxidation of soot (in 10% O$_2$/Ar, with and without NO$_x$) than the physical mixtures, except for Co$_3$O$_4$. However, in view of the loading of the Co-impregnated sample relative to the physical Co$_3$O$_4$/soot mixture (10 *vs.* 200 wt-%), it can be concluded that impregnation is highly beneficial for the soot oxidation activity of Co$_3$O$_4$ as well.

Table 1. *Overview of the effects of NO$_x$ and/or CO on the catalytic activity of Cr$_2$O$_3$, CuO and Co$_3$O$_4$ in the oxidation of soot. The effect is indicated by the average oxidation rate in the presence of the component indicated, relative to the activity in 10% O$_2$ in Ar.*

Catalyst	Contact	NO	CO	NO/CO
Cr$_2$O$_3$	Impregnated	4	0.3-0.5	3-4
CuO	Impregnated	3-4	3	3
Cr$_2$O$_3$	'Tight'	3	1	---
CuO(*ex* nitrate)	'Tight'	4	2-3	---
CuO(875)	'Tight'	---	1-1.5	---
Co$_3$O$_4$(*ex* nitrate)	'Tight'	1.5-2	0.5	---
Co$_3$O$_4$(875)	'Tight'	---	0.5-0.8	---
Cr$_2$O$_3$	'Loose'	>>*	---	---
CuO	'Loose'	>*	---	---
Co$_3$O$_4$	'Loose'	>>*	---	---
Non-catalytic**	---	4	1	3-4

* The rate in O$_2$ in Ar was very small: > and >> indicate that there is a considerable effect.
** Compare chapter 6 of this thesis.
--- Not determined

The necessity of 'tight contact' conditions for a high catalytic soot oxidation activity of (bulk) transition metal oxides in 10% O$_2$ in Ar, was already extensively discussed by Neeft [7] and in chapters 3 and 4 of this thesis. The results presented here show that the soot oxidation rate of catalyst/soot physical mixtures in the presence of NO$_x$ is also contact dependent. The activity of 'loose contact' catalyst/soot mixtures in NO$_x$ was found to be lower than that of the corresponding 'tight contact' mixtures. Nonetheless, the 'loose contact' effect of a catalyst in NO$_x$ is significantly higher than the effect in 10% O$_2$ in Ar. The presence of Co$_3$O$_4$ did not affect the soot oxidation rate in 10% O$_2$ in Ar, whereas a considerable effect was observed in NO$_x$ (figure 11). The influence of NO$_x$ and CO on the catalytic soot oxidation rate will be further discussed in the next three paragraphs.

10.4.2. CuO-catalyzed soot oxidation

The oxidation profile of CuO (*ex* nitrate) shows a rise in the oxidation rate with soot conversion in 10% O$_2$ in Ar, which is less pronounced for the Cu-impregnated soot sample at 550 K, and not observed for CuO(875). Neeft ascribed such a rising-type profile to a combined mechanism, in which both the number of contact points between the catalyst and soot, and the formation of surface oxygen complexes (SOCs), is important [7, 17]. Furthermore, redistribution of the catalyst might also cause an activity increase with soot conversion, as was suggested for *e.g.* MoO$_3$. The discrepancy between the oxidation profiles obtained for CuO(875) and CuO(*ex* nitrate) was already addressed in chapter 9 of this thesis and might be attributed to a higher surface area of CuO(875) than CuO(*ex* nitrate) (approximately 20 m^2.g^{-1} *vs.* <1 m^2.g^{-1}). An increased amount of direct contact points diminishes the contribution of

SOCs to the oxidation profile relative to the contribution of lattice oxygen and the so-called interface reaction mechanism [7].

Three reasons can be proposed for the increased soot oxidation activity of CuO catalysts in the presence of CO (1000 ppm in 10% O$_2$ in Ar, figure 3): *(i)* CO slightly reduces the copper surface, thereby increasing the effectivity in the activation of oxygen, *(ii)* CO slightly reduces the copper surface, followed by a redistribution of the reduced copper species, and subsequently an increase in the number of contact points and thus an increase in the oxidation rate, and *(iii)* CO oxidation causes a localized temperature increase of the catalyst, and thus an enhanced soot oxidation rate. As CO oxidation was not observed at 575 K over Cu-impregnated soot, the last explanation does not seem likely. Moreover, although CO oxidation was observed during the Co$_3$O$_4$ catalyzed soot oxidation, the soot oxidation rate was negatively affected. The second proposition *(ii)* is contradictory to the fact that the CO oxidation activity in NO$_x$ decreases as a function of soot conversion, while the opposite is expected if redistribution of the catalyst occurred. Neeft also argued, referring to the Tammann temperature, that redistribution of CuO-particles is not very likely at 550 K [7].

Jernigan found an increasing CO-oxidation activity in the series Cu > Cu$_2$O > CuO [12]. Although experimental evidence for the formation of a reduced copper surface has not been presented, it seems likely that surface defects, and a slightly reduced copper surface, are created by reaction of CO with oxygen associated with CuO (compare chapter 9), causing a higher effectivity in the activation of oxygen and thus a higher soot oxidation rate.

For the Cu-impregnated sample, CO oxidation was only observed in the presence of NO$_x$, because NO$_2$ is a stronger oxidant than O$_2$ (reaction 1):

$$NO_2 + CO \quad \rightarrow \quad NO_x + CO_2 \tag{1}$$
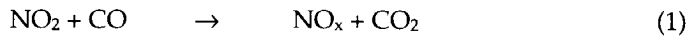
Reaction (1) explains the higher NO concentration, measured in the presence than in the absence of CO (figure 2) and the slightly lower soot oxidation rate in NO$_x$ with, than without CO: CO is in competition with soot for reaction with NO$_2$ (reaction (3)).

The decreasing activity of Cu-impregnated soot in the CO/NO$_2$ reaction as a function of soot conversion, might be explained by *(i)* sintering of the active copper (oxide) species during soot oxidation or *(ii)* a symbiosis between CO and soot: CO slightly reduces the copper surface, thereby enhancing the soot oxidation rate, while at the same time carbothermic reduction of the catalyst surface provides active sites for the oxidation of CO. Both explanations might be valid, although sintering of the active species seems to be more likely.

The rate enhancement, and the high NO concentration found for Cu-impregnated soot and CuO/soot physical mixtures, relative to an empty reactor (figure 2), can be explained by reactions (2) and (3):

$$2\,NO + O_2 \quad \leftrightarrow \quad 2\,NO_2 \tag{2}$$

$$NO_2 + \text{'C'} \quad \rightarrow \quad CO + NO \qquad (3)$$
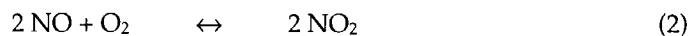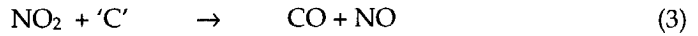
The catalyzed soot oxidation rate is higher than the non-catalyzed rate in NO_x/O_2 (figure 2). Although CuO was shown to possess a catalytic activity for reaction (2) (figure 12), the oxidation rate in NO_x/O_2 is related to the intensity of contact between the catalyst and soot, just like in O_2/Ar. In view of the higher NO_2 conversion in the presence, than in the absence of CuO, the enhancement of the oxidation rate cannot be explained solely by an enhancement of NO_2 reformation, and non-catalytic occurrence of reaction (3). CuO is likely to be catalytically active for reaction (3) in 'tight contact'. This is schematically shown in figure 13. In fact, NO facilitates the transport of activated oxygen. Oxygen is activated on the catalyst surface, followed by reaction with NO, yielding NO_2. NO_2 might react non-catalytically with soot, yielding surface oxygen complexes (SOCs), CO/CO_2, and NO, or decompose on the catalyst surface in the vicinity of the catalyst/soot interface, yielding activated oxygen and NO. The (activated) oxygen species deposited on the catalyst surface might spill-over to, or react *via* the oxidic lattice with the soot particle, yielding SOCs and/or CO and CO_2. Summarizing figure 13, several reactions might contribute to the overall reaction rate and the soot oxidation profile in the presence of NO_x, such as the catalyzed and non-catalyzed oxidation of soot by NO_2, and the catalyzed oxidation by O_2. The use of the NO/NO_2 reaction for the catalytic removal of diesel soot particles is further evaluated in paragraph 10.4.5.
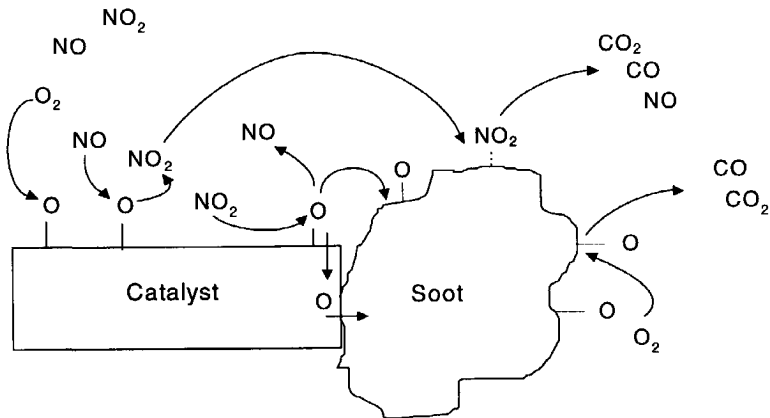
Figure 13. Schematic representation of the interactions of NO, O_2, and NO_2 with a catalyst/soot mixture.

10.4.3. Cr$_2$O$_3$-catalyzed soot oxidation.

A constant-type oxidation profile is found for the Cr$_2$O$_3$ catalyzed soot oxidation, in agreement with observations of Neeft [7] (figure 6). Cr-impregnated soot shows a rapid decay of the reaction rate in O$_2$ up to a conversion level of 0.3 (figure 5) at 550 K. Unfortunately, the profile was not recorded at higher conversion levels, but the exponential decay seems to level off to a more constant reaction rate. This is corroborated by the profile of Cr-impregnated soot without pretreatment, which was presented elsewhere [13].

CO negatively affected the oxidation rate of Cr-impregnated soot at 575 K, whereas it did not affect the catalytic activity of Cr$_2$O$_3$ in 'tight contact' physical mixtures at 675 K. CO oxidation, according to reaction (1), was not observed. The reason for the negative effect of CO at 575 K is likely to be caused by CO and/or CO$_2$ adsorption on the catalyst surface. Bijsterbosch showed that at 550 K CO and CO$_2$ adsorption on relatively small Cr$_2$O$_3$ particles yields chromium carbonates, which show minor activity in oxidation reactions [14]. At 675 K, these carbonates are less stable, explaining the fact that CO, as a net result, did not effect the Cr$_2$O$_3$-catalyzed soot oxidation at 675 K.

NO$_x$ enhances the soot oxidation rate of Cr-impregnated soot and Cr$_2$O$_3$/soot physical mixtures considerably. Cr$_2$O$_3$ was shown to be an effective catalyst for reaction (2), explaining the high 'loose contact' activity in NO$_x$/O$_2$ (figures 12 and 13). However, an increase in the intimacy of contact considerably enhanced the soot oxidation rate (compare figures 5, 7, and 12). As was visualized in figure 13, decomposition of NO$_2$ on the catalyst surface in the vicinity of a soot particle, followed by oxygen spill-over, increases the overall soot oxidation rate. The contribution of this reaction-sequence to the overall oxidation rate in NO$_x$ is diminished, if the distance between a catalyst and a soot particle is increased, due to loss of contact.

10.4.4. Co$_3$O$_4$ catalyzed soot oxidation

CO negatively affected Co$_3$O$_4$ catalyzed soot oxidation at 650 K (Co$_3$O$_4$ (875)) and at 675 K (Co$_3$O$_4$(ex nitrate)), while Co$_3$O$_4$ was shown to be a very effective CO oxidation catalyst. However, Co$_3$O$_4$(*ex* nitrate) showed an increasing CO concentration as a function of soot conversion. It can be suggested that sintering causes the deactivation of the catalyst in CO oxidation. However, the Co$_3$O$_4$(875) catalyst was prepared by calcination at 875 K, while the soot oxidation reaction was conducted at 650 K. Furthermore, the CO conversion seems to be a function of the reaction rate in soot oxidation (figure 10). Following the reasoning given for CuO catalyzed CO and soot oxidation, CO is likely to slightly reduce the Co$_3$O$_4$ surface. In chapter 8 it has already been argued that a slightly reduced surface might hinder oxygen transport through the catalyst surface layer. Obviously, this negatively affects the soot oxidation rate. At the same time, carbothermic reduction might

enhance the amount of vacancies (reactive sites for oxygen activation), contributing to a high CO conversion, in agreement to the results of Jernigan [12]. CO adsorption or carbonate formation is not very likely to take place at 675 K and to cause the lower soot oxidation rate [15]. An explanation for the fact that CO promotes CuO-catalyzed soot oxidation and diminishes the Co_3O_4-catalyzed soot oxidation, as a result of a similar effect (i.e. a slightly reduced surface), is related to the oxidation mechanism. Spill-over might play a considerable role in the CuO catalyzed soot oxidation (chapter 7), whereas it was shown not to take place in Co_3O_4 catalysis. Apparently, activation of oxygen, followed by spill-over, is promoted by a slightly reduced surface, whereas transport of oxygen through the surface layer, needed for reaction at the catalyst/soot interface, is hindered.

NO considerably enhanced the soot oxidation rate and changed the oxidation profile of Co_3O_4-catalyzed soot oxidation. Co_3O_4 was shown to be an active NO_x oxidation catalyst. Following the reasoning of CuO catalyzed soot oxidation, the resulting oxidation profile might be caused by contributions of the *non*-catalytic soot oxidation by NO_2 and the catalytic oxidation of soot by NO_2. However, as discussed previously, oxygen spill-over is less likely to play a role in Co_3O_4 catalysis [18]: reaction of an activated oxygen with soot, deposited on the catalyst surface by NO_2 decomposition, occurs solely at the catalyst/soot interface, after incorporation in the surface layer of Co_3O_4 [7,18]. The contribution of the NO_2/soot reaction is corroborated by the NO concentration profile: compared to an empty reactor, a relatively high NO concentration is observed in the soot conversion range of 0.25-0.7.

10.4.5 Evaluation of the possibilities to use the catalytic soot/NO_x reaction for the removal of soot from diesel exhaust streams

If a practical operation of the NO_x/soot reaction is considered for the catalytic oxidation of diesel soot, three possibilities can be thought of, which are schematically shown in figure 14. In fact, one would want to use a catalytic cycle, as visualized in figure 15. NO is catalytically oxidized into NO_2, followed by reformation of NO by (catalytic) reaction of soot with NO_2. The NO/transition metal oxide combination provides a bifunctional catalyst, where the role of NO is to improve the efficiency of the transition metal oxide by transporting activated oxygen.
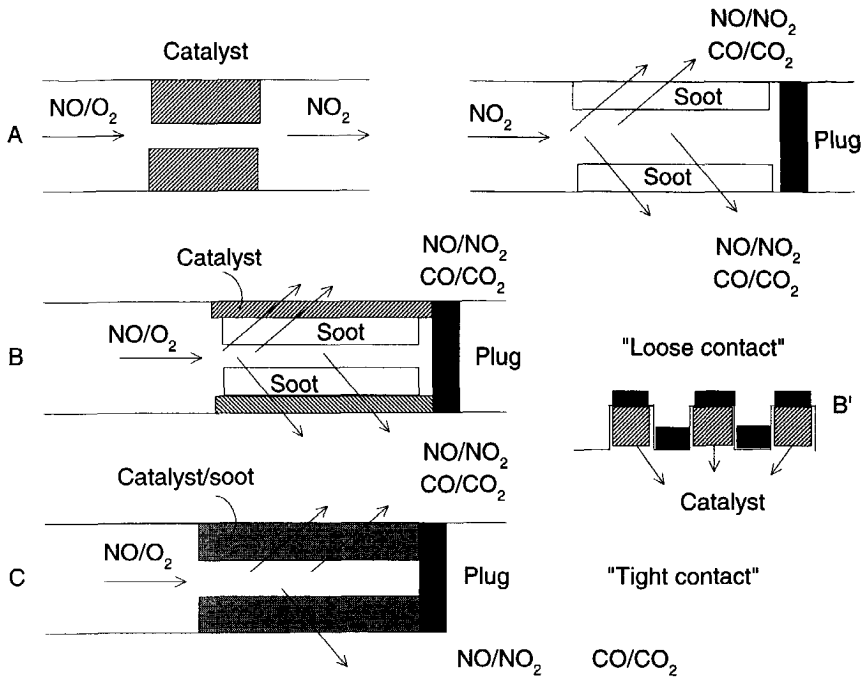
Figure 14. Schematic representation of the practical application of the NO$_x$/O$_2$ reaction in the catalytic removal of soot from diesel exhaust.

In situation A, which has been tested in practice by Johnsson Matthey using a Pt-catalyst [19], the catalyst is completely separated from the soot particles, which are collected in a monolithic filter [7,16]. The catalyst converts NO into NO$_2$, which non-catalytically reacts with soot in the filter. In this situation, a more or less stoichiometric reaction of NO$_2$ with soot is used to produce CO and CO$_2$. Indeed, for Euro I and higher type of diesel engines, the average amount of soot and NO$_x$ present in diesel exhaust is such, that this reaction covers a complete conversion of the carbonaceous part of the particulate [7]. Nevertheless, the use of a catalyst, coated on the walls of the channels of a monolithic filter, as is schematically represented by situation B, seems to be more appropriate, but not ideal, as the NO$_x$/O$_2$ stream first diffuses through the soot particulate layer, before can hit the catalyst. In fact, this situation represents a 'loose contact' situation, and is practically feasible. Situation B could be optimized by using structured channels, as depicted in situation B'.
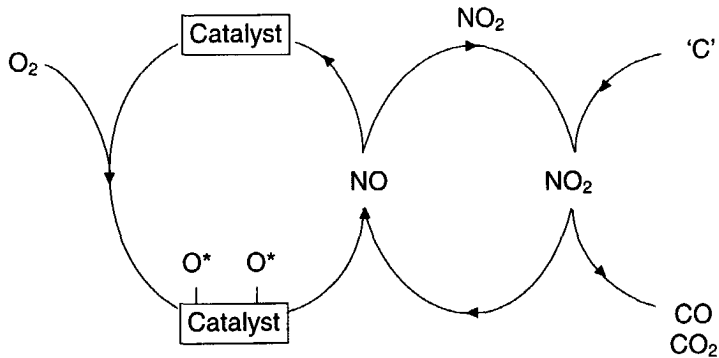
Figure 15. Catalytic cycle, using NO as catalyst. O_2 is activated on the catalyst surface, followed by conversion of NO into NO_2. Subsequently NO_2 reacts with soot, yielding NO, CO and CO_2.

In situation C, as depicted in figure 14, a catalytic cycle of NO/NO_2 seems to be possible, which is schematically shown in figure 15. From the 'loose contact' reaction rates (figure 11) it can be calculated that each NO molecule has a turn-over number up to 10. However, the highest NO_x/soot reaction rates can be obtained, if the catalyst and soot are totally intermixed, *i.e.* in a 'tight contact', or, even better, in an impregnated situation. Solutions, which enable such a situation in practice are currently under investigation. One option is to make use of so-called diesel fuel additives, which function as precursors for active metal oxide species. Very small oxidic particles are formed simultaneously with soot upon combustion of the diesel fuel in the engine, yielding a highly dispersed active phase in the soot particles. A high activity in the NO and soot oxidation is expected, based on the results of the impregnated samples dealt with in this paper.

Concluding, the effectivity of NO_x as a catalyst in the oxidation of soot, is related to the distance between the oxidic catalyst and soot. An impregnated situation results in the highest soot oxidation rates, and can be established in practice by the use of diesel fuel additives. The effects of other constituents of diesel exhaust on the catalytic activity for the oxidation of NO and soot, such as unburned (aliphatic) hydrocarbons, and especially SO_2, have to be further investigated. This has already been emphasized by Cooper and Thoss [16], who used a Pt-catalyst for the oxidation of NO into NO_2 and the subsequent oxidation of soot by NO_2.

10.5. Conclusions

- Impregnated samples were found to show a higher activity than 'tight contact' and 'loose contact' physical mixtures of soot and the corresponding Transition Metal Oxides (TMO) in 10% O_2 in Ar.

- Addition of NO$_x$ to the oxidizing medium (10% O$_2$ in Ar) enhances the rates of Cr$_2$O$_3$, Co$_3$O$_4$ and CuO catalyzed soot oxidation (physical mixtures as well as impregnated samples). The rate enhancement is explained by the catalyzed formation of NO$_2$ and the catalyzed and non-catalyzed reaction of soot with NO$_2$.
- Addition of CO enhances the soot oxidation rate in the presence of CuO, whereas it inhibits the Co$_3$O$_4$ catalyzed soot oxidation and hardly effects Cr$_2$O$_3$ catalysis.
- The effectivity of the NO$_2$/soot reaction increases with an increasing catalyst/soot interaction.
- Removal of NO$_x$ from diesel exhaust should be applied after removal and oxidation of the soot particles.

10.6. *References*

[1]   E.S. Lox, B.H. Engler and E.Koberstein, in Proceedings of Catalysis and Automotive Polution Control, Amsterdam, 1991, pp. 291-321.
[2]   A.F. Ahlstrom and C.U.I. OdenBrand, Appl. Catal. 60 (1990) 143.
[3]   A.F. Ahlstrom and C.U.I. OdenBrand, Appl. Catal. 60 (1990) 157.
[4]   J.P.A. Neeft, M. Makkee and J.A. Moulijn, Appl. Catal. B: Env. 8 (1996) 57.
[5]   D.W. McKee, J. Catal. 108 (1987) 480.
[6]   D.W. McKee, Carbon, 8 (1970) 623.
[7]   J.P.A. Neeft, 'Catalytic oxidation of soot-Potential for the reduction of diesel particulate emissions', PhD Thesis TU Delft, (1995), chapter 7.
[8]   G. Mul, chapter 8 of this thesis.
[9]   J.P.A. Neeft, M. Makkee, J.A. Moulijn, J.A. Saile and K.L. Walker, IMechE, C517/013 (1996) 233.
[10] G. Mul, chapter 5 of this thesis.
[11] S. Imamura, H. Sawada, K. Uemura and S. Ishida, J. Catal. 109 (1988) 198.
[12] G.G. Jernigan and G.A. Somorjai, J. Catal. 147 (1994) 567.
[13] G. Mul, F. Kapteijn and J.A. Moulijn, Prepr. Pap. -Am. Chem. Soc., Div. Fuel Chem. 41 (1996) 230.
[14] J. Bijsterbosch, 'Copper based catalysts for CO oxidation and NO$_x$ reduction', PhD Thesis University of Amsterdam (1993), chapter 2.
[15] G. Busca, R. Guidetti and V. Lorezelli, J.Chem.Soc.Faraday Trans.I, 86 (1990) 989.
[16] B.J. Cooper and J.E. Thoss, SAE Paper 890404, (1989) 171.
[17] G. Mul, chapter 9 of this thesis.
[18] G. Mul, chapter 8 of this thesis.
[19] P.N. Hawker, Platinum Metals Rev. 39 (1995) 2.
[20] E. Ito, R.J. Hultermans, P. M. Lugt, M.H.W. Burgers, M.S. Rigutto, H. van Bekkum, and C.M. vd Bleek, Appl. Catal. B: Env. 4 (1994) 95.

SUMMARY AND CONCLUDING REMARKS

Introduction

Regarding the emission of hydrocarbons and nitrogen oxides (NO_x), diesel engines are environmentally friendlier than otto engines. However, they are main contributors to the emission of particulate matter. The particulates, consisting of soot (*i.e.* the carbonaceous part), adsorbed poly-aromatic hydrocarbons (PAH's, compounds which are toxic and thought to have a carcinogenic effect), sulfates and inorganic substances, are blamed for decreasing environmental conditions, particularly in big cities. The exhaust gases of otto engines can be cleaned by so-called platinum/rhodium based three way catalysts and at present otto engines in combination with a three way catalyst are significantly cleaner than diesel engines. Unfortunately, platinum/rhodium catalysts cannot be used for the clean-up of diesel-exhaust gas, because it contains a relatively high amount of oxygen: the reaction of CO with NO, essential in the three way catalysis, does not take place in the presence of oxygen.

A possibility for the clean-up of diesel exhaust, is to remove particulates by collection in a ceramic filter (a so-called wall-flow monolith) in a first step, and subsequently convert NO_x into harmless N_2 and O_2. Possible processes for the conversion of NO_x have been discussed in other dissertations [1,2]. This thesis deals with the conversion of the particulates, or, more specifically, the oxidation of the carbonaceous part of the particulates (soot). Oxidation can be accomplished with the oxygen content present in diesel exhaust, and is required to prevent plugging of the ceramic filter. However, soot oxidation occurs non-catalytically at 875 K, while diesel exhaust temperatures are usually below 675 K. Hence, catalytic oxidation is needed. In practice, the most convenient way is to coat the catalyst to the wall of the monolith [3]. In this thesis, several techniques have been used to study the activity of catalysts in soot oxidation, such as a flow reactor setup (the so-called six-flow), thermogravimetric analysis (TGA), infrared (IR) spectroscopy and high vacuum equipment to study the behavior of catalysts in $^{18}O_2$. Subsequently, the activity of chlorine based catalysts (chapters 3 and 4), alkali metal based catalysts (chapters 5 and 6), and transition metal based catalysts (chapters 7,8,9 and 10) are dealt with.

IR analysis of catalyst/soot mixtures

In chapter 1, the reader is introduced to literature dealing with IR analyses of coal, soot, and related carbonaceous materials. Many IR analyses performed in the 1950s-1970s, were aimed to elucidate the composition of coal and its structure. Furthermore, extensive *in-situ* FT-IR studies of the pyrolysis and oxidation of coal and other carbonaceous materials have been performed in the 1980s-1990s. These studies are described and the observed spectral phenomena evaluated, including an extensive description of the assignments of the various IR bands to oxidic and hydrogen containing functionalities. Also chemical methods to justify the assignments of the

surface species are dealt with, such as the specific reaction of hydroxylic species with acetic acid. The oxygen containing functional groups formed by oxidation of chars, carbon black, and coal, appear to be quite similar and rather independent of the carbonaceous material. Functionalities such as acid anhydrides, lactones, carboxylic acids, ether-like groups, and hydroxyls can be identified quite well.

In chapter 2, DRIFT spectroscopy is evaluated for the (*in-situ*) analysis of catalyst/soot mixtures in air at elevated temperatures. Carbonaceous materials are strong absorbers of IR radiation. To increase the quality of the IR spectra, usually KBr is used as a diluent. However, several metal oxides, like V_2O_5 and MoO_3, are shown to react with KBr. Changes occurring in the V_2O_5 spectrum can be explained by the formation of potassium vanadates. Furthermore, the *in-situ* DRIFT analysis of metal chlorides in KBr, which are very active in soot oxidation, is affected by the formation of eutectics. This results in melting and/or oxidation below the temperatures characteristic for the pure metal chlorides. Additionally, oxygenated species on the soot surface might react with KBr, yielding potassium phenoxide and benzoate type complexes. Hence, if the *in-situ* DRIFT analysis of the interactions between soot, oxygen and transition metal oxides is aimed for, the use of KBr as a diluent is not recommended. Si powder can be used as an alternative, although it has a higher overall extinction coefficient than KBr. Another alternative is to use a recently discovered carbonaceous material, Fullerene C60, as a soot model compound. C60 has a low overall extinction coefficient, and only four specific IR bands. Upon oxidation, C60 is shown to yield oxygen containing functionalities quite similar to those observed in the spectra of oxidized soot. Throughout this thesis, *ex-situ* DRIFT spectroscopic analyses are presented, *i.e.* pretreatment of catalyst/soot mixtures in a thermobalance or a flow reactor setup, followed by room temperature analysis in KBr. Fullerene C60 was used for *in-situ* measurements.

Contact between soot and catalyst

The activity of oxidic catalysts in soot oxidation is found to be strongly dependent on the intensity of contact between the catalyst and soot. Two types of contact in physical mixtures are evaluated throughout this thesis. Simple shaking of a bulk metal oxide and soot in a sample bottle is indicated by 'loose contact', and extensive mixing of the catalyst and soot in a mechanical ball mill by 'tight contact'. Furthermore, catalyst/soot mixtures have been prepared by impregnation, using a dissolved nitrate precursor of the catalyst in ethanol. Usually, the highest activity for a single metal oxide is obtained after impregnation, followed by 'tight contact' physical mixtures. Unfortunately, the contact achieved in a diesel filter is essentially 'loose contact' [3]. Many metal oxide catalysts completely loose their activity under these conditions. 'Tight contact' systems have been used for mechanistic studies throughout this thesis. A better understanding of the activity of metal oxides might lead to the development of active and applicable catalysts.

Chlorine containing catalysts

A Cu/K/Mo/Cl soot oxidation catalyst has been reported in the literature as being active in 'loose contact' around 670 K. Several copper-molybdates and potassium-molybdates, potentially present in this catalytic system, have been tested individually on their activity (chapter 3). Although these oxides induce soot oxidation between 685 K and 720 K in 'tight contact', the oxidic catalysts only show a high activity above approximately 790 K in 'loose contact'. Hence, the 'loose contact' activity of the Cu/K/Mo/Cl catalysts is not explained by the presence of an oxidic compound. DRIFT and XRD analyses have shown that addition of KCl to $CuMoO_4$ followed by calcination at 950 K in air, eventually results in the formation of a mixed potassium-copper-molybdate. Simultaneously, several volatile copper, potassium and chlorine containing compounds (*e.g.* K_2CuCl_4) are formed. These copper and chlorine containing compounds possess a high 'loose contact' soot oxidation activity between 600 and 690 K. The activity of the Cu/K/Mo/Cl catalyst will be maintained as long as Cu_2OCl_2 can be reformed by reaction of copper molybdates with KCl, which serves as a chlorine supplier. It is not surprising that deactivation of the catalytic system is a serious problem.

The 'loose contact' activity in the oxidation of soot and the stability of metal chlorides is further discussed in chapter 4. $HgCl_2$, $CaCl_2$, $BaCl_2$, $CoCl_2$, and $NiCl_2$ show little activity. Hydrated $BiCl_3$ and $FeCl_3$ are converted in air into $BiOCl$ and $FeOCl$, which have a moderate soot oxidation activity. $MoCl_5$ is converted into the corresponding metal oxide and also shows a moderate 'loose contact' activity. $PbCl_2$, $CuCl_2$, and $CuCl$ are the most active catalysts; the soot oxidation temperature is lowered by 200-275 K. The activity of metal chlorides is thought to be induced by *in-situ* formation of intimate contact between the soot and the metal chloride *via* 'wetting' and/or gas phase transport. A correlation between the melting point and the catalytic activity was found. Furthermore, a catalytic cycle is proposed involving activation of oxygen on the surface of the (oxy)chloride, followed by transfer of activated oxygen to the soot surface. DRIFT analyses show that this results in the formation of carbon surface oxygen complexes, CO and CO_2. Practical application of metal chlorides for the removal of soot from diesel exhaust is not recommended, because they suffer from instability and/or exhibit undesired high vapor pressures.

Alkali metal oxide-based catalysts

The application of potassium salts in the catalytic oxidation of carbonaceous materials has received considerable attention, mainly because of its potential application in commercial coal gasification processes. An extensive DRIFT study on the catalytic oxidation of soot by K_2CO_3, K_2MoO_4, and the nitrates of various alkali metals (Na, K, Rb, and Cs), is described in chapter 5. The spectra of potassium benzoate, potassium phenoxide, alkali metal carbonates and catalytically oxidized fullerene C60 have been used for the assignment of various absorption bands and

reveal the nature of the present alkali metal species. Alkali benzoates are formed upon alkali metal catalyzed soot oxidation in air, as well as alkali metal oxide species attached to the carbon surface. The initial oxidation activity is dependent on the intensity of contact between soot and catalyst, the dispersion of the catalyst and the stability of the potassium precursor: in physical mixtures, the soot oxidation activity increases in the series $KNO_3 < K_2MoO_4 < K_2CO_3$ (chapter 6). Decomposition of the precursors is suggested to yield active oxidic clusters. Based on literature dealing with alkali catalyzed carbon gasification, absorption bands in the 1100-1150 cm^{-1} region and around 620 cm^{-1} are assigned to CO_2, chemisorbed on the oxidic alkali metal species. Absorption bands around 1140 cm^{-1} have also been observed in the spectra of partially converted CaO/soot samples, corroborating the assignment to chemisorbed, *i.e.* non-carbonate CO_2 (chapter 5). The effects of NO_x and CO (other constituents of diesel exhaust) on the activity of potassium based catalysts, are discussed in chapter 6. NO_x negatively affects the oxidation rate of potassium impregnated soot at temperatures below 600 K, which is explained by chemisorption of NO_2 on the oxidic clusters and KNO_3 formation. Above 600 K, nitrate formation does not occur, and the soot oxidation rate is enhanced by a contribution of the 'C'/NO_2 reaction to the overall reaction rate. CO positively affects the potassium catalyzed soot oxidation rate, irrespective of the reaction temperature. This is tentatively explained by a slightly lower oxidation state of the active oxidic potassium cluster, which prevents deactivation by NO_2 and/or CO_2 chemisorption. Because of (i) a very low 'loose contact' soot oxidation activity, (ii) a low NO and CO oxidation activity, and (iii) a possible deactivation by NO_2 or CO_2 chemisorption at diesel exhaust temperatures, the use of potassium-based catalysts for the catalytic removal of soot from diesel exhaust seems to be not feasible. Furthermore, it can be anticipated that, due to the high volatility of alkali oxides and peroxides, deactivation of the catalytic coatings will occur.

Transition metal oxide-based catalysts

Ex-situ DRIFT analyses of partially converted catalyst/soot mixtures and *in-situ* analyses of catalytic fullerene C60 oxidation (chapter 7), revealed that several transition metal oxides (Cr_2O_3, MoO_3, V_2O_5, and CuO) promote the formation of carbon surface oxygen complexes (SOCs). Fe_2O_3 and Co_3O_4 do not enhance the formation of these SOCs in 10% O_2 in Ar and prevent the formation of SOCs in ozone. The latter is tentatively explained by recombination of activated oxygen species on the catalyst surfaces.

Carbothermic reduction of metal oxides does not yield SOCs. Apparently, lattice oxygen is not directly involved in the catalytic formation of these complexes. Indications for chemical interactions between metal oxides and either soot or C60, such as M-O-C bonds, have not been found. Spill-over of activated oxygen from the Cr_2O_3-, MoO_3-, V_2O_5-, and CuO surfaces onto the soot surface is likely to explain the catalytic formation of SOCs.

The soot oxidation mechanism was further investigated by treatment of physical mixtures of soot and several transition metal oxides (Cr_2O_3, Co_3O_4, Fe_2O_3, MoO_3, V_2O_5, and K_2MoO_4) in $^{18}O_2$ at 625-675 K in a high vacuum batch reactor (chapter 8). By analysis of the reaction products ($C^{16}O$, $C^{18}O$, $C^{16}O_2$, $C^{16}O^{18}O$ and $C^{18}O_2$), it was shown that the amount of gas-phase oxygen incorporated in the gaseous products, increases in the series $K_2MoO_4 < V_2O_5 < MoO_3 < Co_3O_4 = \gamma\text{-}Fe_2O_3 < \alpha\text{-}Cr_2O_3$. The experimental results agree well with oxygen exchange data given in the literature: less than one monolayer is exchangeable for Co_3O_4, a monolayer for Fe_2O_3 and Cr_2O_3 and the entire bulk for MoO_3 and V_2O_5. An adapted redox mechanism is proposed for Fe_2O_3 and Co_3O_4 catalyzed soot oxidation in which only a small fraction of lattice oxygen (located in the surface layer, defined as surface oxygen) is available. Surface oxygen of Cr_2O_3 is also found to be involved in the oxidation mechanism. Moreover, based on the relatively high fraction of ^{18}O labeled products and the results of the DRIFT experiments, a spill-over mechanism, involving so-called *super* surface oxygen, is proposed for Cr_2O_3 catalysis. Furthermore, a combination of a spill-over mechanism and a redox mechanism, including oxygen from the bulk, is proposed for MoO_3 and V_2O_5. Finally, a so-called push-pull mechanism is proposed for K_2MoO_4, because carbothermic reduction of K_2MoO_4 was not observed in the absence of gas phase oxygen, whereas in the presence of oxygen extremely high amounts of lattice oxygen were incorporated in the gaseous products CO and CO_2.

The activity of Cr_2O_3, Co_3O_4, CuO, and MnO_x in the oxidation of CO and soot, is further evaluated in chapter 9, including the effects of promotion by Ag or Au. The existence of different oxidation mechanisms was corroborated by the occurrence of different oxidation profiles. So-called exponential decay-type, rising-type, and constant-type profiles have been found. Moreover, the catalytic activity of transition metal oxides in the oxidation of soot appeared to be largely determined by the available surface area and the number of catalyst/soot contact points. A negative effect of Au on the soot oxidation activity of the investigated metal oxides is explained by a partial coverage of the metal oxide surface with inactive Au. The similarity in activity order found for Co_3O_4, CuO and MnO_x in the oxidation of CO and soot, suggests an effect of the metal-oxygen bond strength on the oxidation activity and the involvement of a redox mechanism, in agreement with the results presented in chapter 8. An associative mechanism might explain the CO oxidation activity of MnO_x catalysts at relatively low temperatures, as a step in the CO oxidation profile has been observed. An associative mechanism cannot explain soot oxidation activity: soot is immobile and does not migrate to active sites.

The addition of K, Ag or Cu to V_2O_5 negatively affects the soot oxidation activity, ascribed to a diminished reducibility of oxygen anions in the vanadium bronzes. A positive effect of the addition of Ag to Co_3O_4, CuO, and MnO_x on the soot oxidation activity was observed, ascribed to a high intrinsic activity of transition metal supported Ag_2O species, which are reoxidized by the transition metal oxides. It is concluded that the synergism between Ag and a transition metal oxide in the

oxidation of soot is based on beneficial redox properties of the catalytic system, and that these catalysts might be useful in practice, when applied as diesel fuel additives.

The effects of NO_x and CO on the catalytic soot oxidation activity of Cr_2O_3, Co_3O_4, and CuO is discussed in chapter 10. Addition of NO_x to O_2/Ar enhances the oxidation rate, irrespective of the intensity of contact between the catalyst and soot, which is attributed to the NO_2/soot reaction, yielding NO, CO and CO_2. NO might be reoxidized into NO_2 over the catalyst to close a catalytic cycle. The NO/transition metal oxide combination provides a bifunctional catalyst, where the role of NO is to improve the efficiency of the transition metal oxide by transporting activated oxygen. In 'loose contact', the primary function of the catalyst is to catalyze the oxidation of NO, whereas in 'tight contact' the NO_2/soot reaction is also likely to be catalyzed.

The effect of CO is strongly dependent on the catalyst: CO promotes the CuO catalyzed soot oxidation, it hardly affects the Cr_2O_3 activity, and suppresses the Co_3O_4 activity. Several tentative explanations for the observed phenomena are presented, based on the redistribution, sintering, and the oxidation state of the catalyst.

Recommendations for further research

In order to develop a highly active catalyst for soot oxidation at diesel exhaust temperatures, the main issue to be solved is the contact problem. An efficient transport of the reactant (activated O_2) from the activator (the catalyst) to the substrate (soot) has to be accomplished. This can be established by (i) improving the contact (decreasing the catalyst/soot distance, or increasing the number of catalyst/soot contact points) and (ii) enhancement of the effectivity of activated oxygen.

The results described in this thesis indicate that the activity of Cu/K/Mo/Cl catalysts, and metal chloride containing catalysts in general, is based on (i): the mobility and volatility of the active species induces a redistribution ('tight contact'), and an enhanced number of catalyst/soot contact points. However, volatile active species cannot be used in practice, obviously, because the active material will be lost and introduced into the environment. Mobility is less likely to yield a rapid deactivation, while the *in-situ* formation of 'tight contact' conditions might be achieved. An oxidic cocktail with a low melting point might possess a high mobility and a low volatility. The liquid phase catalyst could be anchored to the wall of the filter. Several aspects of these so-called supported liquid phase catalysts have to be considered such as catalyst loss (volatility), and the sticking probability of the soot particulates in the melt, which is related to the 'wetting' properties of the metal oxides. A liquid phase does not result in 'tight contact' conditions *per se*.

The number of catalyst/soot contact points can also be increased by lowering the average particle size of the catalyst. Throughout this thesis, impregnated systems were found to display a high soot oxidation activity. In practice, the impregnated situation might be established by the use of diesel fuel additives, which function as precursors for active metal oxide species. Very small oxidic particles are formed simultaneously

with soot upon combustion of the diesel fuel in the engine, yielding a highly dispersed active phase in the soot particulates. In this application various transition metal oxides could be chosen, while the synergetic effect of Ag-based catalyst could be exploited by combining a Ag-additive and a transition metal-additive, like *e.g.* Ag_2O/CuO. Blocking of the filter by the formed oxidic ashes and the emission of the additives are important aspects that need to be considered.

Option (ii) might be established in practice by the use of NO. The feasibility of the NO_x/soot reaction for the oxidation of soot, is evaluated in chapter 10. Oxidation of soot by NO_2 occurs already with considerable rates at the diesel exhaust temperatures. Several aspects of bifunctional catalysis, where the role of NO is to improve the efficiency of the transition metal oxide by transporting activated oxygen, have to be further investigated. The effect of other constituents of diesel exhaust on the catalytic activity for the oxidation of NO and soot, such as unburned (aliphatic) hydrocarbons, and CO, is one of them. More important even, is the possible formation of SO_3 by reaction of SO_2 with O_2, which increases the particulate content of diesel exhaust [3]. Fortunately, low sulfur levels in diesel fuel can be expected in the next decades, due to stringent legislation.

References

[1] R.J. Hultermans, 'Selective Catalytic Reduction of NO_x', PhD Thesis, Delft University of Technology, 1995.
[2] E. Ito, 'Development of Zeolite Catalysts for NO_x Reduction with NH_3 in Diesel Exhaust Gas', PhD Thesis, Delft University of Technology, 1996.
[3] J.P.A. Neeft, 'Catalytic Oxidation of Soot-Potential for the Reduction of Diesel Particulate Emissions', PhD Thesis, Delft University of Technology, 1995.

SAMENVATTING

Reiniging van diesel uitlaatgas is noodzakelijk om het milieu te sparen en de volksgezondheid te waarborgen. Met name de verwijdering van NO_x en roet uit diesel uitlaatgas zou de (milieu) vervuiling aanzienlijk kunnen verminderen. Aan de TU Delft wordt een project uitgevoerd, dat de ontwikkeling behelst van een systeem voor de verwijdering van zowel NO_x als roet uit diesel uitlaatgas. Mogelijke processen voor de omzetting van NO_x en de daar bij behorende katalysatoren, zijn beschreven in andere dissertaties [1,2].

Dit proefschrift beschrijft de verwijdering en met name de omzetting (oxydatie) van de roet deeltjes in relatief onschadelijk CO_2. Een keramisch filter is de meest praktische oplossing voor de initiële verwijdering van deeltjes uit het diesel uitlaatgas. Om te voorkomen dat dit filter in zeer korte tijd verstopt raakt, is omzetting noodzakelijk. Hiervoor kan zuurstof, dat aanwezig is in diesel uitlaatgas, worden aangewend. De oxydatie van roet vindt echter pas met aanzienlijke snelheid plaats bij ongeveer 875 K (600 °C), terwijl de temperatuur van diesel uitlaatgas meestal niet veel hoger is dan 675 K (400 °C). Daarom is ofwel een kunstmatige verhoging van de temperatuur noodzakelijk, ofwel de toepassing van een katalystor, die er voor zorgt dat de roet deeltjes bij lage temperatuur snel genoeg worden omgezet. Deze katalysator kan als laagje op de wanden van het filter worden aangebracht, of aan de brandstof worden toegevoegd (als een zogenaamd brandstof additief). De fundamentele inzichten die in dit proefschrift worden beschreven, hebben met name betrekking op de eerste methode.

In de dissertatie van J.P.A. Neeft is reeds een aanzet gegeven voor de ontwikkeling van een goede roet oxydatie katalysator [3]: met name de beschrijving van experimentele methoden voor de bepaling van de activiteit, de selectie van potentieel bruikbare katalysatoren, en een aanzet tot de beschrijving van het werkings mechanisme zijn van belang geweest voor het onderzoek dat wordt beschreven in de voor u liggende dissertatie. Om de werking van katalysatoren in de oxydatie van roet nader te bestuderen, is met name Fourier Transform (FT) Infrarood (IR) spectroscopie toegepast, omdat met deze analyse techniek zowel roet, als de verschillende katalysatoren gekarak-teriseerd kunnen worden. In het eerste, inleidende, hoofdstuk van dit proefschrift wordt de toepassing van FT-IR spectroscopie in de karakterisering van steenkool en andere koolstof bevattende materialen nader toegelicht. Er wordt aangetoond, dat de samenstelling van steenkool niet substantieel verschillend is van die van (partieel geoxydeerd) dieselroet. De interpretatie van de IR spectra van steenkool, die uitgebreid in de literatuur worden beschreven, kan dus worden aangewend voor de verklaring van spectra van (geoxydeerd) roet.

In hoofdstuk 2 worden de experimentele methoden voor de FT-IR analyse van katalysator/roet mengsels bij diesel uitlaatgas temperaturen (dat is *in-situ*) nader toegelicht. Enkele (rekenkundige) technieken die worden toegepast in FT-IR spectroscopie worden behandeld in Appendix I. Het gebruik van diffussie reflectie

(Diffuse Reflectance Infrared Fourier Transform, DRIFT) spectroscopie, de neveneffecten van het gebruik van verdunningsmiddelen en de toepassing van fullereen C60 ('Bucky Ball') als roet-modelverbinding voor spectroscopische analyse, komen achtereen-volgens aan de orde. Hoewel in de IR spectroscopie KBr veel als verdunningsmiddel wordt toegepast, blijkt het met verschillende metaal oxyden, zoals V_2O_5 en MoO_3, een reactie aan te gaan, waarbij diverse vanadaten en molybdaten respectievelijk worden gevormd. Bovendien is gebleken dat KBr interacties met zuurstof houdende complexen op het roet oppervlak vertoont. Daarom is gezocht naar een oplossing om het gebruik van KBr als verdunningsmiddel te vermijden. Si-poeder bleek een redelijke oplossing te zijn. Nog beter is het gebruik van fullereen C60 als roet model verbinding. Zo kan zonder het gebruik van een verdunningsmiddel een hoge spectrale kwaliteit bereikt worden.

Roet oxydatie katalysatoren kunnen worden onderverdeeld in drie catagoriën. Katalysatoren op basis van chloriden, alkali metaal oxyden, en overgangs metaal oxyden worden achtereenvolgens in deze dissertatie behandeld. De activiteit van een gepatenteerde Cu/K/Mo/Cl katalysator wordt beschreven in hoofdstuk 3. De actieve componenten van deze katalysator blijken CuCl en Cu_2OCl_2 te zijn. Deze verbindingen worden gevormd door reactie van kopermolybdaten met KCl, die in ruime mate aanwezig zijn in de Cu/K/Mo/Cl katalysator. Helaas hebben koper chloriden een aantal vervelende eigenschappen. Ze zijn vluchtig, en komen daardoor in het milieu terecht, en bovendien kunnen ze de vorming van dioxynes katalyseren. Het moge duidelijk zijn dat koper chlorides niet in de praktijk kunnen worden toegepast. Ook het gebruik van andere metaal chloriden blijkt aanzienlijke nadelen te hebben, waarvan vervluchtiging de belangrijkste is (hoofdstuk 4). De experimenten met metaal chloriden hebben echter wel het belang van het contact tussen een katalysator en roet en de mogelijke rol van zuurstof complexen op het roet oppervlak in het oxydatie mechanisme aangetoond.

De toepassing en het mechanisme van alkali metaal oxyde gekatalyseerde roet oxydatie is uiteengezet in de hoofdstukken 5 en 6. De actieve verbinding blijkt een alkali oxyde cluster te zijn, dat via zuurstof bindingen aan het oppervlak van roet gebonden zit. Ook de vorming van zogenaamde benzoaten is aangetoond. De aanwezigheid van NO_x bevordert alkali gekatalyseerde roet oxydatie boven 600 K. Echter, bij temperaturen lager dan 600 K, deactiveert chemisorptie van NO_2 deze katalysatoren. Deze deactivering, en de te verwachten vervluchtiging van de actieve componenten, maken alkali oxyden niet aantrekkelijk voor praktische toepassing.

De activiteit van overgangs metaal oxyden wordt uitgebreid behandeld in hoofdstukken 7 tot en met 10. Allereerst wordt door middel van DRIFT spectroscopie aangetoond dat deze metaal oxyden zich verschillend gedragen ten aanzien van de vorming van zuurstof complexen op het roet oppervlak (hoofdstuk 7). Fe_2O_3 en Co_3O_4 geven geen aanleiding tot de vorming van deze complexen, terwijl Cr_2O_3, MoO_3, V_2O_5 en CuO dit bevorderen. Het laatste wordt verklaard door zogenaamd "spill-over" van geactiveerde zuurstof. Blijkbaar vindt recombinatie van dit

geactiveerde zuurstof op het oppervlak van Fe_2O_3 en Co_3O_4 plaats, voordat zuurstof bevattende complexen op het roet oppervlak gevormd kunnen worden.

Het roet oxydatie mechanisme is verder onderzocht door gebruik te maken van $^{18}O_2$, waardoor onderscheid gemaakt kan worden tussen gas fase zuurstof en zuurstof uit het metaal oxyde rooster. Uit de resultaten volgt dat voor zowel Fe_2O_3 en Co_3O_4, als voor Cr_2O_3 geldt, dat reductie en heroxydatie van het metaal oxyde oppervlak een belangrijke rol speelt. Van MoO_3, V_2O_5 en K_2MoO_4 speelt niet alleen zuurstof dat zich aan het oppervlak van het metaal oxyde bevindt, maar tevens zuurstof dat dieper in het rooster gelegen is, een belangrijke rol in het oxydatie mechanisme reactie (hoofdstuk 8). Gebaseerd op de resultaten van hoofdstuk 7 en 8, blijkt dus dat drie typen zuurstof een rol spelen in de roet oxydatie: zuurstof dat zich op het oppervlak van het metaal oxyde bevindt (*super* surface, dat de vorming van zuurstof complexen via "spill-over" op het roet oppervlak veroorzaakt), zuurstof in de buitenste laag van het metaal oxyde oppervlak (surface) en zuurstof dat zich in het rooster bevindt (lattice).

In hoofdstuk 9 is onderzocht of door middel van modificaties van metaal oxyden de roet oxydatie activiteit zou kunnen worden verhoogd. In de literatuur is een positief effect in de oxydatie van CO beschreven, ten gevolge van de modificatie van metaal oxyden met Au of Ag. Uit de metingen beschreven in hoofdstuk 9 volgt dat Au een negatief effect heeft op de roet oxidatie, terwijl zilver een positief effect blijkt te hebben. Bovendien geven de bevindingen in hoofdstuk 9 nog eens aan dat de intensiteit van het contact tussen het metaal oxyde en het roet oppervlak een bepalende factor is voor de uiteindelijk gemeten activiteit van het metaal oxyde (de grootte van het initiële oppervlak van het metaal oxyde speelt een belangrijke rol). Verder blijkt dat, in overeenstemming met de resultaten van hoofdstuk 8, het zuurstof dat geassocieerd is met het metaal oxyde, waarschijnlijk een belangrijke rol speelt in het oxydatie mechanisme. Het negatieve effect van Au kan verkaard worden door een gedeeltelijke bedekking van het oppervlak van het metaal oxyde met Au, wat zelf niet aktief in de roet oxydatie is. Hierdoor wordt het aantal katalysator/roet contact punten verlaagd en zo de efficiëntie van zuurstof transport van het metaal oxyde naar het roet deeltje. Het effect van zilver kan verklaard worden door aan te nemen dat zilver oxyde een hoge intrinsieke activiteit voor de roet oxydatie bezit. De functie van het overgangs metaal oxyde is de activering van zuurstof dat via het zilver oxyde oppervlak met roet reageert. Met andere woorden, de aanwezigheid van zilver versnelt het transport van geactiveerd zuurstof naar het roet deeltje.

In hoofdstuk 10 worden de effecten van NO_x en CO op de roet oxydatie activiteit van Cr_2O_3, Co_3O_4 en CuO nader bediscussieerd. NO_x (dat is een mengsel van NO en NO_2) blijkt de roet oxydatie te bevorderen. Dit is het gevolg van de niet gekatalyseerde "Roet/NO_2" reactie. Wanneer de intensiteit van contact tussen de katalysator en het roet gering is, is de primaire functie van het metaal oxyde om NO om te zetten in NO_2. In principe is sprake van zogenaamde bifunctionele katalyse, waarbij NO de effectiviteit van het metaal oxyde verhoogd, door efficient transport

van geactiveerd zuurstof naar het roet deeltje. Uit metingen met verschillende contact intensiteit tussen de roetdeeltjes en de katalysator, blijkt echter dat de "Roet/NO_2" reactie ook gekatalyseerd wordt. Hierbij speelt de omzetting van NO_2 in NO en geactiveerd zuurstof (O^*) op het metaal oxide oppervlak waarschijnlijk een belangrijke rol.

Hoewel de kennis over het werkings mechanisme van verschillende typen katalysatoren aanzienlijk is vergroot, heeft dit slechts tot aanwijzingen voor de ontwikkeling van een mogelijke systeem in de praktijk geleid, en niet tot een werkend systeem. Het tegendeel is zelfs waar: een veel belovende Cu/K/Mo katalysator blijkt totaal niet geschikt te zijn om in de praktijk te worden toegepast. Behalve nieuwe wetenschappelijke inzichten, laten de bevindingen in dit proefschrift zien dat een mogelijk actieve katalysator de geactiveerde reactant (zuurstof), efficient naar het substraat (roet) moet kunnen transporteren.

Momenteel wordt onderzoek verricht aan mobiele katalysatoren (waardoor het contact tussen de katalysator en de roet deeltjes kan worden verbeterd) en wordt de toepassing van verschillende katalytische additieven aan de diesel brandstof nader onderzocht. Hierdoor wordt de afstand tussen de katalysator en roet verminderd, wat een efficienter transport van zuurstof mogelijk maakt. Mogelijkerwijs kan ook de "roet/NO_x" reactie uitkomst brengen. NO zorgt eveneens voor een efficient transport van geactiveerd zuurstof.

Het verdient aanbeveling om het effect van andere gasvormige componenten die aanwezig zijn in diesel uitlaatgas, zoals CO, H_2O, en koolwaterstoffen, op de katalytische activiteit van metaal oxyde katalysatoren nader te onderzoeken. Belangrijker is nog de mogelijke vorming van SO_3 ten gevolge van de reactie van SO_2 met zuurstof, wat een bijdrage levert aan het 'deeltjes gehalte' van diesel uitlaatgas [3]. Gelukkig ligt een laag zwavel gehalte van de diesel brandstof in het verschiet, ten gevolge van steeds strenger wordende wetgevingen.

Referenties

[1]   R.J. Hultermans, 'Selective Catalytic Reduction of NO_x', PhD Thesis, Delft University of Technology, 1995.

[2]   E. Ito, 'Development of Zeolite Catalysts for NO_x Reduction with NH_3 in Diesel Exhaust Gas', PhD Thesis, Delft University of Technology, 1996.

[3]   J.P.A. Neeft, 'Catalytic Oxidation of Soot-Potential for the Reduction of Diesel Particulate Emissions', PhD Thesis, Delft University of Technology, 1995.

APPENDIX 1

The principles and instrumentation of FT-IR spectroscopy

1. General concepts of IR spectroscopy

Spectroscopy deals with the interaction of electromagnetic waves with matter. The electromagnetic spectrum encompasses an enormous range of wavelengths and frequencies. The visible region of the spectrum (400-800 nm) is relatively small compared to other spectral regions. The infrared region, which is of interest here, includes the frequencies (in wavenumbers) of 12500 to 20 cm^{-1}.

Energy is proportional to frequency, according to equation 1, in which ΔE, h and v represent the difference between two energy levels, Planck's constant and the frequency, respectively.

$$\Delta E = hv = h\frac{c}{\lambda} = hc\sigma \qquad (1)$$

As v equals c/λ (in which c represents the speed of light and λ the wavelength), and the wavenumber (σ) equals $1/\lambda$, the energy is directly proportional to the wavenumber. The total energy of a molecule is a sum of electronic, vibrational and rotational contributions (equation 2). Transitions in vibrational and rotational energy are of interest in IR spectroscopy, which require 3-50 $kJ.mol^{-1}$ and 0.5-5 $kJ.mol^{-1}$, respectively.

$$E_{total} = E_{electr} + E_{vib} + E_{rot} \qquad (2)$$

The vibration of a simple diatomic molecule with an internal frequency can be modeled by two balls connected by a string. The oscillation frequency is described by equation 3, in which k and m_r represent the force constant and reduced mass, respectively.

$$v = \frac{1}{2\pi}\sqrt{\frac{k}{m_r}} \qquad (3)$$

The reduced mass is expressed by equation 4, in which $m1$ and $m2$ represent the mass of atoms 1 and 2:

$$m_r = \frac{m_1 m_2}{m_1 + m_2} \qquad (4)$$

Equations (3) and (4) enable the calculation of frequency differences between *e.g.* $C^{18}O_2$ and $C^{16}O_2$: the higher mass of the ^{18}O atom, compared to the ^{16}O atom, causes a shift of the absorption frequencies to lower wavenumbers (approximately 60 cm^{-1} for $C^{18}O_2$ relative to $C^{16}O_2$).

2. Electromagnetic radiation and its wave properties

Although electromagnetic radiation can act both as waves and particles it is necessary to deal with waves (including parameters like wavelength, frequency and amplitude) to understand the principles of Fourier Transformed spectroscopy. An important feature of waves is that they can be superpositioned. The principle of superposition states that when two (or more) waves traverse the same space, a displacement occurs which is the sum of the displacements caused by individual waves. Mathematically this can be written as (A is amplitude, v is frequency, φ is phase, and t is time):

$$y = A_1 \sin(2\pi v t + \varphi_1) + A_2 \sin(2\pi v t + \varphi_2) + \dots \qquad (5)$$

In equation (5) y represents the resultant force field. Complex wave forms such as square waves, can be described by the summation of several sine waves with different amplitude and frequency. The equations of the individual waves can be calculated by a mathematical operation called a Fourier transformation (named after Jean Fourier, a French mathematician (1768-1830)). To accomplish the resolution of a complex wave form into its sine or cosine components is rather tedious. However computers made it possible to exploit the power of Fourier transformations on a routine basis.

3. The principles of the Michelson interferometer

An FT-IR instrument is equipped with a Michelson Interferometer. A schematic diagram is shown in figure 1.
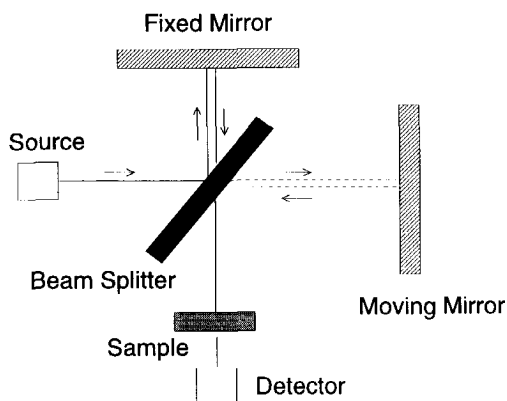
Figure 1. Schematic diagram of the Michelson interfero-meter.

When monochromatic radiation (*e.g.* emitted by a laser) enters the interferometer, the beam impinges on the beam-splitter, which transmits approximately 50% of the radiation to a moving mirror and reflects the other 50% to a fixed mirror. After reflection of the two beams, they are recombined. If the movable and fixed mirrors are equidistant from the beamsplitter, the two parts of the recombined beam are totally in phase and the intensity is twice the intensity of the individual waves. If the difference in path length, called the retardation, is half a wavelength, the resultant intensity will be zero. By changing the position of the movable mirror, the path length is changed and the intensity of the wave leaving the interferometer as well. If the mirror is moved with a constant velocity (V_m) the intensity varies sinusoidally and can be described by equation (6) for a monochromatic source, in which $I(\delta)$ represents the intensity at the detector, σ the wavenumber of the monochromatic source and δ the so-called retardation, which is related to the position of the moving mirror:

$$I(\delta) = 0.5I(\sigma)\left\{1+\cos(2\pi\delta\sigma)\right\} \qquad (6)$$

The intensity at the detector equals the intensity of the monochromatic source ($I(\sigma)$) if δ corresponds to n times the wavelength (n=1,2,3,4,.....).

If the source does not emit monochromatic radiation, but polychromatic radiation, containing every possible frequency (ranging from zero to infinity), equation 6 can be written as equation 7, which is one-half of a cosine Fourier transform pair (compare equation (5)):

$$I(\delta) = \int_0^\infty B(\sigma)\cos(2\pi\delta\sigma).d\sigma \qquad (7)$$

In equation 7 the factor $B(\sigma)$ is introduced to account for the fact that the interferometer usually does not split the beam exactly in half and that the detector response and the amplifier behavior are frequency dependent. Furthermore, only the modulated component of equation (6), *i.e.* $0.5I(\sigma)\cos(2\pi\delta\sigma)$, is important in spectroscopic measurements and taken into consideration. The other half of the Fourier transform pair is given in equation 8:

$$B(\sigma) = 2\int_0^\infty I(\delta)\cos(2\pi\delta\sigma).d\delta \qquad (8)$$

Fourier transformed infrared spectroscopy consists of recording $I(\delta)$ and then mathematically transforming this relation to one that gives $B(\sigma)$, which describes the frequency spectrum.

At $\delta=0$ all frequencies are in phase, so a center burst arises. Figure 2 shows a typical example of an experimentally recorded intensity as a function of retardation, which can be visualized in the 'optical bench setup' option in the Nicolet Omnic™ software.
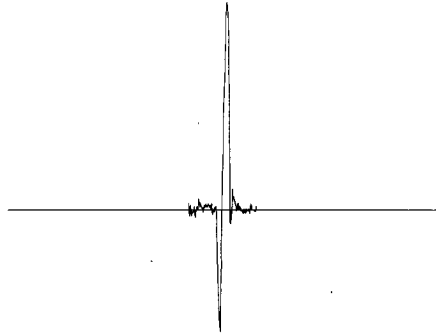

Figure 2. *Representation of the experimental detector intensity as function of the retardation.*

Equation 8 can only be calculated in a certain interval, because the emitted radiation of the IR-source is finite (400-4000 cm⁻¹) and the mirror-drive has a finite length δ. This can be explained as follows.
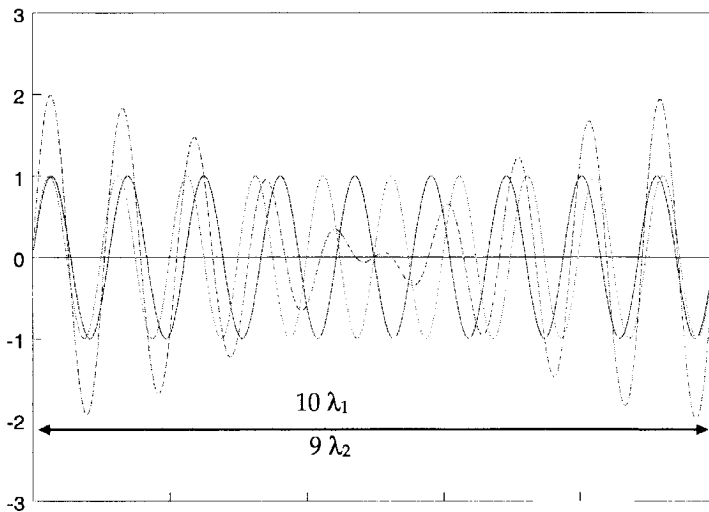
Figure 3. *Diagram to explain that the resolution is determined by the retardation. The interferograms of each line are given, as well as the resultant of the two interferograms, showing that they become in phase at a retardation of $(0.1\ \sigma_1)^{-1}$, that is $10\ \lambda_1$.*

If two wavelengths are considered (λ_1 and λ_2), corresponding to frequencies σ_1 and σ_2 and only separated by $\Delta\sigma=0.1\sigma_1$, it can be shown that they will become out of phase at a retardation of $0.5(\Delta\sigma)^{-1}$, i.e. ($5\lambda_1$), and in phase when the retardation is $(\Delta\sigma)^{-1}$. Thus, to go through one complete period of the beat frequency, needed for a complete resolution of frequencies σ_1 and σ_2, a retardation of $(\Delta\sigma)^{-1}$ is required. Intuitively and mathematically it can be concluded that the best resolution ($\Delta\sigma$) of an interferometer with a maximum retardation of Δ_{max} is given by $\Delta\sigma=(\Delta_{max})^{-1}$ (in cm^{-1}). By restricting the maximum retardation of the interferogram to Δ_{max} cm, the complete interferogram (δ ranging from $-\infty$ to ∞) is in fact multiplied by a truncation function, $D(\delta)$, which is unity between $\delta=-\Delta_{max}$ (minimum retardation) and Δ_{max} (maximum retardation) and zero outside these borders. However, significant negative lobs will appear on the sides of an absorption profile at a certain frequency by using this so-called box-car truncation-function or *apodization*. A correction manipulation has to be carried out on the Fourier transformation. The use of a triangular function, or a so-called Happ-Genzel *apodization*, suppresses the formation of sidelobs. The spectra shown in this thesis were corrected by the Happ-Genzel method, which can be selected in the Omnic™ software.

The spectral quality can be further improved by adding zeros to the interferogram. This so-called *zero-filling* is incorporated in the Omnic™ software and yields a smoother spectrum after Fourier transformation, as stepping between each data point is more or less prevented.

4. Advantages of Fourier Transformed Spectroscopy

Dispersive IR instruments (containing grids and/or prisms) need long measurement times: the spectrum is made up of different individual transmittance measurements at equally spaced frequency or wavelength intervals, and the measurement of a spectrum in a range of 500 cm^{-1} to 5000 cm^{-1} with a 3 cm^{-1} resolution requires typically 12.5 minutes to be completed. Besides the long measurement time, another disadvantage of dispersive instruments is the relatively low signal to noise ratio. This is caused by the narrow slits, which have to be used to obtain a high resolution. The signal to noise ratio in a certain spectrum can be improved by enlarging the number of spectra recorded. Generally, a signal to noise ratio improves with the square root of the number (n) of measurements (S_n and N_n represent the averaged signal, and noise respectively).

$$\frac{S}{N} = \frac{S_n}{N_n} * \sqrt{n} \qquad (9)$$

If one spectrum requires 12.5 minutes to be recorded, it is obvious that it would need enormous analyzing times to obtain a high resolution spectrum with a high signal to noise ratio. In Fourier Transform (FT) spectroscopy all resolution elements are collected simultaneously, reducing the time required to obtain a spectrum (this is called time domain spectroscopy). An improvement of the signal to noise ratio of at least 40 times

can be accomplished, using FT measurements, compared to dispersive measurements (this is known as the Fellgett advantage). Other advantages are the high wavelength precision and the large energy throughput to the detector, which are known as the Jacquinot advantages.

DANKWOORD

Zo, nu kom ik aan het minder officiële gedeelte van dit dankwoord. Uiteraard verdienen mijn kamergenoten Emile en Paul een pluim dat ze het met twee van die 'druk-spoken', d.i. Wridzer en mij, hebben uitgehouden. Wridzer, zonder jou zou mijn tijd aan de TU Delft heel wat saaier zijn verlopen, en dat behoeft verder geen commentaar. Jean-Paul en Mark hebben ook een belangrijke bijdrage aan de plezierige uren aan de TU Delft geleverd. Jean-Paul als klaverjas-maat (Wridzer en Mark, en ook Jacob en Floor hadden geen schijn van kans) en Mark als muziek-maat (wat Scarlett niet altijd waardeerde). Hierbij mag ook Bastiaan niet onvermeld blijven (Ti Bedippie Perip). Verder wil ik John apart noemen, omdat ik de samenwerking in het diesel project zeer leuk heb gevonden. Vooral in het manipuleren van Jacob om hem in onze ideeen te doen geloven, zijn we geloof ik goed geslaagd. Hopelijk wordt onze artikelen-serie snel geaccepteerd. Ook wil ik Jan-Remmert nog bedanken voor de gezelligheid op 't lab en tijdens Carbon '95, en de vele tips voor het verwerven van een Post-Doc positie. Tenslotte wil ik Xander en Matthijs nog apart noemen. Tafeltennis blijft een leuk spelletje, zelfs als je soms wel eens wordt afgedroogd....

Verder hebben natuurlijk ook alle andere leden van de groep industriële katalyse een belangrijke bijdrage aan de gezelligheid tijdens voetbal toernooien, zeil weekenden, schaatsen, het Ardennenweekend, fietsen in de Eifel etc. geleverd: alle *IO's, staf en ander personeel, bedankt !

Dan ben ik nu gekomen aan mijn ouders, die ik wil bedanken voor het enthousiasme dat ze altijd voor mijn plannen omtrent onderwijs en levensloop hebben getoond. En tja, dan nu nog degene die volgens mij het langst heeft uitgezien naar dit dankwoord. Welnu Regine, eigenlijk is het niet nodig om je hier te bedanken. Hopelijk heb ik je de afgelopen vier jaar wel duidelijk genoeg gemaakt dat ik je steun, enthousiasme, en gewoon je stimulerende aanwezigheid thuis altijd zeer heb gewaardeerd. Maar..., bij deze dan.

Guido, Januari 1997.

LIST OF PUBLICATIONS

Articles

G. Mul, J.P.A. Neeft, F. Kapteijn, M. Makkee, J.A. Moulijn, *"Soot oxidation catalyzed by a Cu/K/Mo/Cl catalyst: Evaluation of the chemistry and Performance of the catalyst"*,
Appl. Catal. B: Env. 6 (1995) 339-352.

G. Mul, F. Kapteijn, J.A. Moulijn, *"Catalytic Oxidation of Model Soot by Metal chlorides"*, Appl. Catal. B: Env. (1996), Accepted.

G. Mul, F. Kapteijn, J.A. Moulijn, *"DRIFT analysis of Surface Oxygen Complexes on soot formed by metal oxides"*, Prepr. Pap. - Am. Chem. Soc. Div. Fuel Chem.
41(1996) 230-236.

Contributions to publications

Carola B. Hansen, Guido Mul, Roland B.J. Tabor, Wiendelt Drenth, *"Mechanistic Study of Decomposition of cyclohexyl hydroperoxide catalysed by manganese(III) tetraarylporphyrins"*, Recl. Trav. Chim. Pays-Bas, 112 (1992) 497-502.

Freek Kapteijn, Guido Mul, Gregorio Marbán, José Rodriguez-Mirasol and
Jacob A. Moulijn, *"Decomposition of Nitrous oxide over ZSM-5 Catalysts"*,
Proc. 11th Int. Congres on Catal., Baltimore, USA (1996).

J.P.A. Neeft, G. Mul, F. Kapteijn, M. Makkee, and J.A. Moulijn, *"Feasability study towards a Cu/K/Mo/Cl soot oxidation catalyst for application in diesel exhaust gases"*,
Appl. Catal. B: Env. (1996), accepted.

J.P.A. Neeft, G. Mul, F. Kapteijn, M. Makkee, J.A. Moulijn, *"Catalytic oxidation of soot : part III - The effect of preoxidation of soot on the catalytic activity"*,
Fuel (1997), in preparation.

Abstracts

G.Mul, J.P.A. Neeft. F. Kapteijn, M. Makkee and J.A. Moulijn, *"Soot oxidation catalysed by a Cu/K/Mo/(Cl) catalyst: Evaluation of the chemistry and performance of the catalyst"*. Book of Abstracts-Europcat II, 1995, p. 306-306.

G. Mul, J.P.A. Neeft, F. Kapteijn, M. Makkee, and J.A. Moulijn, *"Soot oxidation catalyzed by a Cu/K/Mo/Cl catalyst: evaluation of the chemistry and performance of the catalyst"*, Proc. 22nd Biennial Conference on Carbon, 16-21 July 1995, San Diego,
USA (1995) 650-651.

G. Mul, F. Kapteijn, and J.A. Moulijn, *"Drift analysis of carbon-oxygen species on Printex-u after catalytic oxidation by metal oxides in air, nitrous oxide and ozone"*, Proc. 22nd Biennial Conference on Carbon, 16-21 July 1995, San Diego,
USA (1995) 554-555.

In preparation

G. Mul, J.P.A. Neeft, F. Kapteijn, J.A. Moulijn, *"Catalytic oxidation of soot :*
Part II - Formation of Surface Oxygen Complexes on soot, catalyzed by transition metal oxides",
Fuel (1997).

G. Mul, C. Doornkamp, F.Kapteijn, J.A. Moulijn, *"Catalytic oxidation of soot :*
Part V - An $^{18}O_2$ Study", J. Catal. (1997).

G. Mul, F. Kapteijn, J.A. Moulijn, *"A DRIFT spectroscopic study of the potassium catalyzed soot*
oxidation.", Carbon (1997).

G. Mul, F. Kapteijn, J.A. Moulijn, *"On the application of KBr in in-situ DRIFT*
studies of catalytic reactions: The reaction of KBr with transition metal oxides.", Vibrational
Spectroscopy (1997).

G. Mul, F. Kapteijn, J.A. Moulijn, *"The effect of NO_x and CO on the rate of the transition metal*
oxide catalyzed soot oxidation: an exploratory study", Appl. Catal. B: (1997).

CURRICCULUM VITAE

Guido Mul werd geboren op 23 juli 1969 in Hoorn. De middelbare school werd gevolgd aan de rijks-scholen gemeenschap 'West-Friesland', alwaar hij in 1987 het Gymnasium β diploma behaalde. Vervolgens werd de scheikundige studie gevolgd aan de Universiteit Utrecht, met als keuzevakken fysisch organische chemie en anorganische chemie. Het hoofdvak werd eveneens bij de afdeling anorganische chemie uitgevoerd (Prof. dr. ir. J.W. Geus) met als onderwerp 'De ontwikkeling van een aluminium fosfaat gedragen ijzeroxyde absorbens voor hoge temperatuur ontzwaveling van kolengas'. Het doctoraal examen werd afgelegd in september 1992.

Vanaf november 1992 tot november 1996 werd een promotie onderzoek uitgevoerd aan de TU Delft bij de afdeling industriële katalyse onder de titel van dit proefschrift. Dit onderzoek werd uitgevoerd onder leiding van Prof.dr. J.A. Moulijn en Dr. F. Kapteijn en werd financieel mogelijk gemaakt door SON/NWO.